Tunable Hydrogel-Polyester Combination Scaffolds for Tissue Engineering Purposes

Thesis submitted to obtain
the degree of Master of Science in Chemistry by

Jasper VAN HOORICK

Academic year 2013 - 2014

Promoter: prof. dr. Peter Dubruel
Copromoter/Supervisor: prof. dr. Sandra Van Vlierberghe

"None but those who have experienced them can conceive of the enticements of science. In other studies you go as far as others have gone before you, and there is nothing more to know; but in a scientific pursuit there is continual food for discovery and wonder."(Frankenstein-Mary Shelley 1818)

Acknowledgement

Unfortunately, to sufficiently express my gratitude to everyone who deserves it, I would have to write an additional thesis consisting solely of an acknowledgement, so in conclusion I would like to express my gratitude to all the members from the group, for their hospitality and kindness. And I sincerely hope that this year will be the start of successful future cooperations.

Thank you very much for everything PBM,

Table of contents

1. Introduction

1.1 Problem statement

Low back pain is one of the most common complaints throughout the modern western society.[1][2][3][4][5] It can lead to a chronic disability for 10% of the patients resulting in a huge economic burden for society. Lower back pain often goes concomitant with intervertebral disc (IVD) degeneration.[3][4][6] As a result, tissue engineering (TE) solutions for IVD gained increasing attention during the last decade.

The spinal column is one of the largest components of the human skeleton. It serves a dual role as it provides trunk flexibility while supporting the upper body weight.[7][8] In addition, it has to function as an armor for the spinal cord and the nerve roots that pass through.[9] The spine is composed of 33 stacked vertebrae, which sandwich an IVD. 24 of these vertebrae form a flexible part while 9 vertebrae form a rigid part inside the pelvis. [7]

The IVDs act as the joint between the separate spinal column vertebral bodies. They are responsible for flexibility and load transmission throughout the spine.[5] When they degenerate, they lose height and therefore affect the entire spinal column, resulting in back pain and/or a loss of mobility of the spinal column. In the long term, the degeneration of IVDs can result in spinal stenosis which is the main cause of back pain for the elderly.[2]

The cause of IVD degeneration is not fully defined, yet it is anticipated to be the result of a combination of factors including natural aging, mechanical compression, biological factors, smoking, etc.[4][5][10][11] Interestingly, IVD degeneration typically occurs in an earlier stage compared to the degeneration of other musculoskeletal tissues. The first signs of degeneration can already be observed in about 20% of youngsters aging from 11 to 16 years old.[2][6]

1.2 Spinal anatomy and pathophysiology

1.2.1 Anatomy of the intervertebral discs

An IVD is a rather avascular system,[8] consisting of three main regions including the nucleus pulposus (NP), the annulus fibrosus (AF) and the cartilaginous end-plates. [2] (see Figure 1, left)

The NP is the gelatinous core of the IVD,[3] with the major component being water (cfr. 65-85% of its total weight).[2][5][12] It contains randomly organized collagen fibers and radially aligned elastin fibers embedded in a highly hydrated proteoglycan (PG) gel. The main PG present is aggrecan which generates an osmotic pressure originating from the presence of chondroitin

sulphate and keratan sulphate chains responsible for hydration.[2][10] In addition, the NP consists of a low density of chondrocyte-like cells embedded in a disorganized matrix mainly consisting of type II collagen fibers. It shows fluid-like behavior, yet acts as an elastic solid upon mechanical loading.[13] The shear modulus G* ranges from 7 to 21 kPa[14] while its compressive elastic modulus varies between 3 and 15 kPa.[15]

The AF is more fibrous-like and consists of 15 to 20 concentric lamellae. These lamellae contain parallel aligned collagen fibers, primarily type I, which are oriented at an angle of 62 degrees relative to the spinal axis at the edges of the AF. The center of the AF mainly consists of collagen type II fibers oriented at an angle of about 45 degrees relative to the spinal axis. [3][7][12][16] The angle of the fibers of one lamellae layer is rotated over 180° in comparison to the fibers of the previous layer.[13] Furthermore, the AF contains proteoglycans and elastin fibers which connect the different lamellae thereby generating a high axial strength.[16] In addition to collagen and elastin fibers, the AF contains elongated, fibroblast-like cells which are aligned parallel with the collagen fibers.[2] The cells maintain the complex extracellular matrix (ECM) structure to preserve the biomechanical properties of the AF.[5] The AF is characterized by a shear modulus G* of 540 kPa.[17]

Finally, the cartilaginous end plates are thin horizontal layers consisting of an outer osseous component and an inner hyaline cartilage region.[8] The central region consists of a hydrated PG gel which is reinforced by collagen fibrils.[8] It enables diffusion of nutrients and waste to and away from the disc.[13] The end plates act as an interface between the IVD and the vertebral body. Furthermore, they prevent the NP from bulging into the vertebral bone.[8] In addition, similar to the additional IVD components, they mainly consist of collagen fibers aligned parallel with the vertebral bodies. [2] The end plates are characterized by a shear modulus G* of 440 kPa.[17]

Collagen is the major component of the IVD as it accounts for 90% of its dry weight. It serves important mechanical properties as it absorbs water, together with the PG's, creating a swelling pressure which is large enough to maintain a distance between the loaded vertebrae. Compressive loads are supported mostly by the pressurization of the NP, in combination with the minimal hydraulic permeability of the AF thereby preventing the NP to burst. The bending and shear stresses on the spine are borne mostly by the mechanically robust AF.[5] In addition, the collagen fibers inside the end plates serve an anchoring function for the IVD to the vertebral bones. [2]

Various interesting features can be distinguished when considering IVD tissue. First, the presence of long, thin cytoplasmic cell projections can be observed which are typically absent in cells of

any other articular cartilage. It can be anticipated that they serve as sensors and communication devices for mechanical strain within the tissue.[2] Secondly, there is an almost complete absence of blood vessels and nerves in the entire IVD. If present, they are only observed in the outer lamellae. [2][8] This feature causes a poor nutrient supply throughout the IVD. In addition, this also leads to poor regeneration capacities[10][18] as the cells are completely dependent on passive diffusion of nutrients through the end plates and subsequently the ECM. The nutrient transport is thus very dependent on the composition of the ECM.[2] Finally, the IVD contains a higher amount of PG compared to articular cartilage.
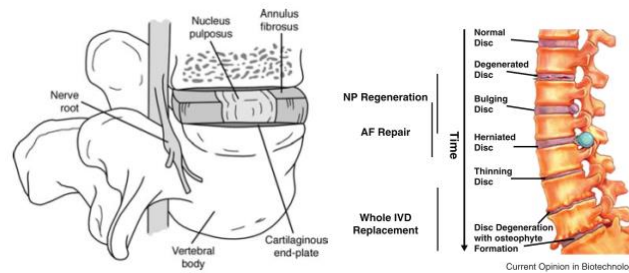
Figure 1: Spinal segment consisting of two vertebral bodies and an intervertebral disc (left)[2]**; Overview of several stages occurring during IVD degeneration including the time scale of possible interventions (right).**[5]

1.2.2 Pathophysiology of the intervertebral disc

Disk degeneration disease (DDD) has significant consequences on the three parts of the IVD. During skeletal maturation, the boundaries between the NP and the AF start to fade and the NP loses some of its elasticity as it becomes gradually more fibrotic and less gel-like.[19][20] The latter results in a drastic reduction of the biomechanical properties of the IVD.[3] Another important aspect in DDD is an increase in endplate calcification.[21]

The origin of these phenomena can be traced back to changes occurring inside the IVD. At an early age, notochordal cells are present in IVDs.[11] Interestingly, these cells can generate large amounts of ECM. However, upon maturation these cells gradually disappear, thereby reducing ECM (re)generation. In addition, enzymatic breakdown of the proteoglycans results in a reduction of the hydration of the NP. The endplate calcification reduces nutrient flow to the NP and the AF resulting in necrosis of ECM synthesizing chondrocytes. The above-mentioned process gives rise to a decreased ECM regeneration. As a result, the PG degradation is further accelerated. [2][22][23][21] Finally, a drop in type II collagen content is observed while an increase in type I collagen is observed inside the NP. [14][23]

The degradation of IVDs can result in several types of IVD failure including the occurrence of tears in the AF resulting in bulging of the disc, herniation of the disc and loss of disc height due to a reduction of the water content. [5] (see Figure 1: right)

The loss in water content due to a reduction of the PG present in the NP, reduces the ability to maintain osmotic pressure upon mechanical load. The latter further increases the loss of fluid and the stress exerted on the AF, leading to compression of the IVD. In addition, a height reduction in one IVD generates an increased stress on other parts of the spine, resulting in a synergistic effect of spinal complications and finally spinal stenosis.[2] Furthermore, the presence of aggrecan prevents vascular and neural ingrowth. As a result, the degradation of PG's gives rise to an increase of vascular and neural ingrowth, which is anticipated to be an attempt of the body to increase nutrient supply in order to restore the IVD.[8] The presence of nerves in a load bearing system causes additional back pain as these nerves experience compressive forces.[24][2]

Another important aspect is the reduced organization of the collagen fibers inside the AF which affects the biomechanical properties to a great extent.[2] The drop in biomechanical properties of the AF can result in concentric tears (cfr. intervertebral disc disruptions, IDD) upon load.[2] Through these tears, the NP can be (partially) extruded, leading to bulges and disc herniation,[22] causing chronic pain because of the pressure exerted on adjacent nerves.[2](see Figure 1: right)

1.3 Conventional clinical therapies

Current treatments for low back pain associated with IVD degeneration are aiming at reducing discomfort and treating the symptoms rather than repairing the mechanical function of the IVD.[2][3] They typically do not address the loss of disc height nor the mechanical functions associated with IVD degeneration.[3] They can even further induce the degeneration due to alterations in biomechanics[3] which result in a necessity for additional surgical interventions.[25]

A first set of treatments are conventional, non-invasive techniques consisting of oral analgesics and physical therapies. However, these treatments tend to focus more on pain relief rather than addressing the cause of the problem. Furthermore, it typically takes months before 'satisfactory' results are obtained.[2]

Secondly, some minimally invasive techniques aim at reducing the pressure exerted on the nerves which is caused by bulging and disc herniation. The above-mentioned techniques are referred to as nucleotomy, (micro)discectomy and annuloplasty[24] and imply that part of the IVD, generally the NP, is removed to reduce the pressure exerted on the nerves.[22][2][26] Although instant pain relief can be observed in the short term, these techniques can lose their benefits because of the poor regeneration properties of the IVD and the possible occurrence of additional degeneration during longer timeframes.[16]

Alternatively, there currently exist two major invasive approaches to treat intervertebral defects.[25] Spinal fusion or arthrodesis[13] fuses two vertebral sections around the damaged IVD. It is currently the standard treatment for degenerative disk disease.[9] A second technique includes a complete surgical removal of the traumatized IVD and its replacement by an artificial one.[4][9][27][28][29][30] The latter technique has emerged as an alternative for spinal fusion to address a possible loss of biomechanical properties. Recently, progress has already been realized in this field by applying rapid manufacturing as a tool to construct patient-specific implants.[31] Although this technique offers some benefits over spinal fusion, it still exhibits significant drawbacks including a limited biocompatibility, inconsistent mechanical behavior which induces additional stress on the column[27], a poor fixation which could lead to fusion[28][29] and the production of wear debris on repetitive mechanical loads which can induce inflammatory responses.[5][16][29][30](see Addendum A.I :Table 5)

1.4 Tissue engineering treatments

Tissue engineering is a scientific research field which aims at the development of novel technologies to address the numerous challenges faced when dealing with tissue repair. On the one hand, it aims at suitable alternatives for conventional organ transplants and all of its associated hurdles. On the other hand, alternative treatments are also targeted for currently unsatisfying treatments including IVD degeneration.[32] A promising approach in this respect is the use of biomaterials as starting compounds for functional scaffolds. Ideally, the scaffolds developed should closely resemble the natural ECM while showing a predetermined macroscopic shape. They can be introduced at the site of a tissue defect [22] to act as a support for stem cell adhesion, differentiation and proliferation, in order to finally result in the generation of new tissue.[32][33][34][35][36] An overview of the applied cell sources is given in Addendum A.II.1

As a result to the lack of fundamental treatment, increasing attention has been paid recently to alternative, more sustainable treatments which focus on restoring disc height and biomechanical functions by introducing tissue engineering approaches.[2][13][22][37][38]

A first approach to engineered IVDs is whole organ culture.[39] The focus thereby lays on understanding the mechanisms behind IVD degeneration and the factors which enhance disc regeneration ex vivo. Several factors are studied in that respect including the effect of mechanical stresses exerted and nutrient supply on the cell viability[18], several areas of the IVD which show increased or decreased cell proliferation, etc. The above-mentioned studies are key to realize the regeneration of IVDs.[5]

Three methods are currently under investigation for IVD regeneration including AF repair, NP repair or replacement and total IVD replacement. The selection and the success rate of the different approaches are often depending on timing and the nature of the observed degeneration.[5] (see Figure 1:Right)

1.4.1 Nucleus Pulposus replacement

As the early symptoms of IVD degeneration can be attributed to transformations occurring inside the NP, a lot of research is focused on augmenting or regenerating the NP.[19][40][41][25] In general, the studies aim at increasing the PG content to restore the hydraulic pressure inside the NP, which is crucial for its mechanical function. [5][38] The regeneration of the NP can be extremely useful in the early stages of DDD prior to AF degradation.[42](see Figure 1:right)

Two approaches exist to realize an increase in PG content. First, the cells present in the NP can be stimulated to upregulate their ECM production by administering growth factors such as TGF-β and BMP-2.[3][6][38][23][36][38][36] Unfortunately, although these growth factors result in an increase of the major ECM components collagen and glucosaminoglycans (GAGs) [6][38][23][36], they can also lead to ossification of the AF. [43] Furthermore, the successful introduction of growth factors in the NP has proven to be quite challenging, as a straightforward injection only generates short-term effects. [16][38] The optimal approach is to introduce the growth factors in a more permanent way by for instance gene transfer therapy.[6] Applying this approach implies the introduction of a gene responsible for growth factor production into the target cells which ideally results in a continuous production of the growth factor.[2] Alternatively, the introduction of new cellular material might be essential as IVD tissue is characterized by a very low cellular density and DDD decreases this density even further. As a result, a stimulation of the ECM production in the native cells will not yield sufficient ECM.[3] To address this cellular shortage, research is also performed to investigate the possibilities to introduce new cellular tissue in the IVD. [44] A dual approach combining growth factors with the introduction of new cellular tissue is anticipated to give the best result.[19][23]

In order to introduce cells, injectable biomaterials or cell-seeded scaffolds can be applied. The former are generally in situ cross-linkable hydrogels showing similar biomechanics compared to the native NP.[21][42][45] Alternatively, a cell-seeded scaffold can be useful for more extensive injuries.[5] A non-exhaustive overview of the materials and cell sources required is shown in Addendum A.I: Table 6.

Injectable procedures show some benefits compared to methods which require surgical implantation. First, injectable procedures are minimally invasive thereby reducing potential

6

inflammatory responses.[46][47] Furthermore, the slightest tissue damage present as a consequence of a surgical intervention can be accelerated upon mechanical loading, which leads to a faster degradation.[19] Secondly, the injection of a biomaterial ensures the entire void present in the IVD to become filled,[14][15] thereby improving implant fixation and reducing the risk of implant migration.[17] However, the success rate of injectable materials is also affected by the resealing strategy applied for the AF post injection.[25] Upon improper sealing of the puncture, the NP can be excluded through the hole upon mechanical loading.[48][49] Although some studies exist during which only cells are injected[44][50], superior results are generally obtained when combining cells with injectable biomaterials to increase viability. A wide variety of hydrogel materials has already been applied for this purpose including collagen, [10][51][52][53] cellulose composites, [42] gelatin, [23] hyaluronic acid(HA)-gelatin-adipic acid dihydrazide, [14] hyaluronic acid , [54] hyaluronan, [12] polyethyleneglycol/hyaluronic acid/pentosan polysulphate (PEG/HA/PPS), [15] ferulic acid-gelatin/chitosan/glycerol phosphate, [55] collagen II/PEG/HA, [47] hyaluronic acid/gelatin/adipic acid dihydrazide (oxi-HA/ADG), [17] poly(ethylene glycol) PEG, [49] platelet rich plasma(PRP), [56] chitosan [21] (see Addendum A.I :Table 6).

The use of scaffolds for NP regeneration also poses some benefits, as they provide additional support in withstanding the mechanical loads exerted on the IVD during cell proliferation thereby increasing cell viability. [11][26][48] Ideally, the scaffold applied should possess a similar or slightly higher stiffness than native tissue. Conversely, in case the stiffness exceeds a critical value, subsidence through the endplates can occur.[48][54] A second advantage of scaffolds is that they provide space for new cells and ECM to be synthesized while enabling diffusion of nutrients and waste, in contrast with injectable methodologies.[40] Unfortunately, the application of scaffolds requires invasive procedures, thus increasing possible inflammatory responses[46] while augmenting the risk of damaging nerves and adjacent tissue upon implantation. Furthermore, since the scaffolds can never completely fill the entire void, there exists a risk related to possible scaffold migration.[17] As a result, the success of an implantable scaffold is very dependent on the implantation procedure.[48] To date, a plethora of materials is already under consideration to produce suitable NP scaffolds including alginate, [22] collagen, [38][48] silk-fibrin hyaluronic acid (HA) composites, [19] poly-glycolic acid/hyaluronic acid (PGA/HA), [20] collagenII/hyaluronan/chondroitin-6-sulphate composites, [57][40] poly-lactic/glycolic acid PLGA, [11][58] HA, [59] poly-lactic acid (PLA).[60] (see Addendum A.I: Table 6)

1.4.2 Annulus fibrosus regeneration

Since the biomechanical properties of the IVD are the result of the combinatory properties of the NP and the AF, augmenting the NP as such will not result in satisfactory results for all degeneration types.[16] Furthermore, damage to the AF upon introduction of an artificial NP often results in an increase of AF degeneration which can induce NP depressurization.[5] In order to address these issues, research is also ongoing on TE of the AF.[5][16][36][54] (see Addendum A.I: Table 7)

One of the key issues in the development of suitable AF scaffolds is the simulation of the lamellar structure, as this provides the key mechanical properties to the AF. [16][37] In the absence of a well-organized scaffold architecture including the angular orientation of fibers relative to the spinal axis, the cells are unable to organize their ECM into the highly organized fiber network present in the AF, while the latter is essential to ensure sufficient mechanical properties.[61] Another obstacle related to AF engineering is the fact that the AF is poorly nutritioned and under continuous mechanical load, which decreases cell viability significantly. As a result, tremendous differences can arise between *in vitro* and *in vivo* studies.[61]

The applied materials to produce scaffolds are often fibrous in an attempt to mimic the network of collagen lamellae present in natural AF tissue.[5] The main difficulty is situated in obtaining a suitable fiber orientation which mimics the collagen fibers present in the natural AF.[37] The necessary fibers can be obtained from a variety of resources including synthetic and natural [13][37][62] (e.g. silk) followed by processing by for instance electrospinning. [36][61][63][64] In addition, some promising results have already been obtained using rapid manufacturing techniques to closely mimic the complex natural structure of the AF.[4][65] The application of rapid prototyping for scaffold production generates a highly powerful tool to produce patient-specific scaffolds with a very accurate structure compared to the native AF, while enabling the introduction of suitable biomechanical functions.[37] In addition, a superior porosity can be obtained over electrospun fibers which results in an improved nutrient flow towards the cells. [37] As a result, rapid prototyping is typically preferred over electrospun scaffolds.[31]

In order to develop AF scaffolds, a wide variety of materials is currently applied, as indicated in Addendum A.I: Table 7, including collagen,[66] silk,[13][37][62] poly-caprolactone (PCL),[61][63][67] poly-urethane (PU),[4][68] PU-Poly carbonate (PC),[64] alginate/chitosan,[69] fibrin,[70] and PLA[36][71].

Research has already shown the potential of introducing interesting features when performing tissue engineering of the AF. For example, the application of RGD sequences on silk fibers

resulted in a more inner AF-like cellular behavior. This thus might be considered as a tool to locally finetune the scaffolds to acquire superior native AF-mimicking properties.[62] Another feature includes the incorporation of growth factors such as TGF-β1 which results in an increase of GAG and collagen production.[36] In addition, anti-inflammatory drugs (e.g. berberine) can be applied to reduce inflammatory effects associated with the surgical implantation.[63] Alternatively, when the surface polarity of a scaffold is modified, the cell viability and collagen production can also be influenced.[64][71] Finally, research has already illustrated that the inter-lamellar ECM is of utmost importance to increase the tensile properties of the AF scaffold.[61] Several studies have also shown the potential of partial AF regeneration to restore local defects (e.g. the hole created through NP replacement) which significantly increases the success rate of NP regenerative procedures.[36][70] Ideally, hydrogels should be applied for this approach as they can be injected and cross-linked in situ. When a bio-interactive cross-linker is applied, the hydrogel can be sealed locally via a connection to the native tissue.[70]

1.4.3 Complete intervertebral disc regeneration

Most of the above-mentioned approaches aim at restoring a damaged IVD. However, in case the degeneration has already proceeded to a critical extent, a full replacement is required[5] by implanting a prosthetic device or by applying a tissue engineered construct. A tissue-engineered IVD possesses several benefits over conventional prostheses including:

- no wear debris formation upon repeated load cycles[30]
- tunable (long-term) mechanical properties which can improve as a function of time[72][73]
- absence of antigenicity and the ability to completely bio-integrate[59][74]

In addition, single tissue engineered parts of the IVD can cause issues related to a proper attachment of the NP to the AF and vice versa.[75] As a result, recently attention has also been paid to TE of complete IVDs.[76] To this end, a combination of different materials and specific arrangements is required in order to simulate the fibrous AF and the gelatinous NP.[5]

In order to combine the two IVD components, a variety of methods exists including molding [72][73][77][74][78], electrospinning followed by injection[59] or cutting and crosslinking[75]. Together with a wide variety of production methods, a broad series of materials can be applied to develop complete IVD-mimicking scaffolds. A non-exhaustive overview is provided in Addendum A.I: Table 8 and includes PCL+agarose,[72][76] gelatin+acellular cartilage, [79] Demineralized bonematrix gelatin (DBMG)/collagenII/hyaluronate/chondroitin-6-sulphate,[75]

silk/fibrin/HA,[77] collagen/alginate,[74][78][80] poly-glycolic acid (PGA)/alginate,[73] and PLA/HA [59][81].

Complete IVD regeneration has already faced some challenges, as often the ECM content inside the NP of complete IVD constructs was lower than in case of regeneration of only the NP. The latter phenomenon is anticipated to occur as a consequence of insufficient nutrient supply in larger *in vitro* and *in vivo* systems.[72]

To increase the scaffold bio-interactivity, research has already been performed by applying compounds which are generally present in the native tissue to serve as scaffold materials. Using this approach, the ECM of a native IVD can be closely mimicked thereby enhancing cell interaction and differentiation.[75]

To date, IVD tissue engineering has mainly been performed *in vitro*. However, the results of some *in vivo* studies were already promising, as it appeared that a poor nutrient supply and mechanical loading did not preclude cell viability and ECM production. Furthermore, promising results were also obtained with respect to bio-integration.[74][78] However, the surgical procedure applied is a main issue determining the success rate as it has already been observed that the implants in rats fail when the posterior longitudinal ligament is destroyed upon implantation of the construct.[74] To give an idea over future developments and perspectives a brief overview is provided in Addendum A.II.2.

1.5 Overview of applied materials

1.5.1 Hydrogel-based materials

Hydrogels are polymer networks which are able to absorb large amounts of water without dissolving.[82][83][84] A polymer network originates in the linkage of several polymer chains through cross-linking points (cfr. junction knots), preventing the material from dissolving in the presence of large amounts of water.

Hydrogels can be classified according to their crosslinking procedure as there exist several methods to generate hydrogels including chemical and physical strategies.[85] Two major hydrogel classes can thus be distinguished (i.e. physically cross-linked materials and chemically cross-linked hydrogels).

A wide range of hydrogel-based materials is currently under investigation for tissue engineering purposes.[82] First, natural polymers including chondroitin sulphate, hyaluronic acid, chitosan, cellulose, alginate, collagen, gelatin,[86][87] etc can be considered. Secondly, there also exist

hydrogels composed of synthetic polymers including pluronics,[88][89] PVA,[90] pHEMA,[85] PEG,[91][92], etc.

In the present work, gelatin will be selected as hydrogel because of its bio-interactive properties, being a derivative of collagen which is one of the major ECM components. [83][87][93][94][95][96] Furthermore, gelatin is cheap,[97] FDA approved[14] and bioresorbable as it can be enzymatically degraded in the presence of collagenase.[93][94] Gelatin owes its excellent bio-interactive properties among other to the presence of the peptide motif arginine-glycine-aspargine (RGD) in its backbone which can easily interact with the integrins of cells.[98][99]

In addition, gelatin is a natural, physically crosslinkable hydrogel characterized by an upper critical solution temperature (UCST). The UCST of gelatin typically lies around 37°C which is not optimal for tissue engineering purposes as it is very close to body temperature.[14] This issue can be circumvented by chemically crosslinking gelatin, which will be discussed in detail in section 1.5.1.3.

1.5.1.1 Physically cross-linked hydrogels

Physically cross-linked gels obtain their insoluble character from the presence of physical interactions between the different polymer chains. They are often referred to as reversible hydrogels as their crosslinking forces are a lot weaker than chemical bonds. In addition, they can often be reversed by varying one or several environmental factors including the ionic strength, the pH, the temperature, etc.[83][85] There exist three major physical crosslinking mechanisms: ionic crosslinking, temperature-induced crosslinking and crosslinking through crystallization.

a) Ionic crosslinking

Ionic crosslinking can crosslink polyanionic compounds by introducing polyvalent cations and vice versa. This approach can combine two chains with a univalent charge using a bivalent cation in a so-called egg box model. A typical example of such hydrogels is alginate of which its mannuronic and guluronic acid residues can be crosslinked in the presence of bivalent calcium cations.[85][100] (see Figure 2)
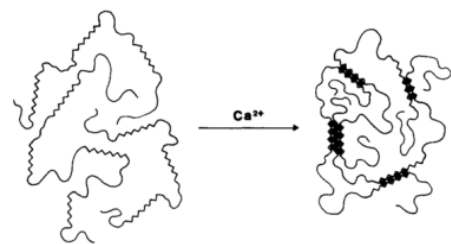
Figure 1: Ionic crosslinking of alginate by means of bivalent calcium ions

b) Crosslinking through crystallization
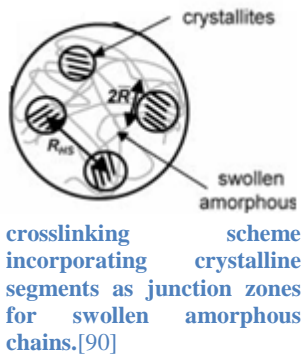
Crosslinking via crystallization results in a gel by the presence of parts of the polymer chains which crystallize together forming junction zones. The latter results in a partially crystalline hydrogel network, as observed for polyvinylalcohol (PVA).[85][90] (see Figure 3)

crosslinking scheme incorporating crystalline segments as junction zones for swollen amorphous chains.[90]

c) Temperature-induced crosslinking

Some materials show gelation properties upon temperature variations.[82] These properties are often the result of an arrangement of the polymer chains as a result of several van der Waals interactions including inter-chain hydrogen bonding.[82] Two material types can typically be distinguished including UCST materials (cfr. above this temperature they dissolve while below this temperature, they gelify) and lower critical solution temperature (LCST) hydrogels (cfr. hydrogels are formed above this critical temperature). Examples of such hydrogels are gelatin and pluronics which are characterized by a UCST and a LCST respectively.[83][89][101] [102]

1.5.1.2 Chemically crosslinked hydrogels

Chemically crosslinked materials are generated by introducing crosslinks using covalent bonds. Depending on the nature of the covalent bonds, chemically crosslinked hydrogels can be divided into two categories including irreversible and reversible crosslinked materials.

1.5.1.2.1 Irreversible crosslinking

Most of the chemically crosslinked hydrogels are permanent or irreversible hydrogels. These materials are obtained by introducing covalent bonds inside the network which join several polymer chains in order to obtain irreversible hydrogels. Several strategies exist in order to obtain a cross-linked network.

a) Cross-linking by radical polymerization

In this approach, several vinyl monomers are polymerized in the presence of a multifunctional cross-linker,[85] thereby generating a polymer network in one single step (e.g. poly(2-hydroxyethyl methacrylate, pHEMA). However, prior to application, the
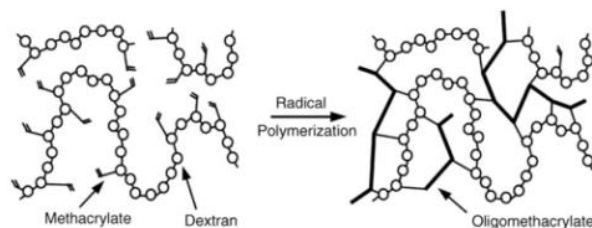
Figure 3: Crosslinking of methacrylated dextran through a radical polymerization.[85]

unreacted monomers need to be removed as these reactive compounds might possess adverse

biological effects.[83] Furthermore, this technique can be used to crosslink water-soluble polymer chains after derivatization with polymerizable groups[85] (e.g. dextran derivatized with glycidyl methacrylate).[103] (see Figure 4)

b) *Cross-linking by reaction of complementary groups*

A lot of water-soluble polymers are characterized by the presence of functional groups including -OH, -COOH and -NH$_2$. Interestingly, these functionalities can be applied to cross-link the polymer chains by reacting them with complementary reagents.[85] For example, amines can react quite easily with carboxylic acids using conventional carbodiimide coupling chemistry to generate e.g. gelatin hydrogels. [82][104]

c) *Cross-linking by high-energy irradiation*

High-energy irradiation can be applied to produce cross-linked hydrogels by irradiating a polymer solution containing vinyl functionalities. By the high-energy irradiation, radicals can be formed on the polymer chain by e.g hemolytic scission of C-H bonds. These radicals can initiate polymerization.[85]

d) *Enzymatic crosslinking*

Some enzymes can catalyze the covalent reaction between certain polymer chains. For example, the introduction of glutaminyl groups on PEG enables crosslinking by glutaminase in the presence of poly(lysine-co-phenylalanine).[85][105] This approach can be very interesting for the development of injectable, in situ crosslinkable hydrogels.[53]

1.5.1.2.1 Photoreversible crosslinking

A photo-reversible hydrogel can be obtained by introducing functional groups which can reversibly dimerize upon irradiation with different wavelengths.[106] (see Table 1) The obtained hydrogels combine the benefits of strong covalent interactions with the ease of reversible hydrogel manipulation observed for physically cross-linked materials.[34][107] In addition, these materials do not require the presence of potentially toxic photo-initiators to result in hydrogel formation.[34]

1.5.1.3 Crosslinking strategies for gelatin B

Gelatin can be crosslinked using various strategies. A frequently applied approach includes the introduction of crosslinkable (meth)acrylamide functionalities through the reaction of the primary amines of (hydroxy)lysine with (meth)acrylic anhydride. [82][86][87][108][109][110][111][112][113][114][115] The obtained gelatin derivatives can subsequently be polymerized using a redox-, a photo- or a thermal initiator upon applying the suitable trigger.

In addition, many research groups have already utilized glutaraldehyde as crosslinker [116][117][118] or conventional carbodiimide chemistry to couple the amines with 1-ethyl-3-(3-dimethyl aminopropyl) carbodiimide (EDC)-activated carboxylic acids (in the presence of N-hydroxysuccinimide, NHS). [82][119][120][121][122] Alternatively, the potential of enzyme-mediated crosslinking in the presence of transglutaminase and tyrosinase has already been studied to introduce covalent linkages in gelatin-based hydrogels.[123] However, the above-mentioned procedures typically result in irreversibly crosslinked networks. To date, only a limited number of research groups have already

Figure 4: : Overview of commonly applied crosslinking strategies for gelatin: Methacrylamide-functionalized gelatin obtained through the reaction with methacrylic anhydride (A), thiolated gelatin obtained through the reaction with N-acetyl-homocysteine thiolactone (B), thiolated gelatin obtained through the reaction with Traut's reagent(C) and crosslinking scheme for gelatin using EDC and NHS (D)[168]

assessed the feasibility of realizing reversible crosslinking. Generally, the network formation is then based on the electrostatic interactions occurring in the presence of oppositely charged polyions. For example, Farris et al. have combined positively charged gelatin and negatively charged pectin to develop reversible physical hydrogels.[124] In order to realize reversible covalent crosslinks, Van Vlierberghe et al have already introduced thiol moieties using Traut's reagent or N-acetyl-homocysteine thiolactone.[125] In the presence of an oxidant (e.g. oxygen or hydrogen peroxide), disulfide linkages can be introduced which can again be converted into thiols (cfr. covalent crosslinks are broken) when a reducing agent is added (e.g. dithiotreitol). Figure 5 depicts a non-exhaustive overview of the most commonly utilized gelatin derivatives and crosslinking schemes applied. For an exhaustive list of all crosslinking methodologies applied so far for gelatin, some excellent reviews can be consulted.[126][127] In the present work, the emphasis will be placed on methacrylation of the amine and carboxylic functionalities present in the gelatin backbone.

An interesting alternative to introduce reversible covalent crosslinks, is the application of photo-responsive moieties (as briefly discussed in section 1.5.1.2.1.) including anthracene, cinnamic acid, thymine, stilbene and coumarin as they are capable of undergoing photo-reversible dimerization upon applying a suitable UV-induced trigger. [128]

Generally, $[4\pi + 4\pi]$- or $[2\pi + 2\pi]$-cycloadditions occur depending on the applied moiety (see Table 1). In the present work, emphasis will be placed on $[2\pi + 2\pi]$-cycloaddition as coumarin

will be selected as proof-of-concept to develop photo-responsive gelatin. Dimerization occurs through the transfer of electrons from one molecule (i.e. the donor) to a second (i.e. the acceptor). The transfer typically occurs from the most energetic electrons in the donor (i.e. the electrons which are present in the highest occupied molecular orbital (HOMO)) to the lowest unoccupied molecular orbital (LUMO) of the acceptor. (see When light with a wavelength of above 350 nm is applied, an electron can transfer from the HOMO of the alkene in coumarin to the LUMO. The development of photo-responsive gelatin has already been scarcely reported as well. [129]
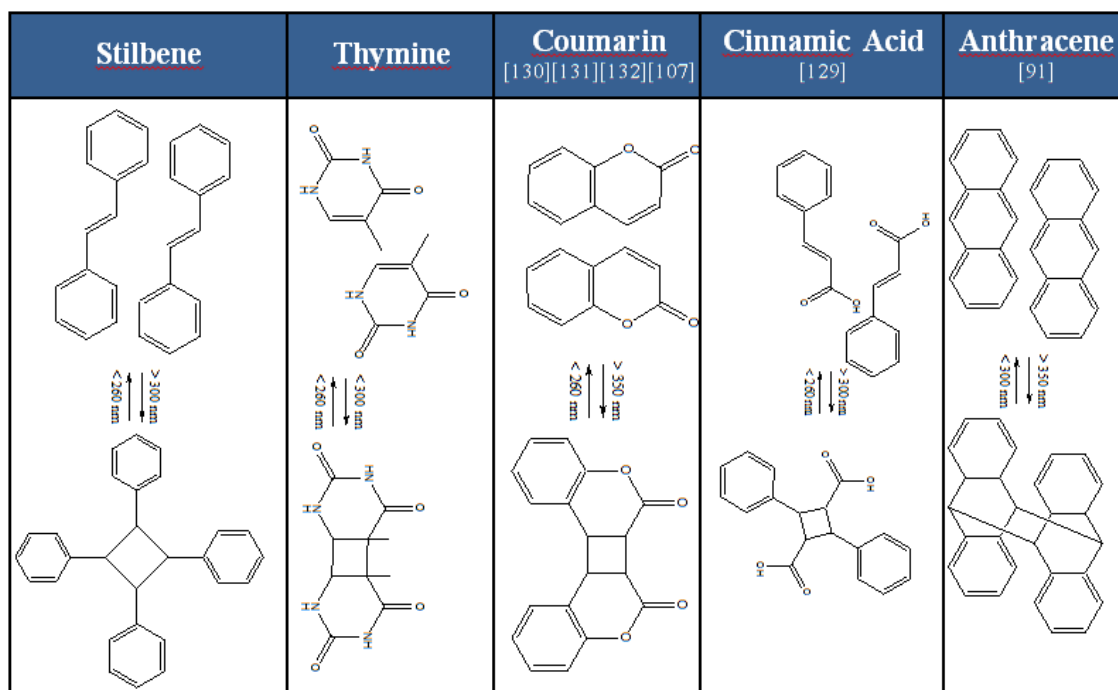
Table 1: Overview of compounds able to undergo Photo-reversible dimerization by application of a suitable UV-trigger.

1.5.1.4 Hydrogel applications

Hydrogels have many applications, yet the most ubiquitous one is the use of pHEMA for the development of soft contact lenses.[130] In addition to ocular applications, hydrogels can also be applied as drug delivery vehicles,[84] but the present study focusses on hydrogels for tissue engineering purposes.

Hydrogels possess several interesting characteristics rendering them suitable for regenerative medicine. Their mechanical properties closely resemble the mechanical behavior of certain tissues. Moreover, as they enable the transport of oxygen, salts, nutrients and metabolites, they can be considered ideal materials for cell cultivation. [15][19][131] In addition, hydrogels possess a very low dry polymer level implying that they will not disturb the patient's immune system to a great extent. [46][132] Hydrogels are also extremely versatile as they can be functionalized with bioactive compounds to mimic the ECM in order to increase the biocompatibility.[131] If in situ crosslinking is possible, they are concomitant with minimally invasive procedures including

injection to realize introduction in the body.[14][46] Finally, they also enable the incorporation of drugs to reduce negative body responses or growth factors to increase the cell proliferation.[14][15]

The tissue engineering applications of hydrogels are nearly limitless as a lot of research has already illustrated the versatility of hydrogel materials and, more specifically, gelatin. [82][96][108][110][133][134]

1.5.2 Polyester-based materials

Polyesters are interesting materials to be applied for tissue engineering applications as they possess degradable ester linkages incorporated in their backbone. Both bulk degradation and surface erosion can occur by hydrolytic chain scission of the ester bonds.[131][135][136] Polyesters consist of monomer units linked together through ester bonds. These chains can be formed through polycondensation between a carboxylic acid and an alcohol or ring opening polymerization of lactones or cyclic diesters. [136](see Figure 7)

1.5.2.1 Overview of polyester types

Several types of biodegradable polyesters exist and can be classified into two subcategories including linear or aliphatic polyesters and aromatic polyesters (see Figure 6).[137]

In the present master thesis, poly(lactic acid) (PLA) will be selected as it is a relatively cheap, renewable polyester with excellent biodegradability, biocompatibility and processing properties.[138][139] Furthermore the mechanical and degradation properties of
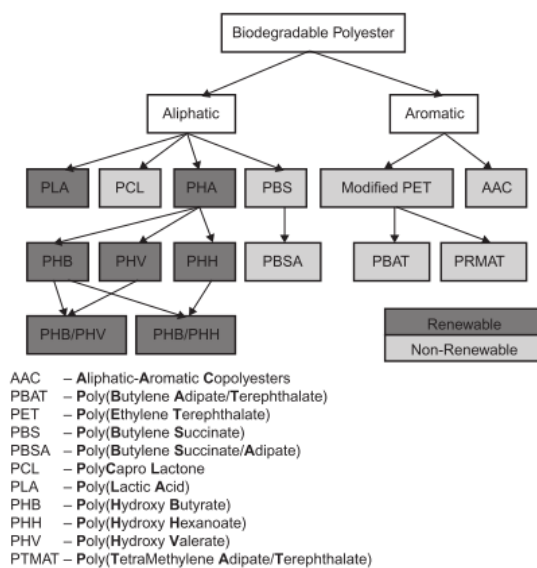
Figure 5: Overview of biodegradable polyesters.

the material can be tailored by variations in the processing conditions, influencing the crystal structure.[140] In addition, the PLA surface can be modified with functional groups through aminolysis to tune its biochemical properties in a straightforward manner.[138][141][142] Moreover, PLA has already proven its potential as scaffold material in the field of tissue engineering and IVD regeneration.[60][101][135][140][141][143][144]

Two general approaches exist for PLA synthesis including polycondensation of lactic acid and ring opening polymerization (ROP) of a cyclic lactide (see Figure 7). The selection of the

production method depends on the desired molecular weight and the obtained polymer properties.[137] Generally, low molecular weight compounds are obtained by polycondensation while high molecular weight polymers are yielded through ROP.[137]

Three PLA types can be distinguished including PLLA (cfr. composed of L-lactic acid units), PDLA (cfr. composed of D-lactic acid) and PDLLA (cfr. consisting of a mixture of L- and D-lactic acid units). The majority of PLA occurs in the L-form as this stereoisomer of lactic acid is more commonly produced in bacterial systems while it is the only stereoisomer which can be synthesized by mammals.[137] The stereochemical aspect has a large impact on the melting point, the crystallization rate and properties and the mechanical properties. PLLA and PDLA are semi-crystalline polymers with a crystallinity of about 70%, a glass transition temperature of around 50-60°C and a melting temperature of 180°C. As a consequence of its high crystallinity, it shows a lower degradation rate in contrast to PDLLA, which is an amorphous polymer. Interestingly, blending of PLLA and PDLA leads to an increase of the melting temperature up to 230°C.[137]

1.5.2.2 Overview of polyester applications

PLA is a commonly applied material with applications in the biomedical and the pharmaceutical field due to its excellent biocompatibility and biodegradability. Furthermore, PLA is used widely in domestic applications including garments, food packaging, bottles, cups and transaction cards, etc.[137][145] Furthermore, as increasing attention is currently paid to a sustainable environment and the renewability of materials, the share of PLA in everyday life applications is anticipated to further grow.

1.6 Scaffold development

Scaffolds are interesting tools to create functional implants starting from stem cells grown in culture as an alternative to transplantation of entire organs.[132] They can be constructed starting from a range of materials including natural, synthetic and semi-synthetic polymers.[94]

When a suitable scaffold is produced, living cells can be seeded followed by cell proliferation and differentiation. After successful proliferation, the seeded scaffold is introduced in the human body to replace the tissue defect thereby facilitating the construction of new tissue.[132]

Typically, scaffolds have to perform several functions in tissue engineering. First, they should act as a guide for cell growth showing a suitable macrostructure. Simultaneously, they should mimic the natural cell environment and possess suitable surface properties. [33][34][93][94][146] Secondly, they have to maintain sufficient mechanical support while the biodegradable scaffold is gradually replaced by newly formed tissue.[34][93][94][132] Scaffolds therefore need to be biocompatible, biointeractive, three-dimensional and very porous with interconnective pores allowing a continuous flow of nutrients and waste products throughout the scaffold. [134][147] In addition, they should possess a high surface to volume ratio and show controllable degradation rates leading to non-toxic degradation products.[34] They should also show a defined mechanical strength[35] comparable to the surrounding tissue.[32][99][132][148][149] In order to generate structures with the above-mentioned properties, several techniques exist with their specific benefits and drawbacks. Ideally, a combination of different technologies might offer the best alternative.[93][150][151]

1.6.1 Solid Freeform Fabrication

Solid freeform fabrication (SFF) is the general term covering all techniques that enable the production of objects through the sequential delivery of energy and/or materials.[146] However, several other terms are also commonly applied in the field of SFF including 3D printing and rapid prototyping (RP). Allthough the term 3D printing is often used to refer to al SFF techniques, strictly speaking 3D printing actually involves the use of a binder on a powdered material, while the term RP originates from the first solid freeform fabrication techniques which generated prototypes during product development.[34][146][101] Since no material is lost during the process and no (toxic) solvents are required for the production of structures, it can be considered as a fast, a clean, a cost-effective and a material-efficient technique. As a result, it is also applicable when small material quantities are available in early stages of research.[34][101][152]

SFF has grown into a very hot topic over the last years,[65] in part because of the expiration of an important patent on fused deposition modeling (FDM) in 2009.[153] The latter was the starting point for a boom in the development of SFF devices, resulting both in the optimization of the technology as well as a decrease in the price. [34][101][154][155] Because of the increased accessibility of RP, the range of applicable materials which can be processed has also expanded significantly.

SFF techniques show some interesting advantages in contrast to conventional methodologies applied for scaffold fabrication including soft particle leaching, electrospinning, supercritical CO_2 treatment, gas foaming, etc. [101][131][148][149][156][157][158] For the latter approaches, the

18

scaffold architecture is mainly process-determined rather than design-driven while the pore interconnectivity is often insufficient.[147] A true benefit of SFF over these conventional technologies is its ease to generate whatever macro-form showing a controlled interconnective porous microstructure.[4][93][94][95][101][134][135][149][150][159] This interconnectivity is essential as it enables the transport of nutrients and metabolites throughout the scaffold, resulting in a more uniform cell distribution and increased proliferation.[32][147]

The large architectural freedom of this technology renders it promising for the development of patient-specific tissue engineering scaffolds.[131][152] Starting from a 3D computer aided design (CAD) which can be obtained through non-invasive procedures including computed tomography (CT) or nuclear magnetic resonance imaging (MRI), exact architectural replicas of the tissue defect with a well-defined microstructure can be generated.   [4][34][131][147][152][158] [159][160][161][162] When a 3D design is obtained, it can be processed by software which slices the model mathematically into

Figure 7: General engineering strategy using rapid prototyping techniques (left).[132]

horizontal layers to be deposited in a layer-by-layer fashion by the SFF device.[34][132][146] (see Figure 8)

SFF can also be used for tuning the mechanical properties of the produced scaffolds by varying the geometrical inner structure.[147][150] Since this technique can replicate very specific designs, it enables the fabrication of 3D scaffolds showing a varying multiple layer design which results in regions with varying mechanical properties within the same scaffold. This characteristic can be important when considering spinal repair,[150][161] especially when mimicking the complex AF structure in which the angular alignment of the collagen fibers gradually changes from the edges towards the center.[2][4]

Two general approaches for scaffold development exist including direct and indirect RP. Direct RP scaffolds are directly produced from a biomaterial and can be surface modified with bio-active compounds to render them more biocompatible.[146] Indirect RP is a method to generate a scaffold using a mold which is produced with rapid prototyping techniques.[101][131][160]

SFF techniques can be divided in three subcategories including laser-based, nozzle-based and printer-based systems.[101] Laser-based systems apply photo-polymerization to introduce

19

crosslinks in the polymer materials or to generate polymer chains in a monomer solution.[159][163] Nozzle-based systems apply extrusion/dispension of (pre)polymers, while the printer-based class employs a powder bed and deposits a binder that fuses the particles. In the present work, the applied SFF techniques will be Fused Deposition Modelling (FDM)[153] (i.e. a nozzle-based system)(discussed in depth in section 2.3) and two-photon-polymerization (2PP) (i.e. a laser-based system)(discussed in depth in Addendum A.II.4[93][131]

1.6.2 Cryogel formation: An introduction

An alternative methodology to develop porous scaffolds is the application of a cryogenic treatment to create cryogels. They can be formed starting from a monomer or a crosslinkable polymer solution with the capability to gelify during a single step process at sub-zero temperatures just below the solvent crystallization point. At this temperature, a moderately frozen solution is obtained.[95][164][115] As a result, most of the solvent is frozen with the exclusion of areas where some unfrozen solvent remains present (i.e. the non-frozen liquid microphase, NFMLP). In these NFLMPs, an increase in the concentration of the crosslinkable precursors is created (cfr. cryoconcentration) while the potential with respect to chemical or physical crosslinking remains present.[82][115] Only in these NFLMPs, the material crosslinking will occur, leading to gel formation while the frozen solvent crystals act as porogens.[95][99] Upon thawing of these frozen solvent crystals, a porous interconnective network is retained showing a high polymer gel concentration in the pore walls which leads to the significant mechanical strength observed in cryogels. This process is schematically demonstrated in Figure 9. [35][97][99]

The pore interconnectivity occurs because the ice crystals of the solvent grow until they find another solvent crystal, thereby creating channels inside the crosslinked material.[95] By varying certain parameters such as the freezing temperature or the polymer concentration prior to freezing, the pore size of the obtained scaffold can be fine-tuned resulting in a size ranging from a few to hundreds of micrometers.[35][95][97][99][164]

Cryogels are promising scaffold materials because of the straightforward processing technique, the presence of interconnective pores, [98][164] their controllable degradation rate upon selecting an appropriate material, the absence of additional (toxic) organic solvents required for processing[99] and their high mechanical strength while showing a great elasticity.[35][97][99] Due to their mechanical properties, cryogels can be a promising tool in the formation of the soft NP upon tissue engineering the IVDs.[2]

There also exist some drawbacks when using cryogels. Since the architecture is process- driven rather than design-driven, a lot of time and effort needs to be invested in optimizing the different parameters including the polymer concentration, the freezing temperature and duration (cfr. to generate moderately freezing conditions to prevent complete freezing of the solution), the concentration of the crosslinker and the initiator, the number of freezing cycles applied (to increase the mechanical properties by secondary crystal formation), etc.[35][82]
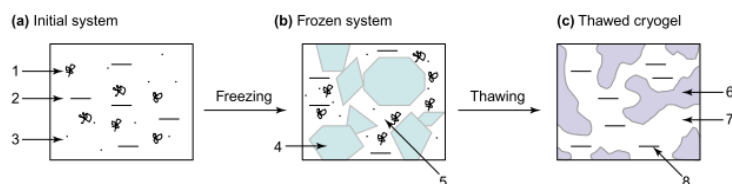
Figure 9: Principle of cryogel formation; 1. macromolecules in a solution, 2. solvent, 3. low-molecular solutes, 4. polycrystals of frozen solvent, 5. unfrozen liquid microphase, 6. polymeric framework of a cryogel, 7. macropores, 8. Solvent.[164]

1.7 Master thesis objectives

The aim of the present work includes the derivatization of gelatin in order to optimize the hydrogel properties towards tissue engineering applications, more specifically, for spinal repair. First, crosslinkable functionalities (i.e. methacrylamides, methacrylates and coumarin derivatives) will be incorporated into gelatin to enable photopolymerization in the presence of a suitable photo-initiator upon applying UV irradiation. To this end, two strategies will be elaborated and evaluated. In a first approach, coumarin functionalities will be introduced on the gelatin backbone. Interestingly, because of the photo-reactive dimerization potential of coumarin, the formation of a reversible hydrogel network can be accomplished. In parallel, both methacrylate as well as methacrylamide functionalities will be introduced on gelatin by reacting the amines and the carboxylic acid moieties present with methacrylic anhydride and amino-ethyl methacrylate respectively. These activated double bonds can subsequently be linked through photo-polymerization by applying UV-irradiation in the presence of a suitable photo-initiator, thereby resulting in a hydrogel network. Moreover, the mechanical properties of the obtained hydrogel will be tuned by varying the amount of cross-linkable functionalities present. The obtained hydrogels will then be characterized using HR-MAS ^{1}H-NMR spectroscopy,[111] swelling tests and rheology. As a result the developed hydrogel can then become a suitable candidate for NP regeneration.

In addition, a combination of the photo-crosslinkable hydrogel precursor with 3D printed PLA scaffolds will be evaluated. The combination of both techiques could lead to materials exhibiting the correct mechanical properties for AF repair, combined with the excellent cell-interactivity

exhibited by the gelatin material. To this purpose, two approached will be assessed. In a first approach, the developed methacrylamide functionalized gelatin derivatives developed will be introduced into 3D printed PLA scaffolds followed by inducing porosity using a cryogenic treatment or 2PP in order to develop porous, AF-mimicking scaffolds for spinal tissue engineering. The scaffolds developed will be characterized in depth using, among other, optical microscopy, micro-computed tomography, scanning electron microscopy and compression tests to enable the assessment of, among other, the porosity, the microstructure and the mechanical properties.

Secondly, the potential of performing photo-crosslinking of a hydrogel precursor in the presence of cells will be assessed as a proof of concept for two photon polymerization (2PP) (see Addendum A.II.4) to obtain well defined microstructures. To characterize this methodology, several tests(Presto Blue staining, ALP staining, Live/dead staining, gene expression tests) will be performed to obtain an insight of the effect of applying a UV treatment to a seeded hydrogel.

2. Results and Discussion

2.1 Synthesis and Characterization of Gelatin Derivatives as Hydrogel Building Blocks.

In the present work, gelatin was selected as one of the starting materials because of its biocompatibility and its cell-interactive properties which can be attributed to the presence of Arg-Gly-Asp (RGD) motifs in the gelatin backbone[165]. Gelatin is a biopolymer derived from collagen as discussed in section 1.5.1. It is composed of a wide variety of amino acids which are linked through amide linkages,[166] resulting in a linear backbone with several functionalities present in the side chains. An overview of the amino acid composition of the gelatin applied in the present work is presented in Table 2.

Amino Acid composition	Gelatin B Bovine hides (g/100g)
Aspartate	5,01 ± 0,14
Glutamate	9,2 ± 0,20
Serine	2,76 ± 0,05
Histidine	0,61 ± 0,01
Glycine	22,12 ± 0,59
Threonine	2,18 ± 0,05
Arginine	6,74 ± 0,14
Alanine	8,76 ± 0,18
Tyrosine	0,21 ± 0,01
Valine	2,63 ± 0,08
Methionine	0,86 ± 0,02
Hydroxylysine	1,26 ± 0,03
Phenylalanine	1,76 ± 0,04
Isoleucine	1,68 ± 0,04
Ornithine	0,97 ± 0,04
Leucine	3,24 ± 0,07
Lysine	3,49 ± 0,08
Proline	14,35 ± 0,40

Table 2: Amino acid composition of the gelatin type applied in the present work.[167]

2.1.1 Development and Characterization of Methacrylamide-modified Gelatin (Gel-MOD)

The methacrylation of gelatin B was accomplished by the reaction of the primary amines present in gelatin B with methacrylic anhydride. The reaction resulted in the introduction of crosslinkable methacrylamide functionalities.

Gelatin type B contains several amino acids with pendant free amines including (hydroxy)lysine, histidine, arginine and ornithine. At a pH of 7.3, the guanidium group of arginine is protonated, rendering this amine inactive towards a nucleophilic attack. In addition, although the imidazole group of histidine is prone to reaction, unstable products will be formed. As a result, only the

primary amines of (hydroxy)lysine and ornithine are partially deprotonated, rendering them suitable to enable reaction.[168] As the reaction continues and deprotonated amines are modified, the acid-base equilibrium ensures a continuous generation of deprotonated amines able to react with methacrylic anhydride. Using the amino acid composition presented in Table 2 to determine the amount of reactive amines, a total of 0.0385 mol amines are present in 100 g gelatin B.[168][169]
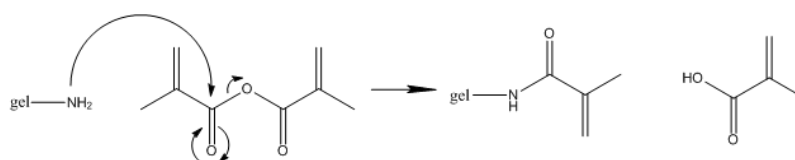
Figure 10: Scheme illustrating the methacrylation of gelatin B.

Gelatin B was dissolved in PBS buffer (pH 7.3) at 40°C under vigorous mechanical stirring. After complete dissolution, 2.5 equivalents of methacrylic anhydride were added relative to the amount of free amines present in the gelatin solution. After 1 hour, the gel-MOD was purified through dialysis against Milli-Ro water (Molecular weight cut off (MWCO): 12000-14000) at 40°C and isolated by lyophilization.

The degree of substitution (DS) was determined by ^{1}H-NMR spectroscopy using D_2O as solvent at an elevated temperature (40°C) to prevent gelation through the formation of triple helices. An example of a ^{1}H-NMR spectrum of gelatin B which was reacted with 2.5 equivalents methacrylic anhydride is shown in Figure 11.
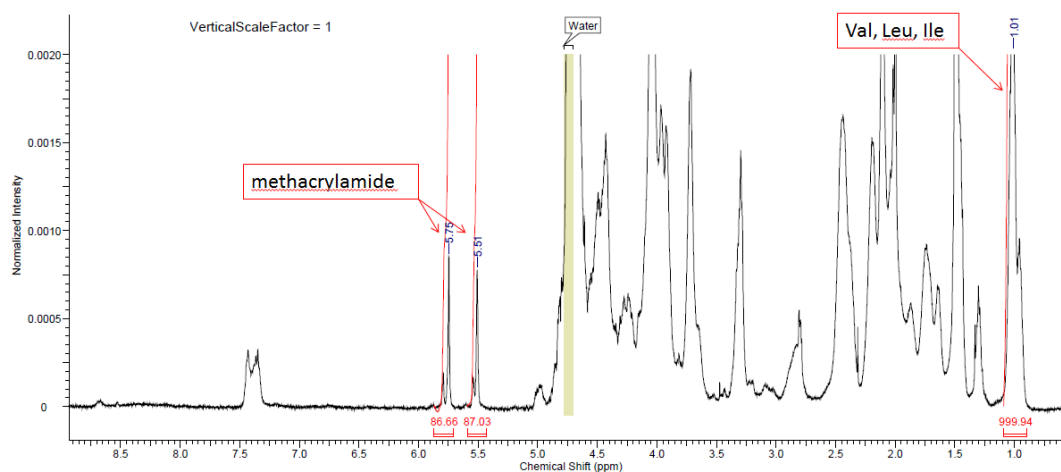
Figure 11: ^{1}H-NMR spectrum of Gel-MOD through the reaction with 2.5 equivalents methacrylic anhydride.

As gelatin consists of more than 20 different amino acids (see Table 2), a complex ^{1}H-NMR spectrum is typically obtained, yet, a complete elucidation of the spectrum was beyond the scope of the present work. The current study only aims at the quantification of the DS by examining the

characteristic peaks present in the spectrum as a consequence of the reaction. The reference peak selected is present at 1.12 ppm, which corresponds to the resonance of the valine (Val), the leucine (Leu) and the isoleucine (Ile) side chains (see Figure 12). These hydrophobic alkyl side chains can be considered chemically inert and can therefore serve as a suitable reference signal.
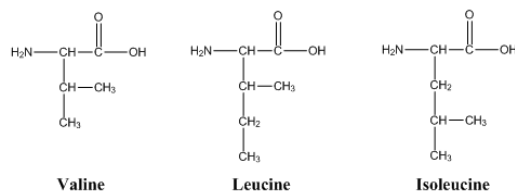
Figure 12: Amino acids present in gelatin B which are applied as NMR reference signal.

The reference peak corresponds with 18 protons and 0.3836 mol/100g gelatin which can be calculated using Table 2. By comparing the integration of the signal corresponding to the characteristic methacrylamide peaks with the integration of the reference signal and taking into account the total amount of primary amines available for reaction (i.e. 0.0385 mol/100g) the DS can be calculated as indicated in equation (1).

$$DS_{Amines}(\%) = \left[\frac{\frac{\left(\frac{(I_{5.51ppm}+I_{5.75ppm})}{2}\right)}{0.0385\frac{mol}{100g}}}{\left(\frac{I_{1.01ppm}}{0.3836\,mol/100g}\right)} \right] * 100 \qquad (1)$$

2.1.2 Development and Characterization of Methacrylate-modified Gel-MOD (Gel-MOD-AEMA)

In order to further increase the mechanical properties of crosslinked gel-MOD hydrogels, additional crosslinkable functionalities were also incorporated on gel-MOD. The latter was achieved by introducing additional methacrylate functionalities onto the carboxylic acids present in aspartate and glutamate present in gelatin B (see Figure 13). The overall amount of carboxylic acids prone to reaction can be calculated from the amino-acid composition of gelatin B (Table 2, cfr. 100 g gelatin B contains 0.1098 mol carboxylic acids). The coupling reaction was executed through a condensation reaction of the amines of amino-ethyl methacrylate (AEMA) and the carboxylic acids present in gelatin via their activation using N,N-(3-dimethylaminopropyl)-N-ethyl carbodiimide (EDC).[85] As EDC is often used as a zero-length crosslinker for several biopolymers containing amines and carboxylic acids, the DS of the starting material (i.e. gel-MOD) was required to be sufficiently high to prevent crosslinking of the residual unreacted amines after addition of EDC. [85][119][120][121][122][168][170]
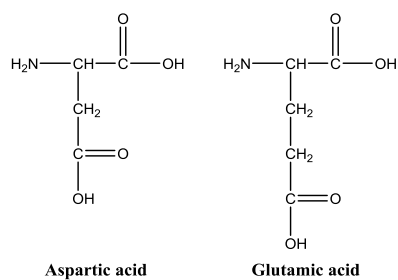
Figure 13: Amino-acids present in gelatin B containing carboxylic acids in their side chain.

Gel-MOD was dissolved in degassed DMSO under inert atmosphere at 50°C under continuous stirring. To activate and stabilize the carboxillic acids 1 equivalent of EDC and 1.5 equivalents of NHS were added. After one hour of reaction time, 2 equivalents of AEMA and 0.01 equivalents of inhibitor (4-ter-butyl catechol) were added to prevent spontaneous crossslinking of the incorporated methacrylate functionalities. After overnight reaction the gel-MOD-AEMA was purified through via dialysis against Milli-Ro (MWCO: 12000-14000 Da) at 40°C and isolated by lyopilization.
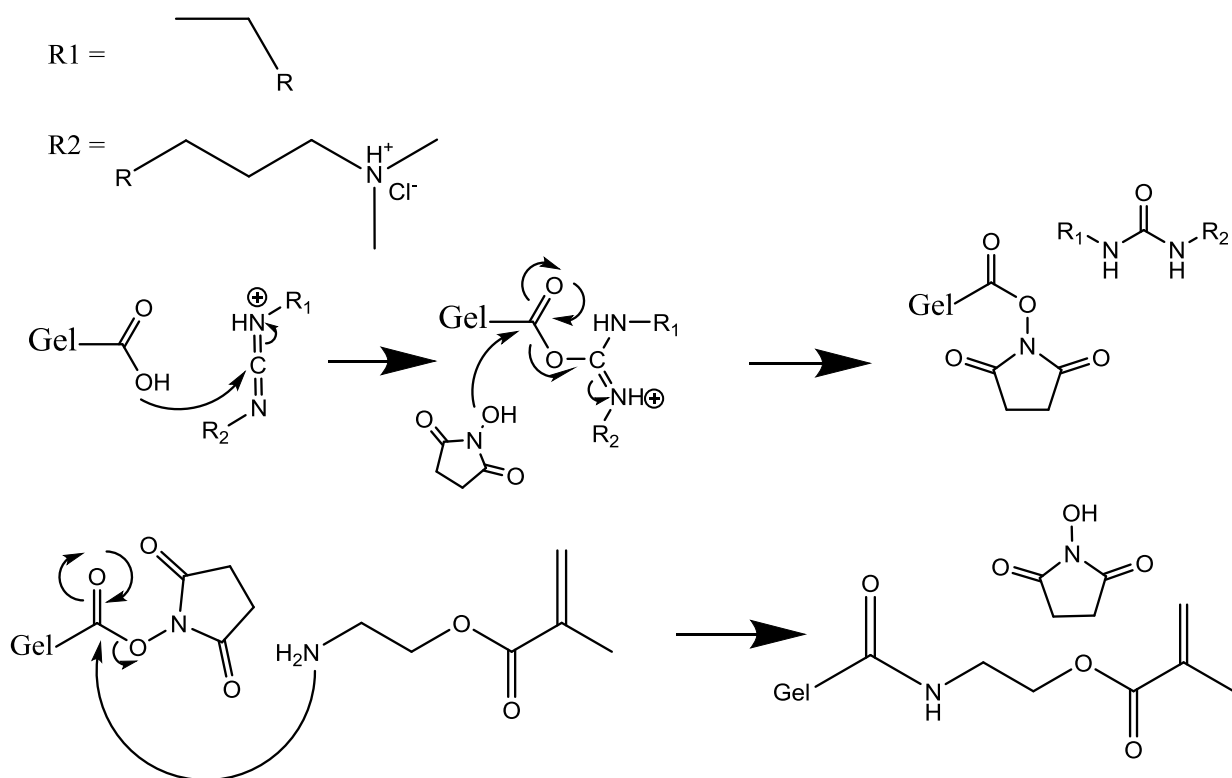
Figure 14: Reaction scheme of gel-MOD-AEMA in DMSO.

The DS was quantified using ^{1}H-NMR spectroscopy at an elevated temperature (40°C) using D_2O as solvent. An example of a ^{1}H-NMR spectrum of Gel-MOD-AEMA using 2 equivalents AEMA is shown in Figure 15.
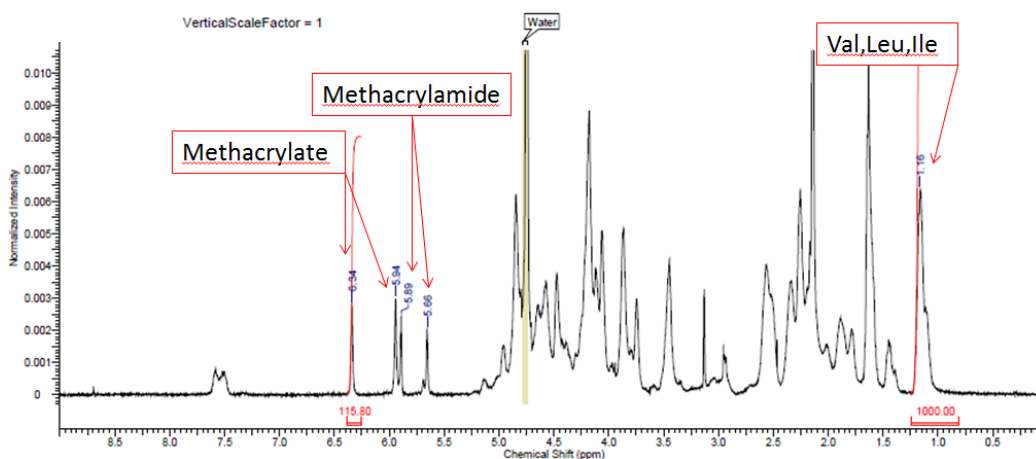
Figure 15: ^{1}H-NMR spectrum of Gel-MOD-AEMA after reaction with 2 equivalents AEMA.

In the ^{1}H-NMR spectrum, the presence of two additional characteristic peaks can be observed compared to the spectrum of gel-MOD. These peaks can be attributed to the methacrylate functionalities introduced in gel-MOD through the reaction with AEMA. As there is a slight overlap between the signal at 5.94 ppm of the methacrylate with one of the methacrylamide signals, only the peak at 6.34 ppm was taken into account for the quantification of the DS.

Comparing the integration of the characteristic methacrylate signal with the integration of the reference signal of Val, Leu, Ile (see section 2.1.1) yields the DS of the carboxylic acids when the total amount of carboxylic acids present in the gelatin is taken into account (i.e. 0.1098 mol/100g).

$$DS_{Carboxyllic\ acids}(\%) = \left[\frac{\frac{I_{6.34ppm}}{0.1098\frac{mol}{100g}}}{\left(\frac{I_{1.12ppm}}{0.3836\ mol/100g}\right)} \right] * 100\ \% \tag{2}$$

2.1.3 Development and Characterization of Photo-Reversible Gelatin (Gel-Coumarin)

2.1.3.1 Synthesis of epoxide-modified 7-hydroxycoumarin

A first step required to enable the functionalization of gelatin with coumarin is the derivatization of the hydroxyl functionality of 7-hydroxycoumarin into an epoxide to enable a nucleophilic attack of the deprotonated amines present in gelatin (cfr. S_N2 reaction). The functionalization was performed through a nucleophilic substitution using epichlorohydrin in alkaline conditions.

27
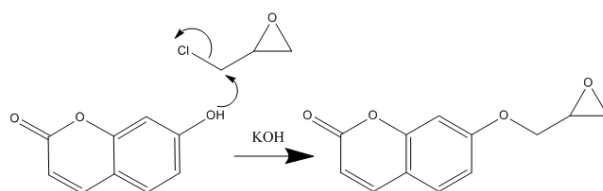
7-Hydroxycoumarin was first dissolved in ethanol. Next, an aqueous solution of KOH was added after which the mixture was stirred at room temperature. After 30 minutes, epichlorohydrin was added and the temperature was increased to 100°C followed by stirring for 2.5 hours while refluxing. Subsequently, the solvent was evaporated in a rotary evaporator at 40°C under reduced pressure. The dry residue was purified through extraction with chloroform which was subsequently evaporated in a rotary evaporator under reduced pressure. A final purification step was performed by means of recrystallization in warm ethanol followed by filtration.[171][172]

2.1.3.2 Functionalization of gelatin B with 7-epoxypropoxycoumarin

The coupling of 7-epoxypropoxycoumarin to gelatin B was performed through an S_N2 type reaction using the deprotonated amines present in gelatin as nucleophile (see section 2.1.1) to induce an epoxide ring opening reaction. The reaction was performed in dimethylsulfoxide (DMSO) as 7-epoxypropoxycoumarin is too hydrophobic to dissolve in an aqueous solution.
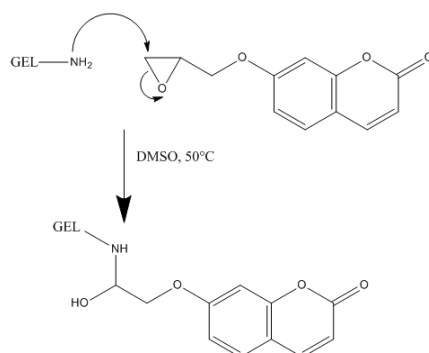
The DS was quantified using ^{1}H-NMR spectroscopy using d-DMSO as solvent at an elevated temperature (i.e. 50°C). An example of a ^{1}H-NMR spectrum of gel-coumarin compared with the spectrum of gelatin B is shown in Figure 18.
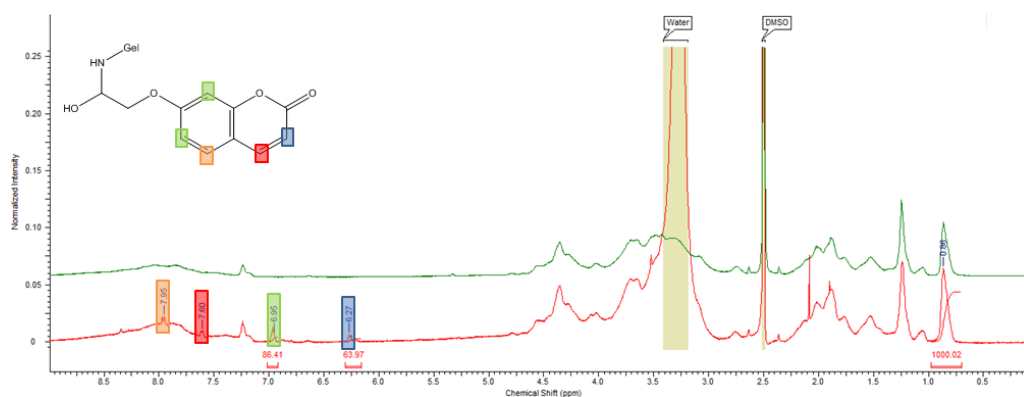
Figure 18: ^{1}H-NMR spectrum of gel-coumarin (red) versus gelatin B (green).

The aromatic peaks of the coumarin functionalities can be distinguished at 6.25, 6.96 ppm, 7.60 and 7.95 ppm. The quantification was performed by comparing the integration of the Val, Leu, Ile reference peak at 0.86 ppm (see section 2.1.1), which corresponds to 18 protons, with the integration of the characteristic coumarin peak at 6.96 ppm which corresponds to 2 protons. Again, the total amount of free amines (0.0385 mol/100g) was taken into account to enable the determination of the DS. The other peaks were not taken into account for quantification purposes as the peaks around 7.60 and 7.95 ppm overlap with the signal of the aromatic side chains of Tyrosine and Phenylalanine present in the gelatin B backbone.

$$DS_{Amines}(\%) = \left[\frac{\frac{(I_{6.96ppm})}{2}}{0.0385\frac{mol}{100g}} \middle/ \left(\frac{I_{0.86ppm}}{0.3836\ mol/100g} \right) \right] * 100 \tag{3}$$

A maximum DS of 45% was obtained.

2.1.4 Characterization of the physical gelation behavior of the gelatin hydrogel precursors

Depending on the functionalization of gelatin, a difference in physical gelation properties can potentially occur as the moieties introduced can hamper the formation of triple helices.[125] Several aspects can play a role in this process including the molecular weight, the hydrophilicity/hydrophobicity and the substitution degree of the incorporated functionalities. In contrast with unmodified gelatin and gel-MOD, the gel-MOD-AEMA derivative developed was soluble at room temperature. Previously, the same phenomenon has already been observed for gel-MOD-DOPA. For that derivative, the carboxylic acids of gelatin were functionalized with dopamine, whereas for gel-MOD-AEMA amino-ethylmethacrylate was introduced.[170] Both for gel-MOD-DOPA as well as for gel-MOD-AEMA, the amines and the carboxylic acids present in gelatin have been consumed during the modification. As a result, it was anticipated that this

29

modification could potentially inhibit the formation of triple helices to a certain extent. To further investigate this phenomenon, differential scanning calorimetry (DSC) was performed on several gelatin derivatives developed via a protocol described by Prado et al.[173]

DSC is a characterization method which enables to determine phase transitions inside a material (e.g. glass transition temperature (T_g) and melting temperature (T_m)). In this method, the required heat applied to a sample is quantified relative to the heat applied to a reference sample for a certain change in the temperature at a predetermined rate. When a material undergoes a certain phase transition, it requires additional or less energy compared to the reference sample. By plotting these differences in applied heat (cfr. the enthalpy) versus the temperature, a thermogram is obtained in which the phase transitions are visualized as peaks or shifts in the base line which represents the heat capacity (C_v).
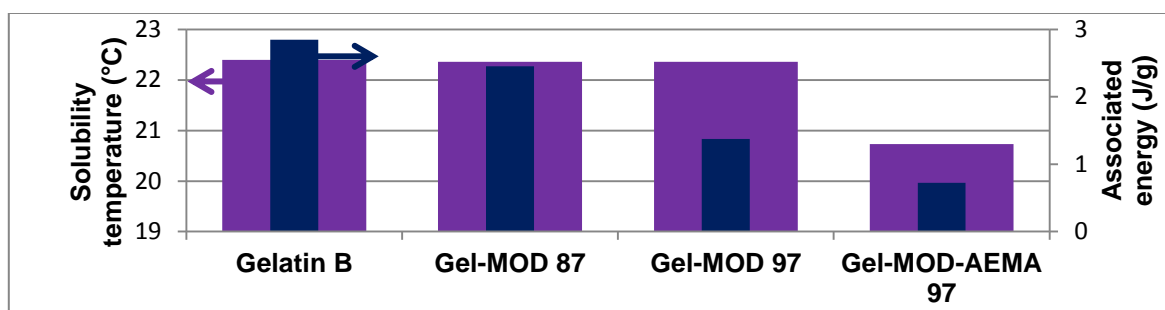
Figure 19: Plot depicting the UCST and the associated heat exchange for gelatin B, gel-MOD 87 (DS$_{amines}$ 87%), gel-MOD 97 (DS$_{amines}$ 97%) and gel-MOD-AEMA (DS$_{amines}$ 97%; DS$_{carboxylic\ acids}$ 41%).

In the present study, the difference in applied heat to the gelatin solutions (10 w/v%) was monitored using miliQ water as a reference (see Addendum D.I for thermograms). Figure 19 depicts the influence of the modification on the heat exchange and the UCST of the material. Interestingly, the modification of the amines of gelatin does not influence the UCST, yet, it will inhibit the formation of triple helices to some extent as reflected by the smaller difference in heat capacity upon dissolution. Furthermore, this effect is more pronounced upon increasing the degree of modification of the primary amines. For gel-MOD-AEMA, a weak transition could still be observed despite the room temperature solubilizing behavior. However, this transition takes place at a lower temperature while the energy associated with this transition is drastically decreased. These results further support the postulated idea that the modification of both the amines as well as the carboxylic acids will partially inhibit the formation of triple helices.

2.2 Development and characterization of UV-crosslinked gelatin hydrogel films

As briefly discussed in section 1.5.1, gelatin B is a material which is characterized by UCST behavior. As the UCST (i.e. 22°C see section 2.1.4) is not ideal for tissue engineering applications because of hydrogel solubilization upon *in vivo* application, the introduction of crosslinkable methacrylate and methacrylamide functionalities is essential. In the present work, crosslinking was performed by applying UV-irradiation in the presence of a suitable photo-initiator. A photo-initiator is a light-sensitive compound which can absorb energy from UV-VIS irradiation to transfer to an excited singlet state. When returning to the ground state, the absorbed energy is dissipated through the fracture of a chemical bond, resulting in radical formation. These radicals can then react with the double bonds present in functionalized gelatin to induce polymerization which results in the formation of a hydrogel network.

In the present work, Irgacure 2959 (i.e. 2-hydroxy-1-[4-(hydroxyethoxy)phenyl]-2-methyl-1-propanone) was selected as photo-initiator because of its proven cytocompatability.[174][86] Irgacure 2959 is a Norrish type I indicator which implies that it will undergo a photochemical α-cleavage upon relaxation resulting in the formation of two radical compounds including a benzoylradical and a hydroxylalkylradical (see Figure 20).
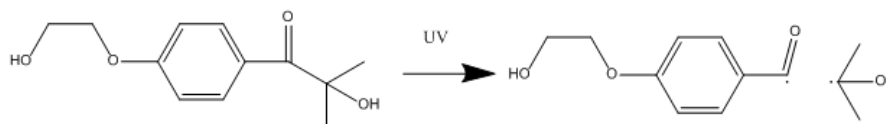
Figure 20: Scheme demonstrating the photocleavage of Irgacure 2959 upon applying UV irradiation.

To enable the characterization of the different gelatin derivatives, a crosslinked hydrogel film was produced via a film casting approach. In this method, a hydrogel solution containing the photo-initiator is injected between two glass plates separated by a silicone spacer. When the mold is sufficiently filled, it is stored at 6°C to induce physical gelation followed by photocuring by applying UV-A irradiation for 30 minutes (see Figure 21).
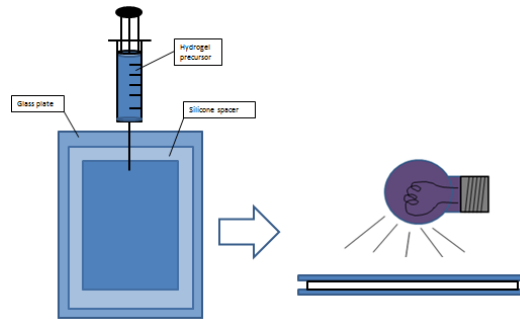
Figure 21: Scheme demonstrating the film casting and crosslinking principle.

Using this method, four different hydrogel films were prepared with a thickness of 0.5 mm (see Table 3). The various derivatives were generated via the strategies described in sections 2.1.1 and 2.1.2 with the exception of gel-MOD (DS 97%) and gel-MOD-AEMA (DS 97%) which underwent two subsequent methacrylation cycles to yield a higher DS (i.e. 97%).

Sample type	DS (NH$_2$)	DS (COOH)
gel-MOD 82	82 %	-
gel-MOD 97	97 %	-
gel-MOD-AEMA 87	87 %	30 %
gel-MOD-AEMA 97	97 %	27 %

Table 3: Overview of the different hydrogel films developed.

2.2.3 Determination of the gel fraction of the crosslinked hydrogel films

The gel fraction of a hydrogel material represents the insoluble weight fraction of a dried hydrogel. It provides an indication of the crosslink efficiency as the unreacted chains will remain soluble at 37°C and will thus leach out of the sample during incubation above the UCST. In order to evaluate the gel fraction, the mass of a freeze-dried film was determined followed by an overnight incubation in distilled water at 37°C. After the incubation period, the gel was freeze-dried again prior to determination of its dry mass. The masses obtained prior to and after incubation were subsequently compared to determine the gel fraction using the following formula:

$$gel\ fraction\ (\%) = \frac{w_{d,after\ incubation}}{w_{d,before\ incubation}} * 100\% \tag{4}$$

$$w_d = dry\ weight$$

Figure 22 shows an overview of the gel fractions obtained for the different hydrogel films after 30 minutes UV-A irradiation. Generally, a relatively high gel fraction was obtained which is beneficial for tissue engineering applications, as the probability for leaching out of potentially harmful hydrogel precursors will be limited. The gel-MOD (DS 97%) film exhibited a significantly (T-test, p<0.05) lower crosslinking degree which is anticipated to originate from the lower molecular weight of the hydrogel derivative due to additional hydrolysis during the second
32

methacrylation cycle. A lower molecular weight results in a shorter chain length and thus in a reduced number of crosslinkable functionalities present per chain.
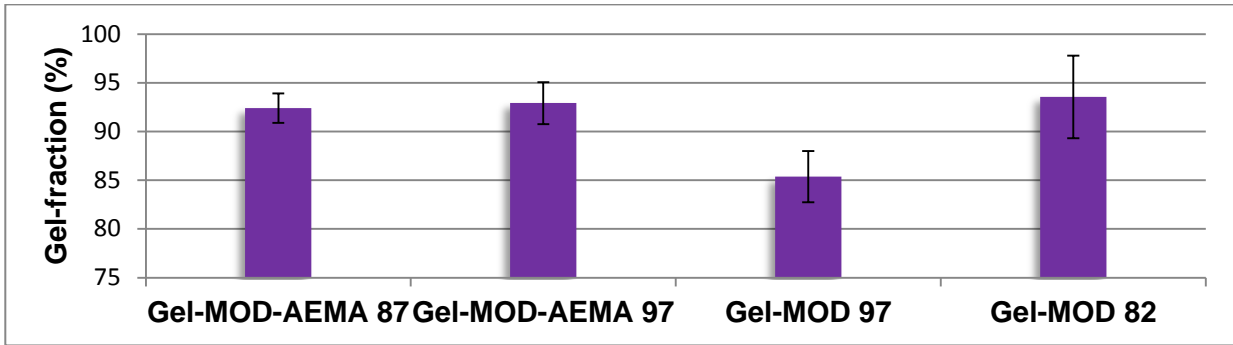
Figure 22: Plot depicting the gel fractions of the prepared hydrogel films.

2.2.4 Determination of the swelling degree of the hydrogel films

The swelling degree of a hydrogel material is an important characteristic as it determines the maximal amount of water it can absorb. This parameter is very relevant when aiming at tissue repair as it provides insight in the cellular environment to be created (e.g. diffusion rate of nutrients and waste throughout the hydrogel). In order to determine the swelling degree of the hydrogel films, samples with a diameter of 12 mm and a thickness of 0.5 mm were freeze- dried followed by determining the initial dry mass. Next, the samples were incubated in a phosphate buffered saline (PBS) solution at 37°C to mimic *in vivo* conditions. At predetermined time points, the samples were removed from the solution and their mass was determined after gently dipping with tissue paper to remove residual water present on the surface. The swelling degree was calculated by dividing the difference in mass between the swollen hydrogel and the initial dry hydrogel by the initial dry mass. In order to correct for the loss of the sol fraction during the experiment, the initial masses were corrected using the data obtained from the gel fraction experiments (see Addendum D.II and section 2.2.3).

$$Swelling\ degree\ (\%) = \frac{w_h - w_d}{w_d} * 100\% \qquad (5)$$

$$w_d = \left(\frac{gel\ fraction\ (\%)}{100}\right) * w_{d,before\ the\ experiment} \qquad (6)$$

$$w_d = corrected\ dry\ weight \qquad w_h = hydrated\ weight$$
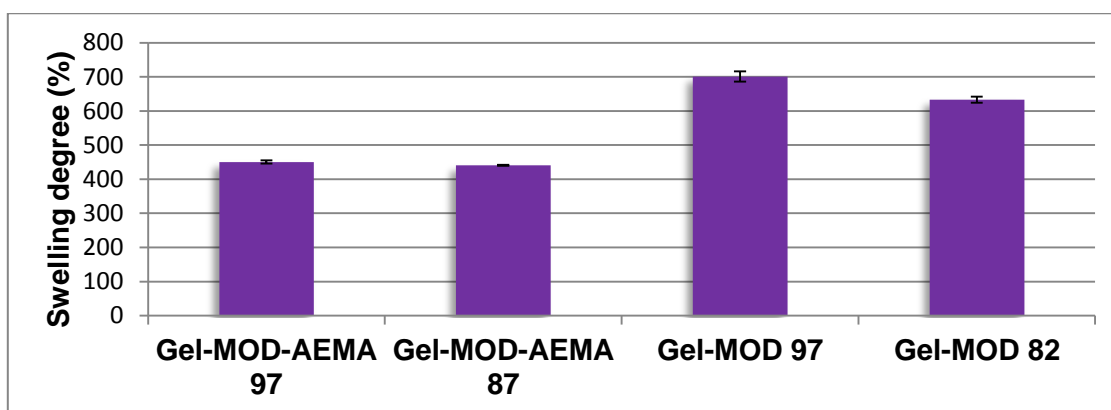
Figure 23: Plot depicting the equilibrium swelling degrees for the prepared hydrogel films.

Figure 23 depicts the equilibrium swelling degrees obtained in the swelling experiment. As anticipated, the plot reveals that gel-MOD-AEMA hydrogels exhibit a much lower swelling degree as the gel-MOD hydrogels. As the introduction of the AEMA functionalities doubled the amount of crosslinkable groups present in the gelatin, a denser network possessing more junction knots per volume unit was formed. These crosslinking points will limit the swelling capacity as this is an osmotically driven process and the mobility of the polymer chains inside the network is hampered. Surprisingly, the gel-MOD (DS 97%) hydrogels exhibit a significantly higher swelling degree (T-test, $p < 0.05$) compared to the gel-MOD (DS 82%) hydrogels despite a larger degree of methacrylation. This observation can be explained by the decrease in molecular weight of the gel-MOD (DS 97%) due to the occurrence of additional hydrolysis during the second methacrylation cycle. This reduction yields shorter chains with fewer crosslinkable functionalities per chain, generating a network with less crosslinking points.

2.2.5 Determination of the crosslink density using HR-MAS ^{1}H-NMR spectroscopy

In order to perform a quantitative characterization of the crosslink efficiency of the produced hydrogel films, high resolution magic angle spinning (HR-MAS) ^{1}H-NMR spectroscopy has been applied in the present work.

In contrast with conventional ^{1}H NMR spectroscopy, HR-MAS NMR spectroscopy enables the characterization of crosslinked polymer networks which show sufficient mobility upon swelling in a deuterated solvent. Using this approach, line broadening effects originating in the presence of dipolar coupling and magnetic susceptibility are minimized.[175][176] HR-MAS NMR spectroscopy applies a fast rotation (cfr. of kilohertz order) on the sample at a magic angle of 54.7°(θ) relative to the static magnetic field. This rotation neutralizes the line broadening effects defined by a $(3\cos^2\theta - 1)/2$ orientation dependence from the spectrum.[175] In addition, swelling of the hydrogel material in a deuterated solvent reduces the line width even further as it enables the polymer to obtain an increase in rotational mobility.[111] Consequently, materials with a

34

higher degree of crosslinking (DC) will experience a reduction in polymer chain mobility which results in broader peaks as compared to materials with a lower DC.[177]

To determine the DC, the integration of the signals corresponding to the methacrylamide and/or the methacrylate functionalities present in gel-MOD and gel-MOD-AEMA respectively have been compared before and after sample crosslinking. The signals were first normalized using the Val/Leu/Ile signal at 1.1 ppm in order to ensure a quantitative comparison. The degree of crosslinking was then calculated from the difference between these normalized values using the following equation:

$$DC(\%) = \left[\frac{\left(\frac{I^i_{5.75ppm} + I^i_{6.20ppm}}{I^i_{1.1ppm}} \right) - \left(\frac{I^c_{5.75ppm} + I^c_{6.20ppm}}{I^c_{1.1ppm}} \right)}{\left(\frac{I^i_{5.75ppm} + I^i_{6.20ppm}}{I^i_{1.1ppm}} \right)} \right] * 100 \ \% \tag{7}$$

$$i = initial\ uncrosslinked\ material \quad c = crosslinked\ material$$

The crosslink efficiency of the methacrylamide and the methacrylate functionalities was also determined separately by applying the above-mentioned formula excluding either of both signals (see Addendum D.III).
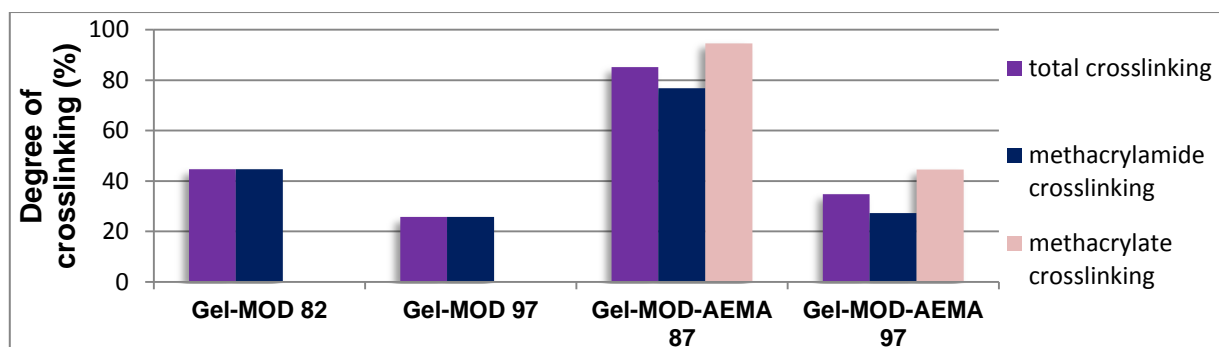
Figure 24: Crosslink efficiency of the methacrylamide and the methacrylate functionalities as well as the combined efficiency of both functionalities determined using HR-MAS ^{1}H-NMR spectroscopy.

Figure 24 depicts the obtained crosslinking degree both for the methacrylate as well as for the methacrylamide functionalites and combinations thereof for the hydrogel films developed. The results illustrate that crosslinking was less proficient for the films with a higher amount of methacrylamide functionalities (i.e. gel-MOD, DS 97% versus gel-MOD, DS 82%), which is in agreement with the gel fraction determination and the swelling behavior (see Figures 22 & 23) and results from the reduction in molecular weight of gel-MOD (DS 97%). Interestingly, the AEMA derivatives exhibit a higher crosslinking degree. The latter was anticipated as an increase in the amount of crosslinkable functionalities will increase the probability for two functionalities to reside in close proximity to one another during UV irradiation. In addition, the crosslinking of

35

the methacrylate functionalities seems to be more efficient compared to the crosslinking of the methacrylamide functionalities.

2.2.6 Rheological evaluation of gelatin-based hydrogel films

Rheology studies the deformation of flow and matter under the influence of a certain applied stress. It provides the ability to study materials with a mechanical behavior which cannot be described using conventional elasticity and Newtonian fluid mechanisms. Polymers are materials whose mechanical behavior can typically not be described using the conventional theories discussed below in brief.

The mechanical behavior of a material can typically be described using two ideal theories. On the one hand, an ideal elastic material will undergo a reversible deformation proportional to the applied tension. The deformations in these materials can be described using Hooke's law (cfr. spring model).[83][168]

$$\tau(t) = G * \gamma(t)$$

$$\tau = shear\ stress \qquad G = shear\ modulus \qquad \gamma = strain$$

On the other hand, ideal viscous materials will undergo an irreversible deformation proportional to the applied tension and time and inverse to the viscosity. These deformations can be described using Newton's law (cfr. the dashpot model).[83][168]

$$\tau(t) = \eta * \dot{\gamma}(t)$$

$$\tau = shear\ stress \qquad \eta = viscosity \qquad \dot{\gamma} = shear\ rate$$

Typically, polymers undergo visco-elastic behavior, which is a combination of both. They will undergo a partial reformation with a delay when the applied stress is removed. To examine these materials, rheology (also referred to as dynamic mechanical analysis) is often applied to perform an oscillatory assay. In the present work, rheology was performed using a plate-plate geometry. In this geometry, the sample is placed onto a glass plate under which a UV light source is mounted and which can be triggered on demand. A second plate is then placed on top at a predetermined distance (i.e. gap) to ensure close contact with the sample. The tests were performed by applying a controlled shear strain characterized by an oscillatory sine function:

$$\gamma(t) = \gamma_0 \sin(\omega t)$$

$$\gamma_0 = amplitude \qquad \omega = frequency$$

The corresponding shear stress is then a phase-shifted sine function:

$$\tau(t) = \tau_0 \sin(\omega t + \delta)$$

$$\delta = phase\ shift\ angle$$

δ = 0° for ideal elastic behavior, δ = 90° for ideal viscous behavior and 0° < δ < 90° for visco-elastic behavior (see Figure 25).
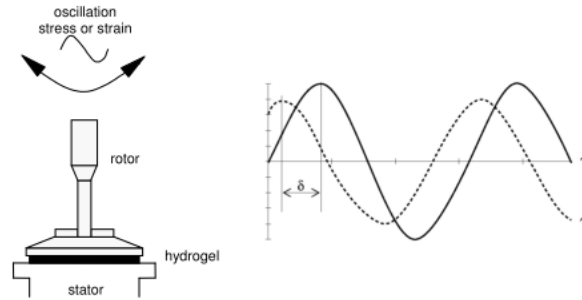
Figure 25: Preset shear strain function $\gamma(t)$, and resulting shear stress function $\tau(t)$(left), applied during a rheological experiment (right).[168]

Two important parameters for the characterization of visco-elastic materials include the storage modulus G' and the loss modulus G''. G' is a measure for the energy stored during deformation which will reverse deformation after removal of the applied load and is thus associated with the elastic behavior of the sample. G'' corresponds with the energy consumed by the sample during the deformation and is associated with the viscous behavior of the material.[83][168]

$$G'(\omega) = \frac{\tau_0}{\gamma_0} \cos(\delta)$$

$$G''(\omega) = \frac{\tau_0}{\gamma_0} \sin(\delta)$$

In order to determine the linear visco-elastic range (LVE range) of the gelatin hydrogels, an amplitude scan was performed on a crosslinked gel-MOD (DS 82%). This measurement was performed in order to select a suitable strain to be applied during the consecutive measurements. To determine the LVE range, the sample was subjected to increasing strain at a constant oscillation frequency at a stable temperature (21°C) (see Figure 26, left). The LVE range of gel-MOD stretches from 0 to around 0.3% strain. For the consecutive measurements, a preset strain of 0.05% was selected. A frequency sweep was performed at a constant temperature (21°C) and a constant strain of 0.05%. The recorded mechanical spectrum revealed that both the elasticity modulus as well as the viscosity modulus of the material are characterized by a pronounced plateau. Consequently 1 Hz was chosen as a frequency for all measurements.
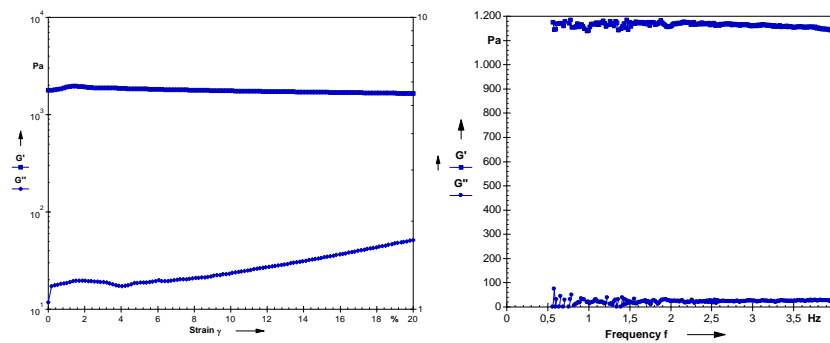
Figure 26: Amplitude sweep of crosslinked gel-MOD (DS 82%, 2 mol% Irgacure 2959) (left) and frequency sweep of crosslinked gel-MOD (DS 82%, 2 mol% Irgacure 2959) (right).

The rheological experiments have been performed to compare the mechanical properties of gel-MOD-AEMA and gel-MOD and to determine to what extent the introduction of additional methacrylate functionalities will result in an increase in mechanical properties. In a typical experiment, an uncrosslinked sample was positioned between the plates of the rheometer, followed by applying UV irradiation enabling the monitoring of the crosslinking effect on the mechanical properties. As gel-MOD-AEMA does not form a physical gel at room temperature, the sample was in situ cooled to 5°C for 15 minutes to enable physical gelation prior to the rheological measurement.

Figure 27 depicts the influence of the UV crosslinking on the storage modulus and the loss modulus for two gelatin derivatives (i.e. gel-MOD-AEMA 97 versus gel-MOD 97). The plots indicated that the initial storage modulus decreases with increasing degree of modification due to a poorer physical gelation as already discussed in section 2.1.4. Secondly, the increase in storage modulus upon UV crosslinking of gel-MOD-AEMA is about two times higher compared to the gel-MOD derivative.
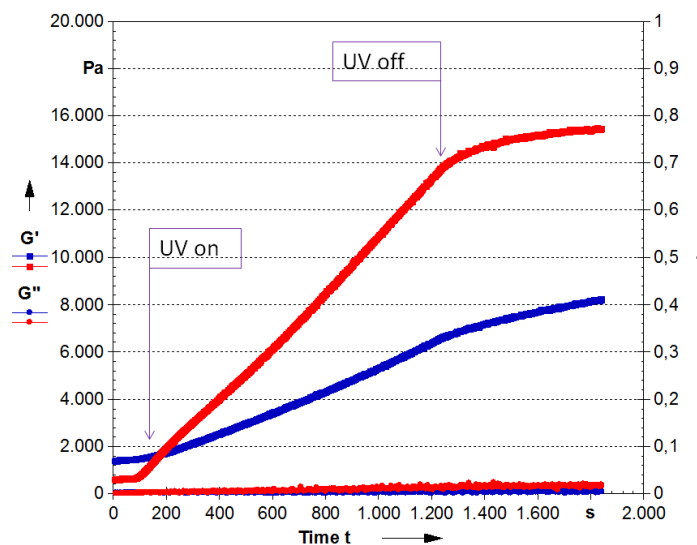
Figure 27: Monitoring of mechanical behavior under the influence of photo-crosslinking of gel-MOD (DS 97%) (blue) and gel-MOD-AEMA (DS 97%) (red).

2.2.7 Evaluation of the biocompatibility of the hydrogel films

The cell work on the hydrogel films was performed in the Tissue Engineering Group of Prof. Maria Cornelissen (Department of Basic Medical Sciences, UGent). The hydrogel films were sterilized using ethylene oxide (cold cycle) while the hydrogel precursors were sterilized through filtration.

2.2.7.1 Live/dead staining

In live/dead staining experiments, the cell viability is assessed by the addition of calcein-AM (i.e. the acetoxymethyl ester of calcein) and propidium iodide to the cell-seeded films. The non-fluorescent calcein-AM dye is a lypophillic compound which can pass through the cellular membrane. Inside the viable cells, calcein-AM is converted into a green fluorescent calcein by intracellular esterases (see Figure 28). Propidium iodide (PI) on the other hand cannot penetrate the cell membranes of living cells. However, in dead cells, the membrane is no longer intact and PI will gain access to the nucleic acids where it will intercalate thereby inducing a red fluorescence of dead cells (see Figure 28). A combination of both effects leads to a qualitative image obtained via confocal microscopy revealing the living and dead cells.
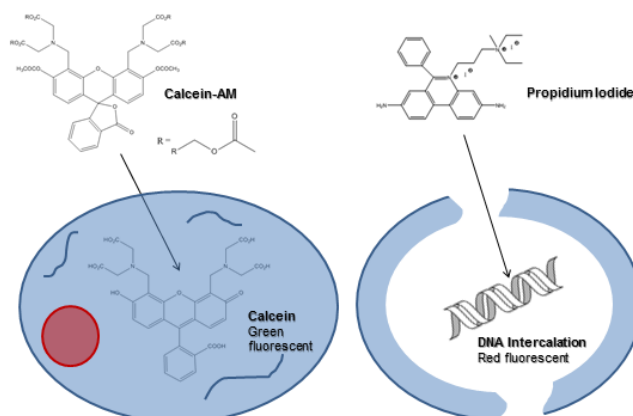
Figure 28: Principle of live/dead staining

Confocal microscopy is a form of microscopy most often applied in biomedical science to obtain images of 3D samples which were labeled with a fluorescent probe. Conventional light microscopy does not allow the generation of a high resolution image as fluorescence of specimens out of the focal plane would interfere with the measurements. To address this issue confocal microscopy is used where rather than complete illumination of the sample, confocal microscopy applies one or more focused beams of light to scan the entire sample. The sample can then be visualized by moving the point illumination through the sample resulting in only local detection of fluorescence and merging all these images into one high resolution composite image.[178]
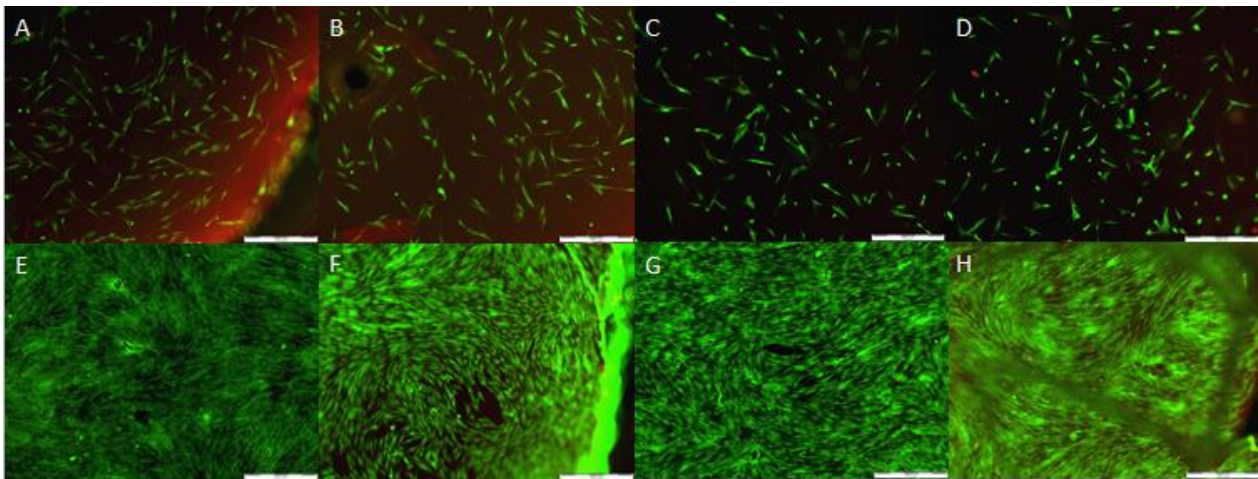
Figure 29: Live/dead staining images obtained 1 and 7 days after seeding for gel-MOD 82 (A,E), gel-MOD 97 (B,F), gel-MOD-AEMA 87 (C,G) and gel-MOD-AEMA 97 (D,H), (scale bars represent 500µm).

Evaluation of the images obtained 1 and 7 days after seeding of the hydrogel films with human foreskin fibroblasts (HFF) using the live/dead staining assay resulted in some interesting observations. It seems that all samples exhibited nice cell attachment and cell proliferation results. In addition, only few dead cells were visible on the samples after 1 day with almost no dead cells present after 7 days. These observations prove that the introduction of extra crosslinkable methacrylates does not negatively influence the biocompatibility of the gelatin hydrogels.

2.2.7.2 Qualitative determination of cytotoxicity on hydrogel precursors: MTT assay
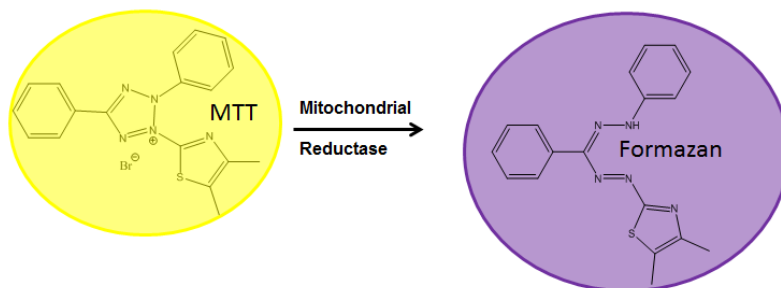
Figure 30: Principle of MTT assay

3-(4,5-dimethythiazol-2-yl)-2,5-diphenyl tetrazolium bromide (MTT) is a yellow dye, which colors purple upon reduction by mitochondrial succinate dehydrogenase. When the yellow dye enters the cells, it will be reduced in the mitochondria to yield an insoluble dark purple formazan product.(see Figure 30) After solubilization of the cells in an organic solvent, the formazan reagent can be measured using spectrophotometry. As the reduction will only take place in metabolically active cells, the spectrophotometry results give an indication of the metabolic

activity. When the results are quantified relatively to a control experiment, an estimation for the cell viability can be obtained.[179]
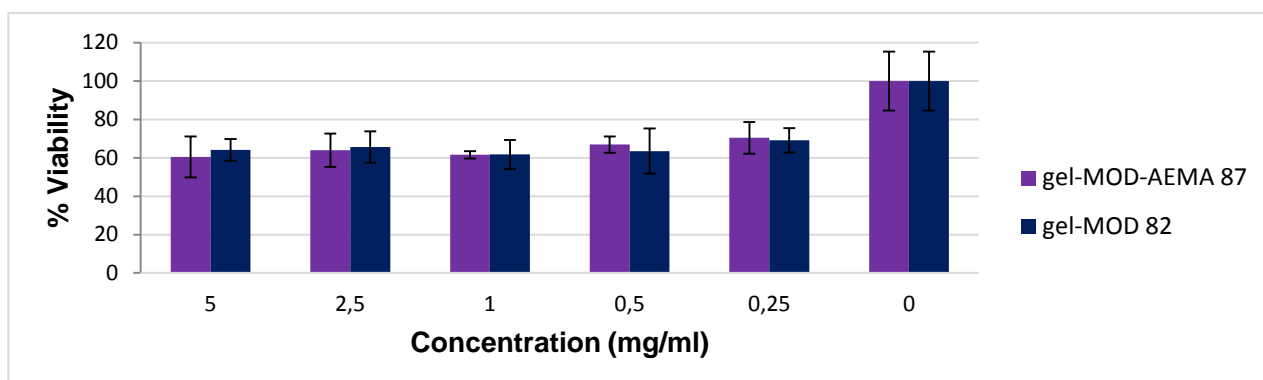
Figure 31: Plot depicting the cytotoxicity for several concentrations of hydrogel precursors gel-MOD, DS 82% and gel-MOD-AEMA, DS 87%) relative to a control.

Figure 31 depicts the influence of several concentrations of uncrosslinked hydrogel precursors both for the gel-MOD-AEMA (DS 87%) material as for gel-MOD (DS 82%) material. A comparable decrease in cell viability is observed both for the gel-MOD (DS 82%) as well as for gel-MOD-AEMA (DS 97%) relative to the tissue culture plate control group. This decrease in cell viability probably originates from the presence of methacrylate and methacrylamide functionalities as well as factors which can be ascribed to the gelatin base material. However, the cytotoxicity of the gel-MOD-AEMA precursors is not significantly different compared to the cytotoxicity of the gel-MOD precursors which have a proven biocompatibility.[86][134] Another interesting observation is the fact that the cell viability remains practically constant for various concentrations of hydrogel precursors. This remarkable observation indicates that the methacrylates/methacrylamides do not exhibit a cytotoxic effect, and the decrease in cytotoxicity might be attributed to other factors.

2.2.8 Conclusions and future perspectives

The introduction of additional methacrylate functionalities by the modification of the carboxylic acids present in the gelatin backbone hydrogel is a viable method to obtain a biocompatible hydrogel with higher mechanical properties. Cytotoxicity studies revealed no increase in the cytotoxicity of gel-MOD-AEMA both for the crosslinked as well as for the reactive precursors compared to gel-MOD despite the presence of additional crosslinkable functionalities. Furthermore, swelling tests and HR-MAS NMR spectroscopy measurements indicated that the crosslink efficiency in gel-MOD-AEMA was substantially higher compared to gel-MOD. However, the different characterization experiments also revealed that the application of a second

methacrylation cycle to yield a gel-MOD with a higher DS, has a negative influence on the mechanical properties of the material. This effect probably originates in a decrease of the molecular weight of the hydrogel precursors resulting in fewer crosslinkable functionalities per chain. These observations have to be further investigated by applying gel permeation chromatography (GPC) and viscosimetry for molecular weight determination. In addition, additional rheological characterization needs to be performed on Gel-MOD-AEMA derivatives with different degrees of substitution.

2.3 Production of poly-lactic acid scaffolds using fused deposition modelling

The aim of the present study was to apply a combination of poly-lactic acid (PLA) and gelatin B derivatives for the production of hydrogel-polyester combination scaffolds for tissue engineering purposes. The PLA scaffolds ensure sufficient mechanical properties while the gelatin derivatives introduced typically increase the bio-interactivity and the biocompatibility of the final construct.

The PLA scaffolds were produced using fused deposition modelling (FDM). This equipment applies a thermoplastic polymer filament as starting material which is fed through a heated nozzle using rollers. The heat of the nozzle melts the material and by movement of the nozzle in the X-Y plane, the material can be deposited. [101][132][149] (see Figure 32) After the deposition of a 2D layer in the X-Y plane, the platform moves downwards to enable the deposition of a subsequent layer, thereby generating a 3D structure.[154][152] The different layers are connected because the molten polymer causes the previously deposited layer to soften.[159] Fused deposition modelling can generate structures with a resolution in the micrometer range, which is mainly limited by the nozzle diameter.[159]
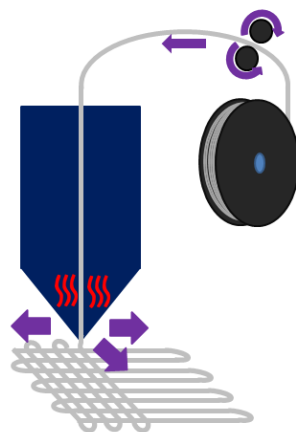
Figure 32: Scheme of FDM principle.

The FDM technique exhibits an additional advantage over other nozzle-based systems since the continuity of the filament prevents the material from intruding inside the pores (for a reasonable

distance) prior to solidification. As a result, no additional (potentially toxic) support materials are required which typically have to be removed afterwards.[159]

The majority of FDM applications are currently situated in the field of hard tissue replacement since FDM does not enable the application of hydrogel materials typically required for soft tissue engineering.[132] The main drawback of of the FDM principle is the requirement to start from preshaped, solid polymer filaments exhibiting specific dimensions and properties to enable their feed through the rollers towards the nozzle.[149]

2.3.1 Overview of printing parameters for fused deposition modelling

In order to realize reproducible 3D scaffolds, several printing parameters can be finetuned including the nozzle diameter, the printing temperature, the printing speed, the layer height and the starting material. A first essential parameter in the FDM process is the nozzle diameter as it is the limiting factor regarding the minimal width of the polymer struts which can be realized. In the present work, the applied nozzle possessed a diameter of 400 μm, limiting the theoretical minimum strut width to 400 μm.[180] In addition to the nozzle diameter, the printing temperature can also affect the FDM process to a great extent. It determines the viscosity of the extruded polymer and the required time to enable solidification of the polymer thereby affecting potential post-extrusion deformations. The selection of a minimal printing temperature results in the lowest deformation after extrusion, rendering it possible to bridge larger gaps without strut collapse inside the pores. PLLA possesses a melting temperature in the range of 170°C-180°C (i.e 167°C for the applied filament, see thermogram in Addendum E.I), incidently, the printing temperature needs to surpass at least 170°C.[181][182] However, a too low temperature generally results in an inferior attachment between superposing layers. Conversely, a critically high printing temperature will result in a high fluidity thereby reducing the control over the deposited layer and potentially inducing thermal degradation.[182] The printing temperature for the PLA scaffolds developed in the present work was set at 195°C.

The printing speed affects several factors involving the scaffold production including the required printing time for each scaffold developed. Increasing the printing speed decreases the scaffold production time and aids in bridging the pores. However, an excessive printing speed results in an inhomogeneous deposition of polymer material which results in differences of the strut width throughout the scaffold. By selecting the printing speed critically low, poor bridging of the pores becomes apparent ,consequently, the lateral porosity becomes poor. The applied printing speed for the scaffold production throughout the present work was set at 11 mm/s.

The height of the printed layers determines to a great extent the lateral porosity of the scaffold. A low layer height results in small pores, rendering the scaffold less suitable for tissue engineering purposes. The maximum layer height is determined by the feed rate of the filament. If the layer height is set too high, the subsequent layer can no longer attach to the previous layer rendering controlled deposition impossible. Herein, the layer height was set at 0.3mm, which is about the limit of the printing device in combination with the PLA filament. The selected layer height resulted in relatively large pores which facilitates the subsequent introduction of gelatin inside the printed PLA scaffold.

The printing material is a key aspect in FDM as it determines to a great extent the above-mentioned parameters because of differences in the melting temperature of the polymer applied and the viscosity of the polymer melt. The melting temperature of PLA is greatly influenced by its composition (cfr. PLLA, PDLA, PDLLA and blends) and its molecular weight as already discussed in section 1.5.2.1.[137][181][182] In this study, the applied material is a transparent PLLA filament possessing a molecular weight of 16426 Da. The Gel Permeation Chromatography (GPC) and ^{1}H and ^{13}C- NMR spectroscopy results are included in Addendum E.I.

2.3.3 Generation of a 3D model for scaffold printing

In order to produce the PLLA scaffolds, two approaches have been evaluated. The first approach consisted of the generation of a 3D model using CAD software. The 3D model included a 15*15*15 mm cube containing square pores of 500*500 μm in three dimensions as depicted in Figure 33 A and B. The 3D model was subsequently sliced using Cura slicing software prior to printing using the Ultimaker 1.
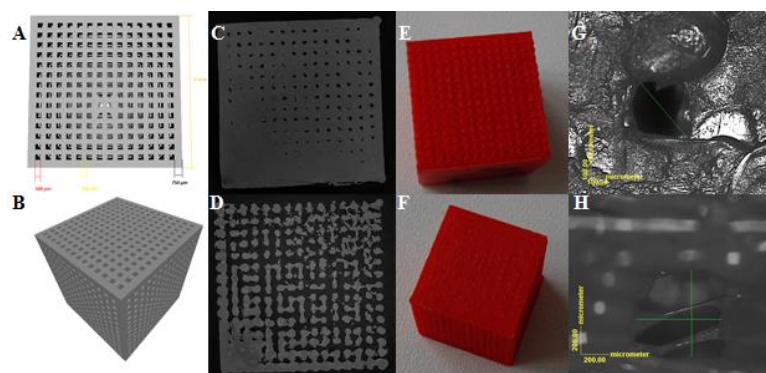
Figure 33: Images (top view - E & side view - F) of scaffolds produced using a CAD Model (A & B) generated using micro-Computed Tomography (μ-CT) (C & D) and optical microscopy (G & H).

A visual evaluation of the produced scaffolds combined with optical microscopy and μ-Computed Tomography (μCT) illustrated the presence of inhomogeneous pore shapes and sizes

and the absence of a fully interconnected porous network (see Figure 33 C-F). These observations indicated that even upon fine-tuning several processing parameters the CAD model remained too complex for the Ultimaker 1when relatively small dimensions were applied.

In order to address these shortcomings, a second approach was elaborated to realize the scaffold production which enabled the direct control over the movement of the printing head using commands introduced into the printer via a Gcode file (see Addendum E.II). By the input of direct commands, scaffolds could be printed under a continuous flow of PLLA melt in a meander-like fashion. This approach not only results in superior mechanical properties since the complete scaffold is produced starting from a continuous PLLA strand, but also significantly reduces printing errors originating from an interrupted extrusion process. In order to generate the Gcode files, a program was written in Visual Basic for Applications (VBA) (see Addendum E.III). This program processes the input of several parameters including the pore size, the macroscopic size, the amount of layers to be deposited and the printing temperature to generate a Gcode file which can be transferred to the Ultimaker 1. The application of this program ensured an additional benefit over the CAD approach as a wide variety of scaffold/pore sizes can be produced without the need to develop novel CAD designs upon changing the scaffold dimensions and/or the pore size.
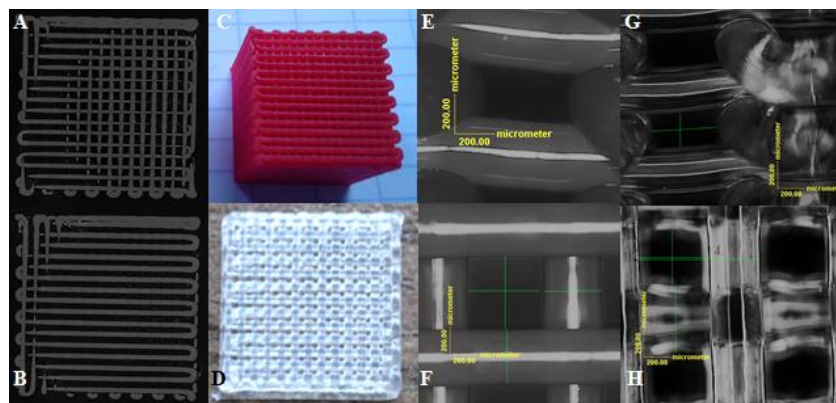
Figure 34: Overview of scaffolds developed starting from Gcode generation: µCT images (A, B); visual images of a scaffold produced using a colored filament (C) and a transparent filament (D); optical microscopy images from the side (E, G) and the top (F, H) of a scaffold using a colored and a transparent filament respectively.

2.3.4 Characterization of the Printed Scaffolds

2.3.4.1 Visual Evaluation

Visual evaluation of the scaffolds produced via Gcode already resulted in some interesting benefits compared to the CAD scaffolds. For instance, the presence of a more reproducible and a homogeneous porous network was observed when applying Gcode.(see Figure 33 E and F and Figure 34 C and D and Figure 35)
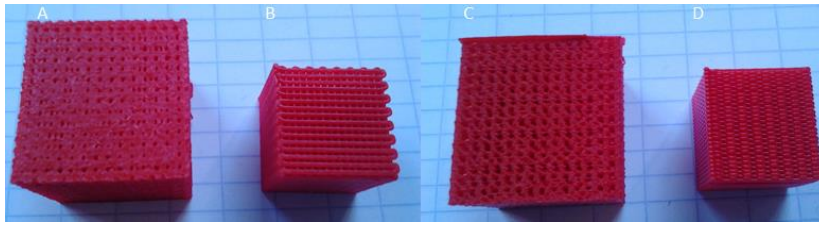
Figure 35: Comparison between a scaffold produced through CAD design (A,C) and a scaffold produced using a Gcode file (C,D) viewed from the top and the side respectively.

2.3.4.2 Optical Microscopy

In optical microscopy, a magnified image of the sample is produced through the use of visible light in combination with a series of lenses and diaphragms to realize different magnifications and a variety of contrasts respectively. The sample is illuminated from the top and the resulting image can be recorded using a camera. In a subsequent step, the recorded images can be processed using software to measure the pore size of the sample.

The visual observations were further confirmed by measuring 5 pores using optical microscopy (see Figure 34 D, E, F and G). Figure 34 confirmed that the morphology of the pores in the scaffolds developed using Gcode was more reproducible as demarcated square pores were observed in contrast with the pores observed in the CAD scaffolds (see Figure 33 G and H).

In order to denote the difference in a quantitative manner, 5 pores in four different scaffolds were measured using optical microscopy to enable comparison between both strategies. For these purposes the CAD model was enlarged to 2*2*2 cm to generate an overall porosity resulting in a theoretical pore size of 666µm, for comparison purposes Gcode scaffolds with a pore size of 666µm were printed. The results are depicted in Figure 36 depicting both the average pore size as the theoretical pore size for both methods. An analysis of variance (ANOVA) between the several scaffolds produced by either method was in agreement with the observations made visually. There was no significant difference ($p>0.05$) between the average pore size of the scaffolds produced via the Gcode method while the CAD scaffolds differed significantly ($p<0.01$) in average pore size. This analysis confirmed the more uniform pore size distribution for the scaffolds printed using the Gcode relative to the pore size distribution of the scaffolds produced using the CAD model (see Figure 36). In addition, the average pore size of each scaffold was calculated and compared to the theoretical pore size.
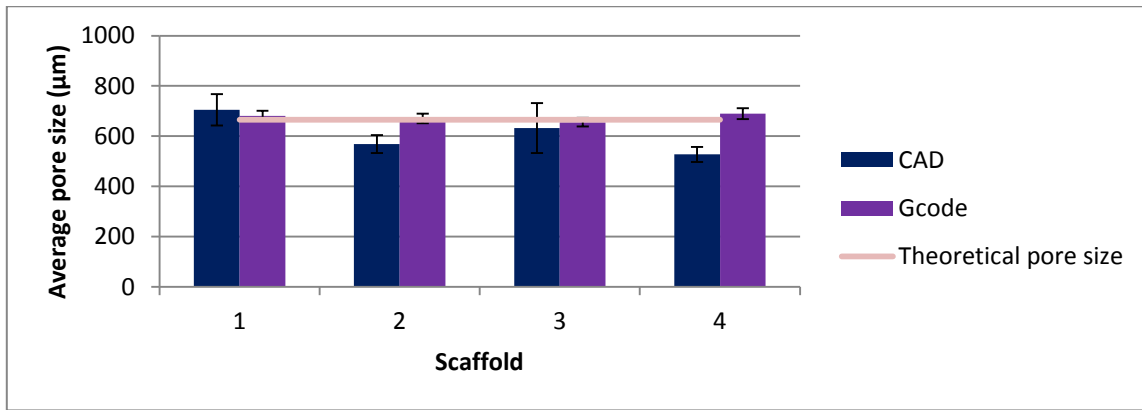
Figure 36: Plot of the average pore sizes for scaffolds obtained via both methods compared to their theoretical pore size. The error bars depict the standard deviation on the obtained pore size.

2.3.4.3 Micro-Computed Tomography

Computed tomography (CT) is a non-destructive visualization technique which uses X-rays to generate an image of the sample. The benefit of this visualization technique can be attributed to the fact that images of the interior of the sample can be obtained without the requirement of sample destruction. For this purpose, X-rays are sent through the sample. As the X-rays interact with the sample, a shadow is projected on the detector, generating a planar image or a radiograph of the sample. In order to generate a 3D image of the sample, it is rotated around a fixed axis in the X-ray field. This rotation enables the recording of multiple planar images on the detector. These planar images can then be processed via specialized software to generate visual reconstructions of axial slices of the sample. In a next step, these obtained reconstructions can be merged, yielding 3D visualizations of the samples containing a detailed view on the inner structure.[183][184]
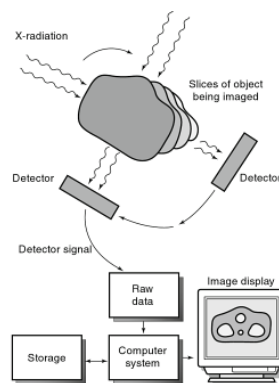
Figure 37: Working principle of computed tomography. [183]

The most common application of CT can be found in the world of medicine where it is used as a powerful diagnostic tool.[183] The resolution for clinical applications is limited (i.e. a few 100 µm) due to regulations concerning maximum allowed radiation doses.[183][184] However, for

material characterization, the applied dose is of secondary importance. As a consequence, superior resolutions can be achieved (i.e. 1 µm).[184]

Comparison between the µ-CT images of the scaffolds produced using both approaches confirmed the observations established using visual characterization and optical microscopy. The inner structure and the pore morphology of the CAD scaffolds were less uniform compared to the inner structure of the Gcode scaffolds (see Figure 33 C, D and Figure 34 A, B). In addition, Figure 33 C also demonstrates the absence of a completely interconnected porous network as already discussed in section 2.2.3. Figure 34 A and B shows the presence of a continuous PLA strand printed in a meander-like fashion in the Gcode scaffolds as opposed to Figure 33 D and E which exhibit rough edges due to printing errors (cfr. an interrupted extrusion process).

2.3.4.4 Assessment of mechanical properties through compression tests

The mechanical properties of the produced PLA scaffolds were assessed by determining the Young's modulus via compression tests. The Young's modulus or the compressive elastic modulus E is a measure for the material stiffness. Considering the function of the IVD, the resistivity of the scaffold developed against compressive forces exerted is of primary importance (see also section 1.2.1).[8]

Compressive stress-strain experiments are mainly performed using a setup in which the sample is gradually compressed by applying a certain force until a predetermined maximum is reached. Typically, the material deformation (generally in mm) is monitored as a function of the applied force (in N). After converting the output of these measurements into stress (i.e. $\sigma = F/A_0$, applied force divided by the sample surface area) and strain (i.e. $\varepsilon = (L_0-L)/L_0$, deformation divided by sample height), a stress-strain curve can be plotted. Generally, different characteristic regions can be distinguished in stress strain plots including the linear elastic region, the pseudo-elastic region, the yield point and the plastic region.[83][185]
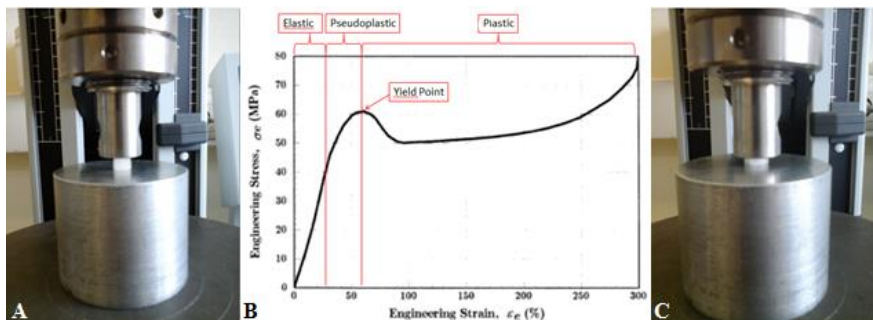
Figure 38: Image of a scaffold prior to (A) and after compression (C); example of a typical stress-strain curve for a semi-crystalline thermoplastic polymer exhibiting the different characteristic regions (B).[185]

Compression tests were only performed on scaffolds produced using the Gcode approach as the characterization through the above-mentioned methods indicated that the CAD scaffolds were less favorable for the intended application (i.e. tissue engineering) (see also sections 2.2.4.1-2.2.4.3).

An example of a stress-strain plot obtained after compression of a PLA is depicted in Figure 38. The Young's modulus can be calculated from the slope of the linear area in the elastic region on the stress-strain plot (see inset Figure 39).
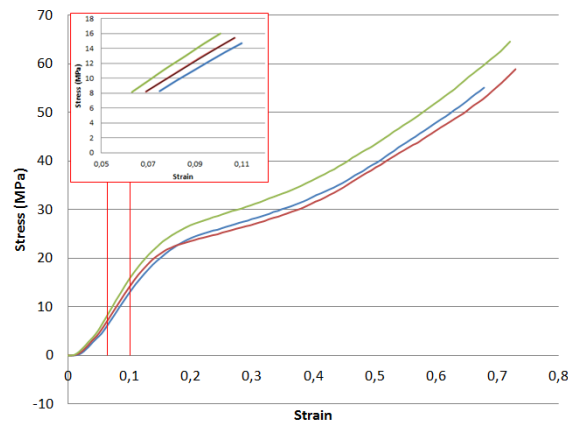
Figure 39: Stress-strain plot of a PLA scaffold. The inset shows a magnification of the elastic region.

The experiments revealed that the Young's modulus of the scaffolds developed can be influenced by adjusting several parameters. Figure 41 (left) shows the influence of the pore size and the sample aging time (i.e. time between development and characterization through compression). Figure 41indicates that the mechanical properties of the scaffold can be fine-tuned by varying the pore size. Smaller pores result in stiffer structures. However, when the pore size is lower than a critical value, the scaffold becomes less suitable for the targeted application as the efficiency to introduce a gelatin cryogel into the scaffolds developed decreases. The plot also reveals an influence of the sample aging time on the mechanical properties. This phenomenon is generally referred to in literature as "physical aging".[186] The "physical aging" phenomenon occurs because PLA is generally stored at a temperature (i.e. room temperature) below, yet close, to its glass transition temperature (T_g)(i.e. 61°C see Addendum E.I). At this temperature, the polymer is present in a thermodynamically unstable state. This unstable state originates from the rapid cooling of the PLA after deposition. The rapid cooling "freezes" the polymer chains drastically, thereby reducing their segmental mobility.[187] To overcome this instability, the polymer will slowly transfer to an equilibrium state through slow segmental rearrangements.[186][188] These rearrangements will in their turn result in the creation of locally ordered domains and at the same time, in a reduction of the free volume of the polymer.[186][189][187] Figure 40 depicts the

influence of "physical aging" on the crystallineity present in the sample, quantified by DSC as the required melting energy upon heating (see thermograms in Addendum E.IV).
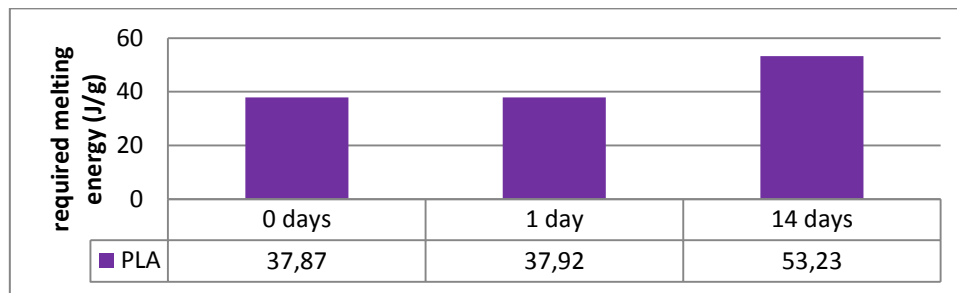
Figure 40: Plot depicting the increase in required energy for melting of the printed PLA as a result of 'physical aging'.

The presence of the locally ordered domains and the reduction of the free volume render it more difficult to transfer a locally applied strain throughout the entire sample, thereby reducing the elasticity and increasing the brittleness.[187] The increase in brittleness can be observed by the increase of the Young's modulus as elasticity drops concomitantly.[187] Figure 41 (right panel) reveals the influence of the printing temperature on the Young's modulus. The results illustrate that at a printing temperature of 190°C, a slight drop in Young's modulus can be observed relative to the scaffolds printed at higher temperatures. The origin of this drop in elastic modulus is anticipated to be attributable to the inferior attachment of superposing layers due to the lower printing temperature (see section 2.2.2.2). The results enabled the selection of the optimal printing temperature (i.e. 195°C) as increasing temperatures are anticipated to induce thermal degradation of the scaffolds. [182] In conclusion, both the pore size as well as the printing temperature are important features when it comes to fine-tuning the mechanical properties of scaffolds.
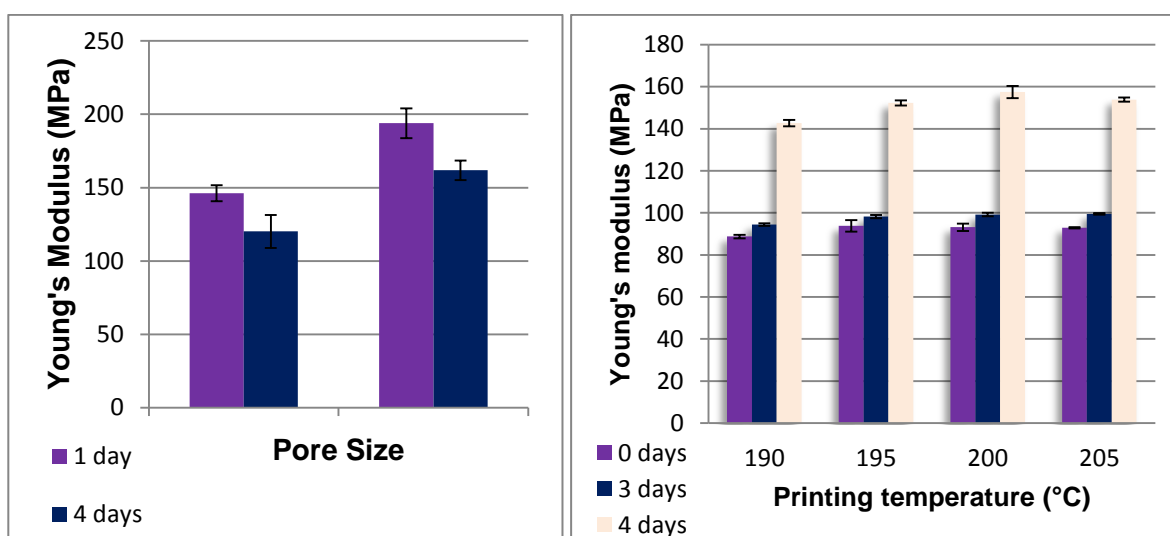
Figure 41: Plot revealing the influence of the pore size and the sample aging time on the Young's modulus for PLA scaffolds (left); Influence of printing temperature and sample aging time on the Young's modulus of PLA scaffolds with a pore size of 450 µm (right).

2.4 Development of Poly Lactic Acid-Hydrogel Combination Scaffolds

In order to increase the biocompatibility and the bio-interactivity, a gelatin-based hydrogel was selected to be combined with the PLA scaffolds developed. As previously discussed (see section 2.1), the material was methacrylated (gel-MOD) to enable covalent crosslinking ensuring stability upon *in vitro* or *in vivo* application. For the combination of both materials, two approaches have been selected. On the one hand, a gel-MOD hydrogel was introduced in the PLA scaffold which was subsequently UV crosslinked and exposed to a cryogenic treatment followed by lyophilization prior to cell seeding. On the other hand, a gel-MOD solution was blended with MC3T3 preosteoblast cells prior to introduction in the PLA scaffolds followed by UV crosslinking.

2.4.1 Development of PLA-cryogel combination scaffolds

In a first part, the cryogel approach was selected as this method enables the generation of an interconnected porous gelatin network. The cryogenic treatment was applied to obtain a certain degree of control over both the hydrogel pore size as well as its geometry within the PLA scaffold.[156] The cryogel-PLA combination scaffolds were obtained using a multistep process. First, the PLA scaffolds were immersed in gel-MOD (DS 82%) solutions of different concentrations (i.e. 2, 5 and 10 w/v%) containing a suitable photo-initiator (2 mol% Irgacure 2959) (see Figure 42). The solution containing the scaffolds was then exposed to a vacuum treatment for five minutes enabling optimal intrusion of the gel-MOD throughout the PLA scaffolds (see Figure 42: **3**). In a second step, the gel-MOD containing scaffolds were stored at 6°C for 1 hour to induce physical gelation of the hydrogel. Afterwards, the scaffolds were exposed to UV-A light for two hours to enable a photo-induced radical polymerization of the methacrylamide functionalities present in gel-MOD (see Figure 42: **4**). Next, the scaffolds were exposed to a cryogenic treatment followed by lyophilization (see Figure 42: **6,7**).
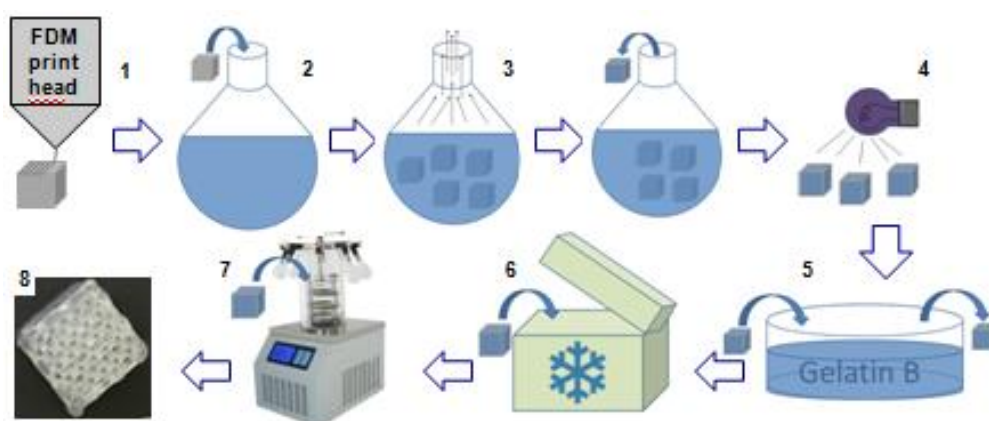
Figure 42: Scheme of the principle to introduce Gel-MOD cryogels in PLA scaffolds.

2.4.1.1 Cryogenic treatment of PLA-gel-MOD combination scaffold

For the application of a cryogenic treatment, a cryo-unit was selected which was designed and manufactured in close collaboration with the central workshop of Ghent University. The device consists of an aluminum mold which can be cooled to a predefined temperature in a controllable fashion by means of a thermostat, using isopropanol as cooling liquid. In addition to conventional cooling, the device also contains thermoelectric coolers (TEC) or Peltier elements at the bottom of the aluminum mold which enables the introduction of temperature gradients up to 30°C between the top and bottom of the mold. The Peltier elements - also referred to as a solid state heat pump - contain an array of n- and p- type semiconductors. By means of electron/gap interactions and associated excitation/relaxation effects, heat is transferred. Basically, when an electron moves from the copper conductor to the p-type semiconductor at the hot side, it needs to fill a hole. In order to fill this hole, the energy of the electron will be lowered, resulting in a release of heat. In essence, these holes travel through the p-type semiconductor until they reach the cold side of the p-type semiconductor where the electron needs to gain energy to travel through the copper conductor again absorbing heat in the process. Similarly, the electron from the copper conductor needs to increase its energy when reaching the cold side of the n-type semiconductor absorbing heat in the process until it falls back to its lower state to enter the copper conductor at the hot side. [110][156][168][190]

Two types of PLA-cryogel scaffolds have been developed by applying a cryogenic treatment. On the one hand, scaffolds have been produced by applying a temperature gradient of 30°C between top and bottom of the scaffold. It was anticipated that this methodology would result in scaffolds containing vertical channels with a decreasing diameter from top to bottom of the cryogel. [110][156][168] In addition, scaffolds were produced without applying a temperature gradient, leading to a more uniform porosity throughout the entire scaffold.[110][156][168] For both approaches, the cryogenic treatment consisted of a controlled temperature decrease at a rate of 0.15°C/min until a temperature of -30°C was reached as described by Van Vlierberghe *et al* (2007).[156]

An important drawback of the application of cryogels for tissue engineering purposes is the presence of a non-porous skin at the outer material surface.[168] This non-porous skin can greatly reduce the cell seeding efficiency while at the same time diminish the transport of nutrients and waste throughout the cell-seeded scaffold. In order to prevent skin formation, the scaffolds were immersed in a gelatin B solution prior to the cryogenic treatment to generate a dissolvable skin (see Figure 42: **5**). Incubation in water at 37°C prior to cell seeding will then result in the dissolution of this non-porous gelatin skin. [156][168][190]

2.4.1.2 Characterization of PLA-cryogel combination scaffolds

2.4.1.2.1 Visualization through digital microscopy

Digital microscopy is a technique which applies the same principle as conventional optical microscopy but with the substitution of the ocular lens by a semiconductor charge-coupled device (CCD) image sensor to capture the picture. By controlling the movement of the lenses, the software can record several images focusing on different sample depths to generate a complete image in which all these focal planes are combined to realize an overall sharp image.
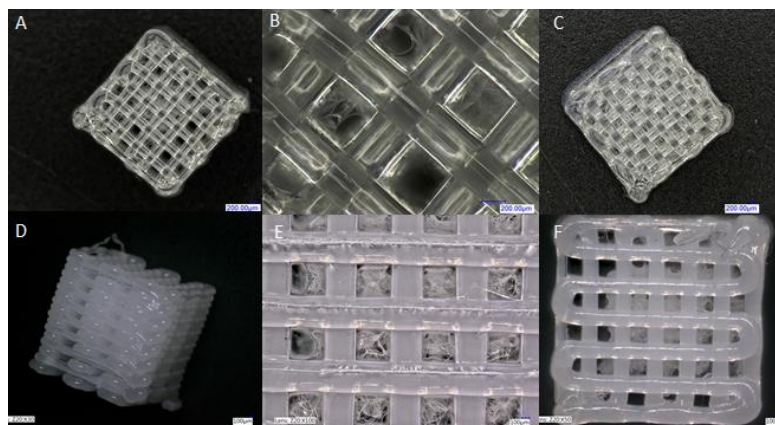
Figure 43: Digital microscopy images of a PLA-gel-MOD (2w/v%) combination scaffold developed in the absence of a temperature gradient before (A & B) and after incubation in water (D, E, F) and PLA-gel-MOD (5w/v%) combination scaffold prior to incubation (C).

The images obtained via digital microscopy revealed the presence of a gel-MOD cryogel structure inside the pores of the PLA scaffolds (see Figure 43(A, B & C). However, the combination scaffolds obtained using a 2w/v% gel-MOD solution clearly reveal the absence of gelatin towards the edges of the scaffolds. The origin of this phenomenon can be attributed to two effects. First, the 2w/v% gel-MOD solution is less viscous and gives rise to a slower physical gelation which resulted in a partial leaching out during the physical gelation (1 hour, 6°C) prior to UV crosslinking. To remove unreacted gel-MOD from the scaffolds, they were incubated for 12 hours in milliQ water at 37°C (see Figure 43 D, E and F). The gelatin hydrogel can still be observed, which indicated that the PLA scaffolds enable the penetration of UV irradiation and thus the photo-polymerization of the introduced gelatin.

2.4.1.2.2 Visual evaluation using scanning electron microscopy

In scanning electron microscopy (SEM), an electron beam is generated which is directed towards the sample via electron lenses. When the electrons collide with the sample, a variety of radiation types can be observed including backscattered electrons, secondary electrons, photons, visible light and heat. The backscattered and secondary electrons are monitored using a detector which

generates a sample image. To avoid a build-up of charges inside the sample, the sample is coated with gold by a low vacuum sputtering technique. This coating renders the sample conductive allowing it to be grounded, thereby removing all charges present.[191]
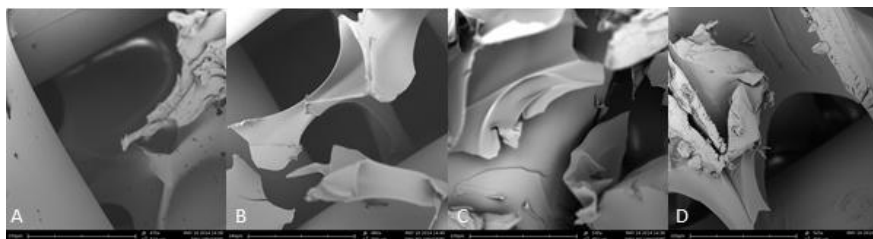
Figure 44: SEM images of the gelatin microstructure inside the PLA scaffolds at the center of the scaffolds: (A) 5 w/v% with temperature gradient; (B, C and D) 2, 5 and 10 w/v% without temperature gradient respectively.

Figure 44 reveals the gelatin microstructure present inside the PLA scaffolds, as obtained through SEM. The density of this microstructure was clearly a lot more pronounced in the 5 and 10w/v% gelatin concentrations as compared to the 2w/v% concentrations.. The scaffolds produced using a 2 w/v% gel-MOD solution (Figure 44 B) clearly exhibit more pores as compared to the scaffolds produced using a 5 and a 10 w/v% gel-MOD solution (Figure 44,A, C and D. In addition, a skin of crosslinked gel-MOD appears to encapsulate the PLA struts which is anticipated to enhance the cell adhesion to the polymer struts (see Figure 45).
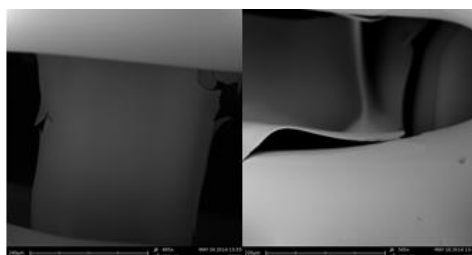
Figure 45: SEM images of gelatin covering the PLA struts of a scaffold produced using a 10 w/v% gel-MOD solution.

2.4.2.2.3 Non-destructive evaluation using micro-computed tomography

The use of μ-CT enables the 3D visualization of the PLA-gelatin combination scaffold even towards the core of the scaffold without the need for sample destruction. The reconstructed slices were in agreement with the observations obtained from digital microscopy. The images of the scaffolds generated using a 2 w/v% gelatin solution showed the absence of gel-MOD towards the edges of the scaffold as a result of leaching out prior to and during UV-crosslinking (Figure 46, A & C). However, the slices of the scaffolds obtained using a 5 and a 10 w/v% gelatin solution reveal a porous gelatin structure throughout the PLA scaffolds (see Figure 46, B, D and E).
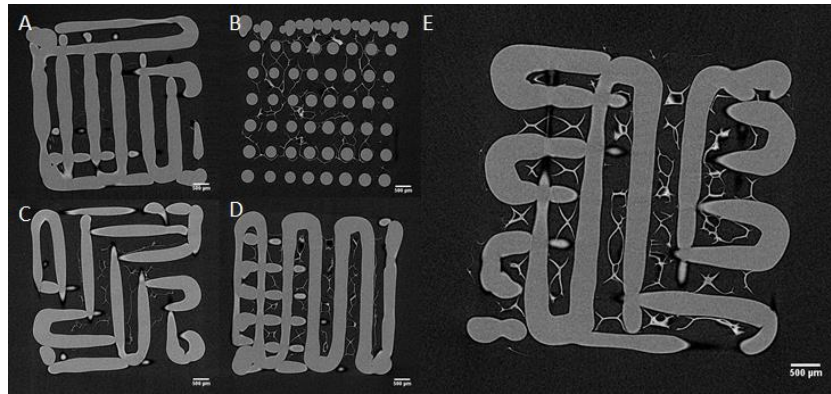
Figure 46: Image reconstructions of PLA-gel-MOD combination scaffolds obtained through μ-CT: 2 w/v% and 5 w/v% gel-MOD in the presence of a temperature gradient (A & B respectively) versus 2 w/v%, 5 w/v% and 10 w/v% gel-MOD without temperature gradient (C, D & F respectively).

2.4.2.2.4 Evaluation of the water uptake capacity of the PLA-gel-MOD combination scaffolds

The water uptake capacity is an important characteristic of scaffolds developed as cell carriers for tissue engineering applications. In order to quantify the water uptake capacity of the gel-MOD cryogels inside the PLA scaffolds, the scaffolds were immersed in PBS buffer at 37°C to mimic *in vivo* conditions. At regular time points, the water uptake of the scaffolds was determined by quantifying mass differences between the dry and the hydrated scaffolds:

$$Water\ uptake\ capacity\ (\%) = \frac{w_{ht,hydrated} - w_{d,dry}}{w_{d,dry}} * 100\ (\%)$$

The maximum water uptake capacity of all scaffolds developed was determined. In addition, both the influence of applying a temperature gradient during the cryogenic treatment as well as the gelatin concentration applied (2, 5 and 10 w/v%) on the swelling capacity was evaluated (see Figure 47). As a reference, the water uptake capacity of a blank PLA scaffold containing no gelatin was also assessed.
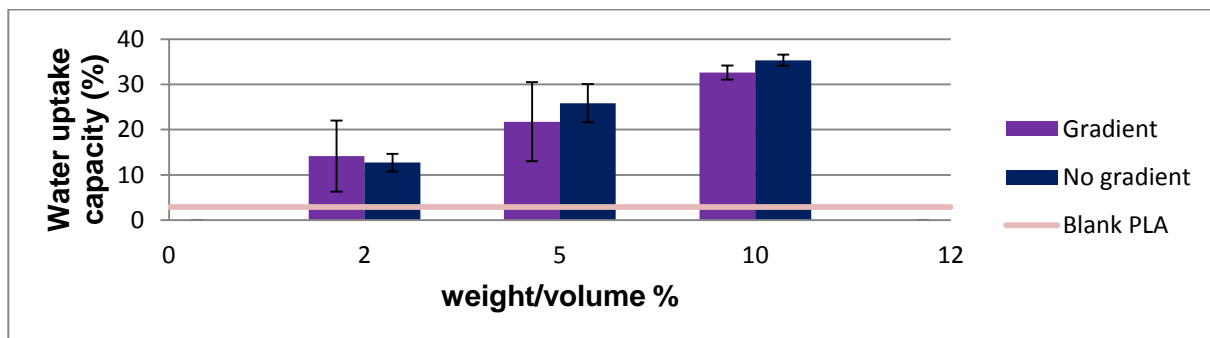
Figure 47: Maximum water uptake capacity of the PLA-gel-MOD combination scaffolds with varying gelatin concentrations.

55

A first interesting aspect included the fact that the maximum water uptake was attained almost instantaneously. This effect might be attributed to the fact that a volume increase of the gelatin is obstructed partially by the presence of the PLA struts. In addition and surprisingly, an increase in water uptake capacity was observed for increasing gelatin concentrations. The latter is contradictory to the results of Van Vlierberghe *et al* which illustrated an increase in water uptake capacity of gelatin-based cryogels upon decreasing the gelatin concentration.[109] As higher gelatin concentrations lower the porosity of the cryogel, a larger obstruction towards water uptake can be anticipated. In addition, higher polymer concentrations generally result in a higher crosslinking degree and consequently, a lower water uptake.[168] However, the obtained results can be explained by evaluating the digital microscopy and the μ-CT images. Due to the poorer physical gelation and the reduced viscosity of the lower gelatin concentrations (i.e. 2 and 5 w/v% versus 10 w/v%), part of the gel-MOD solution was leached out from the scaffolds containing the lowest gelatin concentration prior to crosslinking. As the dry gelatin fraction in the PLA scaffolds increases with increasing gelatin concentration, the water uptake capacity of the scaffolds will increase concomitant (see Figure 47).

Furthermore, Figure 47 reveals an increase in water uptake capacity for scaffolds which were produced in the absence of a temperature gradient during the cryogenic treatment. However, an ANOVA test proved this difference to be statistically insignificant ($p > 0.05$).

2.4.1.3 Conclusions and future perspectives

The application of a cryogenic treatment to introduce a porous, crosslinked gelatin microstructure inside a 3D printed PLA scaffold is a suitable technique to develop PLA-hydrogel combination scaffolds. Despite the introduction into the PLA scaffolds, the porous gelatin microstructure exhibited a very fast maximum water uptake. However, further optimization still needs to be performed with respect to the procedure for introducing low concentrations of gel-MOD solutions to prevent leaching out from the PLA scaffolds. A potential solution for this problem might be to enable the physical gelation to occur when the scaffolds are still immersed in the gelatin solution, followed by removing the scaffolds from the gel prior to UV-curing.

2.4.2 Combination of PLA scaffolds with cell-encapsulated gel-MOD solution

The UV crosslinking of a MC3T3 cell encapsulating gel-MOD solution introduced in a PLA scaffold was evaluated as a pilot experiment towards two photon polymerization (2PP) of a cell encapsulating gelatin solution introduced in the PLA scaffolds to generate a predefined, structurally tailored hydrogel microstructure inside the PLA scaffold (see Addendum A.II.4). In order to assess the viability of this concept, the cell survival after UV-crosslinking is a key

element. To this end, PLA scaffolds were immersed in a solution containing gel-MOD dissolved in cell medium in the presence of 0.05 wt% Irgacure® 2959 and MC3T3 cells (i.e. mouse pre-osteoblasts), followed by UV-induced crosslinking (see Figure 48). After seven days, the scaffolds were stimulated with differentiation medium (DM). The cell viability and the ability to proliferate were characterized using different techniques including presto blue staining and live/dead staining. In order to verify whether the cells maintained their differentiation potential in the osteogenic lineage after UV-curing, alkaline phosphatase (ALP) staining and gene expression with quantitative reverse transcription polymerase chain reaction (qRT-PCR) for RUNX2 and osteocalcin were performed by Marica Marcovic of the Institute of Materials, Science and Technology at the Vienna University of Technology.
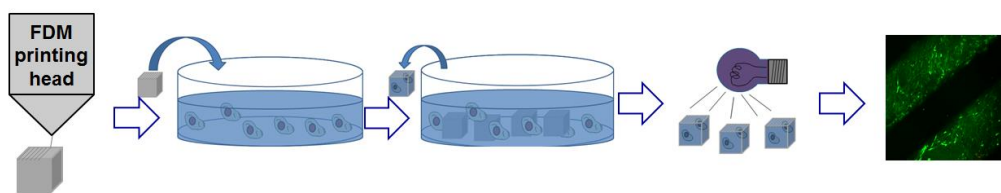
Figure 48: Scheme demonstrating the general principle of introducing a cell-gel-MOD solution inside a PLA scaffold.

2.4.2.1 Characterization of the cell viability and the proliferation

2.4.2.1.1 Determination of the metabolic activity using Presto Blue staining

In order to determine the metabolic activity of the cells encapsulated in the combination scaffolds at certain time points, Presto blue staining was performed. Presto Blue is a resazurin-based solution which can be applied to determine cell viability in a quantitative manner. The reagent contains a blue compound (i.e. resazurin) which is able to pass through the cell barrier. Inside a metabolically active cell, the resazurin will be reduced rapidly generating resorufin which is red in color and highly fluorescent. By measuring the obtained fluorescence, a quantitative assessment of the metabolic activity can be realized.
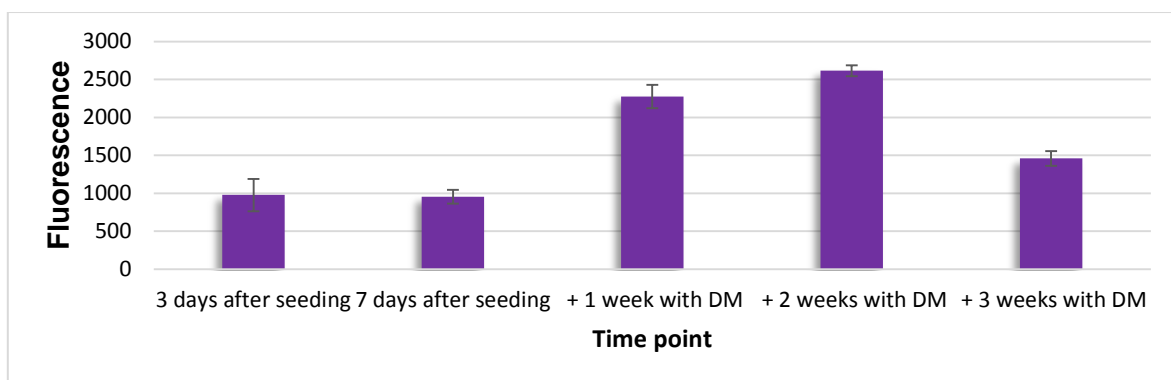
Figure 49: Results of a presto blue assay revealing the observed fluorescence at different time points.

Evaluation of the generated fluorescence in the scaffolds after Presto Blue staining confirmed an increase in cell proliferation with a maximum after 3 weeks in culture. This increase in metabolic activity probably originates from two effects. On the one hand, the cell proliferation increases, which results in a higher overall metabolic activity. In addition, introducing the differentiation medium is likely to increase the metabolic activity of the viable cells.

In parallel with the presto blue staining, an estimation of the cell number was realized through DNA isolation (see Table 4). At a maximum fluorescence, the cell number estimation revealed that the amount of cells present was close to the initially seeded 500000. This demonstrates that cells can sufficiently survive the harsh UV-crosslinking conditions. After 3 weeks, a drop in cell number and metabolic activity was observed. The reason for this phenomenon remains unclear to date. A possible explanation might be that the scaffolds have become saturated with mature osteoblasts at this point and because of the slow degradation of the scaffolds, the cells are not provided with enough additional space, inducing cell apoptosis.

Time line	Metabolic activity (fluorescence)	Cell number estimation
3 days after seeding	977 ± 212	-
7 days after seeding	954 ± 92	160000
+ 1 week with DM	2274 ± 155	365000
+ 2 weeks with DM	2615 ±70	420000
+ 3 weeks with DM	1459 ± 98	260000

Table 4: Monitored metabolic activity obtained via presto blue staining and comparison with the estimated cell number based on DNA isolation.

2.4.2.1.2 Qualitative evaluation of cell viability through live-dead staining

The live/dead staining images were obtained using confocal microscopy. Figure 50, A reveals the presence of a few dead cells, probably as a consequence of the UV irradiation. Interestingly, Figure 50, B depicts an almost complete absence of dead cells indicating that cell proliferation occurred. Three weeks after the addition of DM, however, an increase in dead cells was again observed, which is in agreement with the results obtained via Presto Blue staining and DNA quantification (see Figure 50, C).
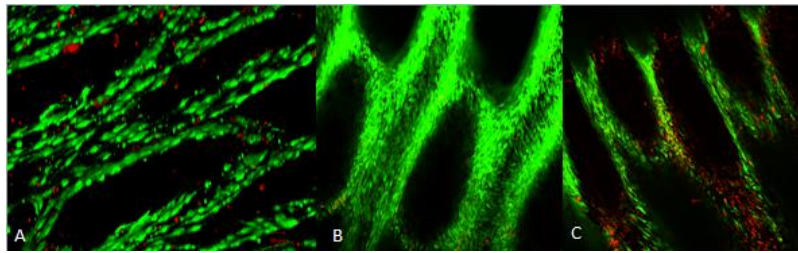
Figure 50: Confocal microscopy images obtained from live/dead staining after 1 week, 2 weeks and 3 weeks in the presence of differentiation medium (A, B and C respectively)

In addition to the qualitative results regarding cell viability, an elongated cell morphology was observed which is an indication that the cell adhesion onto the gelatin encapsulated PLA struts was successful.

2.4.2.1.3 Evaluation of the differentiation potential using alkaline phosphatase staining

Alkaline phosphatase (ALP) is an enzyme which plays an important role in osteogenesis [192]. Therefore, staining of the scaffolds with a compound that exhibits green fluorescence in the presence of ALP (i.e. ALP LIVE stain) is a powerful tool to enable the qualitative evaluation of osteogenesis. Cells undergoing osteogenesis will typically give rise to a green fluorescence which can be visualized using confocal microscopy.
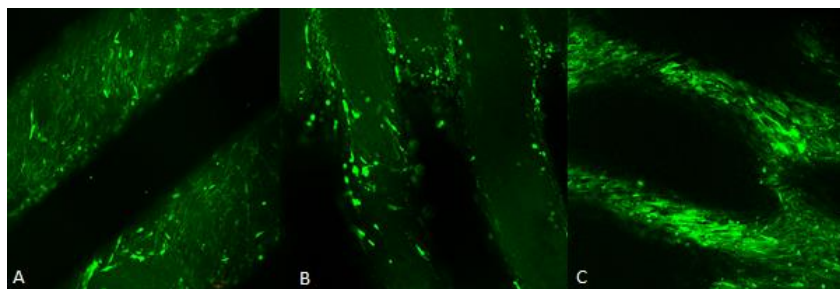
Figure 51: ALP staining of the cell-encapsulating scaffolds revealing cells undergoing osteogenesis after 1 week in DM (A), 2 weeks in DM (B) and 3 weeks in DM (C).

The confocal microscopy images after ALP staining revealed an increase in the amount of cells exhibiting green fluorescence as a function of time. Even after three weeks, an increase in osteogenesis was still observed despite the drop in cell number, proving that the osteoblasts are mature, mineral-forming and healthy osteoblasts.

2.4.2.1.4 Gene expression evaluation using qRT-PCR

Quantitative real time polymerase chain reaction (qRT-PCR) is a method which is used to amplify and quantify a target sequence in a DNA molecule simultaneously. In a first step cDNA is synthesized using RNA as a template sequence. Next, the cDNA is amplified using a primer and reverse transcriptase in the presence of a substance marked with a fluorophore which enables

the number of 'copies' to be quantified via the detection of fluorescence. In qRT-PCR, the presence of a particular DNA sequence is measured after each PCR amplification cycle.[193]

In the present work, the target genes were RUNX2 and osteocalcin as these genes are important markers in the osteogenesis process. The plots in Figure 52 reveal an initial increase for the RUNX2 gene which is generally detected in pre-osteoblasts and increases in immature osteoblasts. After 2 weeks in DM, a down-regulation in the RUNX2 gene is observed, alongside an up-regulation in osteocalcin. These results indicate the presence of mature osteoblasts as upon maturation, the production of RUNX2 is inhibited.[194]
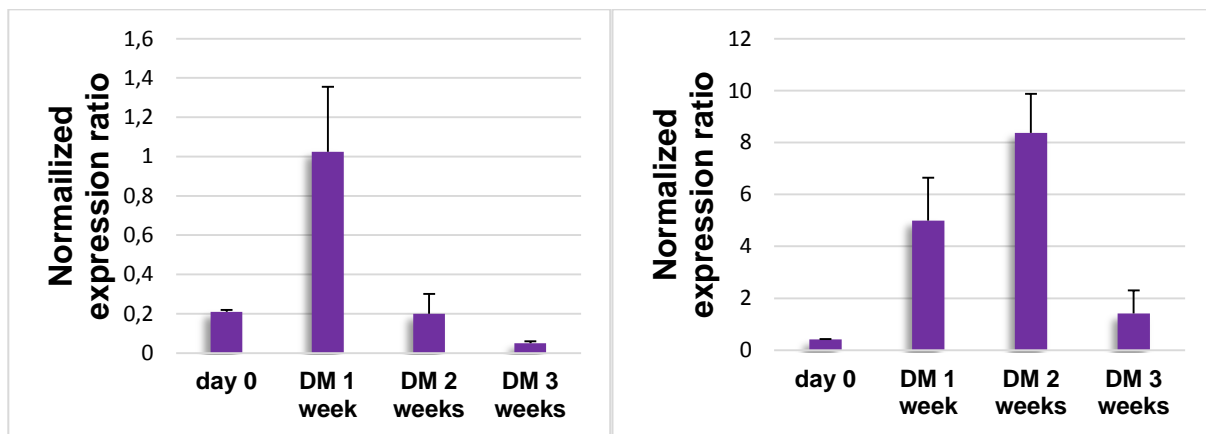
Figure 52: Plots revealing the RUNX2 (left) and osteocalcin (right) gene expression in the cell-encapsulating scaffolds at different time points.

2.4.3 Conclusions and future perspectives

The combination of the different cell characterization assays results in some key observations. Not only do the cells survive the harsh UV-crosslinking conditions, their differentiation potential is preserved as after stimulation, the presence of osteogenesis proved the differentiation from pre-osteoblasts to mature osteoblasts. However, an increase in cell death alongside a drop in metabolic activity was observed after three weeks in differentiation medium. This phenomenon is probably occurring as a result of spatial obstruction, originating from the slow scaffold degradation. Ongoing work includes the comparison of the cell response using scaffolds generated via the cryogel approach with the scaffolds generated by UV-crosslinking cell-encapsulating gel-MOD solutions introduced in the PLA scaffolds. The latter strategy will yield the most viable approach towards cell seeding efficiency, viability and proliferation to be applied in future work aiming at tissue engineering.

3. General conclusions and future perspectives.

The ultimate goal of the present study was to clear the road towards the application of 2PP to generate a cell-encapsulated, predefined, structurally tailored hydrogel microstructure inside a PLA scaffold obtained via FDM. As this method would drastically increase the cell seeding efficiency, combined with the ability to tailor the scaffold towards the optimal morphology, ideal conditions can be realized for the envisioned tissue engineering approach. Ideally, the applied hydrogel materials should exhibit both sufficient mechanical strength as well as a beneficial bio-interactivity.

In a first part, gelatin type B was successfully derivatized to yield photo-crosslinkable hydrogel precursors. These derivatizations included among other the reaction of the amines and the carboxylic acids present in the gelatin backbone with methacrylic anhydride and/or aminoethylmethacrylate respectively to yield gel-MOD and gel-MOD-AEMA. Moreover, gelatin type B was also derivatized with coumarin functionalities in order to obtain a reversible, initiator-free crosslinkable system. Although this derivatization was proven successful via ^{1}H NMR spectroscopy, the successful crosslinking has not yet been achieved to date. Further research will be performed towards the application of lasers to realize coumarin dimerization and thus reversible crosslinking of gelatin. In addition, preliminary experiments have been performed towards the introduction of a photo-initiator (i.e. Irgacure 2959) on the gelatin backbone to yield an in situ crosslinkable hydrogel material. The details of these experiments were however not incorporated in the present work due to time constraints.

In a second part, the gel-MOD and gel-MOD-AEMA derivatives were successfully crosslinked by applying UV irradiation in the presence of Irgacure 2959 to develop 2D films for characterization purposes. An in-depth characterization using a plethora of assays including HR-MAS ^{1}H-NMR spectroscopy, gel-fraction determination, swelling experiments and rheology indicated that the incorporation of additional methacrylate groups in gel-MOD not only increased its mechanical properties, but also increased the crosslink efficiency. In addition to the increase in mechanical properties, preliminary cytotoxicity tests revealed that a comparable cell viability was observed as for gel-MOD. These observations were apparent both for the materials in crosslinked as well as in the uncrosslinked state. These results are remarkable as a substantial increase in double bonds is present in gel-MOD-AEMA relative to gel-MOD. These preliminary cell tests are extremely promising towards future applications of gel-MOD-AEMA as gel-MOD has already proven its success in the field of tissue engineering. [86][134][168] The results therefore clear the road towards the application of gel-MOD-AEMA for tissue engineering applications. In

addition, the substantial increase in mechanical properties should render gel-MOD-AEMA very suitable towards the application of 2PP as this is anticipated to result in a better geometric reproduction of the applied CAD model.
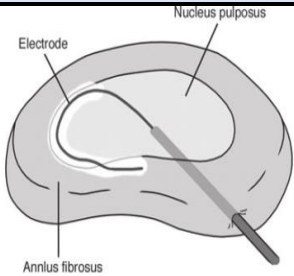
In a third part, 3D scaffolds have been produced using FDM to investigate the potential of a combination of a PLLA scaffold for its mechanical properties with a gelatin hydrogel for its bio-interactive properties. To generate reproducible PLA scaffolds, a custom program was written in VBA which enables a precise control over the pore size and the external dimensions of the scaffolds produced via FDM. These PLA scaffolds were then combined with a gel-MOD hydrogel which was subjected to a cryogenic treatment to introduce a porous microstructure inside the PLA scaffolds. In parallel, a cell-encapsulating gel-MOD solution was combined with the PLA scaffolds prior to crosslinking to assess the cell viability after applying a UV treatment for crosslinking purposes. The obtained PLA-cryogel combination scaffolds were characterized using a variety of methods including digital microscopy, µCT and SEM. These methods illustrated the presence of a porous gelatin network inside the PLA scaffolds. However, at present, cell studies on the combination scaffolds are still ongoing. Interestingly, for the second approach, the biological assays in which MC3T3 preosteoblasts were encapsulated into the gel-MOD solution prior to crosslinking were promising. Preliminary cell work not only indicated a high cell viability after UV-irradiation, but also illustrated that the cells maintained their ability to differentiate into mature osteoblasts.
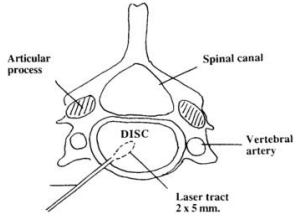
The results obtained in the present study not only revealed the success of the encapsulation of cells in the hydrogel precursors to increase cell seeding efficiency, but also proved that the developed hydrogel materials in combination with PLA scaffolds are promising tools towards the targeted aim. The combination of two different material classes with various SFF techniques is a valuable approach to yield perfectly tailorable scaffolds for tissue engineering purposes.

Addendum A (Introduction): Tables and additional information.

A.I Tables

Table 1: Overview of clinically applied IVD degeneration treatments

Conventional treatments				
Methodology	**Description**	**Benefits**	**Drawbacks**	**Illustration**
conventional physiotherapy	a combination of oral analgesics, exercise and physiotherapy [2]	* non-invasive * no revalidation	*symptomatic treatment *it takes months to obtain 'satisfactory' results	
Chemoenucleolysis	* treatment of herniatic IVD when conventional methods have failed *chympopain injected directly in NP, dissolves proteoglycans shrinks bulging disc, leaves AF intact [2][56][26]	*Back pain is diminished instantly *minimally invasive procedure	*complications(anaphylaxis) *Healing after nucleotomy is observed by formation of vascular tissue through ruptures in the bony endplates, can cause pain	 I50DDM degeneration of NP in disc 10 days after injection
Ozone chemonucleolysis	*treatment of herniatic IVD *injection of ozone/oxygen mixture into paravertebral musculature and in the herniated zone [2]	* painless *Well-tolerated	*insufficient published data to show the effects of treatment	
Minimally invasive procedures				
Methodology	**Description**	**Benefits**	**Drawbacks**	**Illustration**
Annuloplasty				
IDET (intradiscal electrothermal therapy)	* alternative to vertebral body fusion *treatment for crhronic discogenic lower backpain *thickens collagen, leading to a contraction and a diminishment in vascular and neural ingrowth *An electrode is inserted in the defective area and heated to 90°C [2][195]	*minimally invasive *Patient is discharged on the same day *can lead to a reduction of annular fissures *can increase the stability of the disc itself *low cost	*not possible for inflammatory arthritis, medical or metabolic conditions that exclude proper follow up *limited amount of long term results availiable *thermocoagulation of the nociceptors within the annular walls can occur *possible complications: catheder breakage, post IDET disc herniation, infection, abscess, spinal cord damage *moderate evidence to prove effectiveness of the treatment	 Schematic picture showing the introduction of the electrode into an IVD.
RFA (radiofrequency annuloplasty)	*treats patients with chronic low back pain, often the result of internally disrupted discs *discTRODE™ cannula is inserted in outer disc tissue under X-ray guidance *Radio frequency current flows through the electrode, locally heating the adjacent tissue, coagulating and thickening the collagen present. [2]	*minimally invasive *low cost *few side effects compared to surgical options	*complications: catheter breakage, nerve root injuries, discitis, disc herniation, epidural abscess, spinal cord damage *only short term evidence for benefits	

IDB (Intra discal Biacuplasty) (kapural)	*new annuloplasty procedure *bipolar system of two RF electrodes is used *electrodes are placed on opposite posterolateral sides of the defective annulus fibrosus [2][24]	*minimally invasive *lower peak temperature compared to IDET leads to better tolerance *short procedure *can be used in discectomized discs *relative ease for placement of electrodes compared to RFA and IDET	*insufficient long-term data on long term effects.	 X-ray image showing the placement of both electrodes
Percutaneous disc decompression				
Laser discectomy	* patients with herniated IVD * A laser is inserted into the NP by means of a catheter with fluoroscopy *laser irradiation, removes small portions of the NP, enabling the herniation to shrink. [2][196]	*minimally invasive *patients can return home the same day *very localized tissue removal *can be applied on patients with spinal stenosis and IDD	*scarcity of clinical trials * steep learning curve for the surgeon *Increases difficulty level for surgeon *moderate evidence for success	 Needle positioning for laser disc decompression
RF coblation (Plasma discectomy)	* patients with herniated IVD *The device is entered into the NP through a needle guided by fluoroscopy *NP is ablated with RF when introducing the device *tissue is transferred to gas by molecular dissociation, which is removed through the needle *after removal of the device, coagulation takes place by thermally treatment of the canal which leads to a denaturation of nerve fibers [2]	*minimally invasive	*not applicable to patients with spinal stenosis *loss of disc height of 50%, severe disc degeneration *spinal fraction *tumor *moderate evidence of success	
Mechanical disc decompression	*dekompressor is a handheld device, connected to a helical probe, the probe rotates thus sucking out milled tissue from the NP *The dekompressor is placed into the IVD using fluoroscopic guidance [2]	*minimally invasive *short surgical procedure times	*results on this procedure are still limited *moderate evidence of success	 Placement of the device into the inflamed disc on a skeletal model
manual PLD (percutaneous lumbar discectomies)	A probe is inserted, slicing tissue in the IVD, which is succequently sucked out. [2]	*minimally invasive *relatively short surgical procedure times	*varying results	
Regional endoscopic techniques				
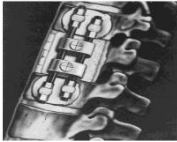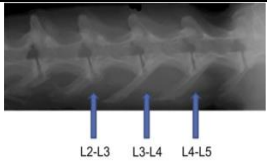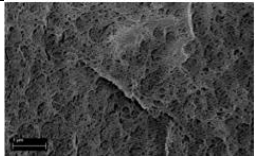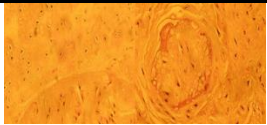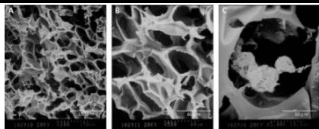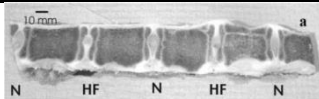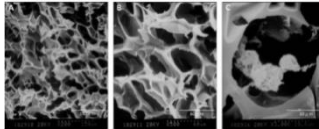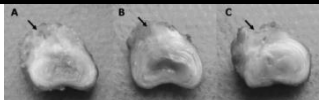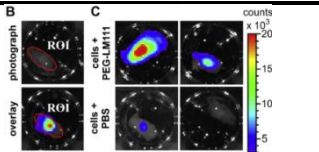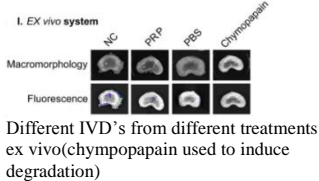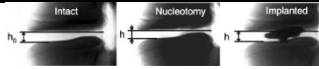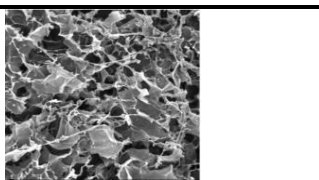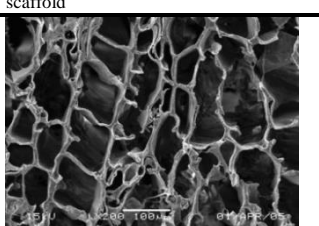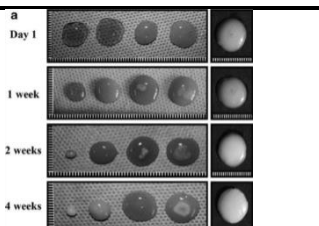
Lumbar discectomy	Using an endoscope inserted through a needle, very local pieces of the prolapsed disc can be removed under direct vision [2]	*ultimate form of minimally invasive spinal surgery *immediate pain relief *patient can go home within 24 hours		
Major surgical procedures				
Methodology	**Description**	**Benefits**	**Drawbacks**	**Illustration**
Spinal fusion				
	The vertebral bodies adjacent to the traumatized IVD are fused together using somekind of fixation device [9][146]	*reduction of complaints	*No restoration of disc function *may lead to further degeneration of adjacent IVD's due to loss of mechanical function *alters biomechanics of the spinal column	 model of a spinal fusion device attached to the spinal column
Artificial IVD replacements				
	The traumatized IVD is surgically removed and replaced by an artificial one. [4][31][9]	*restoration of the motion of the IVD	*cannot sustain compressive forces *production of wear debris which can induce osteolysis *stress transfer to vertebrae *possibility of implant failure *little long term results	 Model of a IVD implant produced by Rapid manufacturing.

Table 2: Materials applied for tissue engineering of the nucleus pulposus

materia l class	Applied materials	Material properties	Cell source	Description	Benefits/ Drawbacks	Stage	Illustrations
				Injectable			
Collagen	Collagen	*protein *main ECM constituent	*rabbit NP cells *human mesenchym al stem cells (MSC) s	rabbit and human MSCs encapsulated in collagen microspheres containing rabbit NP derived ECM, followed by injection into rabbit IVDs [52][152][152]	+higher hydration level observed +hMSCs survived and synthesized new ECM +increase in type II collagen production and GAGs -further optimization of culture conditions required	*in vitro, 24 days *in vivo, 6 months	X-ray image of inserted NP materials in rabbits
	Collagen II/PEG/H A	*ECM components *4-star PEG is non-toxic cross-linker	*rabbit adipose derived stem cells	*collagen II hydrogels in situ crosslinked 4S-star-PEG cross-linkers [47]	+high NP cell viability +HA stimulates ECM synthesis, proliferation, migration and phenotype maintenance +HA is anti-inflammatory and anti-vascular +ideal setting time (1h) for clinical applications +stable in culture -poor mechanical properties of non-cross-linked collagen II	in vitro, 14 days	Picture of a seeded NP hydrogel
	Atelocolla gen	*ECM component in NP	*rabbit MSCs *bovine NP	*Injectable + in situ cross-linkable *enzymatic crosslinking using mTGase [10][53]	+ideal for injection +good biocompatibility -animal origin, risk for disease transfer -weak mechanical properties -degradative resistance properties -scaffolds size reduction observed after 7 days	in vivo, 8 weeks	
Cellulose	Cellulose composite	*polysaccharide fibers to tune mechanical properties	*human, fetal cartilage cells	injection in the NP in the absence of cells [42]	+mechanical properties are maintained for a long period +in situ UV curing +biocompatible	in vitro, 1 week	Cryo-SEM-image of the composite hydrogel, showing a porous structure
Gelatin	Gelatin	*derived from collagen (ECM component)	*rabbit MSCs	fibrinous gelatin + MSCs + growth factors injected in the NP [23]	+decrease in disc height was slowed down +increase in aggrecan and collagen type II +decrease in collagen type I +lower apoptosis rates +injectable	in vivo, 12 weeks	Presence of a lot of spindle cells in the NP after 12 weeks
	Ferulic acid-gelatin/chi tosan/glyce rol phosphate	*therapeutic effect	*rabbit NP cells	*thermosensitive hydrogel as carrier for ferulic acid in NP repair, liquid at room temperature, turns into a gel at physiological temperatures *FA attached to gelatin through amide bond formation [55]	+no cytotoxicity +good gelation and handling properties for clinical application +FA leads to a reduction in inflammation +upregulation of collagen II and aggrecan +FA prevents proteoglycan degeneration	in vitro, 3 days	

Hyaluronic acid	**oxi-HAG-ADH (hyaluronic acid-gelatin-adipic acid dihydrazide hydrogels) [14]**	*components of ECM in NP	*rabbit NP cells	injectable hydrogel combined with NP cells and cross-linked using EDC and NHS [17]	+sterilizable +comparable visco-elastic properties -crosslinking required -slight drop in cell viability due to unreacted aldehyde groups +no fibrous tissue replacement or disruption of bony end plates +large amount of chondrocytes in center of the disc +no necrosis or inflammation +good cell viability +straightforward +cost-effective	in vitro, 3 days	SEM images of seeded hydrogels after lyophilization
	Hyaluronan HYAFF 120 & HYADD 3	*major component of NP	*pig bone marrow stem cells	*injection of hyaluronan and homologous bone marrow stem cells [12]	+no fibrous tissue replacement or disruption of bony endplates +large amount of chondrocytes in center of the disc +no necrosis or inflammation +good cell viability +straightforward +cost-effective	in vivo, 6 weeks	Comparison between normal NP IVD's (N) and IVD's where the NP is replaced by the injected hyaluronic derivative
	Oxi-HA/ADG	*ECM component	*six month old rabbit NP cells	*injectable oxidized hyaluronic acid/adipic acid dihydrazid [17]	+transform from liquid to solid within minutes +can maintain its shape for at least 5 weeks before degrading +collagen type II and aggrecan synthesis +nice mechanical properties +good biocompatability -some cytotoxicity; not observed when increasing ADH percentage	in vitro, 72 hours	SEM images of seeded hydrogels after lyophilization
PEG	**PEG/HA/PPS (Pentosan polysulphate)**	*HA is ECM component *PEG is a thermoplastic aromatic polyester	*hMSCs	*PEG and HA enzymatically cross-linked using horseradish peroxidase [20]	+PPS aids in viability and chondrogenesis of MSCs +increased ECM production +no significant immunogenicity +crosslinking under physiological conditions +resemblance to natural NP +upregulation of ECM production +no growth factors required -PPs slows gelation speed and diminishes swelling -little difference in viability with or without PPS	*in vitro, 21 days *in vivo, 14 days	Comparison between, discectomized IVD(A): scar tissue, presence of scaffold without serum coating(B) no regeneration and scaffold dipped in serum(C) regeneration
	Laminin functionalized PEG	*PEG is a thermoplastic aromatic polyester *laminin is a protein present in cellular tissue	*porcine NP cells	*injectable laminin functionalized PEG [49]	+suitable gelation time (20 min) +laminin induces adhesion, survival, migration and differentiation +increase in cell retention +Tunable mechanical properties +No need for initiator (addition of free thiols and PEG acrylates)	*in vitro, 14 days *in vivo	In vitro comparison in cell retention between cellulose carrier(above) and carrier free introduction

Platelet rich Plasma (PRP)	PRP (platelet rich plasma)	*blood plasma enriched with platelets	*porcine MSCs	injection of mixtures of MSCs with platelet-rich plasma [56]	+height was increased +increase in mRNA +ECM synthesis +collagen II and aggrecan +good bio-interactivity +low immunogenicity -osteogenesis after 7 days	*in vitro, 4 weeks *in vivo, 2 months	 Different IVD's from different treatments ex vivo(chympopapain used to induce degradation)
Chitosan	Chitosan	*linear polysaccharide with antimicrobial properties	*bovine NP cells	*chitosan injection *in situ crosslinking using genipin [21]	+minimally invasive +good immunogenic properties +temperature induced gelation (37°C) +no detectable leakage through the AF +tunable crosslinking time, ideal for injection -chitosan soluble at physiological pH -poor mechanical properties	*in vitro, 24 hours *in vivo, several months	 Injected chitosan hydrogel in human cadaver IVD

Scaffold introduction				

Alginate	Alginate	*Anionic polysaccharide	*milk goat NP cells	2D alginate discs [22]	+mimics mechanical and cell-adhesive properties of the NP +inexpensive +no adverse tissue reactions -loss of stiffness over time -poor cell-scaffold coupling	in vitro, 4 weeks	
Collagen	Collagen	*ECM protein	none	*Introduction of scaffolds in IVDs explanted from calve cadavers *implant = collagen matrix [48]	+reinforcing and supporting the culture of nucleus cells +slight increase in disc height +mechanical stability comparable to native NP -extrusion of implant through surgically induced defect in AF upon mechanical stress	in vitro	 comparison of disc height between intact, nucleotomized and implanted IVD
	Atelo-collagen	*ECM protein	*rabbit NP cells	scaffold production by lyophilization + TGF-β1 and BMP-2 [38]	+30% increase of ECM +good biocompatibility +good immunogenic properties -atelocollagen is prepared from animals, risk for disease transmission	in vitro, 2 weeks	 SEM image of seeded atelocollagen scaffold
	Collagen II/hyaluronan/chondroitin-6-sulphate composites	*ECM components	*rabbit NP cells	*scaffold constructed using lyophilization [40]	+complete scaffold replacement by vascularized granulation tissue after 84 days +ECM production +disc height decrease retarded +low immunogenicity -collagen II crosslinking required	*in vitro, 7 days *in vivo, 24 weeks	 SEM image of produced seeded lyophilized scaffold
Silk	Silk-fibrin HA composites	*silk is a natural protein fiber *HA is unsulphated glycosaminoglycan present in cartilaginous ECM	*human chondrocytes	*Seeded silk-fibrin hyaluronic acid scaffolds [19]	+silk is added to HA gel to obtain improved mechanical properties +excellent cell interaction +silk slows degradation rates and maintains the mechanical properties +superior mechanical strength -slight drop in cell proliferation compared to HA scaffolds	in vitro, 4 weeks	 Morphological changes upon degradation of different composites after 4 weeks
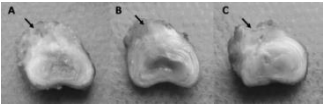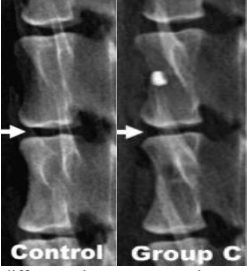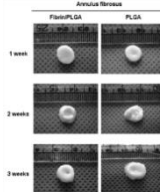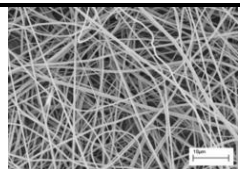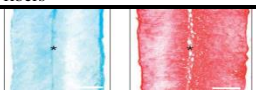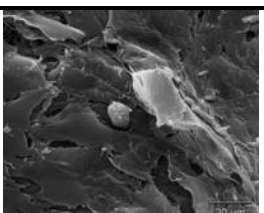
Material class	applied materials	Material properties	Cell source	Description	Benefits/Drawbacks	Stage	Illustration
Poly-(glycolic acid)/Hyaluronic acid	PGA/HA	*HA is a unsulphated GAG present in ECM *PGA is a biodegradable, aliphatic polyester	none	PGLA scaffold incubated in HA and freeze-dried [20]	+increase in height of IVD after 6 months +repair tissue was present in the IVDs +no need for scarce donor cells +only one surgical intervention necessary +long shelf life for the scaffolds	in vivo, 6 months	Comparison between, discectomized IVD(A): scar tissue, presence of scaffold without serum coating(B) no regeneration and scaffold dipped in serum(C) regeneration
Poly (lactide-glycolic acid)	PLGA	*biodegradable aliphatic polyester	*beagle dog NP cells	*cell seeded PLGA scaffold introduced in IVD *scaffolds produced using a mold and a temperature gradient to obtain microtubuli followed by lyophilization [11]	+slower disc degradation +height of discs higher +scaffolds degraded completely after 4 weeks +increase in chondrocyte-like cells and ECM +good biocompatibility +tunable mechanical and degradation properties	in vivo, 8 weeks	difference between control group(discectomized) and seeded implant after 8 weeks

Table 3: Materials applied for tissue engineering of the Annulus Fibrosus

Material class	applied materials	Material properties	Cell source	Description	Benefits/Drawbacks	Stage	Illustration

polyesters	**PLGA/fibrin**	*fibrin is a non-globular protein involved in blood clotting *PLGA is a polyester serving a mechanical function	*rabbit IVD cells	scaffolds produced by solvent casting/salt leaching technique [58]	+increase in ECM +homogenous cell distribution	in vitro, 3 weeks	 Fibrin/PLGA scaffold(left) retains its shape better than a PLGA only(right) scaffold.
	PLLA	*biodegradable aliphatic polyester	*bovine AF cells	*PLLA scaffolds + growth factor TGF-β1 *scaffolds prepared by electrospinning *randomly oriented PLA fibers [36]	+nice mechanical properties +biodegradable +good cell viability +increase in GAG and collagen +thick ECM layer +could be applied as a 'cork' material to close local defects	in vitro, 3 weeks	 SEM image of the PLLA/TGF fibers
	PCL	*biodegradable aliphatic polyester	*bovine MSCs	*aligned electrospun fibers [61]	+slow degradation rate +accumulation of s-GAG and aligned collagen after 10 weeks +successful inter-lamellae connection +comparable tensile modulus +improved mechanical properties -collagen and GAG lower than in native AF -no replication of intra-lammelar collagen organization	in vitro,10 weeks	 Alcian blue and Picrosius red staining of opposing bilayer cross-sections after 10 weeks showing the inter-lamellar space
			*porcine AF cells	*electrospun PCL scaffolds loaded with berberine were compared to electrospun PCL scaffolds [63]	+increase in cell attachment on berberine scaffolds. +no significant cell death +increase in sGAG and collagen content	in vitro,7 days)	 SEM image of the berberine-PCL fibers
Silk	**Silk**	*Natural protein fiber	*rabbit MSCs	* knitted silk fiber scaffolds represent native AF lamellae *comparison between static and dynamic setup [13]	+cells survived under repeated mechanical stress +increase of col II and decrease of col I compared to static culture +similar ECM structure +appropriate mechanical properties -drop in cell numbers and viability upon repeated mechanical cycles	in vitro, 4 weeks	
			*human nasal chondrocytes	scaffolds through diagonal winding of silk fibers to generate the collagen orientation in the lamellae [37]	+alignment along the fibers of chondrocytes and ECM was observed +supported chondrogenic redifferentiation +increase in collagen II and GAG	in vitro, 4 weeks	Image of a produced silk fibroin seeded scaffold after 4 weeks of culturing
	silk-RGD-peptide	*peptidesimmobilization on the surface	*bovine AF cells	*scaffolds produced by salt leaching resulting in sheets *silk scaffolds surface modified with RGD peptide [62]	+little immune response +controllable degradation rate +increase in collagen II and aggrecan +increase in proteoglycans on the RGD modified scaffolds after 14 days -after 8 weeks no significant difference anymore +cells grown on the RGD-modified scaffolds showed more inner AF properties -RGD modified scaffolds showed lower cell count after 8 weeks of culturing	in vitro, 8 weeks	 SEM image of RGD modified, cell seeded scaffold, showing spherical chondrocytes and ECM.
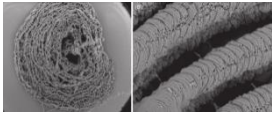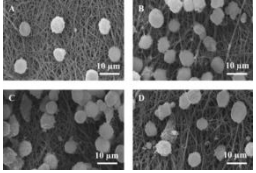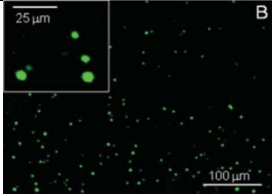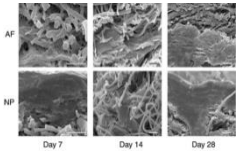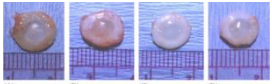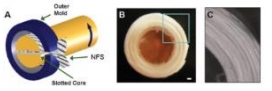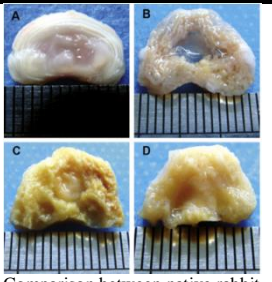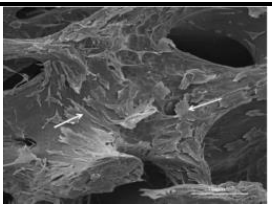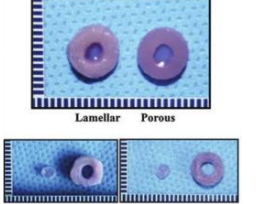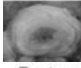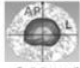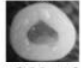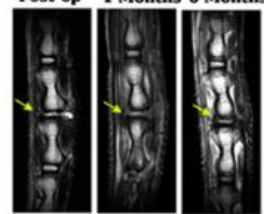
Material class	Applied materials	Material properties	Cell source	Description	Benefits/Drawbacks	Stage	Illustrations
Polyurethane	**PU**	*organic units linked by carbamate bindings	*Bovine IVD cells	*PU scaffold prepared by rapid manufacturing of biodegradable elastic polyurethane [4]	+suitable elastic properties +very precise architecture closely mimicking the natural structure of AF +aligned chondrocytes present +very reproducible scaffold construction -compressive properties in the low range	in vitro, 19 days	 SEM image of the scaffold closely mimicking the structural properties of native AF
	Polyurethane-polycarbonate/Anionic dihydroxyl oligomer (PU-PC/ADO)	*PC-synthetic thermoplastic polymer joined by carbonate bonds *PU-organic units linked by carbamate bindings	*bovine AF cells	*surface modified PU-PC scaffolds using ADO *scaffolds produced by electrospinning [64]	+increase in cell attachment and collagen for ADO scaffolds+spherical cell morphology +ECM production +nice degradation products	in vitro, 7 weeks	 SEM images of AF cells seeded onto the scaffolds, increasing amount of cells with increasing amount of ADO
Alginate	**Alginate/chitosan**	*alginate-polysaccharide obtained from seaweed *chitosan-linear polysaccharide	*canine AF cells	*scaffold construction bywet-spinning followed by lyophilization resulting in felsts with alligned fibers [69]	+good cell compatability +biodegradable +antimicrobial functions +beneficciel scaffold degradation timeframe +cell alignment +deposition of ECM +collagen type I & II and aggrecan expression	in vitro, 10 days	 Image of the fiber scaffolds before(left) and after (right) lyophilization
Fibrin	**genipin-crosslinked fibrin hydrogels**	*non globular protein, involved in blood clotting	*human AF cells	*injectable fibrin hydrogels are obtained by using genipin as a cross linker [70]	+comparable modulus to native AF tissue +tunable mechanical properties +cell compatible +adhesive to AF tissue, can be used for gap filling +injectable +genipin has anti-nflammatory properties -poor mechanical properties	in vitro(culture in 6-wells for up to 7 days)	 Image of calcein stained cells after 7days of culture, a round morphology is clearly observed.

Table 4: Materials applied for tissue engineering of the complete IVD

Material class	Applied materials	Material properties	Cell source	Description	Benefits/Drawbacks	Stage	Illustrations
polyesters	**PLIA+HA**	*HA is an unsulphated GAG present in ECM *PLA is a biodegradable aliphatic polyester	*hMSC	*A PLA scaffold constructed by electrospinning *seeded HA NP injected using a syringe [59]	+biocompatibility +Uniform cell loading in the AF region +similar cell architecture compared to native tissue +ECM production +GAG production +ECM resembled native IVD	in vitro, 28 days	 SEM images of the seeded scaffold, increasing amounts of ECM were deposited over time

72	**PGA/PLA+ alginate**	*PGA/PLA are biodegradable aliphatic polyesters *alginate is an anionic polysaccharide	* sheep AF and NP cells	*scaffolds produced from PGA fiber mesh coated with PLA to produce AF *seeded alginate hydrogel NP by injection [73][81]	+increase in proteoglycan and GAG +The GAG content in NP was similar to native tissue +comparable mechanical properties +oriented cell structures present +ECM matrix production observed	*in vivo*, 16 weeks	 Images of produced IVD before implantation and after 4.6 and 16 weeks in vivo.
	PCL+ agarose	*PCL is a biodegradable aliphatic polyester	*porcine chondrocytes	*AF = seeded electrospun oriented PCL fibers *NP = cell containing agarose gel [76]	+cellular along the fibers +nice cell viability+nice cell distribution +higher modulus than agarose gel alone	*in vitro*	
			*bovine AF/MSC	*aligned fiber PCL scaffolds produced by electrospinning spot welded together in several layers in a custom mold, core was cut out and replaced by an agarose solution [72]	+mechanical behavior similar to native tissue +distinct cell morphology observed comparable to native tissue +Ordered ECM deposition +reproduction of lamellar structure +accrued collagen and GAG increase +increase in compressive modulus	*in vitro*, 7 days/6 weeks	 Scaffold production(A), image of the obtained scaffold(B), close-up of the layered structure (C)
Gelatin	**Demineralized bone matrix gelatin (DBMG) +collagenII /hyaluronate/chondroitin-6-sulfate**	*collagen/HA/CS are major ECM components	*AF and NP cells from rabbits	*DBMG cut into shape of AF by scalpel prior to lyophilization *CII/HyA sponges prepared and cross-linked to CS through EDC/NHS *NP and AF cross-linkedusing EDC/NHS *2 scaffold regions seeded separately [57]	+Good biocompatability +morphology and histology resembled native IVD. +increase in proteoglycan and hydroxyproline over 12 weeks +ECM production observed over 12 weeks +good proliferation observed over 12 weeks -DBMG materials lack lamellar structure and show weak biomechanical properties	in vivo, 12 weeks	 Comparison between native rabbit IVD(A), produced scaffold(B),after 4-weeks(C) and after 12 weeks(D)
	Bone matrix gelatin (BMG)- acellular matrix (ACECM)	*No cytotoxicity and good biocompatibility	*sheep AF and NP cells	*scaffolds produced out of (porcine)bone matrix gelatin(AF) and acellular cartilage extracellular matrix(for NP). * produced by lyophilization and cross-linking [79]	+no cytotoxicity +biocompatible +Collagen II present in NP, collagen I in AFs -low compressive modulus,	*in vitro*	 SEM image of surface of AF covered by cells
Silk	**Silk+fibrin/ hyaluronic acid**	*HA is a major component of the ECM	*porcine AF cells/chondrocytes	*silk scaffolds were produced by moldinggenerating bothlamellar and porous scaffolds followed by lyophilization *HA/fibrin NP [77]	+AF like tissue formation +NP phenotype present+cells in lamellar structure spread homogeneously + integration between AF and NP showing a transition zone comparable to native IVD +increased collagen and GAG content both in AF as in NP -mechanical properties of silk are lower than native AF	in vitro, 2 weeks	 image of the lamellar(left) and porous(right) scaffolds before and after integration of the NP (2 weeks)

Collagen	collagen+ alginate	*Collagen is a major component of the ECM *Alginate is an anionic polysaccharide	* sheep AF and NP cells	*scaffolds through injection molding using a mold obtained by µ-CT and MRI images. *oversized NP scaffold produced by injection moldingto prevent slipping from the AF scaffold. [74][78][80]	+close match in size and properties +disc space maintained +similar proteoglycan and collagen compared to native IVD tissue +good bio integration +potential in reparation of small defects -2 discs failed rapidly (within 4 weeks) due to surgical removal of an intact posterior longitudinal ligament during surgery	*in vivo, 16 weeks/6 months*	 1)Comparison between native IVD, the image based model and the produced IVD 2)X-ray images of the introduced IVD after operation, A month and after 6 months in a rat tail

A.II Overviews

A.II.1 Overview of available cell sources

Tissue engineering of IVD requires a high number of clinically suitable cells[3] and thus forms one of the main obstacles to date[3][19][22][25] since even healthy IVD and especially the NP are characterized by a low cellular density. In addition, extracting cells from healthy IVDs to repair degenerative IVDs can result in an increased degeneration of the healthy disc.[19] As successful regeneration requires more cells than can be harvested from a single IVD, different cell sources have to be addressed. [3][6][59]

At present, different cell sources are under consideration to enable TE of IVD. First, autologous chondrocytes can be obtained from non-spinal sites[19][25] while autologous disc chondrocytes are typically harvested through a discectomy.[44] The benefits of these cells include their similarity with IVD chondrocytes.[19] In addition, the use of autologous cells excludes immunogenic body responses.[44] Secondly, some researchers address the use of allogeneic IVD cells (i.e. cells from a different individual), but this method raises questions concerning immunological reactions, difficulties related to cell culture and preservation and potential disease transmission. Furthermore, this procedure can cause IVD degeneration in the donor.[57] Finally, mesenchymal stem cells (MSCs)[3][6][10][23][26][51][60][61][197] or bone marrow stromal cells (BMSCs) can be applied as they are not yet differentiated and multipotent (cfr. able to differentiate into a large variety of cell types).[10] The application of MSCs for IVD regeneration holds several advantages including: [3][10][23][59]

- relatively easy to become harvested from bone marrow
- straightforward *in vitro* culture
- self-renewal and expansion behavior
- low immunogenicity ruling out tissue rejection post implantation
- differentiation possible into a variety of cells including cell types present in the AF and the NP

Unfortunately, the application of MSCs also holds some risk as these cells exhibit the ability to transform into a large variety of cells. The latter can become troublesome upon leaking from the implant site and the formation of osteophyte.[25] Interestingly, the *in vitro* manipulation of the cells prior to the implantation (cfr. coculture with NP cells), forms a viable alternative to generate large populations of the appropriate cells to realize TE of the NP.[3][6]

74

A.II.2 Future developments and perspectives

Although there has already been a lot of research performed in the field of IVD TE, there remain some major concerns and obstacles which need to be overcome before a general consensus can emerge on the ideal approach and the optimal materials to be applied. The main obstacles arising in the TE field of IVD are summarized below.

It has been shown that the occurrence of poor nutritional pathways present in traumatized IVDs combined with continuous mechanical stress present in the spinal column can greatly reduce the viability of the introduced cells. [2][11][18][38]   Additional research thus has to be performed towards the optimization of cell growth under these conditions. In addition, only limited research has been performed towards the integration of cartilaginous endplates into the IVD scaffolds. As these plates serve a crucial role in the attachment to the vertebral bones, it might be a promising topic for further studies. [72][75]

The scarcity and suitability of cell sources remains a major hurdle towards the clinical application of tissue engineering of the IVD. Therefore, the optimization, the culture and the preservation methods of suitable cells have to be studied in depth. [16][52][75]   Furthermore, the idea has been rising to apply notochordal cells for regeneration purposes. [57] The cells are present in the embryonic stage and play an organizing role in the PG regulation by other cells. Moreover, they function as a source of cytokines aiding ECM synthesis, but they disappear during infancy. [16][52][75]   However, as they have been attributed a role during cancer development, the main aim of additional research in this field is related to the transfer of their cytokine producing abilities to the IVD. [25]

Although increasing ECM levels are observed in tissue engineered IVDs, they often don't reach native tissue levels, resulting in the need for additional research towards increasing ECM production. [72] In addition, the complex structural properties of the IVD and mainly the AF are issues affecting successful scaffold production. The use of rapid prototyping is anticipated to rise as the dominant scaffold production process, because of its architectural freedom, patient-specific potential and relatively ease of use. [4]

Furthermore a consensus needs to rise on whether to focus on mimicking the biochemical properties of native IVD in scaffolds prior to implantation [21][72], or to aim at improving nutrient supply, rather than tunable mechanical properties. [74] Moreover, although scaffold production is often successful, additional research should be drawn to optimizing surgical

implantation and fixation methods , as often the success of the TE treatment goes concomitant with these procedures. [16]

Although there is a wide variety of TE routes towards novel IVD tissue, there remains a long road ahead. Additional research also has to be performed towards the possibilities enabling *in vivo* characterization in order to be able to start long-term *in vivo* studies without the need to sacrifice the test objects.[49]

A.II.3 Orbital symmetry required to enable suprafacial $[2\pi + 2\pi]$-cycloaddition of two alkenes
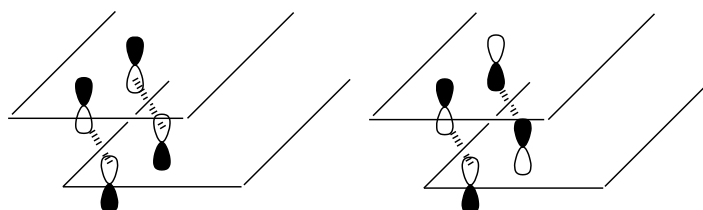
Figure 1: Orbital symmetry required to enable suprafacial $[2\pi + 2\pi]$-cycloaddition of two alkenes.

A.II.4 Two-Photon polymerization (2PP)

Two-photon polymerization is an example of a laser-based technique applying light to initiate the polymerization of a photo-sensitive material. As a result, in contrast with FDM, hydrogel materials can be printed , yet the occurrence of post-drying shrinkage should be taken into consideration.[34] Furthermore, as mild conditions are applied to enable crosslinking, a broad range of materials including thermally unstable materials can be processed.[32][93][135] The latter opens up perspectives to produce biodegradable and cell-interactive scaffolds which are functionalized with proteins or other biological compounds. [32] Interestingly, the fabrication of materials encapsulating cells has also been performed in order to increase the cell seeding efficiency.[34][92][198]

2PP differs from other laser-based SFF techniques because it applies the principle of Two foton absorption for the generation of micro and nanostructures inside a polymerizable solution. This is made possible via the application of a tightly focussed femtosecond pulsed laser beam with laser pulses of 800 nm as opposed to a traditionally applied UV beam. When focussed correctly, this setup enhances the probability for an initiator molecule to simultaneously absorb two long wavelength fotons (cfr. In the near IR range), to result in an energy comparable to the absorption of one short wavelength photon and thus induce a very local polymerization reaction. (see Figure 2(right)).[33][94][101][131][162][199][200] This principle is where this technology differs from conventional stereolithografic processes where 1 foton absorption is applied, and polymerization will occur in the entire area where the laserbeam penetrates the solution.

When applying 2PP, the photo-initiator concentration applied should also be taken into account as these compounds often show some cytotoxicity which negatively influences the cell viability.[32] However, generally the unreacted photo-initiator can be removed by incubating the generated structures in an appropriate solvent.[32]

Since 2PP does not operate in a layer-by-layer fashion, it exhibits the benefit of having nearly no geometrical restrictions in the produced structure. The movement of the focal point through the solution can be seen as a 3D drawing being instantly processed through the solidification of the material as is demonstrated in Figure 2. [33][93][94][131][162][199] Because of this working principle, which differs from other SFF techniques, 2PP exhibits a higher resolution, which can even extend to beyond the diffraction limit. The latter can be achieved by controlling the number and the energy of the applied laser pulses to only just overcome the polymerization energy threshold which results in nanometer precision. [33][93][101][131][135][199]

Interestingly, the resolution of this technique renders it feasible to influence the micro- and nano-topography of the struts, in contrast with other SFF techniques.[93] The ability to control the topography enables the construction of so-called cell sieves which increase the cell seeding efficiency. In addition, 2PP is a promising tool to mimic the ECM to a greater extent thereby increasing cell proliferation.[32][93][150] An improved cell seeding efficiency and an upregulated cell proliferation is not only beneficial from a biological viewpoint, but also from an economical perspective. The economic viability of an engineered scaffold increases in case a lower amount of stem cells is required to fulfil its purpose.[150]

Similar to other SFF technologies, a perfect control in the design enables the construction of scaffolds exhibiting regions with different mechanical properties which is promising towards the construction of IVDs for spinal repair.[32]

The 2PP technique also possesses a disadvantage compared to alternative SFF techniques including FDM as the construction of an entire scaffold requires more time and it lacks the ability to integrate different materials into a single scaffold in a controlled manner.[34]
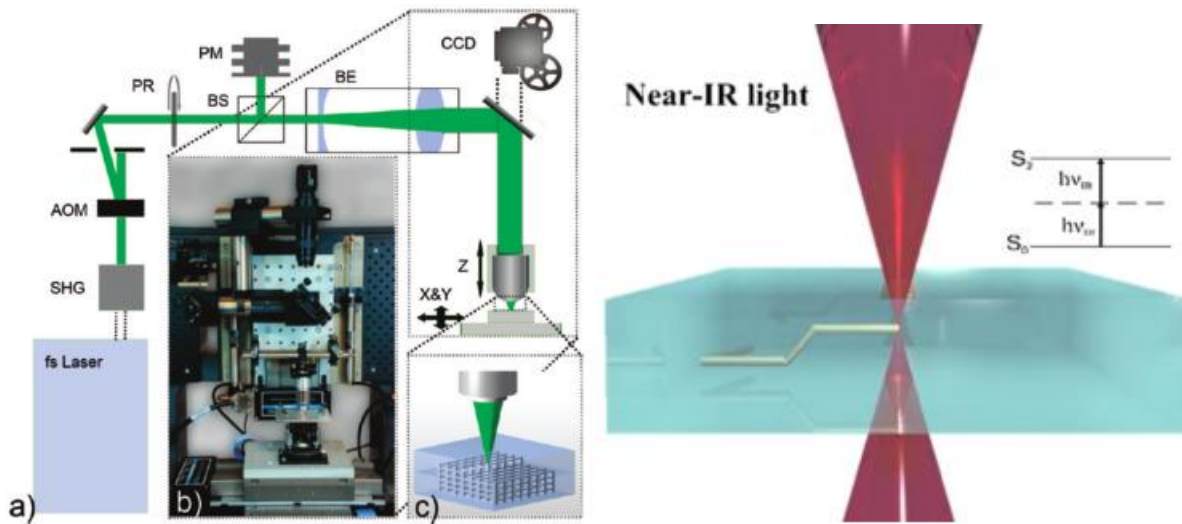
Figure 2: 2PP setup with a pulsed laser beam which is directed through a series of optical devices, resulting in a controllable focal point inside a solution resulting in local photo-polymerization (right);[93] Principle of 2PP with two separate infrared beams (800 nm) are emitted under a certain angle relative to each other resulting in a single focal point with an energy corresponding to a single photon of 400 nm (left).[32]

Addendum B: List of Abbreviations

2PP	Two Photon Polymerization
μ-CT	micro computed tomography
ADG	adipic acid dihydarzide
AF	Annulus Fibrosus
ALP	Alkaline Phosphatase
AEMA.HCL	2-Amino ethyl methacrylate hydrochloride
ANOVA	Analysis of Variance
BMSCs	Bone marrow stromal cells
CAD	Computer aided design
Chloroform-d	Deuterated Chloroform
CCD	Charge Coupled Device
CT	Computed Tomography
D_2O	Deuterium oxide
DBMG	Demineralized bone matrix gelatin
DDD	Disc degeneration disease
DC	Degree of crosslinking
DM	Differentiation medium(αMEM with 50μg/ml L-ascorbic acid and 10mM glycerolphosphate)
DMSO	Dimethyl sulfoxide
DMSO-d6	Deuterated dimethyl sulfoxide
DS	Degree of substitution
DSC	Differential scanning calorimetry
ECM	Extra cellular matrix
EDC	1-ethyl-3-(3-dimethylaminopropyl)carbodiimide
FDA	Food and drug administration
FDM	Fused deposition modeling
FITC	Fluorecein isothiocyanate

GAGs	Glucosaminoglycans
HA	hyaluronic acid
H_2O	Water
HR-MAS NMR	High Resolution Magic Angle Spinning Nuclear Magnetic Resonance spectroscopy
IVD	Intervertebral disc
KH_2PO_4	Potassium hydrogen Phosphate
kPa	kilo Pascal
LCST	lower critical solution temperature
MC-3T3-E1	Mouse preosteoblasts
MEM-alpha	Alpha minimum essential medium
MRI	nuclear magnetic resonance imaging
MSCs	mesenchymal stem cells
MTT	3-(4,5-dimethythiazol-2-yl)-2,5-diphenyl tetrazolium bromide
MWCO	Molecular weight cut off
Na_2HPO_4	Sodium Phosphate
NFMLP	non-frozen liquid microphases
NHS	N-hydroxysuccinimide
NMR	Nuclear magnetic resonance spectroscopy
NP	Nucleus Pulposus
PEG	polyethyleneglycol
PG	Proteoglycan
PGA	Poly-(glycolic acid)
PBS	Phosphate buffered saline
PC	Poly-carbonate
PCL	Polycaprolactone
PDLA	Poly-D-(lactic acid)
PDLLA	Poly-D-L-(lactic acid)
PEG	Poly-(ethylene glycol)
PGA	Poly-(glycolic acid)

80

pHEMA   Poly-(hydroxyethyl methacrylate)

PI   Propidium Iodide

PLA   Poly-(lactic acid)

PLGA   Poly-(lactic/glycolic) acid

PLLA   Poly-L-(lactic acid)

PPS   pentosan polysulphate

PRP   platelet rich plasma

PU   Poly-urethane

PVA   Poly vinyl alcohol

qRT-PCR   quantitative reverse transcription polymerase chain reaction

RGD   Arginine-glycine-aspargine

ROP   ring opening polymerization

RP   rapid prototyping

SEM   Scanning electron microscopy

SFF   Solid freeform fabrication

T_g Glass Transition Temperature

T_m Melting temperature

TCPS   Tissue culture poly-styrene

UCST   Upper Critical Solution Temperature

UV   Ultra violet

VBA   Visual Basic for Applications

Addendum C: Materials and Methods

C.I Materials

1-ethyl-3-(3-dimethylaminopropyl)carbodiimide	Sigma-Aldrich(Diegem, Belgium)
2-aminoethyl methacrylate hydrochloride	Polysciences(Conches, France)
7-hydroxycoumarin (Umbelliferrone)	Sigma-Aldrich(Diegem, Belgium)
Acetone(99.8% pure)	Sigma-Aldrich(Diegem, Belgium)
Alkaline phosphatase live stain A14353	Life Technologies
Chloroform	Sigma-Aldrich (Diegem, Belgium)
Chloroform-d	Sigma-Aldrich (Diegem, Belgium)
Dialysis membrane Spectra/por (MWCO: 12000-14000)	Polylab(Antwerpen, Belgium)
Deuterium oxide(99.9 atom% D)	Aldrich(Bornem, Belgium)
Dimethyl Sulfoxide (99.85), purified via destillation	Acros(Geel, Belgium)
Dimethyl sulfoxide-d6(99.96 atom% D)	Aldrich(Bornem, Belgium)
Epichlorohydrin	Sigma-Aldrich(Diegem, Belgium)
Ethanol	Sigma-Aldrich(Diegem, Belgium)
Fetal Bovine serum F7524	Sigma
Gelatin (type B), isolated from bovine bone by an alkaline process	Rousselot (Ghent, Belgium)
Glycerol phosphate	Sigma
Irgacure 2959 (2-hydroxy-1-[4-(hydroxyethoxy)phenyl]-2-methyl-1-propanone)	BASF(Kaisten, Germany)
L-Ascorbic acid	Sigma
MC-3T3-E1 subclone 4 (CRL-2593)	ATCC-LGC, Standards
Methacrylic anhydride	Aldrich (Bornem, Belgium)
MEM alpha, nucleosides, no ascorbic acid A10490	Life technologies
N-hydroxysuccinimide(98%)	Acros(Geel,Belgium)
Penicillin/Streptomycin (N.1482)	Lonza
Potassium hydrogen phosphate	Acros(Geel, Belgium)
Potassium hydroxide	Chem-lab(Zedelgem, Belgium)

Poly-L-lactic acid filament	Bitsfrombytes.com
Presto Blue A-13261	Life Technologies
SsoFast EvaGreen supermix	Bio-Rad
Sodium chloride	Sigma Aldrich(Diegem, Belgium)
Sodium hydroxide	Aldrich(Bornem, Belgium)
Sodium phosphate (dibasic, anhydrous, p.a.)	Acros (Geel, Belgium)
Tri reagent	Molecular research center, INC
Trypsin-EDTA (T4174)	Sigma

C.II Methods

Compression tests: The compression tests on the PLA scaffolds were performed using a Hounsfield THE Universal tester 10-KM. The required program as well as the data acquisition was performed via QMAT software. The raw data were then analyzed using Microsoft Excel 2010. The samples were subjected to forces of up to 1500N at a rate of 1mm/min.

Confocal microscopy: All confocal microscopy images of the PLA scaffolds were obtained using a ZEIS LSM 700 laser scanning microscope.

Cryogenic treatment: The cooling rate and the final freezing temperature of the cryogels were controlled using a Julabo, type FP40-ME cryostat in combination with a thermo-electric cooler (DuraTec DT12, Marlow industries) for the application of a temperature gradient. The combinatory device was developed in close collaboration with the central workshop of the Faculty of Sciences (Ghent University).

Differential scanning calorimetry: The gelatin thermograms were obtained by adding approximately 40mg of a 10w/v% solution to a T_{zero} pan, As a reference a few droplets of MilliQ were introduced in a hermetic pan prior to sealing using a T_{zero} hermetic lid. For the PLA samples, a quantity of around 5 mg was put into an aluminum T_{zero} pan and an empty pan was applied as a reference. First a temperature ramp of 20.00°C/min was applied to reach a temperature of 60.00°C. The sample was stabilized for 20 minutes. Next a ramp of 10.00°C/mi was applied to 15.00°C, samples were stabilized at 15°C for 20 minutes prior to a temperature ramp of 20.00°C/min until a temperature of -10.00°C was reached followed by a ramp of 5.00°C/min until a temperature of 60.00°C was obtained. For the determination of the glass transition and melting temperature of the PLA filament prior to printing, the sample was heated to 250°C, cooled to -50°C and reheated to 250°C at a rate of 10°C/min. For the determination of the

crystallinity after printing, the samples were stabilized at 20°C prior to heating to 220°C at a rate of 10°C/min. All measurements were performed on a TA instruments Q 2000. The results were analyzed using Q series software.

Digital microscopy: The images of the samples prior to leaching were obtained using a Keyence VHX-2000 series system. The sample images after leaching were otained using a Keyence VHX-5000 series system.

Fused deposition modelling (FDM): All scaffolds developed were printed using an Ultimaker 1 device with a standard printing nozzle with a diameter of 400µm in combination with a transparent PLA filament obtained from bitsfrombytes.com. The gcodes were written using the self-developed scaffold generator v1.8 program written in Visual Basic for Application in Microsoft excel 2010. The CAD designs were generated via Illustrator. The gcode and CAD designs were loaded into the 3D printer using Cura 13.06.4 software.

Gel fraction determination: The gel-fraction experiments on crosslinked hydrogel films were performed on circular films with a diameter of 8mm in milli-Q at 37°C for the course of 12 hours. To incubate the films in Milli-Q tissue cassettes were applied (Thermo Shandon, tissue cassette IV). All measurements were performed in triplicate and the results were reported as mean values, with corresponding standard deviations.

Lyophilization: Lyophilization of the gelatin derivatives occurred via a Christ freeze-dryer alpha I-5.

Micro-computed tomography: The microcomputed tomography images were obtained using a scanner which consists of an open type Feinfocus Tra tube combined with a Varian 2520V Paxscan detector. The samples were scanned via a coned beam with a voxel size of 9.3µm for the combination scaffolds, 12.2µm for the gcode scaffolds and 15µm for the CAD scaffolds. The applied voltage was 100kV with a current of 140µA. To obtain the 2D cross-sections (i.e the X-ray radiographs), a step wise rotation between 0° and 360° around a fixed vertical axis was applied. The 3D reconstructions of the obtained radiographs were realized using Octopus software and the 3D visualization was performed using VGStudio version 2.2.

Nuclear Magnetic Resonance spectroscopy: The ^{1}H-NMR spectra of the coumarin derivatives were obtained using a Brüker Avance 300MHz NMR-spectrometer. The ^{1}H-NMR spectra of the gelatin derivatives were obtained at 40°C using a Brüker WH 500 MHz NMR-spectrometer. The ^{1}H- and ^{13}C-NMR spectra of the PLLA were recorded using the Brüker WH 500 MHz NMR-spectrometer at room temperature. The solvent signals applied for sample preparation were used

as an internal standard for all measurements. Analysis of the spectra was performed via the ACD/1D NMR processor software developed by ACD/Labs.

HR-MAS ^{1}H-NMR Spectrocopy: All HR-MAS NMR spectra were obtained using a Brüker Avance II 700 spectrometer (700.13 MHz) in combination with an HR-MAS NMR probe equipped with a ^{1}H, ^{13}C, [119]Sn and gradient channel. The spinning rate was adjusted to 6 kHz. The samples were obtained by swelling the freeze dried hydrogel samples inside a 4mm zirconium oxide MAS rotor with a volume of 50µL sealed with a teflon cap. To homogenize the samples, manual stirring was performed prior to analysis.

Optical microscopy: All optical microscopy images were obtained by means of an Axiotech 100 reflected light microscope (Carl Zeiss), with reflected-light brightfield for Köhler illumination. The obtained images were characterized using ImageJ software.

Rheology: To investigate the mechanical properties of the hydrogels a rheometer type physica MCR-301 (Anton Paar, Sint-Martens-Latem, Belgium) with a parallel plate geometry was applied. The diameter of the upper plate was 25mm. The samples were placed in between the plates(gap 0.95mm) by pipetting 500 µl of the solution followed by a 15 min gelation period at 5°C. The storage modulus (G') and loss modulus (G") were measured during a 30 minute assay consisting of a 20 min UV crosslinking step followed by a 10 minutes post curing step in the absence of UV-irradiation. The spectra were obtained by the application of an oscillation frequency of 1Hz, a strain of 0.05 and application of a normal force of 0.2N. The crosslinking was performed using an EXFO novacure 2000 UV light source (max. power 20W/cm^2) to apply an irradiation of 4400mW/cm².

Scanning electron microscopy: SEM analysis occurred by means of a Fei Quanta 200F (field emission gun) scanning electron microscope. The scaffolds were cut in half before applying gold coating with an automatic sputter coater K550X using an RV3 two stage rotary vane pump. Finally, dust was removed using compressed air.

Statistical analysis: Statistical analysis to determine whether different means were significantly different was either performed by the application of a two-tailed T-test for the comparison of two values or by a unifactorial analysis of variance (ANOVA) for the comparison of more means. Two values were considered significantly different in case $p < 0.05$.

Swelling experiments: Circular hydrogel films with a diameter of 12mm were incubated in PBS buffer at 37°C. To entrap the films they were placed in tissue cassettes (Thermo Shandon, tissue cassette IV). At predetermined time points the hydrogels were removed from the buffer solution

and gently dipped with paper to remove residual water and weighed. Afterwards the samples were reintroduced into the medium. All experiments were performed in triplicate and the results were depicted as means and plotted together with their standard deviation. These measurements enabled to determine mass differences as a function of time.

Thermogravimetric analysis: The degradation behavior of PLA under the influence of temperature was assessed via thermogravimetric analysis by heating at a rate of 10°C/min while monitoring the difference in mass until a temperature of 800°C was reached. Around 20 mg of sample was loaded into a platinum pan for determination of the mass during the measurement. The measurement was performed using a TA instruments Q50 and the results were analyzed using Q series software.

UV crosslinking: UV-A crosslinking was performed by means of a high performance ultraviolet transilluminator (Ultra Violet Products) at a wavelength of 365nm and an intensity of 8 mW/cm². This setup allows for the irradiation of the sample both from the top as well as from the bottom.

Water uptake capacity of gelatin-PLA combination scaffolds: The gelatin-containing PLA combination scaffolds were immersed in PBS buffer at 37°C. At predetermined time points, they were removed from the solution and extensively dried using paper to remove residual water inside the pores of the PLA scaffolds prior to determination of the mass. All measurements were performed in triplicate and the results were depicted as mean values with corresponding standard deviations. A blank scaffold was also measured as a control experiment.

C.III Overview of synthesis methods

C.III.1 Methacrylation of gelatin B

100 g gelatin B (cfr. 38.5 mmol amines) was dissolved in 1 L phosphate buffer (pH 7.3) at 40°C under continuous mechanical stirring. Next, 2.5 equivalents methacrylic anhydride (14.34 mL, 96.25 mmol) were added after which the solution was stirred vigorously for 1 hour at 40°C. After 1 hour, the reaction mixture was diluted by addition of 1 L Milli-Q. The solution was then dialyzed using Milli-RO (MWCO 12000-14000) for 24 hours at 40°C (cfr. Water changed 5 times). After dialysis, the solution was transferred to petridishes at room temperature to allow physical gelation. After physical gelation, the petridishes were frozen at -20°C enabling the subsequent removal of ice via lyophilization.

To yield gel-MOD with a higher DS, the same protocol was applied to 25 g gel-MOD (DS 86%) with the addition of only 1 equivalent methacrylic anhydride relative to the primary amines originally present in gelatin B (9.625 mmol, 1.434 ml).

C.III.2 Synthesis of gel-MOD-AEMA

10 g gel-MOD (cfr. 10.980 mmol carboxylic acids) was dissolved in 200 ml DMSO at 50°C under reflux conditions in argon atmosphere (three times degassed) under continuous magnetic stirring. After complete dissolution, 1 equivalent 1-ethyl-3-(3-dimethylaminopropyl)carbodiimide (EDC) (cfr. 2100 mg; 10.980 mmol) and 1,5 equivalents n-hydroxysuccinimide (NHS) (cfr. 1895 mg; 16.48 mmol) were added to the mixture. After 30 min of stirring, 2 equivalents of 2-aminoethylmethacrylate hydrochloride (AEMA.HCl) were added (3.6353g; 21.96 mmol) together with 0.01 equivalents of 4-tert-butyl catechol (i.e. inhibitor). The solution was shielded from light and stirred at 50°C overnight. Afterwards, the reaction was precipitated in a tenfold excess of cold acetone and filtered on a glass filter n°4. The precipitate was redissolved in MilliQ and dialyzed using Milli-Ro (MWCO: 12000-14000 Da) at 40°C for 24 hours (water changed 5 times). After dialysis, the solution was transferred to petridishes and frozen at -20°C enabling the subsequent removal of ice via lyophilization.

C.III.3 Synthesis of 7-(2,3-epoxypropoxy)coumarin

3.24 g 7-hydroxycoumarin (20 mmol) was dissolved in 100 ml ethanol under magnetic stirring. Upon dissolution, an aqueous solution of KOH (25% w/v; 1.25g/5 ml) was added. The solution was stirred at room temperature for 30 min followed by the addition of epichlorohydrin (20 ml; 255.73 mmol; 12.79 eq). Next, the mixture was heated to 100°C. After 2.5 hours, the solvent was

completely evaporated at 40°C in a rotary evaporator under a reduced pressure to obtain a dry residue.

The obtained residue was dissolved in MilliQ/chloroform (80/100ml), introduced in a 250 ml-separation funnel and hand-shaken for 5min. Next, the mixture was kept for 2 hours at room temperature to enable the partition into an aqueous and an oil phase. The oil phase (cfr. lower phase, density chloroform: 1.48 g/cm³, density water: 1.00 g/cm³) was then separated from the water phase and washed with MilliQ (80mL) and again kept for 2 hours at room temperature followed by separating the oil phase from the water phase. Next, the solvent of the oil phase was evaporated under reduced pressure to obtain a dry residue.

For further purification, the dry residue was dissolved in warm ethanol (85°C under refluxing) and it was recrystallized at room temperature. The white solid was filtered off using a filter paper (Whatman, No.2 (8μm)), glass filter n°4 (10-16μm)).

C.III.4 Synthesis of gel-coumarin

0.2358279 g 7-(2,3-epoxypropoxy)coumarin (1.155 mmol) was dissolved in 10 ml DMSO in a two-neck flask under reflux conditions under argon atmosphere (2 times degassed) while stirring continuously. Next, gelatin B (1 g, 0.385 mmol amines) was added and the set-up was degassed twice while the temperature was risen to 50°C. The mixture was allowed to react for two days followed by precipitation in a tenfold excess of cold acetone. The precipitate was filtered of on a glass filter (P4) and redissolved in MilliQ water prior to dialysis using MilliRo (MWCO: 12000-14000 Da) for 24 hours at 40°C (water changed 5 times) followed by freezing at -20°C prior to lyophilization.

C.III.5 Buffer composition
Composition of phosphate buffer for the methacrylation of gel-MOD

Substance	CAS	#mmol	MW (g/mol)	theoretical quantity
Na_2HPO_4	7558-79-4	125.2	141.96	17.77 g
KH_2PO_4	7778-77-0	19.95	136.086	6.80 g

*the pH of the buffer was adjusted by the addition of NaOH

Composition of PBS buffer for swelling tests

Substance	CAS	#mmol	MW (g/mol)	theoretical quantity
Na2HPO4	7558-79-4	10	141,96	1,4195 g
KH2PO4	7778-77-0	3	136,086	0,42 g
NaCl	7647-14-5	123	58,44	7,2 g

C.III.6 Production of 2D hydrogel films via film casting

Film casting was performed by dissolving 1 g of the respective gelatin derivative in 9 ml of double-distilled water at 40°C. After complete dissolution, 2 mol% Irgacure 2959 relative to the amount of double bonds was added by the addition of the correct amount of a stock solution of Irgacure 2959 containing 200 mg in 25 ml MilliQ which was allowed to dissolve for 3 hours at 50°C shielded from light. After addition of the Irgacure 2959 solution, additional MilliQ was added to the solution until a total volume of 10 ml was obtained. These solutions were then injected in between two glass plates covered with teflon release foil separated by a 0.5 mm silicone spacer. The materials were allowed to form gels, by the storage at 6°C overnight followed by the application of UV-A irradiation for 30 minutes.

Four films were prepared starting from the following compounds and its respective quantities.

Type	amine substitution	carboxylic acid substitution	# double bonds (mmol)	Irgacure 2959 (mmol)	I2959 stock solution (ml)
gel-MOD (DS 82%)	82 %	-	0.3157	0.006314	0.177
gel-MOD (DS 97%)	97 %	-	0.37345	0.007469	0.209
gel-MOD-AEMA (DS 87%)	87 %	30 %	0.66435	0.013287	0.372
gel-MOD-AEMA (DS 97%)	97 %	27 %	0.66991	0.0133982	0.376

C.III.7 Generation of PLA-cryogel combination scaffolds

1 g gel-MOD (DS 82%, 0.3157 mmol double bonds) was dissolved in either 9, 19 or 49 ml MilliQ at 40°C.After complete dissolution, 2 mol% Irgacure 2959 relative to the amount of double bonds present was added by the addition of the correct amount of a stock solution of Irgacure 2959. The stock solution was prepared by dissolving 200 mg Irgacure 2959 in MilliQ at 50°C shielded from light under continuous stirring. After addition of the Irgacure solution, additional MilliQ was added until respectively a total volume of 10, 20 or 50 ml was obtained to generate solutions with concentrations of respectively 2, 5 or 10 w/v%. . Next, the scaffolds were introduced into the solution followed by a 5 min vacuum treatment. After the vacuum treatment, the scaffolds were taken out from the solution and placed onto a hydrophobic substrate to be stored in the fridge at 6°C for 1 hour to induce physical gelation followed by 2 hours of UV-A irradiation. Next, the scaffolds were dipped in a 10 w/v% gelatin B solution followed by the application of a cryogenic treatment where they were gradually cooled down to -30°C at a rate of 0.15°C/min with or without the application of a 30°C temperature gradient between the top and

the bottom of the cryo-chamber. After the cryogenic treatment, the samples were stored at -20°C followed by removal of ice through lyophilization.

C.IV. *In vitro* biocompatibility

C.IV.1 2D experiments

Cell culture setup

HFF-1 cells (human foreskin fibroblasts, ATCC) were cultured in DMEM glutamax medium (Gibco Invitrogen) supplemented with 10 % foetal calf serum (FCS, Gibco Invitrogen), 2 mM L-glutamine (Sigma-Aldrich, Belgium), P/S (10 U/ml penicillin, 10 mg/ml streptomycin, Gibco Invitrogen) and 100 mM sodium-pyruvate (Gibco Invitrogen). Cells were cultured at 37°C in a humidified atmosphere containing 5% CO_2.

Live/dead staining assay (Adhesion and proliferation on the hydrogel films)

Hydrogel films (diameter 12 mm) were sterilized using ethylene oxide (AZ Sint-Jan, Brugge). Cells were seeded at a density of 40 000 cells/500 µl medium per hydrogel in 24-well culture dishes. Cell adhesion and proliferation were evaluated after 1 and 7 days. Cells cultured on tissue culture polystyrene (TCPS) were taken as a positive control. To visualize cell attachment and distribution on the hydrogels, the cells were evaluated using fluorescence microscopy (Type U-RFL-T, Olympus, XCellence Pro software, Aartselaar, Belgium). A live/dead staining (Calcein AM/propidium iodide) was performed to evaluate cell viability. After rinsing, the supernatant was replaced by 1 ml PBS solution supplemented with 2 µl (1 mg/ml) calcein AM (Anaspec, USA) and 2 µl (1 mg/ml) propidium iodide (Sigma). Cultures were incubated for 10 minutes at room temperature, washed twice with PBS solution and evaluated. Evaluations were done 1 and 7 days post-seeding.

Cytotoxicity assay

HFF-1 cells were seeded in 96-well tissue culture plates at a density of 10 000 cells/well in 200 µl of HFF medium. After 24 h, the medium was withdrawn and 200 µl medium containing gel-MOD/gel-MOD-AEMA (dilution series of 0.5 w/v%, 0.25 w/v%, 0.1 w/v%, 0.05 w/v%, 0.025 w/v%) … was added and incubated for 2 days.

The colorimetric MTT assay was performed to quantify cell viability. The tetrazolium component is reduced in living cells by mitochondrial dehydrogenase enzymes to a water-insoluble purple formazan product, which, in turn, can be solubilized by the addition of lysis buffer and measured using spectrophotometry. The cell culture medium was replaced by 0.5 mg ml^{-1} MTT reagent and cells were incubated for 4 hours at 37°C. After removal of the MTT reagent, lysis buffer (1%

Triton X-100 in isopropanol/0.04 N HCl) was added and incubated for 30 min at 37°C on a gyratory shaker (70 rpm). The dissolved formazan solution was transferred into a 96-well plate and measured spectrosphotometrically at 580 nm (Universal microplate reader EL 800, Biotek Instruments) in triplicate. The amount of viable cells was calculated as a percentage of control cultures.

C.IV.2 3D experiments

All 3D cellular experiments were performed by Marica Markovic ot the institute of materials science and technology at the Vienna university of technology (TU Wien), Austria.

Cell culture setup

MC-3T3-E1 Subclone 4 cells were cultivated in an incubator with a humid atmosphere and 5% carbon dioxide at 37°C in α-MEM with ribonucleases, deoxyribonucleases, 2mM L-glutamine without ascorbic acid with the addition of 10 % fetal bovine serum and 1% of penicillin/streptomycin. The medium was refreshed every other day. The cells were in passage 8.

Upon reaching confluence, the cells were detached by the application of trypsin-EDTA and resuspended in fresh medium for cell counting. The cell counting was performed using a Neubauer chamber in which 10 µL of a known dilution of the cell-containing medium is placed inside a chamber which exhibits a background with squares which each contain 0.1 µL of the diluted solution. This chamber is then placed underneath a microscope and the cells per square are counted. The cell concentration is then given by dividing the number of cells per square by the volume of solution per square. In this way, the cell concentration of the initial solution can be calculated.[201]

After cell counting, the cells were resuspended in a 10 w/v% gel-MOD (DS 82%) solution in α-MEM containing 0.05 w/v% Irgacure 2959 (2.24 mM) to achieve a total of 10 million cells per ml solution.

Introduction of the scaffolds and the Gel-MOD solution containing cells

The scaffolds were wetted with isopropanol for sterilization, followed by air-drying before placement in a 48 well plate. Subsequently, the scaffolds were seeded with 50 µl of the gel-MOD solution resulting in the introduction of approximately 500000 cells per scaffold. Next, the scaffolds were exposed to UV-A irradiation for 10 minutes (365 nm, 4 mW/cm²).

Seven days after seeding, 6 of the scaffolds were stimulated with differentiation medium (DM) (αMEM containing 50µg/ml of L-ascorbic acid and 10 mM glycerolphosphate). The medium was replaced every other day during 3 weeks. Scaffolds without DM stimulation were used as a control experiment.

Metabolic assay

Metabolic tests were performed, 3 and 7 days after seeding and 1, 2 and 3 weeks after stimulation with DM according to the following protocol. 600 µl of PrestoBlue reagent was added to each well containing a scaffold followed by one hour of incubation at 37°C in a humid atmosphere containing 5% of CO_2. Next, the medium from around the scaffolds was pipetted in 96 wells in duplicate, followed by a measure of fluorescence using a Synergy BioTek plate reader. The excitation occurred at 560 nm, the resulting emission was measured at 590 nm. A background correction was made by subtraction of the value obtained by measuring unseeded cell medium. The obtained values were compared to the unstimulated scaffolds and a higher observed fluorescence correlates to a greater total metabolic activity.

Cell counting using Tri reagent

To generate an indication of the cellular number 7 days after seeding and 1, 2 and 3 weeks after differentiation, a cell number estimation was obtained via RNA isolation using Tri reagent according to the following protocol. 1 ml of Tri reagent was added per scaffold followed by standing for at least 5 minutes at room temperature to allow for complete dissociation of nucleoprotein complexes. Next, the samples were vortexed prior to transfer of the solution to a clean PCR tube. The solutions where then homogenized by application of an IKA Ultra Turrax T10 homogenizer. Next, 0.2 ml of chloroform was added for every ml of Tri reagent followed by 15 seconds of vigorous shaking of the sample. To allow for a phase separation, the samples were then kept for 10-15 minutes at room temperature followed by centrifuging of the mixture at 12000 g for 5-15 minutes at 2-8°C. This centrifugation allows for a separation of the mixture in three phases including a protein-containing red organic phase, a DNA-containing interphase, and an RNA-containing colorless upper aqueous phase.

DNA isolation procedure

The DNA was isolated from the interphase and the phenol-chloroform layer. To precipitate the DNA, the remaining aqueous phase was removed followed by the addition of 0.3 ml of ethanol per ml Tri reagent used in the initial homogenization. The sample was mixed by capping the tube followed by inversion of the sample several times. Next, the samples were incubated for 2-3

minutes at room temperature, followed by centrifugation at 2000 g for 5 minutes at 4°C to precipitate the DNA. The phenol-ethanol supernatant was removed and the DNA was washed with 1 ml of sodium citrate/ethanol solution (0.1% sodium citrate in 10% ethanol, pH 8.5) per ml of initially added Tri reagent prior to a 30 minutes incubation at room temperature. Next, the sample was centrifuged at 2000 g for 5 minutes at 4°C followed by removal of the supernatant. This washing cycle was performed twice followed by the addition of 1.5-2 ml of 75% ethanol solution per ml of the originally added Tri reagent. Next, the samples were incubated for 10-20 minutes at room temperature followed by centrifugation at 2000 g for 5 minutes at 4°C. The supernatant was removed and the DNA was allowed to air dry for 5-10 minutes, taking care not to let the sample run completely dry. Next, the DNA was resuspended in 8mM NaOH by addition of 0.3-0.6ml of the NaOH solution per (50-70mg) of tissue.

Nucleic acid determination

Nucleic acid concentrations were measured using a Synergy Bio Tek plate reader. The number per analyzed sample was calculated via the assumption that one million diploid mouse cells contain 5.8 µg of DNA.

Live/dead staining

Live/dead staining images were obtained 7 days after seeding and 1, 2 and 3 weeks after inducing differentiation according to the following protocol. First, the medium was removed and the cell-containing scaffolds were washed using PBS. Next, 600 µl of a 3 M calcein and 2.5-5 M PI diluted in PBS at 37°C were added to each well. The samples were then incubated for 30 min at 37°C, followed by two washing cycles with warm PBS. Finally, images were recorded using confocal microscopy by applying light of 485 nm for excitation of calcein and 530 nm for PI excitation. The fluorescence occurs at 535 nm for calcein and at 620 nm for PI.

Alkaline phosphatase live stain

The live stain procedure was performed 1, 2 and 3 weeks after stimulation of the cells with DM according to the following procedure. In a first step, the medium of the scaffold containing wells was removed. Next, the seeded scaffolds were washed twice with warm PBS for 2-3 minutes followed by aspiration. Next, a 1:100 diluted AP live stain solution was prepared in PBS. Next, an appropriate amount of the stock solution was placed directly onto the scaffolds followed by a 20-30 min incubation. After the incubation, excess AP live stain solution was removed by applying a 5 min washing step with PBS twice. Prior to visualization using the confocal microscope using a standard FITC filter, fresh PBS was added to the samples.

Gene expression quantification

First, the protocol described for cell counting using tri phase was performed followed by the isolation of RNA.

RNA isolation procedure

The aqueous phase (0.4 ml) was transferred to a 1.5 ml eppendorf tube (PCR clean), followed by the addition of 0.5 ml of 2-propanol per ml tri reagent prior to vortexing of the solution. Next, the sample was kept at room temperature for 5-10 minutes followed by centrifugation at 12000 g during 10 minutes at 2-8°C. The RNA precipitate will be present on the bottom of the tube. To wash the RNA, the supernatant was removed and 1 ml of cold 75% ethanol per ml of Tri reagent was added followed by vortexing and centrifuged at 75000 g for 5 minutes at 2-8°C. This washing sequence was performed twice.

RNA solubilization

The ethanol added for washing was removed via a pipet followed by air drying to remove the residual ethanol. The sample was not completely dried as this will decrease its solubility. Next, an appropriate volume of Ultra-Pure water was added followed by vortexing. This treatment was then followed by a heating step to 55-60°C for 10 minutes after which the samples were cooled to 4°C for 20 minutes.

cDNA synthesis

To determine the gene induction, the isolated RNA was transcribed into cDNA (iScript^{TM} cDNA Synthesis Kit, Bio-Rad). The volume of the applied components per sample were 4 µl of 5x iScript reaction mix, 1 µl of iScript reverse transcriptase and RNA template (100 fg to 1µg total RNA) per µl of nuclease free water added to obtain a total volume of 20µl. The obtained reaction mixture was then incubated for 5 minutes at 25°C, followed by 30 minutes at 42°C and finally 5 minutes at 85°C.

qRT-PCR

The gene induction of osteocalcin and RUNX2 was determined using qRT-PCR with the application of HPRT as a housekeeping gene. The PCR reaction was performed with SsoFast EvaGreen Supermix on a CFX connect (Bio-Rad).

Addendum D

D.I DSC results for different gelatin derivatives
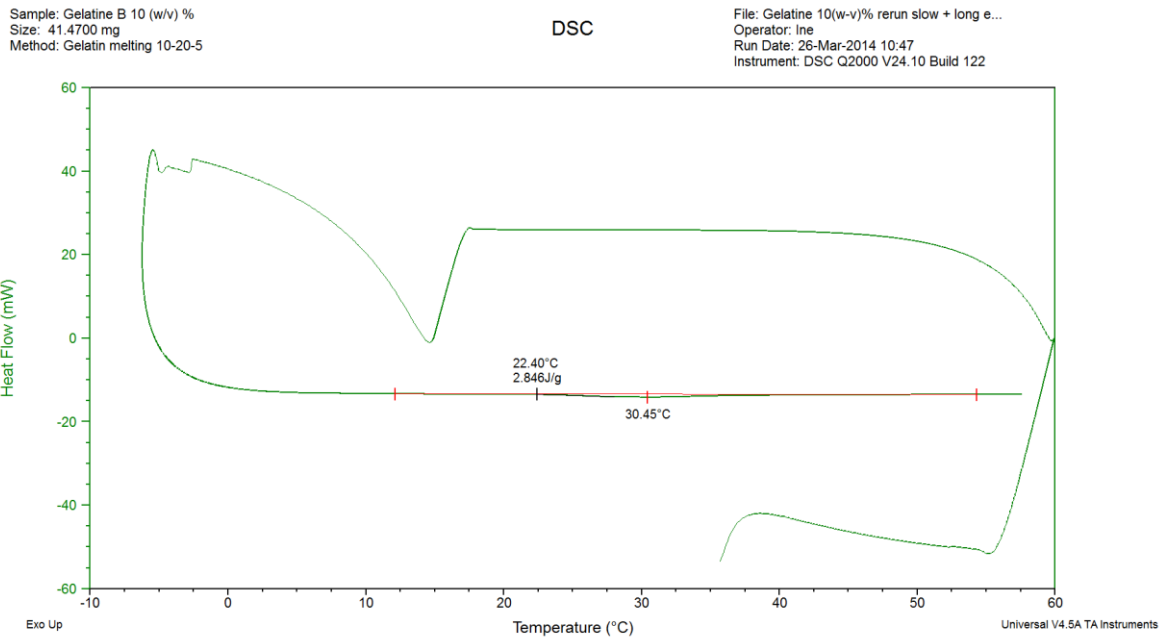
Figure 3: DSC thermogram depicting gelation temperature and heat flow exchange for gelatin B.
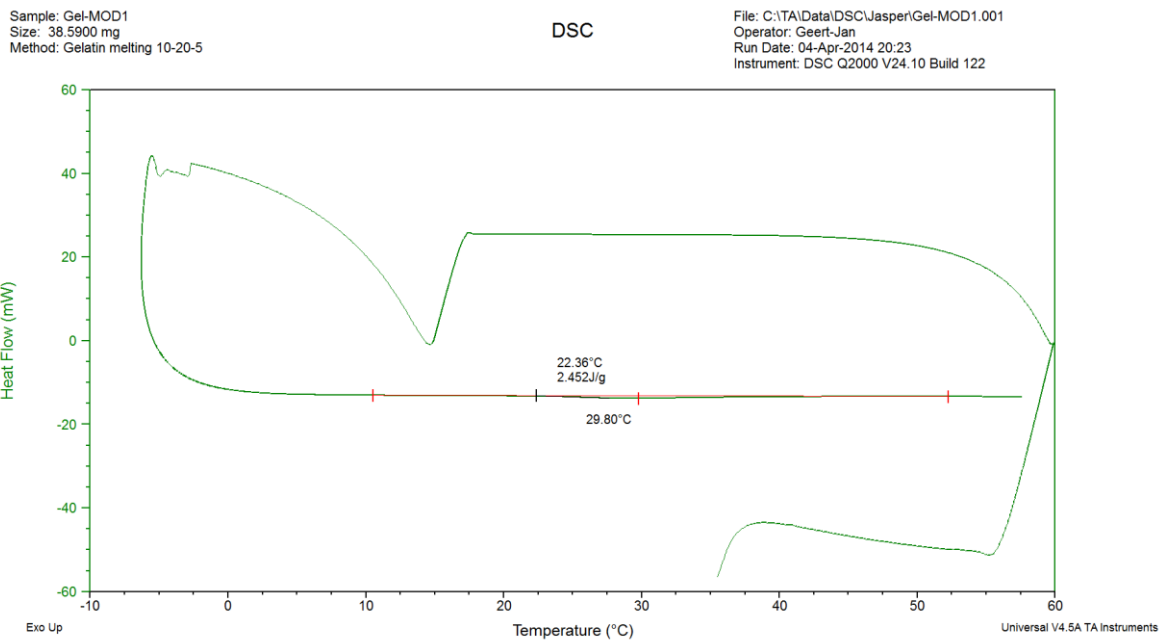
Figure 4: DSC thermogram depicting gelation temperature and heat flow exchange for gel-MOD (87%).
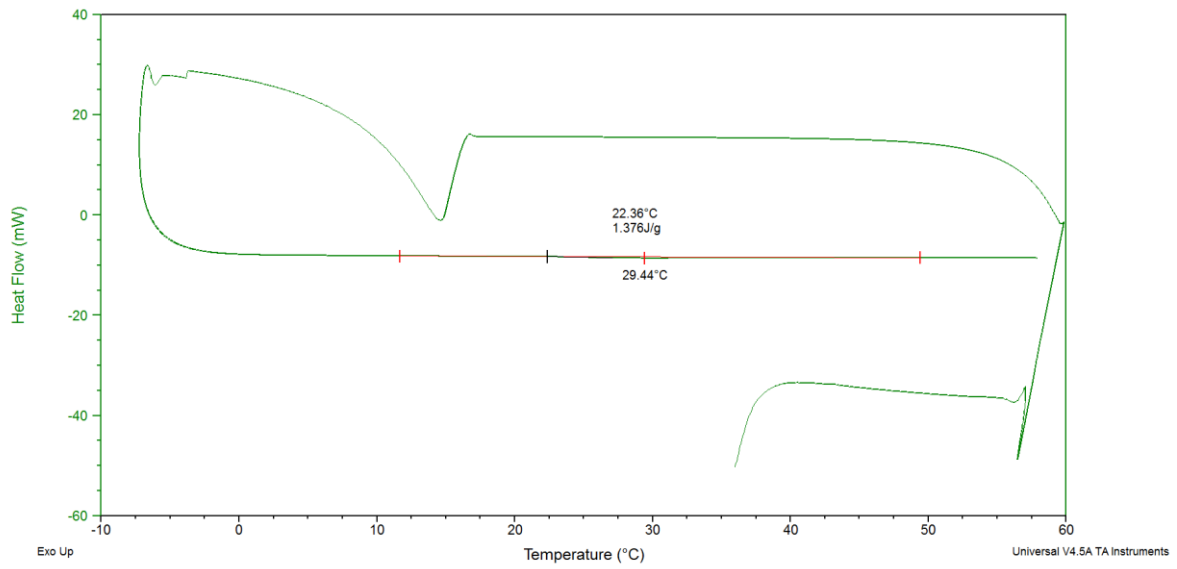
Figure 5: DSC thermogram depicting gelation temperature and heat flow exchange for gel-MOD (97%).
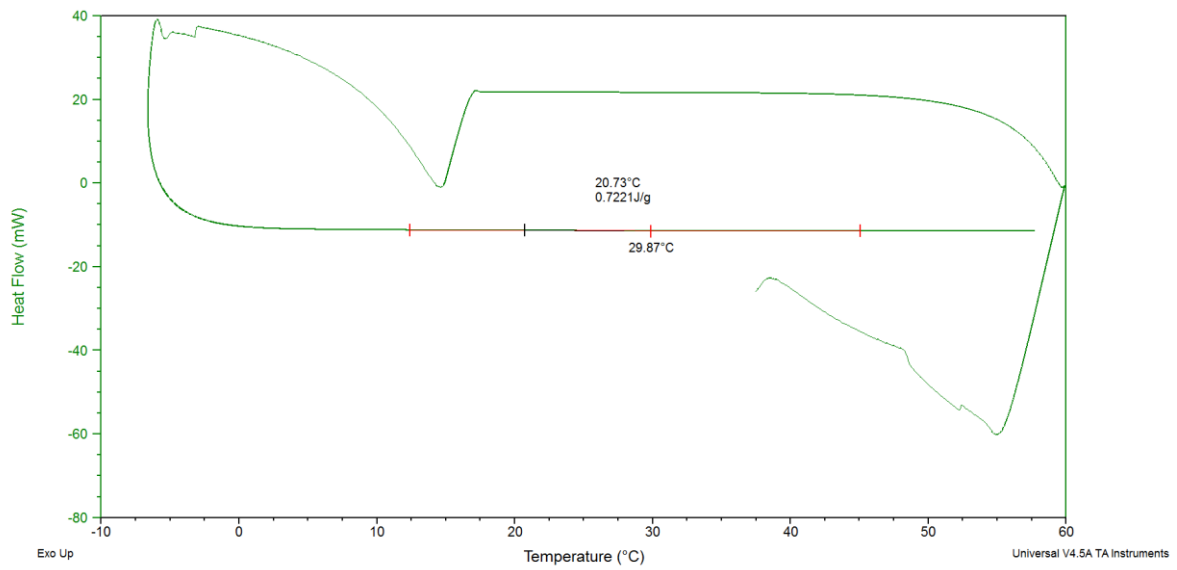
Figure 6: DSC thermogram depicting gelation temperature and heat flow exchange for gel-MOD-AEMA (97%, 41%).

D.II Swelling experiments
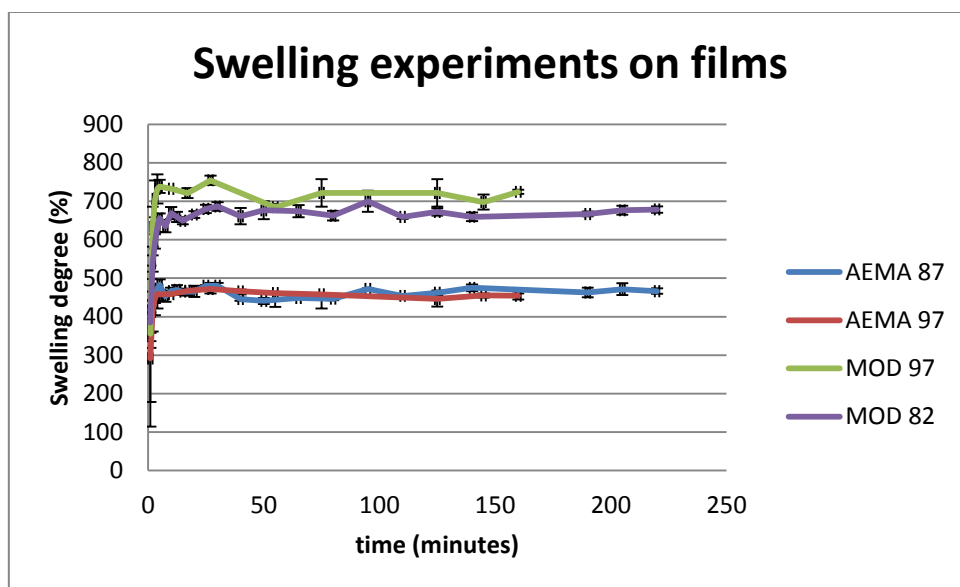
Figure 7: Plot revealing the increase in mass for the gelatin films after incubation in PBS at 37°C versus time.

D.III HR-MAS NMR Spectra
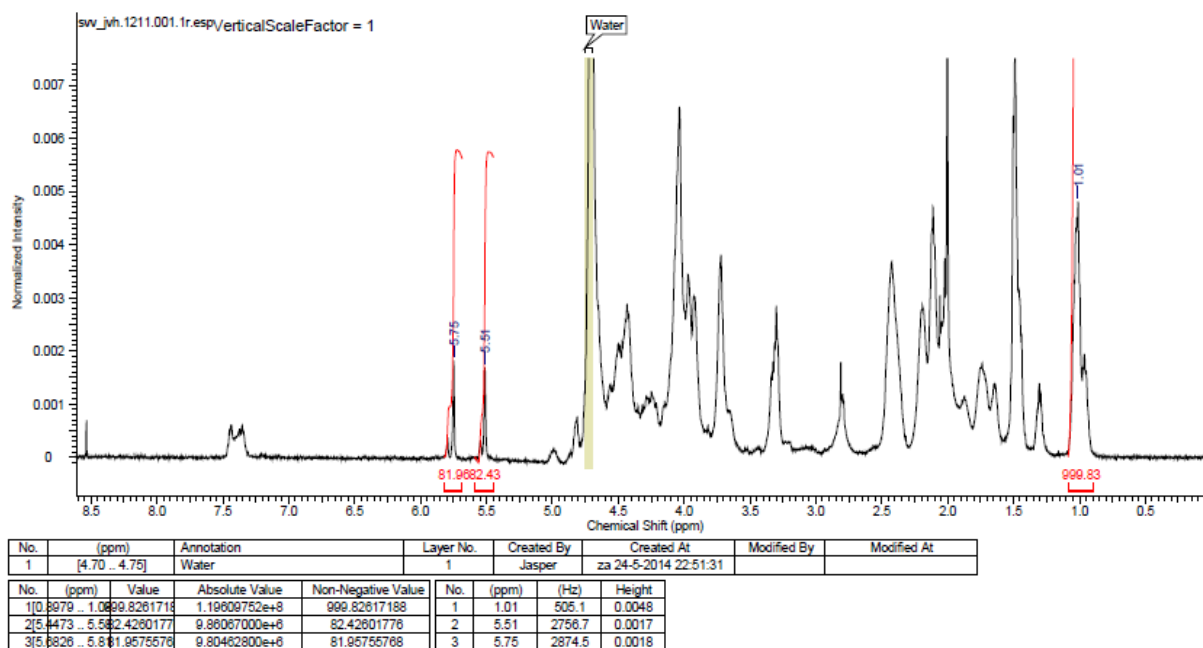
Figure 8: ¹H proton NMR spectrum of gel-MOD 82.
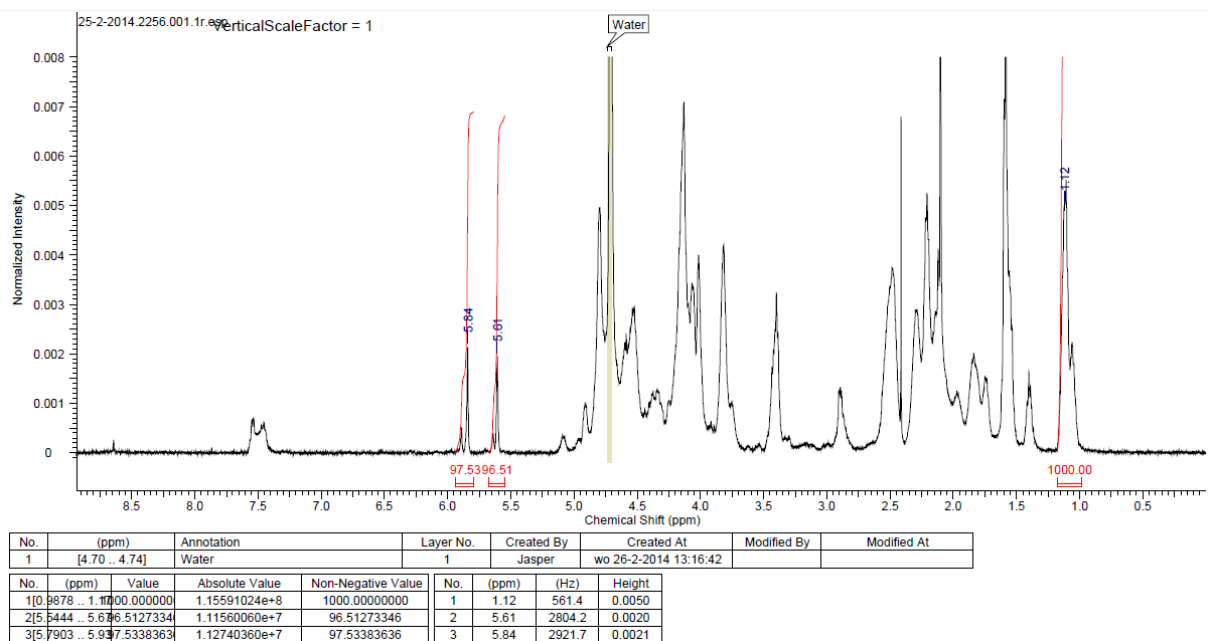
Figure 9: ¹H proton NMR spectrum of gel-MOD 97.

No.	(ppm)	Annotation	Layer No.	Created By	Created At	Modified By	Modified At
1	[4.70 .. 4.74]	Water	1	Jasper	wo 26-2-2014 13:16:42		

No.	(ppm)	Value	Absolute Value	Non-Negative Value		No.	(ppm)	(Hz)	Height
1	[0.9878 .. 1.1]	1000.000000	1.15591024e+8	1000.00000000		1	1.12	561.4	0.0050
2	[5.5444 .. 5.67]	96.5127334	1.11560060e+7	96.51273346		2	5.61	2804.2	0.0020
3	[5.7903 .. 5.93]	97.5338363	1.12740360e+7	97.53383636		3	5.84	2921.7	0.0021
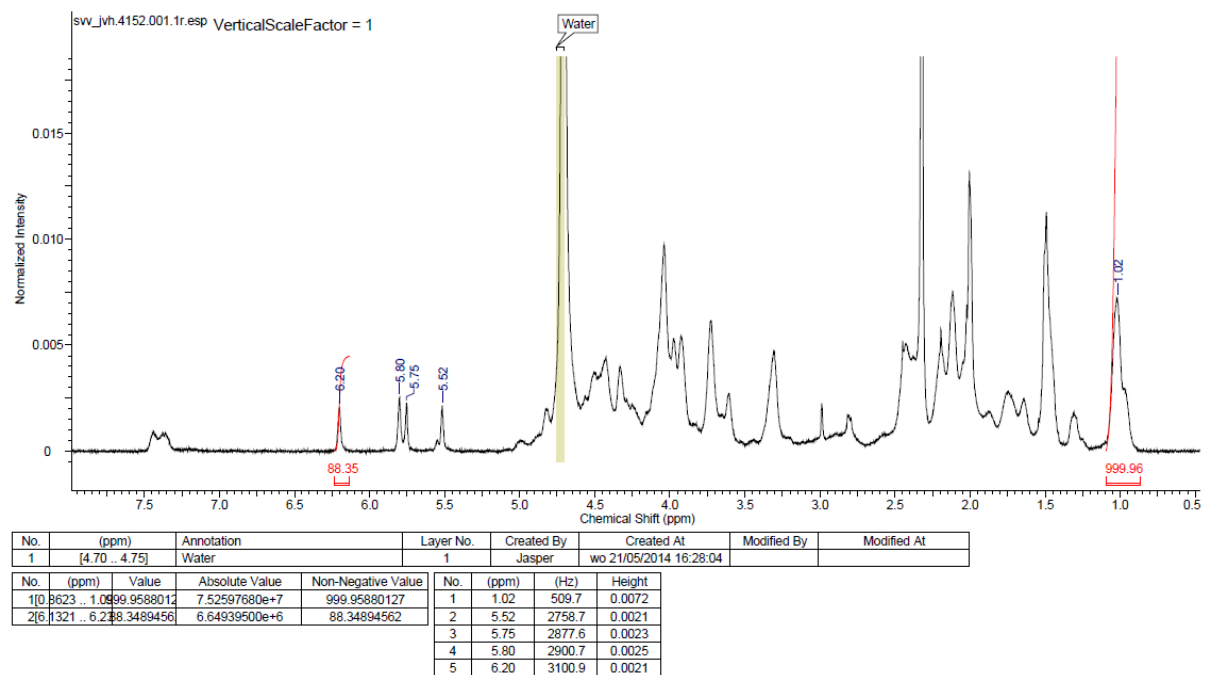
Figure 10: ¹H proton NMR spectrum of gel-MOD-AEMA 87.

No.	(ppm)	Annotation	Layer No.	Created By	Created At	Modified By	Modified At
1	[4.70 .. 4.75]	Water	1	Jasper	wo 21/05/2014 16:28:04		

No.	(ppm)	Value	Absolute Value	Non-Negative Value		No.	(ppm)	(Hz)	Height
1	[0.8623 .. 1.09]	999.9588012	7.52597680e+7	999.95880127		1	1.02	509.7	0.0072
2	[6.1321 .. 6.23]	88.3489456	6.64939500e+6	88.34894562		2	5.52	2758.7	0.0021
						3	5.75	2877.6	0.0023
						4	5.80	2900.7	0.0025
						5	6.20	3100.9	0.0021

Figure 11: ¹H proton NMR spectrum of gel-MOD-AEMA 97.
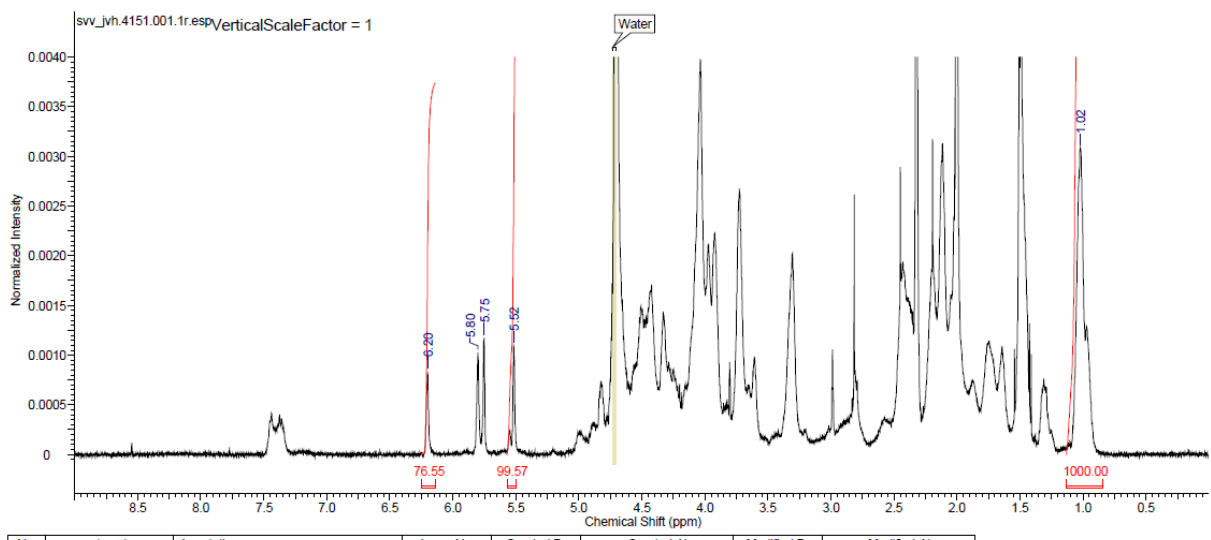
No.	(ppm)	Annotation	Layer No.	Created By	Created At	Modified By	Modified At
1	[4.70 .. 4.73]	Water	1	Jasper	do 17-4-2014 12:19:15		

No.	(ppm)	Value	Absolute Value	Non-Negative Value		No.	(ppm)	(Hz)	Height
1	[0.8423 .. 1.19]	999.9957885	9.09295760e+7	999.99578857		1	1.02	510.0	0.0031
2	[5.4962 .. 5.56]	99.5677261	9.05368900e+6	99.56772614		2	5.52	2759.1	0.0011
3	[6.1409 .. 6.24]	76.5461502	6.96033800e+6	76.54615021		3	5.75	2877.2	0.0012
						4	5.80	2901.5	0.0010
						5	6.20	3101.7	0.0008

Figure 12: HR-MAS Spectrum of gel-MOD 82
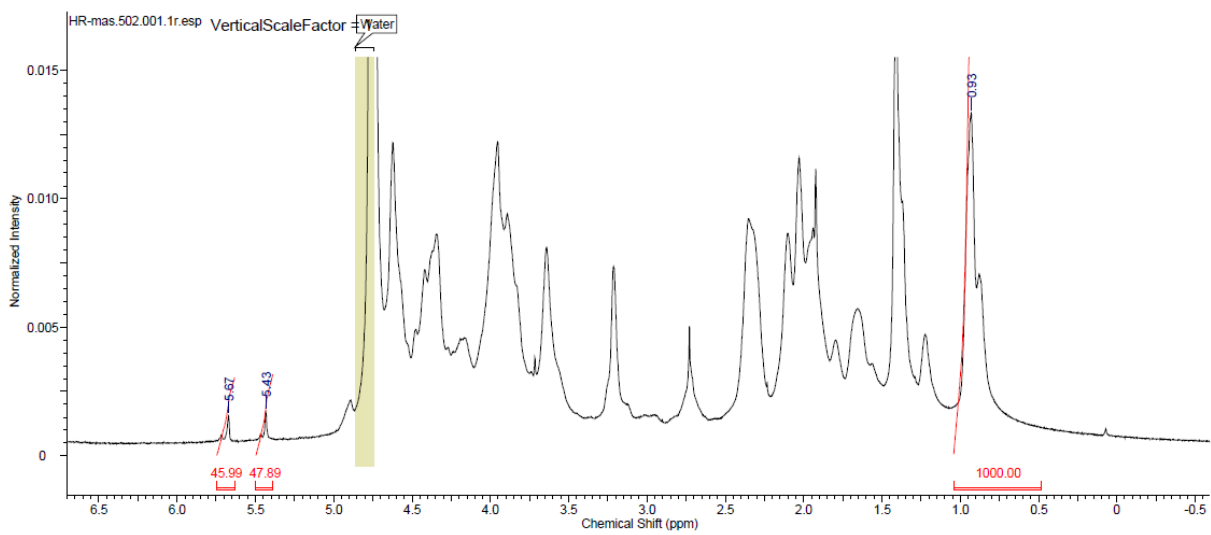
No.	(ppm)	Annotation	Layer No.	Created By	Created At	Modified By	Modified At
1	[4.74 .. 4.86]	Water	1	Jasper	wo 21/05/2014 10:24:21		

No.	(ppm)	Value	Absolute Value	Non-Negative Value		No.	(ppm)	(Hz)	Height
1	[0.4808 .. 1.04]	1000.000000	3.72687760e+7	1000.00000000		1	0.93	651.2	0.0133
2	[5.3887 .. 5.49]	47.8865089	1.78467163e+6	47.88650894		2	5.43	3803.6	0.0017
3	[5.5324 .. 5.74]	45.9904708	1.71400850e+6	45.99047089		3	5.67	3970.9	0.0016

Figure 13: HR-MAS NMR spectrum of gel-MOD 97

No.	(ppm)	Value	Absolute Value	Non-Negative Value	No.	(ppm)	(Hz)	Height
1	[0.2284 .. 0.96	1001.593139	5.76525200e+7	1001.59313965	1	0.88	614.5	0.0132
2	[5.3469 .. 5.43	73.2853393	4.21836400e+6	73.28533936	2	5.38	3766.9	0.0033
3	[5.5872 .. 5.68	71.7826461	4.13186775e+6	71.78264618	3	5.62	3932.4	0.0029
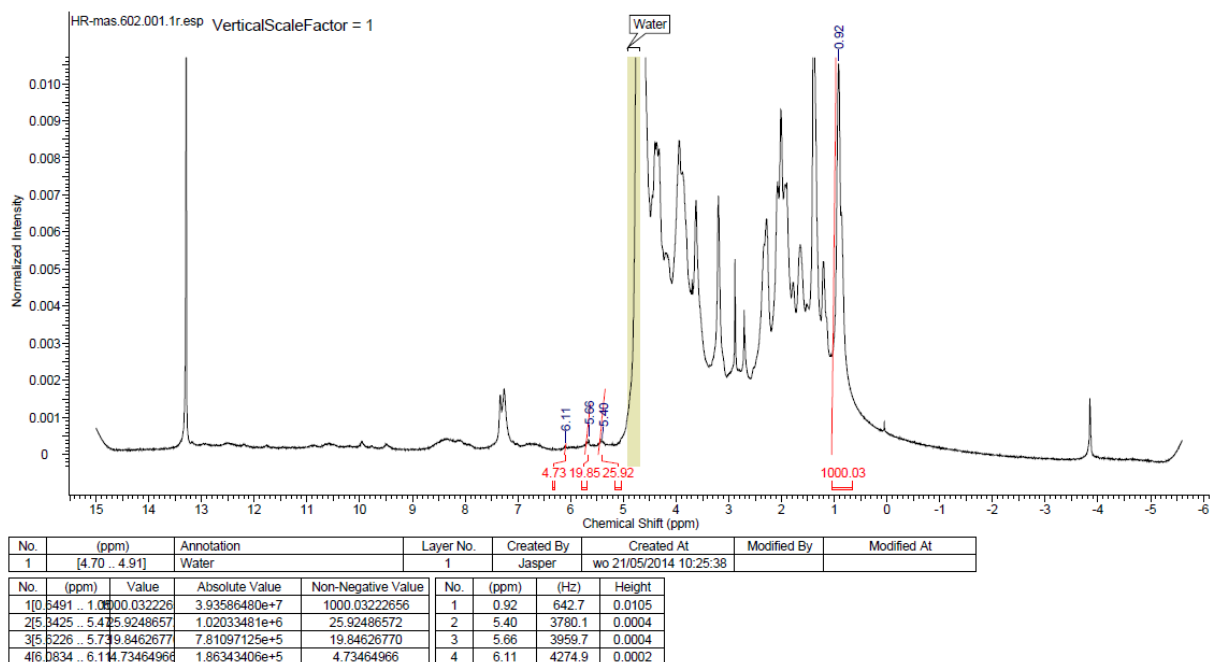
Figure 14: HR-MAS NMR spectrum of gel-MOD-AEMA 87

No.	(ppm)	Annotation			Layer No.	Created By	Created At	Modified By	Modified At
1	[4.70 .. 4.91]	Water			1	Jasper	wo 21/05/2014 10:25:38		

No.	(ppm)	Value	Absolute Value	Non-Negative Value	No.	(ppm)	(Hz)	Height
1	[0.6491 .. 1.06	1000.032226	3.93586480e+7	1000.03222656	1	0.92	642.7	0.0105
2	[5.3425 .. 5.42	25.9248657	1.02033481e+6	25.92486572	2	5.40	3780.1	0.0004
3	[5.6226 .. 5.73	19.8462677	7.81097125e+5	19.84626770	3	5.66	3959.7	0.0004
4	[6.0834 .. 6.11	4.73464966	1.86343406e+5	4.73464966	4	6.11	4274.9	0.0002

No.	(ppm)	Value	Absolute Value	Non-Negative Value
1	0.4791 .. 0.98	1000.000000	3.49375880e+7	1000.00000000
2	5.3453 .. 5.43	71.9572448	2.51401250e+6	71.95724487
3	5.6045 .. 5.70	73.9279632	2.58286475e+6	73.92796326
4	6.0480 .. 6.11	42.4194259	1.48203238e+6	42.41942596

No.	(ppm)	(Hz)	Height
1	0.88	618.1	0.0139
2	5.39	3770.5	0.0029
3	5.63	3940.4	0.0026
4	6.06	4245.0	0.0021

Figure 15: HR-MAS NMR spectrum of gel-MOD-AEMA 97.

101

Addendum E: Production of PLA scaffolds

E.I Pristine PLA Filament DSC, GPC, NMR results
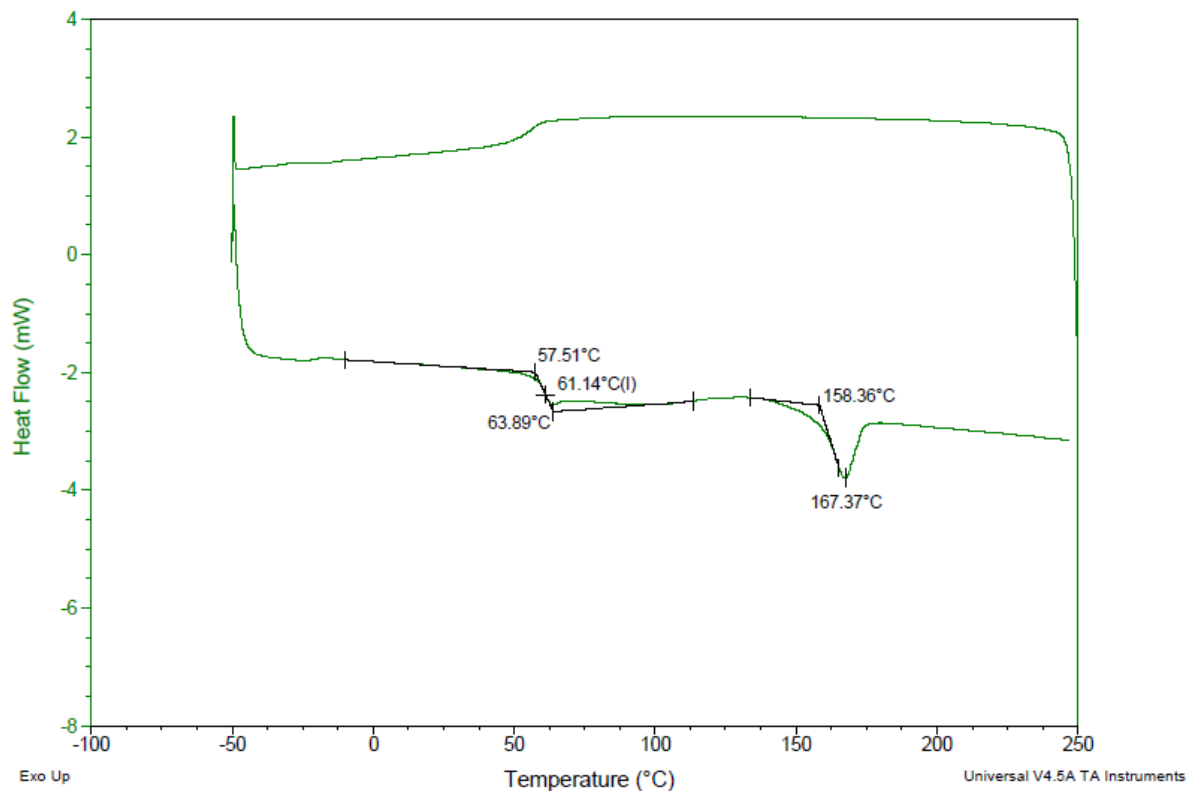
Figure 16: DSC thermogram revealing a glass transition state around 61.14°C and a melting temperature at 167.37°C.
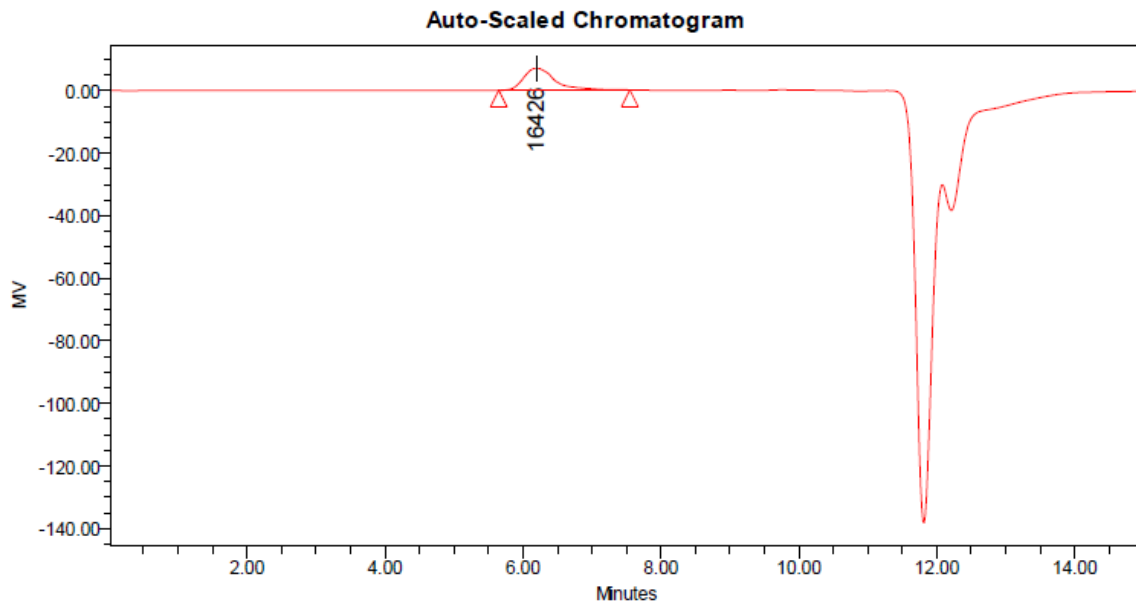
GPC Results

	Dist Name	Mn	Mw	MP	Mz	Mz+1	Mv	Polydispersity	MW Marker 1	MW Marker 2
1		13501	15291	16426	16677	17820		1.132583		

Figure 17: GPC chromatogram of pristine PLA filament yielded a molecular weight of 16426 Da.
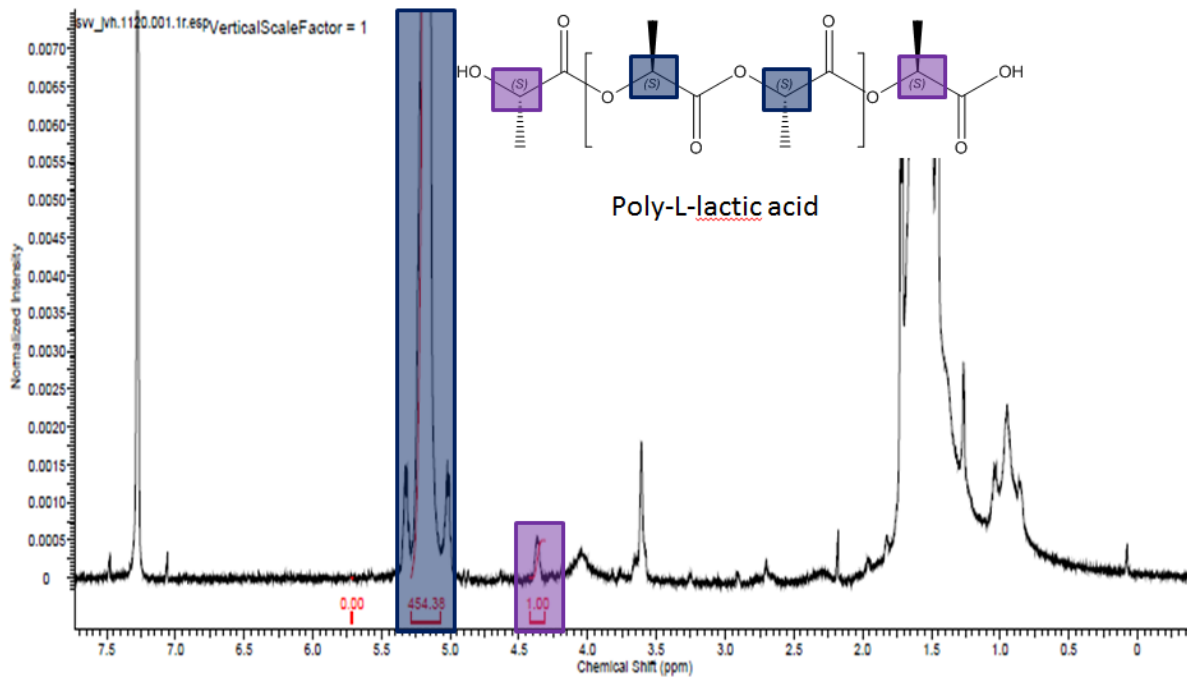
Figure 18: ^{1}H-NMR spectrum of PLLA filament.

$$Mwp = \frac{I\ incorporated}{2 * I\ endgroup} * Mwm$$

$$Mwp = \frac{I_{5.2ppm}}{2 * I_{4,4\ ppm}} * Mwm$$

$$Mwp = \frac{454.38}{2 * 1} * 90.08 = 16420.5\ Da$$

$Mwp =\ polymer\ molecular\ weight \qquad Mwm = monomer\ molecular\ weight$
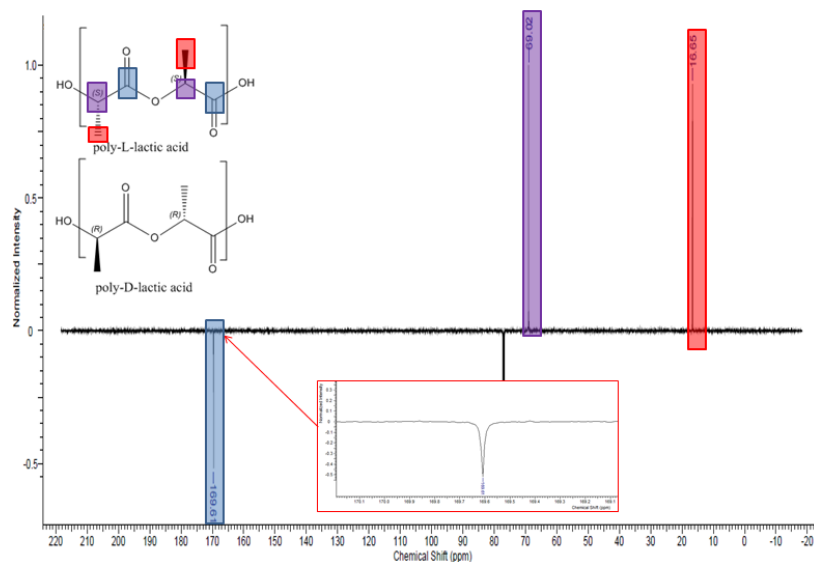
Figure 19: 13C-NMR spectrum of PLLA filament.

The clean signal at 169.61ppm indicates that the PLA filaments are PLLA as the presence of D-lactides would results in the presence of small peaks in the vicinity of this peak as described by Buchatip et al.[181]

103

E.II Example of a Gcode Applied for the Printing of a Scaffold with a pore size of 450 µm and 5*5*3 mm as external dimensions.

```
;Generated with VanHooricksprojects Scaffoldgenerator 1.8
M109 T0 S195.000000
T0
;Sliced at: Tue 13 nov 2013 10:05:05
;Basic settings: Layer height: 0.3 Walls: 0.4 Fill: 0
;Print time: #P_TIME#
;Filament used: #F_AMNT#m #F_WGHT#g
;Filament cost: #F_COST#
G21         ;metric values
G90         ;absolute positioning
M107        ;start with the fan off
G28 X0 Y0   ;move X/Y to min endstops
G28 Z0      ;move Z to min endstops
G1 Z15.0 F9000 ;move the platform down 15mm
G92 E0                    ;zero the extruded length
G1 F200 E3               ;extrude 3mm of feed stock
G92 E0                    ;zero the extruded length again
G1 F9000
M117 Printing...

;total_layers=10
;LAYER:0
M107
G0 F1260 X50 Y50 Z0.30
;TYPE:WALL-OUTER
G1 F660 X50 Y50 E0.17
G1 X55 Y50 E0.255
G1 X55 Y50.85 E0.255
G1 X50 Y50.85 E0.34
G1 X50 Y51.7 E0.34
G1 X55 Y51.7 E0.425
G1 X55 Y52.55 E0.425
G1 X50 Y52.55 E0.51
G1 X50 Y53.4 E0.51
G1 X55 Y53.4 E0.595
G1 X55 Y54.25 E0.595
G1 X50 Y54.25 E0.68
G1 X50 Y55 E0.68
G1 X55 Y55 E0.765
G0 F4680 X55 Y55
;LAYER:1
M106 S255
G0 F1260 X55 Y55 Z0.6
;TYPE:WALL-OUTER
G1 F660 X55 Y55 E0.85
G1 X55 Y50 E0.935
G1 X54.15 Y50 E0.935
G1 X54.15 Y55 E1.02
G1 X53.3 Y55 E1.02
G1 X53.3 Y50 E1.105
G1 X52.45 Y50 E1.105
G1 X52.45 Y55 E1.19
G1 X51.6 Y55 E1.19
G1 X51.6 Y50 E1.275
G1 X50.75 Y50 E1.275
G1 X50.75 Y55 E1.36
G1 X50 Y55 E1.36
G1 F1260 X50 Y50 E1.445
G0 X50.5 Y50.5


…


;LAYER:9
G0 X55 Y55 Z3
;TYPE:WALL-OUTER
G1 F660 X55 Y55 E6.63
G1 X55 Y50 E6.715
G1 X54.15 Y50 E6.715
G1 X54.15 Y55 E6.8
G1 X53.3 Y55 E6.8
G1 X53.3 Y50 E6.885
```

```
G1 X52.45 Y50 E6.885
G1 X52.45 Y55 E6.97
G1 X51.6 Y55 E6.97
G1 X51.6 Y50 E7.055
G1 X50.75 Y50 E7.055
G1 X50.75 Y55 E7.14
G1 X50 Y55 E7.14
G1 F1260 X50 Y50 E7.225
G0 X50.5 Y50.5
M107
;End GCode
M104 S0                      ;extruder heater off
M140 S0                      ;heated bed heater off (if you have it)
G91                                    ;relative positioning
G1 E-1 F300                            ;retract the filament a bit before lifting the
nozzle, to release some of the pressure
G1 Z+0.5 E-5 X-20 Y-20 F9000 ;move Z up a bit and retract filament even more
G28 X0 Y0                              ;move X/Y to min endstops, so the head is out
of the way
M84                          ;steppers off
G90                          ;absolute positioning
```

E.III Self-developed Gcode Generating Program Written in Visual Basic for Applications.

```
Option Explicit
Dim poriegrootte As Double
Dim poriegrootteX As Double
Sub coordinatenevenlagen()

Dim dimensies As Double
Dim poriegrootte As Double
Dim i As Integer
Dim x() As Double
Dim y() As Double
Dim j As Integer
Dim poriegrootteX As Double
i = 3
j = 1
poriegrootte = Worksheets("blad2").Cells(2, 3)   'startwaarden invoeren
poriegrootteX = poriegrootte + 0.4
dimensies = Worksheets("blad2").Cells(4, 3)
Worksheets("blad2").Cells(3, 2) = 50
Worksheets("blad2").Cells(4, 2) = 50
Worksheets("blad2").Cells(3, 1) = 50
Worksheets("blad2").Cells(4, 1) = 50 + dimensies

ReDim y(3)
ReDim x(3)
ReDim E(1)

Do Until (y(i - 1) = (50 + dimensies)) And (x(i - 1) = (50 + dimensies))

    y(1) = 50
    y(2) = 50
    If y(i - 1) = y(i - 2) Then
        y(i) = y(i - 1) + poriegrootteX
        Else: y(i) = y(i - 1)

    End If

    If y(i) > (50 + dimensies) Then y(i) = (50 + dimensies)

    Worksheets("blad2").Cells(i + 2, 2) = y(i) 'y waarde printen

    x(1) = 50
    x(2) = (50 + dimensies)
    If x(i - 1) = 50 And x(i - 2) = 50 Then
        x(i) = (50 + dimensies)
        ElseIf x(i - 1) = (50 + dimensies) And x(i - 2) = (50 + dimensies) Then
        x(i) = 50
        Else: x(i) = x(i - 1)
    End If
```

```vba
        Worksheets("blad2").Cells(i + 2, 1) = x(i) 'x waarde printen

        i = i + 1 'volgende stap
        ReDim Preserve y(i)
        ReDim Preserve x(i)
        ReDim Preserve E(i)
Loop

End Sub
```

```vba
Sub coordinatenonevenlagen()

Dim dimensies As Double
Dim poriegrootte As Double
Dim i As Integer
Dim x() As Double
Dim y() As Double
Dim j As Integer
Dim poriegrootteX As Double
i = 3
j = 1
poriegrootte = Worksheets("blad2").Cells(2, 3)   'startwaarden invoeren
poriegrootteX = poriegrootte + 0.4
dimensies = Worksheets("blad2").Cells(4, 3)
Worksheets("blad2").Cells(3, 4) = (50 + dimensies)
Worksheets("blad2").Cells(4, 4) = (50 + dimensies)
Worksheets("blad2").Cells(3, 5) = (50 + dimensies)
Worksheets("blad2").Cells(4, 5) = 50

ReDim y(3)
ReDim x(3)


Do Until (x(i - 1) = 50) And (y(i - 1) = 50)
    x(1) = (50 + dimensies)
    x(2) = (50 + dimensies)
    If x(i - 1) = x(i - 2) Then
        x(i) = x(i - 1) - poriegrootteX
    Else: x(i) = x(i - 1)

    End If

    If x(i) < 50 Then x(i) = 50

    Worksheets("blad2").Cells(i + 2, 4) = x(i) 'x waarde printen

    y(1) = (50 + dimensies)
    y(2) = 50
        If i = 3 Then
        y(i) = 50
        ElseIf y(i - 1) = 50 And y(i - 2) = 50 Then
        y(i) = (50 + dimensies)
        ElseIf y(i - 1) = (50 + dimensies) And y(i - 2) = (50 + dimensies) Then
        y(i) = 50
        Else: y(i) = y(i - 1)
    End If

    Worksheets("blad2").Cells(i + 2, 5) = y(i) 'x waarde printen

    i = i + 1 'volgende stap
    ReDim Preserve y(i)
    ReDim Preserve x(i)

Loop

End Sub
```

```vba
Sub extrusie()

Dim n As Integer
Dim s As Integer
Dim layer(0 To 50)  As Integer
Dim langgrond As Double
Dim kortgrond As Double
Dim dimensies As Double
Dim temperatuur As Double
Dim lagen As Double
Dim lang As Double
Dim kort As Double
Dim layerHEIGHT As Double
Dim j As Integer
Dim k As Integer     'er moet altijd een laag in een richting
```

106

```vba
Dim E As Double 'totale geextrudeerde hoeveelheid
Dim Z As String
poriegrootte = Worksheets("blad2").Cells(2, 3)   'startwaarden invoeren
poriegrootteX = poriegrootte + 0.4
dimensies = Worksheets("blad2").Cells(4, 3)
lagen = Worksheets("blad2").Cells(6, 3)
temperatuur = Worksheets("blad2").Cells(8, 3)
If temperatuur < 190 Or temperatuur > 250 Then
    MsgBox ("Gelieve een temperatuur tussen 190°C en 250°C te kiezen.")
End If


langgrond = 0.017 * dimensies                 'extrudeerhoeveelhedi grondlaag lang
kortgrond = 0 * poriegrootteX               'extrudeerhoeveelheid grondlaag kort
lang = 0.09155
kort = 0.006 * poriegrootteX
E = 0
k = 4

n = FreeFile()
Open "C:\Documents and Settings\Chris\Mijn documenten\Ultimaker\Output.txt" For Output
As #n

    Print #n, ";Generated with VanHooricksprojects Scaffoldgenerater 1.8"
    Print #n, "M109 T0 S" & temperatuur & ".000000"
    Print #n, "T0"
    Print #n, ";Sliced at: Tue 13 nov 2013 10:05:05"
    Print #n, ";Basic settings: Layer height: 0.3 Walls: 0.4 Fill: 0"
    Print #n, ";Print time: #P_TIME#"
    Print #n, ";Filament used: #F_AMNT#m #F_WGHT#g"
    Print #n, ";Filament cost: #F_COST#"
    Print #n, "G21           ;metric values"
    Print #n, "G90           ;absolute positioning"
    Print #n, "M107          ;start with the fan off"
    Print #n, "G28 X0 Y0   ;move X/Y to min endstops"
    Print #n, "G28 Z0      ;move Z to min endstops"
    Print #n, "G1 Z15.0 F9000 ;move the platform down 15mm"
    Print #n, "G92 E0                    ;zero the extruded length"
    Print #n, "G1 F200 E3                ;extrude 3mm of feed stock"
    Print #n, "G92 E0                    ;zero the extruded length again"
    Print #n, "G1 F9000"
    Print #n, "M117 Printing..."
    Print #n, ""
    Print #n, ";total_layers=" & lagen

For j = 0 To (lagen - 1)
    If j = 0 Then
        E = langgrond + E
        Worksheets("blad2").Cells(2, 7) = E
            Print #n, ";LAYER:0"
            Print #n, "M107"
            Print #n, "G0 F1260 X50 Y50 Z0.30"
            Print #n, ";TYPE:WALL-OUTER"

        E = langgrond + E
Worksheets("blad2").Cells(3, 7) = E
Replace(Worksheets("blad2").Cells(3, 2), ",", ".") & " E" & Replace(E, ",", ".")
        Print #n, "G1 F660 X" & Replace(Worksheets("blad2").Cells(3, 1), ",", ".") & "
        Y" & Replace(Worksheets("blad2").Cells(3, 2), ",", ".") & " E" & Replace(E, ",",
        ".")
Do Until (Worksheets("blad2").Cells(k, 1) < 50)
If Worksheets("blad2").Cells(k, 1) - Worksheets("blad2").Cells(k - 1, 1) = 0 Then
                E = E + kortgrond
            Else
                E = E + langgrond
            End If
            Worksheets("blad2").Cells(k, 7) = E
Replace(Worksheets("blad2").Cells(k, 2), ",", ".") & " E" & Replace(E, ",", ".")
Print #n, "G1 X" & Replace(Worksheets("blad2").Cells(k, 1), ",", ".") & " Y" &
Replace(Worksheets("blad2").Cells(k, 2), ",", ".") & " E" & Replace(E, ",", ".")
            k = k + 1
        Loop
      Print #n, "G0 F4680 X" & (50 + dimensies) & " Y" & (50 + dimensies); ""
      k = 4
    ElseIf j / 2 = Int(j / 2) Then
        E = E + langgrond
        Worksheets("blad2").Cells(2, j + 7) = E
        Print #n, ";LAYER:" & j
                Z = 0.3 + 0.3 * j
```

```vba
Replace(Worksheets("blad2").Cells(3, 2), ",", ".") & " Z" & Replace(Z, ",", ".")
Print #n, "G0 X" & Replace(Worksheets("blad2").Cells(3, 1), ",", ".") & " Y" &
Replace(Worksheets("blad2").Cells(3, 2), ",", ".") & " Z" & Replace(Z, ",", ".")
                    Print #n, ";TYPE:WALL-OUTER"
                E = E + langgrond
        Worksheets("blad2").Cells(3, j + 7) = E
            If k = 4 Then
Replace(Worksheets("blad2").Cells(3, 2), ",", ".") & " E" & Replace(E, ",", ".")
        Print #n, "G1 F660 X" & Replace(Worksheets("blad2").Cells(3, 1), ",", ".") & "
        Y" & Replace(Worksheets("blad2").Cells(3, 2), ",", ".") & " E" & Replace(E, ",",
        ".")
            Else
Replace(Worksheets("blad2").Cells(3, 2), ",", ".") & " E" & Replace(E, ",", ".")
Print #n, "G1 X" & Replace(Worksheets("blad2").Cells(3, 1), ",", ".") & " Y" &
Replace(Worksheets("blad2").Cells(3, 2), ",", ".") & " E" & Replace(E, ",", ".")
            End If
        Do Until (Worksheets("blad2").Cells(k, 1) < 50)

If Worksheets("blad2").Cells(k, 1) - Worksheets("blad2").Cells(k - 1, 1) = 0 Then
            E = E + kortgrond

            Else
            E = E + langgrond
            End If

            Worksheets("blad2").Cells(k, j + 7) = E
If Worksheets("blad2").Cells(k, 1) = (50 + dimensies) And Worksheets("blad2").Cells(k,
2) = (50 + dimensies) Then
Replace(Worksheets("blad2").Cells(k, 2), ",", ".") & " E" & Replace(E, ",", ".")
Print #n, "G1 F1260 X" & Replace(Worksheets("blad2").Cells(k, 1), ",", ".") & " Y" &
Replace(Worksheets("blad2").Cells(k, 2), ",", ".") & " E" & Replace(E, ",", ".")
            Else
Replace(Worksheets("blad2").Cells(k, 2), ",", ".") & " E" & Replace(E, ",", ".")
Print #n, "G1 X" & Replace(Worksheets("blad2").Cells(k, 1), ",", ".") & " Y" &
Replace(Worksheets("blad2").Cells(k, 2), ",", ".") & " E" & Replace(E, ",", ".")
            End If
            k = k + 1
            Loop
            Print #n, "G0 F1260 X" & (50 + dimensies) & " Y" & (50 + dimensies)
            k = 4
    Else
        E = E + langgrond
        Worksheets("blad2").Cells(2, j + 7) = E
        Print #n, ";LAYER:" & j
            If j = 1 Then
            Print #n, "M106 S255"
            Z = 0.3 + 0.3 * j    'Waarde van Z met 0.3 laten toenemen zodat het
platform zakt
Print #n, "G0 F1260 X" & (50 + dimensies) & " Y" & (50 + dimensies) & " Z" &
Replace(Z, ",", ".")
            Print #n, ";TYPE:WALL-OUTER"
            Print #n, "G1 F660 X" & (50 + dimensies) & " Y" & (50 + dimensies) & " E"
& Replace(E, ",", ".")
            Else
            Z = 0.3 + 0.3 * j 'waarde van 2 met 0.3 laten toenemen zodat het platform
zakt
Replace(Worksheets("blad2").Cells(3, 5), ",", ".") & " Z" & Replace(Z, ",", ".")
Print #n, "G0 X" & Replace(Worksheets("blad2").Cells(3, 4), ",", ".") & " Y" &
Replace(Worksheets("blad2").Cells(3, 5), ",", ".") & " Z" & Replace(Z, ",", "."
Print #n, ";TYPE:WALL-OUTER"
            If k = 4 Then
Print #n, "G1 F660 X" & (50 + dimensies) & " Y" & (50 + dimensies) & " E" & Replace(E,
",", ".")
            End If
            End If

        Do Until (Worksheets("blad2").Cells(k, 5) < 50)
If Worksheets("blad2").Cells(k, 5) - Worksheets("blad2").Cells(k - 1, 5) = 0 Then
            E = E + kortgrond
        Else
            E = E + langgrond
        End If
            Worksheets("blad2").Cells(k, j + 7) = E
If Worksheets("blad2").Cells(k, 4) = 50 And Worksheets("blad2").Cells(k, 5) = 50 Then
Replace(Worksheets("blad2").Cells(k, 5), ",", ".") & " E" & Replace(E, ",", ".")
Print #n, "G1 F1260 X" & Replace(Worksheets("blad2").Cells(k, 4), ",", ".") & " Y" &
Replace(Worksheets("blad2").Cells(k, 5), ",", ".") & " E" & Replace(E, ",", ".")
            Else
Replace(Worksheets("blad2").Cells(k, 5), ",", ".") & " E" & Replace(E, ",", ".")
```

```
Print #n, "G1 X" & Replace(Worksheets("blad2").Cells(k, 4), ",", ".") & " Y" &
Replace(Worksheets("blad2").Cells(k, 5), ",", ".") & " E" & Replace(E, ",", ".")
                End If


        k = k + 1
     Loop
     Print #n, "G0 X50.5 Y50.5"
     k = 4
   End If
Next j

     Print #n, "M107"
     Print #n, ";End GCode"
     Print #n, "M104 S0                       ;extruder heater off"
     Print #n, "M140 S0                       ;heated bed heater off (if you have it)"
     Print #n, "G91                               ;relative positioning"
     Print #n, "G1 E-1 F300                          ;retract the filament a bit
before lifting the nozzle, to release some of the pressure"
     Print #n, "G1 Z+0.5 E-5 X-20 Y-20 F9000 ;move Z up a bit and retract filament
even more"
     Print #n, "G28 X0 Y0                            ;move X/Y to min endstops, so
the head is out of the way"
     Print #n, "M84                       ;steppers off"
     Print #n, "G90                       ;absolute positioning"
 Close #n
End Sub
```

```
Sub wissen()
Dim x As Integer
Dim y As Integer
x = 3
y = 1
Do Until Worksheets("blad2").Cells(x, y) = 0
    Do Until Worksheets("blad2").Cells(x, y) = 0 And Worksheets("blad2").Cells(x + 2,
y) = 0
    Worksheets("blad2").Cells(x, y).ClearContents
    x = x + 1
    Loop
x = 2
If y < 7 Then x = 3
y = y + 1
If y = 3 Or y = 6 Then y = y + 1
If y = 7 Then x = 2
Loop
End Sub
```

```
Sub alles()

Call wissen
Call coordinatenevenlagen
Call coordinatenonevenlagen
Call extrusie

End Sub
```

E.IV DSC thermograms for printed PLA samples depending on sample maturity
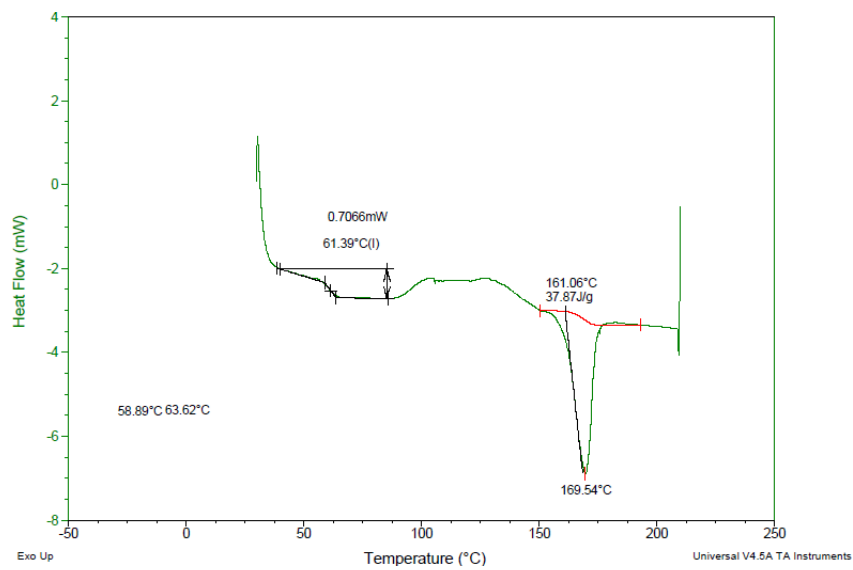

Figure 20: DSC thermogram depicting first heating run of a pristine printed PLA sample.
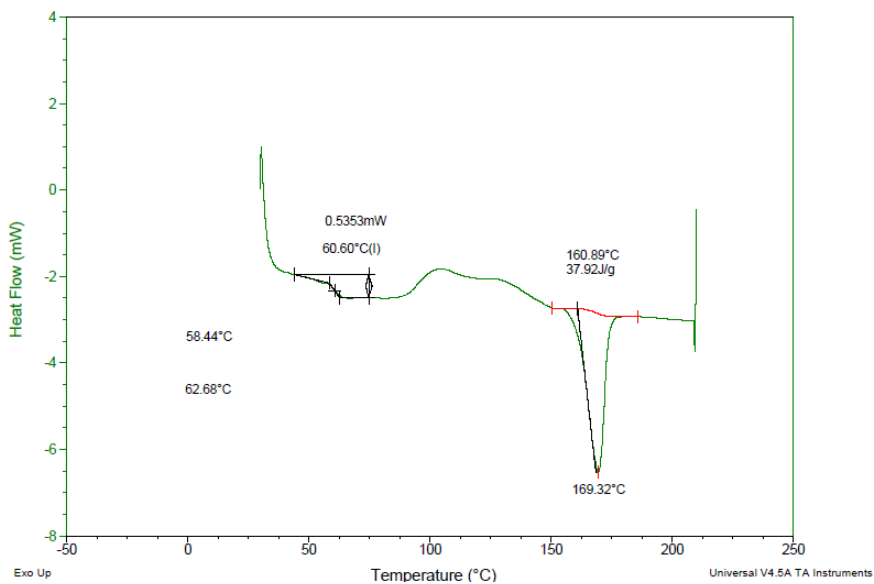

Figure 21: DSC thermogram depicting first heating run of a printed PLA sample which was agedfor 1 weeks at room temperature.
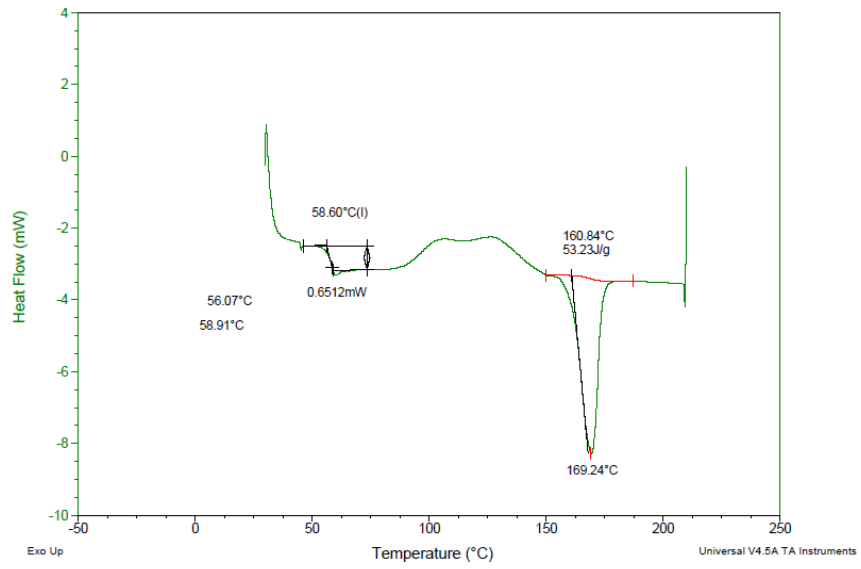
Figure 22: DSC thermogram depicting first heating run of a printed pla sample which was aged for 2 weeks at room temperature. (a more pronounced Tg can be observed)

Addendum F: Submitted abstracts and poster presentations

F.I 2014 Belgian Polymer Group Meeting Poster Presentation

J. Van Hoorick[1], M. Markovic[2], A. Ovsianikov[2], T. Fowler[3], O. Hoffman[3], P. Dubruel[1] and S. Van Vlierberghe[1]

[1]Polymer Chemistry & Biomaterials Group, Ghent University, 9000 Ghent, Belgium
[2]Institute of Materials Science and Technology, Vienna University of Technology (TU Wien), Austria
[3]Dept. Of Pharmacology and Toxicology, University of Vienna, Austria
Jasper.VanHoorick@UGent.be

Ghent University

PBM U-Gent
Polymer Chemistry & Biomaterials Group

MULTIFUNCTIONAL SCAFFOLDS FOR ORTHOPAEDIC TISSUE ENGINEERING APPLICATION: WHEN FUSED DEPOSITION MODELLING MEETS CRYOGELATION

Introduction

The aim of the present work was to develop 3D scaffolds using a combination of fused deposition modeling and a cryogenically treated hydrogel to generate a fully interconnective porous network. (Scheme I) In the present work, two material classes have been applied as starting compounds including polyesters (for their mechanical properties) and crosslinkable gelatin precursors (for their cell-interactive properties).

In parallel, crosslinkable hydrogel precursors containing MT3T3 cells have been introduced into the 3D printed PLA scaffolds, followed by crosslinking through UV irradiation.(Scheme II)
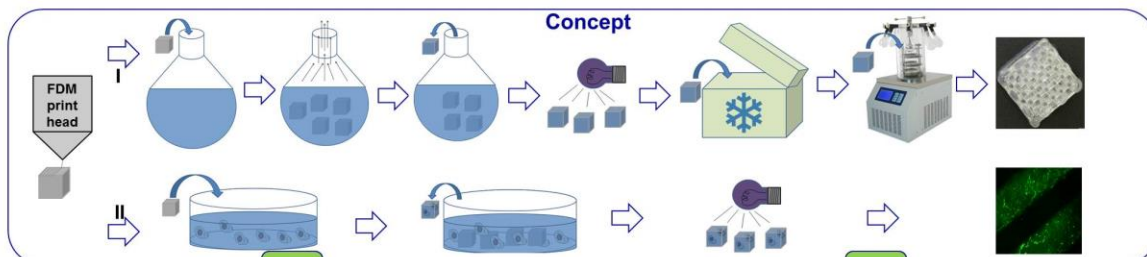
Experimental

In the first approach (I), poly-L-lactic acid scaffolds were generated by fused deposition modeling (Ultimaker). Next, the porous scaffolds were incubated in aqueous methacrylamide-modified gelatin (Gel-MOD, 80%) solutions of varying concentrations (2-10 w/v%) containing 2 mol% Irgacure 2959
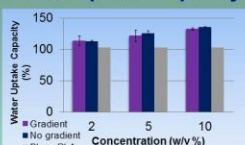
After vacuum treatment, the scaffolds were exposed to UV-light (365 nm) for 2 hours(4), placed in a cryo-unit and cooled from room temperature to -30°C during 5,5 hours (while applying a 30°C temperature gradient). In a final step, the scaffolds were freeze-dried. The scaffolds were characterized using digital microscopy an μ-CT.

In the second approach (II) MC3T3 cells were cultivated prior to resuspension in 10 w/v% Gel-MOD in culture medium containing 0,5 wt% Irgacure 2959. The scaffolds were subsequently seeded with 50 μl of the above mentioned followed by UV-irradiation (365 nm) for 10 minutes.
7 days after seeding scaffolds were stimulated with differentiation medium, Cells were characterized using presto Blue staining for metabolic activity. ALP staining for osteogenic differentiation, live-dead staining with calcein/ propidium lodide and gene expression with qRT-PCR.

Concept

I — FDM print head

II

I

Water Uptake Capacity

Water Uptake Capacity (%) — Gradient / No gradient / Blanc PLA — Concentration (w/v%): 2, 5, 10

The presence of the hydrogel material inside the PLA scaffolds significantly ($p<0,005$) increases the water uptake capacity, with increasing amounts of gel-MOD.

μ-Computed Tomography

5 w/v% no gradient   10 w/v % no gradient   5 w/v% gradient
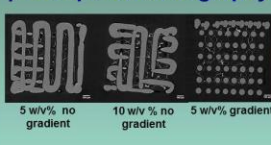
Image slices obtained via μ-Computed Tomograpgy clearly demonstrates the presence of the gel-MOD cryogel throughout the entire scaffold. Even penetrating to the core of the scaffolds.

Digital Microscopy

2 w/v%   2 w/v%   5 w/v%   2 w/v% after leaching   2 w/v% after leaching
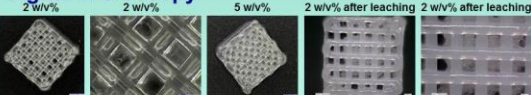
Digital microscopy revealed the gelatin structure in the PLA scaffolds after the cryogenic treatment and after incubation at 40°C to dissolve unreacted gel-MOD
(all images show scaffolds prepared without temperature gradient)

II

Metabolic Activity

Time line	Metabolic activity (fluorescence)	Cell number estimation
3 days after seeding	977 ± 212	
7 days after seeding	954 ± 92	160000
+ 1 week with DM	2274 ± 155	365000
+ 2 weeks with DM	2615 ±70	420000
+ 3 weeks with DM	1459 ± 98	260000

After 3 weeks of cell culture a substantial increase in metabolic activity could be observed. After 2 weeks, the amount of cells present in the scaffolds was close to the initially seeded 500000 cells prior to UV crosslinking. This proves that cell proliferation remained intact after UV crosslinking.

Live/Dead Staining

7 days with DM   14 Days with DM   21 Days with DM
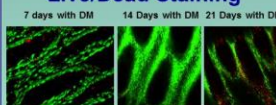
Initially an increase in live/dead ratio was observed followed by a decrease after 3 weeks.

ALP Staining

7 days with DM   14 Days with DM   21 Days with DM
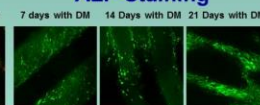
Based on the ALP staining images, an increase in osteogenic differentiation can be observed after 21 days with DM.

Gene Expression Status in the Presence of DM

qRT-PCR was used to investigate gene induction of osteocalcin and RUNX2

Osteocalcin gene expresion — day 0, DM 1 week, DM 2 weeks, DM 3 weeks

RUNX 2 gene expresion — day 0, DM 1 week, DM 2 weeks, DM 3 weeks
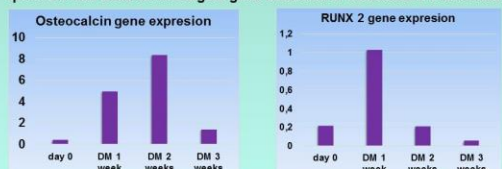
Initially an upregulation in gene expression was observed both for Osteocalcin as wella s for RUNX2. After 3 weeks of stimulation an upregulation of the osteocalcin expression and a downregulation of RUNX2 expression indicates osteogenic differentiation.

Acknowledgement

The authors would like to acknowledge the Research Foundation Flanders (FWO-Flanders) for financial support under the form of a post-doctoral fellowship and a Research Grant ('Development of the ideal tissue engineering scaffold by merging state-of-the art processing techniques', FWO Krediet aan Navorsers).

Conclusion

The UV crosslinking of cell-interactive hydrogel precursos in the presence of suspended cells is a valuable route to introduce cells throughout 3D PLA scaffolds. The positive ALP staining and gene expression status indicate the potential for these printed scaffolds to support osteogenesis. Alternatively, the combination of a gelatin cryogel and a PLA scaffold is a potential candidate for cell seeding purposes in the tissue engineering field.

Tuning the 3D Architecture of Gelatin Hydrogel-PLLA Combination Scaffolds

Jasper Van Hoorick[1], Marica Markovic[2], Aleksandr Ovsianikov[2], Tristan Fowler[3], Oskar Hoffmann[3], Peter Dubruel[1] and Sandra Van Vlierberghe[1*]

[1*]Polymer Chemistry & Biomaterials Research Group, Ghent University, Belgium, sandra.vanvlierberghe@ugent.be
[2]Institute of Materials Science and Technology, Vienna University of Technology (TU Wien), Austria
[3]Dept. of Pharmacology and Toxicology, University of Vienna, Austria

INTRODUCTION
The present work aims at the development of 3D scaffolds using both fused deposition modelling as well as a cryogenic treatment to create a fully interconnected pore network. Two material classes will be applied as starting compounds including polyesters (for their mechanical properties) and crosslinkable gelatin precursors (for their cell-interactive properties).

EXPERIMENTAL METHODS
In a first part, poly-L-lactic acid (PLA) was processed using fused deposition modelling (Ultimaker). Next, the porous PLA scaffolds were incubated in aqueous methacrylamide-modified gelatin (gel-MOD) solutions of varying concentrations (i.e. 2 – 10 w/v%) containing 2 mol% Irgacure 2959. The gelatin applied had a modification degree of 80%. Next, after vacuum application, the scaffolds were exposed to UV-light (365 nm) for 2 hours, placed in a cryo-unit and cooled from room temperature to -30°C during 5.5 hours while applying a temperature gradient of 30°C between top and bottom of the scaffolds. In a final step, the frozen hydrogel-PLA combination scaffolds were transferred to a freeze-dryer to remove the ice crystals. The scaffolds were characterized using micro-computed tomography (μCT) and scanning electron microscopy (SEM). In addition, we assessed the *in vitro* swelling behaviour, the mechanical properties and the degradation behaviour. Furthermore, MC3T3 cells were seeded onto the scaffolds to determine cell interaction, attachment and proliferation.

In parallel, similar hydrogel precursor solutions containing MC3T3 cells were introduced into the 3D printed PLA scaffolds, followed by hydrogel crosslinking through UV irradiation. The scaffolds containing encapsulated cells were characterized using confocal laser scanning microscopy and Presto blue to determine cellular metabolic activity.

RESULTS AND DISCUSSION
First, the efficiency of the UV crosslinking of gel-MOD was assessed after its introduction in the porous PLA. Interestingly, the results indicated that relatively high gel fractions were obtained varying according to the polymer concentration applied which were comparable to the ones obtained in the absence of PLA. *In vitro* degradation tests indicated that the crosslinked gelatin was still prone to degradation in an enzyme containing solution, despite the presence of the surrounding PLA scaffold. Preliminary cell tests showed that upon exceeding a critical gelatin concentration (i.e. 10

w/v%), the presence of cryogels diminished cell migration throughout the PLA scaffolds. Currently, additional cell work is ongoing to optimize the balance between cryogel architecture and stability on the one hand and sufficient cellular infiltration on the other hand. However, the reference samples consisting of crosslinked hydrogel precursors encapsulating MC3T3 cells present in the PLA scaffolds were very promising as indicated in the figures below (scale bars equal 50 μm). After 7 days, an increase in metabolic activity was observed, indicating the occurrence of cell proliferation in the scaffolds. In addition, live-dead stains only showed a limited number of dead cells due to UV crosslinking (see figure below). Moreover, positive ALP staining indicates the potential for these scaffolds to support osteogenesis.
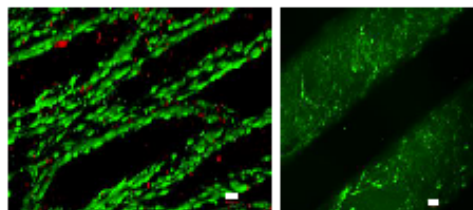
CONCLUSIONS
The UV crosslinking of cell-interactive hydrogel precursors in the presence of suspended cells is a very valuable route to introduce cells throughout 3D PLA scaffolds. Alternatively, the combination of a gelatin cryogel and a PLA scaffold is a potential candidate for cell seeding purposes in the tissue engineering field. Taken together, these results indicate that the applied polymer-related and cryogenic parameters are crucial to determine the optimal cell seeding efficiency and the ultimate cellular infiltration in 3D PLA scaffolds.

REFERENCES
1. Van Vlierberghe S. *et al.*, Biomacromolecules 8: 331-337, 2007

ACKNOWLEDGMENT

Seeding 3D CAD scaffolds with photopolymerizable cell-hydrogel suspension

Marica Markovic[1], Jasper Van Hoorick[2], Sandra Van Vlierberghe[2], Tristan Fowler[3], Oskar Hoffmann[3], Peter Dubruel[2], Aleksandr Ovsianikov[1*]

[1]*Institute of Materials Science and Technology, Vienna University of Technology (TU Wien), Austria*
[2]*Polymer Chemistry & Biomaterials Research Group, Ghent University, Belgium*
[3]*Dept. of Pharmacology and Toxicology, University of Vienna, Austria*

Hydrogels are widely used as 3D matrices for cell growth owing to similarity of their mechanical and diffusivity properties to the natural extracellular matrix (ECM). Furthermore, encapsulation of living cells within the hydrogel allows to produce constructs with high initial cell loading and intimate cell-matrix contact, similar to that of the natural ECM. In this contribution the results of the seeding of macroporous poly-lactic acid (PLA) based scaffolds with the help of photopolymerizable gelatin as a cell delivery material are presented. The 3D scaffolds were produced from PLA in accordance to computer aided design (CAD) model by means of fused deposition modeling (FDM, Ultimaker). A solution of methacrylamide-modified gelatin (gel-MOD) in cell culture medium was used as a cell carrier material for seeding. A 10^7/ml suspension of MC3T3 cells in gel-MOD was introduced into the pores of the scaffold and then photopolymerized. Our results indicate that such seeding procedure facilitates delivering cells into the pores of the scaffolds at high density and homogeneous distribution. The proliferation of the cell within the scaffolds was monitored using a Presto Blue assay for the course of three weeks. The data was verified by DNA quantification at different time points. An upregulation of the osteocalcin expression and a downregulation of RUNX2 indicate the osteogenic differentiation of MC3T3s. These results are confirmed by the positive alkaline phosphatase (ALP) staining. Our findings show that photoinduced encapsulation of cells within a cell-interactive hydrogel is a valuable route to introduce cells throughout 3D scaffolds for bone tissue engineering.

References

[1] E. George, "Low back pain," *Bull. World Health Organ.*, vol. 81, no. 9, pp. 671–676, 2003.

[2] P. P. Raj, "Intervertebral Disc : AnatomyPhysiology-Pathophysiology-Treatment," *World Inst. Pain, Pain Pract.*, vol. 8, no. 1, pp. 18–44, 2008.

[3] S. M. Richardson, R. V Walker, S. Parker, N. P. Rhodes, J. a Hunt, A. J. Freemont, and J. a Hoyland, "Intervertebral disc cell-mediated mesenchymal stem cell differentiation.," *Stem Cells*, vol. 24, no. 3, pp. 707–16, Mar. 2006.

[4] B. R. Whatley, J. Kuo, C. Shuai, B. J. Damon, and X. Wen, "Fabrication of a biomimetic elastic intervertebral disk scaffold using additive manufacturing.," *Biofabrication*, vol. 3, no. 1, p. 015004, Mar. 2011.

[5] K. D. Hudson, M. Alimi, P. Grunert, R. Härtl, and L. J. Bonassar, "Recent advances in biological therapies for disc degeneration: tissue engineering of the annulus fibrosus, nucleus pulposus and whole intervertebral discs.," *Curr. Opin. Biotechnol.*, vol. 24, no. 5, pp. 872–9, Oct. 2013.

[6] Y. Yamamoto, J. Mochida, D. Sakai, T. Nakai, K. Nishimura, H. Kawada, and T. Hotta, "Upregulation of the viability of nucleus pulposus cells by bone marrow-derived stromal cells: significance of direct cell-to-cell contact in coculture system.," *Spine (Phila. Pa. 1976).*, vol. 29, no. 14, pp. 1508–14, Jul. 2004.

[7] L. Ambrosio, A. Gloria, and R. De Santis, *Biomedical composites*. Woodhead Publishing Limited and CRC Press LLC, 2010, pp. 178–200.

[8] R. J. Moore, "The vertebral end-plate: what do we know?," *Eur. Spine J.*, vol. 9, no. 2, pp. 92–6, Apr. 2000.

[9] E. O. Martz, V. K. Goel, M. H. Pope, and J. B. Park, "Materials and design of spinal implants--a review.," *J. Biomed. Mater. Res.*, vol. 38, no. 3, pp. 267–88, Jan. 1997.

[10] D. Sakai, J. Mochida, Y. Yamamoto, T. Nomura, M. Okuma, K. Nishimura, T. Nakai, K. Ando, and T. Hotta, "Transplantation of mesenchymal stem cells embedded in Atelocollagen® gel to the intervertebral disc: a potential therapeutic model for disc degeneration," *Biomaterials*, vol. 24, no. 20, pp. 3531–3541, Sep. 2003.

[11] D. Ruan, H. Xin, C. Zhang, C. Wang, C. Xu, D. Ph, C. Li, and Q. He, "Experimental Intervertebral Disc Regeneration with Tissue-Engineered Composite in a Canine Model," *Tissue Eng.*, vol. 16, no. 7, pp. 2381–2389, 2010.

[12] P. a Revell, E. Damien, L. Di Silvio, N. Gurav, C. Longinotti, and L. Ambrosio, "Tissue engineered intervertebral disc repair in the pig using injectable polymers.," *J. Mater. Sci. Mater. Med.*, vol. 18, no. 2, pp. 303–8, Feb. 2007.

[13] E. Y.-S. See, S. L. Toh, and J. C.-H. Goh, "Effects of Radial Compression on a Novel Simulated Intervertebral Disc–Like Assembly Using Bone Marrow–Derived Mesenchymal Stem Cell Cell-Sheets for Annulus Fibrosus Regeneration," *Spine (Phila. Pa. 1976).*, vol. 36, no. 21, pp. 1744–1751, Oct. 2011.

[14] Y.-C. Chen, W.-Y. Su, S.-H. Yang, A. Gefen, and F.-H. Lin, "In situ forming hydrogels composed of oxidized high molecular weight hyaluronic acid and gelatin for nucleus pulposus regeneration.," *Acta Biomater.*, vol. 9, no. 2, pp. 5181–93, Feb. 2013.

[15] J. E. Frith, A. R. Cameron, D. J. Menzies, P. Ghosh, D. L. Whitehead, S. Gronthos, A. C. W. Zannettino, and J. J. Cooper-White, "An injectable hydrogel incorporating mesenchymal precursor cells and pentosan polysulphate for intervertebral disc regeneration.," *Biomaterials*, vol. 34, no. 37, pp. 9430–40, Dec. 2013.

[16] L. Jin, A. L. Shimmer, and X. Li, "The challenge and advancement of annulus fibrosus tissue engineering.," *Eur. Spine J.*, vol. 22, no. 5, pp. 1090–100, May 2013.

[17] W.-Y. Su, Y.-C. Chen, and F.-H. Lin, "Injectable oxidized hyaluronic acid/adipic acid dihydrazide hydrogel for nucleus pulposus regeneration.," *Acta Biomater.*, vol. 6, no. 8, pp. 3044–55, Aug. 2010.

[18] A. R. Jackson, T.-Y. Yuan, C.-Y. Huang, M. D. Brown, and W. Y. Gu, "Nutrient transport in human annulus fibrosus is affected by compressive strain and anisotropy.," *Ann. Biomed. Eng.*, vol. 40, no. 12, pp. 2551–8, Dec. 2012.

[19] S.-H. Park, H. Cho, E. S. Gil, B. B. Mandal, B.-H. Min, and D. L. Kaplan, "Silk-Fibrin / Hyaluronic Acid Composite Gels for Nucleus Pulposus Tissue Regeneration," *Tissue Eng. Part A*, vol. 17, pp. 2999–3009, 2011.

[20] A. Abbushi, M. Endres, M. Cabraja, S. N. Kroppenstedt, U. W. Thomale, M. Sittinger, A. A. Hegewald, L. Morawietz, A.-J. Lemke, V.-G. Bansemer, C. Kaps, and C. Woiciechowsky, "Regeneration of intervertebral disc tissue by resorbable cell-free polyglycolic acid-based implants in a rabbit model of disc degeneration.," *Spine (Phila. Pa. 1976).*, vol. 33, no. 14, pp. 1527–32, Jun. 2008.

[21] F. Mwale, M. Iordanova, C. N. Demers, T. Steffen, P. Roughley, and J. Antoniou, "Biological evaluation of chitosan salts cross-linked to genipin as a cell scaffold for disk tissue engineering.," *Tissue Eng.*, vol. 11, no. 1–2, pp. 130–40, 2005.

[22] J. L. Bron, L. a Vonk, T. H. Smit, and G. H. Koenderink, "Engineering alginate for intervertebral disc repair.," *J. Mech. Behav. Biomed. Mater.*, vol. 4, no. 7, pp. 1196–205, Oct. 2011.

[23] H. Yang, J. Wu, J. Liu, M. Ebraheim, S. Castillo, X. Liu, T. Tang, and N. a Ebraheim, "Transplanted mesenchymal stem cells with pure fibrinous gelatin-transforming growth factor-beta1 decrease rabbit intervertebral disc degeneration.," *Spine J.*, vol. 10, no. 9, pp. 802–10, Sep. 2010.

[24] L. Kapural, J. P. Cata, and S. Narouze, "Successful treatment of lumbar discogenic pain using intradiscal biacuplasty in previously discectomized disc.," *Pain Pract.*, vol. 9, no. 2, pp. 130–4, 2009.

[25] S. C. W. Chan and B. Gantenbein-Ritter, "Intervertebral disc regeneration or repair with biomaterials and stem cell therapy--feasible or fiction?," *Swiss Med. Wkly.*, vol. 142, no. May, p. w13598, Jan. 2012.

[26] S. C. W. Chan, A. Bürki, H. M. Bonél, L. M. Benneker, and B. Gantenbein-Ritter, "Papain-induced in vitro disc degeneration model for the study of injectable nucleus pulposus therapy.," *Spine J.*, vol. 13, no. 3, pp. 273–83, Mar. 2013.

[27] J. Beaurain, P. Bernard, T. Dufour, J. M. Fuentes, I. Hovorka, J. Huppert, J. P. Steib, J. M. Vital, L. Aubourg, and T. Vila, "Intermediate clinical and radiological results of cervical TDR (Mobi-C) with up to 2 years of follow-up.," *Eur. Spine J.*, vol. 18, no. 6, pp. 841–50, Jun. 2009.

[28] J. S. Harrop, J. a Youssef, M. Maltenfort, P. Vorwald, P. Jabbour, C. M. Bono, N. Goldfarb, A. R. Vaccaro, and A. S. Hilibrand, "Lumbar adjacent segment degeneration and disease after

arthrodesis and total disc arthroplasty.," *Spine (Phila. Pa. 1976).*, vol. 33, no. 15, pp. 1701–7, Jul. 2008.

[29]   S. M. Kurtz, A. van Ooij, R. Ross, J. de Waal Malefijt, J. Peloza, L. Ciccarelli, and M. L. Villarraga, "Polyethylene wear and rim fracture in total disc arthroplasty.," *Spine J.*, vol. 7, no. 1, pp. 12–21, 2007.

[30]   A. van Ooij, S. M. Kurtz, F. Stessels, H. Noten, and L. van Rhijn, "Polyethylene wear debris and long-term clinical failure of the Charité disc prosthesis: a study of 4 patients.," *Spine (Phila. Pa. 1976).*, vol. 32, no. 2, pp. 223–9, Jan. 2007.

[31]   N. De Beer and A. Van Der Merwe, "Patient-specific intervertebral disc implants using rapid manufacturing technology," *Rapid Prototyp. J.*, vol. 19, no. 2, pp. 126–139, 2013.

[32]   a Ovsianikov, M. Malinauskas, S. Schlie, B. Chichkov, S. Gittard, R. Narayan, M. Löbler, K. Sternberg, K.-P. Schmitz, and a Haverich, "Three-dimensional laser micro- and nano-structuring of acrylated poly(ethylene glycol) materials and evaluation of their cytoxicity for tissue engineering applications.," *Acta Biomater.*, vol. 7, no. 3, pp. 967–74, Mar. 2011.

[33]   a. Ovsianikov, a. Ostendorf, and B. N. Chichkov, "Three-dimensional photofabrication with femtosecond lasers for applications in photonics and biomedicine," *Appl. Surf. Sci.*, vol. 253, no. 15, pp. 6599–6602, May 2007.

[34]   F. P. W. Melchels, J. Feijen, and D. W. Grijpma, "A review on stereolithography and its applications in biomedical engineering.," *Biomaterials*, vol. 31, no. 24, pp. 6121–30, Aug. 2010.

[35]   N. Kathuria, A. Tripathi, K. K. Kar, and A. Kumar, "Synthesis and characterization of elastic and macroporous chitosan-gelatin cryogels for tissue engineering.," *Acta Biomater.*, vol. 5, no. 1, pp. 406–18, Jan. 2009.

[36]   G. Vadalà, P. Mozetic, A. Rainer, M. Centola, M. Loppini, M. Trombetta, and V. Denaro, "Bioactive electrospun scaffold for annulus fibrosus repair and regeneration.," *Eur. Spine J.*, vol. 21 Suppl 1, pp. S20–6, May 2012.

[37]   M. Bhattacharjee, S. Miot, A. Gorecka, K. Singha, M. Loparic, S. Dickinson, A. Das, N. S. Bhavesh, A. R. Ray, I. Martin, and S. Ghosh, "Oriented lamellar silk fibrous scaffolds to drive cartilage matrix orientation: towards annulus fibrosus tissue engineering.," *Acta Biomater.*, vol. 8, no. 9, pp. 3313–25, Sep. 2012.

[38]   K.-I. Lee, S.-H. Moon, H. Kim, U.-H. Kwon, H.-J. Kim, S.-N. Park, H. Suh, H.-M. Lee, H.-S. Kim, H.-J. Chun, I.-K. Kwon, and J.-W. Jang, "Tissue engineering of the intervertebral disc with cultured nucleus pulposus cells using atelocollagen scaffold and growth factors.," *Spine (Phila. Pa. 1976).*, vol. 37, no. 6, pp. 452–8, Mar. 2012.

[39]   B. G. M. van Dijk, E. Potier, and K. Ito, "Long-term culture of bovine nucleus pulposus explants in a native environment.," *Spine J.*, vol. 13, no. 4, pp. 454–63, Apr. 2013.

[40]   C.-Q. Li, B. Huang, G. Luo, C.-Z. Zhang, Y. Zhuang, and Y. Zhou, "Construction of collagen II/hyaluronate/chondroitin-6-sulfate tri-copolymer scaffold for nucleus pulposus tissue engineering and preliminary analysis of its physico-chemical properties and biocompatibility.," *J. Mater. Sci. Mater. Med.*, vol. 21, no. 2, pp. 741–51, Feb. 2010.

[41]   G. Paesold, A. G. Nerlich, and N. Boos, "Biological treatment strategies for disc degeneration: potentials and shortcomings.," *Eur. Spine J.*, vol. 16, no. 4, pp. 447–68, Apr. 2007.

[42] A. C. Borges, C. Eyholzer, F. Duc, P.-E. Bourban, P. Tingaut, T. Zimmermann, D. P. Pioletti, and J.-A. E. Månson, "Nanofibrillated cellulose composite hydrogel for the replacement of the nucleus pulposus.," *Acta Biomater.*, vol. 7, no. 9, pp. 3412–21, Sep. 2011.

[43] D. Haschtmann, S. J. Ferguson, and J. V Stoyanov, "BMP-2 and TGF-β3 do not prevent spontaneous degeneration in rabbit disc explants but induce ossification of the annulus fibrosus.," *Eur. spine J.*, vol. 21, no. 9, pp. 1724–33, Sep. 2012.

[44] H. J. Meisel, T. Ganey, W. C. Hutton, J. Libera, Y. Minkus, and O. Alasevic, "Clinical experience in cell-based therapeutics: intervention and outcome.," *Eur. Spine J.*, vol. 15 Suppl 3, pp. S397–405, Aug. 2006.

[45] J. D. Thomas, G. Fussell, S. Sarkar, A. M. Lowman, and M. Marcolongo, "Synthesis and recovery characteristics of branched and grafted PNIPAAm-PEG hydrogels for the development of an injectable load-bearing nucleus pulposus replacement.," *Acta Biomater.*, vol. 6, no. 4, pp. 1319–28, Apr. 2010.

[46] J. M. Anderson, G. Cook, B. Costerton, S. R. Hanson, A. Hensten-Pettersen, N. Jacobson, R. J. Johnson, R. N. Mitchel, M. Pasmore, F. J. Schoen, M. Shirtliff, and P. Stoodley, "Host reactions to biomaterials and their evaluation," in *Biomaterials Science*, 2nd ed., Elsevier, 2004, pp. 293–338.

[47] E. C. Collin, S. Grad, D. I. Zeugolis, C. S. Vinatier, J. R. Clouet, J. J. Guicheux, P. Weiss, M. Alini, and A. S. Pandit, "An injectable vehicle for nucleus pulposus cell-based therapy.," *Biomaterials*, vol. 32, no. 11, pp. 2862–70, Apr. 2011.

[48] H.-J. Wilke, F. Heuer, C. Neidlinger-Wilke, and L. Claes, "Is a collagen scaffold for a tissue engineered nucleus replacement capable of restoring disc height and stability in an animal model?," *Eur. spine J.*, vol. 15 Suppl 3, pp. S433–8, Aug. 2006.

[49] A. T. Francisco, R. J. Mancino, R. D. Bowles, J. M. Brunger, D. M. Tainter, Y.-T. Chen, W. J. Richardson, F. Guilak, and L. a Setton, "Injectable laminin-functionalized hydrogel for nucleus pulposus regeneration.," *Biomaterials*, vol. 34, no. 30, pp. 7381–8, Oct. 2013.

[50] K. Serigano, D. Sakai, A. Hiyama, F. Tamura, M. Tanaka, and J. Mochida, "Effect of cell number on mesenchymal stem cell transplantation in a canine disc degeneration model.," *J. Orthop. Res.*, vol. 28, no. 10, pp. 1267–75, Oct. 2010.

[51] M. Yuan, C. W. Yeung, Y. Y. Li, H. Diao, K. M. C. Cheung, D. Chan, K. Cheah, and P. B. Chan, "Effects of nucleus pulposus cell-derived acellular matrix on the differentiation of mesenchymal stem cells.," *Biomaterials*, vol. 34, no. 16, pp. 3948–61, May 2013.

[52] M. Yuan, K. W. Leong, and B. P. Chan, "Three-dimensional culture of rabbit nucleus pulposus cells in collagen microspheres.," *Spine J.*, vol. 11, no. 10, pp. 947–60, Oct. 2011.

[53] D. O. Halloran, S. Grad, M. Stoddart, P. Dockery, M. Alini, and A. S. Pandit, "An injectable cross-linked scaffold for nucleus pulposus regeneration.," *Biomaterials*, vol. 29, no. 4, pp. 438–47, Mar. 2008.

[54] J. M. Cloyd, N. R. Malhotra, L. Weng, W. Chen, R. L. Mauck, and D. M. Elliott, "Material properties in unconfined compression of human nucleus pulposus, injectable hyaluronic acid-based hydrogels and tissue engineering scaffolds.," *Eur. spine J.*, vol. 16, no. 11, pp. 1892–8, Nov. 2007.

[55] Y.-H. Cheng, S.-H. Yang, C.-C. Liu, A. Gefen, and F.-H. Lin, "Thermosensitive hydrogel made of ferulic acid-gelatin and chitosan glycerophosphate.," *Carbohydr. Polym.*, vol. 92, no. 2, pp. 1512–9, Feb. 2013.

[56] W.-H. Chen, H.-Y. Liu, W.-C. Lo, S.-C. Wu, C.-H. Chi, H.-Y. Chang, S.-H. Hsiao, C.-H. Wu, W.-T. Chiu, B.-J. Chen, and W.-P. Deng, "Intervertebral disc regeneration in an ex vivo culture system using mesenchymal stem cells and platelet-rich plasma.," *Biomaterials*, vol. 30, no. 29, pp. 5523–33, Oct. 2009.

[57] B. Huang, Y. Zhuang, C.-Q. Li, L.-T. Liu, and Y. Zhou, "Regeneration of the intervertebral disc with nucleus pulposus cell-seeded collagen II/hyaluronan/chondroitin-6-sulfate tri-copolymer constructs in a rabbit disc degeneration model.," *Spine (Phila. Pa. 1976).*, vol. 36, no. 26, pp. 2252–9, Dec. 2011.

[58] M. Sha'ban, S. J. Yoon, Y. K. Ko, H. J. Ha, S. H. Kim, J. W. So, R. B. H. Idrus, and G. Khang, "Fibrin promotes proliferation and matrix production of intervertebral disc cells cultured in three-dimensional poly(lactic-co-glycolic acid) scaffold.," *J. Biomater. Sci. Polym. Ed.*, vol. 19, no. 9, pp. 1219–37, Jan. 2008.

[59] L. J. Nesti, W.-J. Li, R. M. Shanti, Y. J. Jiang, W. Jackson, B. a Freedman, T. R. Kuklo, J. R. Giuliani, and R. S. Tuan, "Intervertebral disc tissue engineering using a novel hyaluronic acid-nanofibrous scaffold (HANFS) amalgam.," *Tissue Eng. Part A*, vol. 14, no. 9, pp. 1527–37, Sep. 2008.

[60] S. M. Richardson, J. M. Curran, R. Chen, A. Vaughan-Thomas, J. a Hunt, A. J. Freemont, and J. A. Hoyland, "The differentiation of bone marrow mesenchymal stem cells into chondrocyte-like cells on poly-L-lactic acid (PLLA) scaffolds.," *Biomaterials*, vol. 27, no. 22, pp. 4069–78, Aug. 2006.

[61] N. L. Nerurkar, B. M. Baker, S. Sen, E. E. Wible, D. M. Elliott, and R. L. Mauck, "Nanofibrous biologic laminates replicate the form and function of the annulus fibrosus.," *Nat. Mater.*, vol. 8, no. 12, pp. 986–92, Dec. 2009.

[62] G. Chang, H.-J. Kim, D. Kaplan, G. Vunjak-Novakovic, and R. a Kandel, "Porous silk scaffolds can be used for tissue engineering annulus fibrosus.," *Eur. Spine J.*, vol. 16, no. 11, pp. 1848–57, Nov. 2007.

[63] J. Bao, W. Lv, Y. Sun, and Y. Deng, "Electrospun antimicrobial microfibrous scaffold for annulus fibrosus tissue engineering," *J. Mater. Sci.*, vol. 48, no. 12, pp. 4223–4232, Feb. 2013.

[64] L. Yang, R. a Kandel, G. Chang, and J. P. Santerre, "Polar surface chemistry of nanofibrous polyurethane scaffold affects annulus fibrosus cell attachment and early matrix accumulation.," *J. Biomed. Mater. Res. A*, vol. 91, no. 4, pp. 1089–99, Dec. 2009.

[65] G. T. Klein, Y. Lu, and M. Y. Wang, "3D Printing and Neurosurgery -ready for prime time," *World Neurosurg.*, vol. 80, pp. 228–235, 2013.

[66] Y. Pan, T. Chu, S. Dong, Y. Hao, X. Ren, J. Wang, W. Wang, C. Li, Z. Zhang, and Y. Zhou, "Cells scaffold complex for Intervertebral disc Anulus Fibrosus tissue engineering: in vitro culture and product analysis.," *Mol. Biol. Rep.*, vol. 39, no. 9, pp. 8581–94, Sep. 2012.

[67] N. L. Nerurkar, R. L. Mauck, and D. M. Elliott, "ISSLS prize winner: integrating theoretical and experimental methods for functional tissue engineering of the annulus fibrosus.," *Spine (Phila. Pa. 1976).*, vol. 33, no. 25, pp. 2691–701, Dec. 2008.

[68] M. Yeganegi, R. a Kandel, and J. P. Santerre, "Characterization of a biodegradable electrospun polyurethane nanofiber scaffold: Mechanical properties and cytotoxicity.," *Acta Biomater.*, vol. 6, no. 10, pp. 3847–55, Oct. 2010.

[69] X. Shao and C. J. Hunter, "Developing an alginate / chitosan hybrid fiber scaffold for annulus fibrosus cells," *J. Biomed. Mater. Res. Part A*, vol. 82, no. 3, pp. 701–710, 2007.

[70] R. M. Schek, A. J. Michalek, and J. C. Iatridis, "GENIPIN-CROSSLINKED FIBRIN HYDROGELS AS A POTENTIAL ADHESIVE TO AUGMENT INTERVERTEBRAL DISC ANNULUS REPAIR," *Eur. cells Mater.*, vol. 21, pp. 373–383, 2011.

[71] W. Helen, C. L. R. Merry, J. J. Blaker, and J. E. Gough, "Three-dimensional culture of annulus fibrosus cells within PDLLA / Bioglass s composite foam scaffolds : Assessment of cell attachment , proliferation and extracellular matrix production," *Biomaterials*, vol. 28, no. 2007, pp. 2010–2020, 2010.

[72] N. L. Nerurkar, S. Sen, alice H. Huang, D. M. Elliott, and R. L. Mauck, "Engineered disc-like angle-ply structures for intervertebral disc replacement," *Spine (Phila. Pa. 1976).*, vol. 35, no. 8, pp. 867–873, 2010.

[73] H. Mizuno, A. K. Roy, V. Zaporojan, C. a Vacanti, M. Ueda, and L. J. Bonassar, "Biomechanical and biochemical characterization of composite tissue-engineered intervertebral discs.," *Biomaterials*, vol. 27, no. 3, pp. 362–70, Jan. 2006.

[74] R. D. Bowles, H. H. Gebhard, J. P. Dyke, D. J. Ballon, A. Tomasino, M. E. Cunningham, R. Härtl, and L. J. Bonassar, "Image-based tissue engineering of a total intervertebral disc implant for restoration of function to the rat lumbar spine.," *NMR Biomed.*, vol. 25, no. 3, pp. 443–51, Mar. 2012.

[75] Y. Zhuang, B. Huang, C. Q. Li, L. T. Liu, Y. Pan, W. J. Zheng, G. Luo, and Y. Zhou, "Construction of tissue-engineered composite intervertebral disc and preliminary morphological and biochemical evaluation.," *Biochem. Biophys. Res. Commun.*, vol. 407, no. 2, pp. 327–32, Apr. 2011.

[76] M. Lazebnik, M. Singh, and P. Glatt, "Biomimetic method for combining the nucleus pulposus and annulus fibrosus for intervertebral disc tissue engineering.," *J. Tissue Eng. Regen. Med.*, vol. 5, no. 8, pp. E179–E187, 2011.

[77] S.-H. Park, E. S. Gil, H. Cho, B. B. Mandal, L. w. Tien, B.-H. Min, and D. L. Kaplan, "Intervertebral disk tissue engineering using biphasic silk composite scaffolds," *Tissue Eng. Part A*, vol. 18, no. 5, pp. 447–458, 2012.

[78] R. D. Bowles, H. H. Gebhard, R. Härtl, and L. J. Bonassar, "Tissue-engineered intervertebral discs produce new matrix, maintain disc height, and restore biomechanical function to the rodent spine.," *Proc. Natl. Acad. Sci. U. S. A.*, vol. 108, no. 32, pp. 13106–11, Aug. 2011.

[79] Y. Wu, B. Xu, Q. Yang, X. Li, Y. Zhang, X. Ma, Q. Xia, H. Xu, C. Zeng, and Y. Zhang, "A novel natural ECM-derived biphasic scaffold for intervertebral disc tissue engineering," *Mater. Lett.*, vol. 105, pp. 102–105, Aug. 2013.

[80] R. D. Bowles, R. M. Williams, W. R. Zipfel, and L. J. Bonassar, "Self-assembly of alligned tissue-engineered annulus fibrosus and intervertebral disc composite via collagen gel contraction," *Tissue Eng. Part A*, vol. 16, no. 4, pp. 1339–1348, 2010.

[81] H. Mizuno, A. K. Roy, C. a Vacanti, K. Kojima, M. Ueda, and L. J. Bonassar, "Tissue-engineered composites of anulus fibrosus and nucleus pulposus for intervertebral disc replacement.," *Spine (Phila. Pa. 1976).*, vol. 29, no. 12, pp. 1290–7; discussion 1297–8, Jun. 2004.

120

[82]   S. Van Vlierberghe, P. Dubruel, and E. Schacht, "Biopolymer-based hydrogels as scaffolds for tissue engineering applications: a review.," *Biomacromolecules*, vol. 12, no. 5, pp. 1387–408, May 2011.

[83]   P. Dubruel and F. Du Prez, "Polymer Materials." University of Ghent, Ghent, 2012.

[84]   N. a Peppas, P. Bures, W. Leobandung, and H. Ichikawa, "Hydrogels in pharmaceutical formulations.," *Eur. J. Pharm. Biopharm.*, vol. 50, no. 1, pp. 27–46, Jul. 2000.

[85]   W. E. Hennink and C. F. van Nostrum, "Novel crosslinking methods to design hydrogels," *Adv. Drug Deliv. Rev.*, vol. 64, pp. 223–236, Dec. 2012.

[86]   P. Dubruel, R. Unger, S. Van Vlierberghe, V. Cnudde, P. J. S. Jacobs, E. Schacht, and C. J. Kirkpatrick, "Porous gelatin hydrogels: 2. In vitro cell interaction study.," *Biomacromolecules*, vol. 8, no. 2, pp. 338–44, Feb. 2007.

[87]   S. Van Vlierberghe, S. K. Samal, and P. Dubruel, "Development of Mechanically Tailored Gelatin-Chondroitin Sulphate Hydrogel Films," *Macromol. Symp.*, vol. 309–310, no. 1, pp. 173–181, Dec. 2011.

[88]   J. Schelfhout, P. Dubruel, and S. Van Vlierberghe, "Synthese en karakterisatie van polymeriseerbare Pluronic ⬜ derivaten als kandidaat hydrogelen voor zachte weefselregeneratie," Ghent University, 2013.

[89]   A. Houben, "Design and development of porous Pluronic ® based scaffolds for tissue engineering," Ghent University, 2013.

[90]   R. Ricciardi, G. Mangiapia, F. Lo Celso, L. Paduano, R. Triolo, F. Auriemma, C. De Rosa, D. Chimica, C. Uni, and V. Uni, "Structural Organization of Poly (vinyl alcohol) Hydrogels Obtained by Freezing and Thawing Techniques : A SANS Study," *Chem. Mater.*, vol. 17, no. 5, pp. 1183–1189, 2005.

[91]   Y. Zheng, M. Micic, S. V. Mello, M. Mabrouki, F. M. Andreopoulos, V. Konka, S. M. Pham, and R. M. Leblanc, "PEG-Based Hydrogel Synthesis via the Photodimerization of Anthracene Groups," *Macromolecules*, vol. 35, no. 13, pp. 5228–5234, Jun. 2002.

[92]   K. Arcaute, B. K. Mann, and R. B. Wicker, "Stereolithography of three-dimensional bioactive poly(ethylene glycol) constructs with encapsulated cells.," *Ann. Biomed. Eng.*, vol. 34, no. 9, pp. 1429–41, Sep. 2006.

[93]   A. Ovsianikov, A. Deiwick, S. Van Vlierberghe, P. Dubruel, M. Lena, G. Dräger, and B. Chichkov, "Laser Fabrication of Three-Dimensional CAD Scaffolds from Photosensitive Gelatin for Applications in Tissue Engineering," *Biomacromolecules*, vol. 12, pp. 851–858, 2011.

[94]   A. Ovsianikov, A. Deiwick, S. Van Vlierberghe, M. Pflaum, M. Wilhelmi, P. Dubruel, and B. Chichkov, "Laser Fabrication of 3D Gelatin Scaffolds for the Generation of Bioartificial Tissues," *Materials (Basel).*, vol. 4, no. 12, pp. 288–299, Jan. 2011.

[95]   S. C. Rodrigues, C. L. Salgado, A. Sahu, M. P. Garcia, M. H. Fernandes, and F. J. Monteiro, "Preparation and characterization of collagen-nanohydroxyapatite biocomposite scaffolds by cryogelation method for bone tissue engineering applications.," *J. Biomed. Mater. Res. A*, vol. 101, no. 4, pp. 1080–94, Apr. 2013.

[96]   E. Vanderleyden, L. Van Hoorebeke, E. Schacht, and P. Dubruel, "Comparative Study of Collagen and Gelatin Coatings on Titanium Surfaces," *Macromol. Symp.*, vol. 309–310, no. 1, pp. 190–198, Dec. 2011.

[97]   M. B. Dainiak, I. U. Allan, I. N. Savina, L. Cornelio, E. S. James, S. L. James, S. V Mikhalovsky, H. Jungvid, and I. Y. Galaev, "Gelatin-fibrinogen cryogel dermal matrices for wound repair: preparation, optimisation and in vitro study.," *Biomaterials*, vol. 31, no. 1, pp. 67–76, Jan. 2010.

[98]   T. Vishnoi and A. Kumar, "Conducting cryogel scaffold as a potential biomaterial for cell stimulation and proliferation.," *J. Mater. Sci. Mater. Med.*, vol. 24, no. 2, pp. 447–59, Mar. 2013.

[99]   K.-H. Chang, H.-T. Liao, and J.-P. Chen, "Preparation and characterization of gelatin/hyaluronic acid cryogels for adipose tissue engineering: in vitro and in vivo studies.," *Acta Biomater.*, vol. 9, no. 11, pp. 9012–26, Nov. 2013.

[100] P. Gacesa, "Alginates," *Carbohydr. Polym.*, vol. 8, no. 3, pp. 161–182, Jan. 1988.

[101] T. Billiet, M. Vandenhaute, J. Schelfhout, S. Van Vlierberghe, and P. Dubruel, "A review of trends and limitations in hydrogel-rapid prototyping for tissue engineering.," *Biomaterials*, vol. 33, no. 26, pp. 6020–41, Sep. 2012.

[102] M. Vandenhaute, J. Schelfhout, S. Van Vlierberghe, E. Mendes, and P. Dubruel, "Cross-linkable, thermo-responsive Pluronic® building blocks for biomedical applications: Synthesis and physico-chemical evaluation," *Eur. Polym. J.*, vol. 53, pp. 126–138, Apr. 2014.

[103] P. EDMAN, B. EKMAN, and I. SJOHOLM, "IMMOBILIZATION OF PROTEINS IN MICROSPHERES OF BIODEGRADABLE POLYACRYLDEXTRAN," *J. Pharm. Sci.*, vol. 69, no. 7, pp. 838–842, 1980.

[104] a. . Kuijpers, P. . van Wachem, M. J. . van Luyn, G. H. . Engbers, J. Krijgsveld, S. a. . Zaat, J. Dankert, and J. Feijen, "In vivo and in vitro release of lysozyme from cross-linked gelatin hydrogels: a model system for the delivery of antibacterial proteins from prosthetic heart valves," *J. Control. Release*, vol. 67, no. 2–3, pp. 323–336, Jul. 2000.

[105] J. J. Sperinde and L. G. Griffith, "Synthesis and Characterization of Enzymatically-Cross-Linked Poly (ethylene glycol) Hydrogels," *Macromolecules*, vol. 30, no. 18, pp. 5255–5264, 1997.

[106] X. Yuan, K. Fischer, and W. Schärtl, "Reversible Cluster Formation of Colloidal Nanospheres by Interparticle Photodimerization," *Adv. Funct. Mater.*, vol. 14, no. 5, pp. 457–463, May 2004.

[107] T. Matsuda, M. Mizutani, and S. C. Arnold, "Molecular Design of Photocurable Liquid Biodegradable Copolymers . 1 . Synthesis and Photocuring Characteristics," *Macromolecules*, vol. 33, pp. 795–800, 2000.

[108] S. Van Vlierberghe, V. Cnudde, P. Dubruel, B. Masschaele, A. Cosijns, I. De Paepe, P. J. S. Jacobs, L. Van Hoorebeke, J. P. Remon, and E. Schacht, "Porous gelatin hydrogels: 1. Cryogenic formation and structure analysis.," *Biomacromolecules*, vol. 8, no. 2, pp. 331–7, Feb. 2007.

[109] S. Van Vlierberghe, P. Dubruel, E. Lippens, M. Cornelissen, and E. Schacht, "Correlation between cryogenic parameters and physico-chemical properties of porous gelatin cryogels," *J. Biomater. Sci. Polym. Ed.*, vol. 20, no. 10, pp. 1417–1438, 2009.

[110] S. Van Vlierberghe, P. Dubruel, E. Lippens, B. Masschaele, L. Van Hoorebeke, M. Cornelissen, R. Unger, C. J. Kirkpatrick, and E. Schacht, "Toward modulating the architecture of hydrogel scaffolds: curtains versus channels.," *J. Mater. Sci. Mater. Med.*, vol. 19, no. 4, pp. 1459–66, Apr. 2008.

[111] S. Van Vlierberghe, B. Fritzinger, J. C. Martins, and P. Dubruel, "Hydrogel network formation revised: high-resolution magic angle spinning nuclear magnetic resonance as a powerful tool for measuring absolute hydrogel cross-link efficiencies.," *Appl. Spectrosc.*, vol. 64, no. 10, pp. 1176–80, Oct. 2010.

[112] S. Van Vlierberghe, M. Sirova, P. Rossmann, H. Thielecke, V. Boterberg, B. Rihova, E. Schacht, and P. Dubruel, "Surface modification of polyimide sheets for regenerative medicine applications.," *Biomacromolecules*, vol. 11, no. 10, pp. 2731–9, Oct. 2010.

[113] E. Hoch, T. Hirth, G. E. M. Tovar, and K. Borchers, "Chemical tailoring of gelatin to adjust its chemical and physical properties for functional bioprinting," *J. Mater. Chem. B*, vol. 1, no. 41, pp. 5675–5685, 2013.

[114] T. Billiet, B. Van Gasse, E. Gevaert, M. Cornelissen, J. C. Martins, and P. Dubruel, "Quantitative contrasts in the photopolymerization of acrylamide and methacrylamide-functionalized gelatin hydrogel building blocks.," *Macromol. Biosci.*, vol. 13, no. 11, pp. 1531–45, Nov. 2013.

[115] S. Van Vlierberghe, P. Dubruel, and E. Schacht, "Effect of Cryogenic Treatment on the Rheological Properties of Gelatin Hydrogels," *J. Bioact. Compat. Polym.*, vol. 25, no. 5, pp. 498–512, Aug. 2010.

[116] X. H. Zhu, Y. Tabata, C.-H. Wang, and Y. W. Tong, "Delivery of basic fibroblast growth factor from gelatin microsphere scaffold for the growth of human umbilical vein endothelial cells.," *Tissue Eng. Part A*, vol. 14, no. 12, pp. 1939–47, Dec. 2008.

[117] H. Ishikawa, Y. Nakamura, J. Jo, and Y. Tabata, "Gelatin nanospheres incorporating siRNA for controlled intracellular release.," *Biomaterials*, vol. 33, no. 35, pp. 9097–104, Dec. 2012.

[118] J. Ratanavaraporn, S. Damrongsakkul, S. Kanokpanont, M. Yamamoto, and Y. Tabata, "Osteogenic differentiation of Bone-Marrow -Derived Stem Cells Cultured with Mixed Gelatin and Chitooligosaccharide Scaffolds," *J. Biomater. Sci. Polym. Ed.*, vol. 22, no. 8, pp. 1083–1098, 2011.

[119] H. Staroszczyk, K. Sztuka, J. Wolska, A. Wojtasz-Pająk, and I. Kołodziejska, "Interactions of fish gelatin and chitosan in uncrosslinked and crosslinked with EDC films: FT-IR study.," *Spectrochim. Acta. A. Mol. Biomol. Spectrosc.*, vol. 117, pp. 707–12, Jan. 2014.

[120] H. Sun, F. Zhu, Q. Hu, and P. H. Krebsbach, "Controlling stem cell-mediated bone regeneration through tailored mechanical properties of collagen scaffolds.," *Biomaterials*, vol. 35, no. 4, pp. 1176–84, Jan. 2014.

[121] P. Zhao, C. Deng, H. Xu, X. Tang, H. Hailong, C. Lin, and J. Su, "Fabrication of photo-crosslinked chitosan-gelatin scaffold in sodium alginate hydrogel for chondrocyte culture," *Biomed. Mater. Eng.*, vol. 24, no. 1, pp. 633–641, 2014.

[122] Z. Zhou, J. Chen, C. Peng, T. Huang, H. Zhou, B. Ou, J. Chen, Q. Liu, S. He, D. Cao, H. Huang, and L. Xiang, "Fabrication and physical properties of gelatin/sodium alginate/hyaluronic acid composite wound dressing hydrogel," *J. Macromol. Sci. part A-Pure Appl. Chem.*, vol. 51, no. 4, pp. 318–325, 2014.

[123] P. Taddei, V. Chiono, A. Anghileri, G. Vozzi, G. Freddi, and G. Ciardelli, "Silk fibroin/gelatin blend films crosslinked with enzymes for biomedical applications.," *Macromol. Biosci.*, vol. 13, no. 11, pp. 1492–510, Nov. 2013.

[124]   S. Farris, K. M. Schaich, L. Liu, P. H. Cooke, L. Piergiovanni, and K. L. Yam, "Gelatin–pectin composite films from polyion-complex hydrogels," *Food Hydrocoll.*, vol. 25, no. 1, pp. 61–70, Jan. 2011.

[125]   S. Van Vlierberghe, E. Schacht, and P. Dubruel, "Reversible gelatin-based hydrogels: Finetuning of material properties," *Eur. Polym. J.*, vol. 47, no. 5, pp. 1039–1047, May 2011.

[126]   A. O. Elzoghby, "Gelatin-based nanoparticles as drug and gene delivery systems: reviewing three decades of research.," *J. Control. Release*, vol. 172, no. 3, pp. 1075–91, Dec. 2013.

[127]   R. S. G. Silva and L. a. a. Pinto, "Physical Cross-linkers: Alternatives to Improve the Mechanical Properties of Fish Gelatin," *Food Eng. Rev.*, vol. 4, no. 3, pp. 165–170, Jul. 2012.

[128]   G. Kaur, P. Johnston, and K. Saito, "Photo-reversible dimerisation reactions and their applications in polymeric systems," *Polym. Chem.*, vol. 5, no. 7, p. 2171, 2014.

[129]   K. M. Gattás-Asfura, E. Weisman, F. M. Andreopoulos, M. Micic, B. Muller, S. Sirpal, S. M. Pham, and R. M. Leblanc, "Nitrocinnamate-functionalized gelatin: synthesis and 'smart' hydrogel formation via photo-cross-linking.," *Biomacromolecules*, vol. 6, no. 3, pp. 1503–9, 2005.

[130]   O. WICHTERLE and D. LIM, "HYDROPHILIC GELS FOR BIOLOGICAL USE," *Nature*, vol. 185, no. 4706, pp. 117–118, 1960.

[131]   S. a Skoog, P. L. Goering, and R. J. Narayan, "Stereolithography in tissue engineering.," *J. Mater. Sci. Mater. Med.*, Dec. 2013.

[132]   R. Landers, A. Pfister, U. Hubner, H. John, R. Schmelzeisen, and R. Milhaupt, "Fabrication of soft tissue engineering scaffolds by means of rapid prototyping techniques," *journals Mater. Sci.*, vol. 37, pp. 3107–3116, 2002.

[133]   S. Van Vlierberghe, E. Vanderleyden, V. Boterberg, and P. Dubruel, "Gelatin Functionalization of Biomaterial Surfaces: Strategies for Immobilization and Visualization," *Polymers (Basel).*, vol. 3, no. 4, pp. 114–130, Jan. 2011.

[134]   T. Billiet, E. Gevaert, T. De Schryver, M. Cornelissen, and P. Dubruel, "The 3D printing of gelatin methacrylamide cell-laden tissue-engineered constructs with high cell viability.," *Biomaterials*, vol. 35, no. 1, pp. 49–62, Jan. 2014.

[135]   J. Seppälä, H. Korhonen, R. Hakala, and M. Malin, "Photocrosslinkable polyesters and poly(ester anhydride)s for biomedical applications.," *Macromol. Biosci.*, vol. 11, no. 12, pp. 1647–52, Dec. 2011.

[136]   A. L. Sisson, M. Schroeter, and A. Lendlein, "Polyesters," in *handbook of biodegradable polymers: Synthesis, Characterization and Applications*, First edit., A. Lendlein and A. L. Sisson, Eds. Wiley-VCH Verlag GmbH & Co. KGaA, 2011, pp. 1–21.

[137]   L. T. Sin, A. R. Rahmat, and W. A. W. A. Rahman, *Polylactic acid: PLA biopolymer technology and applications*, 1st ed. Elsevier Inc, 2012.

[138]   Y. Zhu, Z. Mao, and C. Gao, "Aminolysis-based surface modification of polyesters for biomedical applications," *RSC Adv.*, vol. 3, no. 8, p. 2509, 2013.

[139]   F. Du Prez, "Inleiding tot de polymeerwetenschap." Acco, Ghent, 2010.

124

[140] P. Pan, B. Zhu, W. Kai, T. Dong, and Y. Inoue, "Polymorphic Transition in Disordered Poly (L - lactide) Crystals Induced by Annealing at Elevated Temperatures," pp. 4296–4304, 2008.

[141] Y. Zhu, C. Gao, T. He, X. Liu, and J. Shen, "Layer-by-layer assembly to modify poly(l-lactic acid) surface toward improving its cytocompatibility to human endothelial cells.," *Biomacromolecules*, vol. 4, no. 2, pp. 446–52, 2003.

[142] L. Xiao, B. Wang, G. Yang, and M. Gauthier, "Poly (Lactic Acid) -Based Biomaterials : Synthesis , Modification and Applications," in *Biomedical Science, Engineering and Technology*, D. N. Ghista, Ed. Intech, 2012, pp. 247–282.

[143] Q. Meng, M.-C. Heuzey, and P. J. Carreau, "Control of thermal degradation of polylactide/clay nanocomposites during melt processing by chain extension reaction," *Polym. Degrad. Stab.*, vol. 97, no. 10, pp. 2010–2020, Oct. 2012.

[144] F. P. W. Melchels, J. Feijen, and D. W. Grijpma, "A poly(D,L-lactide) resin for the preparation of tissue engineering scaffolds by stereolithography.," *Biomaterials*, vol. 30, no. 23–24, pp. 3801–9, Aug. 2009.

[145] D. Karst and Y. Yang, "Molecular modeling study of the resistance of PLA to hydrolysis based on the blending of PLLA and PDLA," *Polymer (Guildf).*, vol. 47, no. 13, pp. 4845–4850, Jun. 2006.

[146] T. Desmet and P. Dubruel, "The surface Modification of porous biodegradable scaffolds for tissue engineering, produced by rapid prototyping," Ghent University, 2013.

[147] S. Park, G. Kim, Y. C. Jeon, Y. Koh, and W. Kim, "3D polycaprolactone scaffolds with controlled pore structure using a rapid prototyping system.," *J. Mater. Sci. Mater. Med.*, vol. 20, no. 1, pp. 229–34, Jan. 2009.

[148] P. Dubruel and E. Schacht, "Polymers for bio-related applications." 2013.

[149] T. B. F. Woodfield, J. Malda, J. de Wijn, F. Péters, J. Riesle, and C. a van Blitterswijk, "Design of porous scaffolds for cartilage tissue engineering using a three-dimensional fiber-deposition technique.," *Biomaterials*, vol. 25, no. 18, pp. 4149–61, Aug. 2004.

[150] L. Moroni, R. Schotel, D. Hamann, J. R. de Wijn, and C. a. van Blitterswijk, "3D Fiber-Deposited Electrospun Integrated Scaffolds Enhance Cartilage Tissue Formation," *Adv. Funct. Mater.*, vol. 18, no. 1, pp. 53–60, Jan. 2008.

[151] X. Liu and P. X. Ma, "Phase separation, pore structure, and properties of nanofibrous gelatin scaffolds.," *Biomaterials*, vol. 30, no. 25, pp. 4094–103, Sep. 2009.

[152] A. a Mäkitie, J. Korpela, L. Elomaa, M. Reivonen, A. Kokkari, M. Malin, H. Korhonen, X. Wang, J. Salo, E. Sihvo, M. Salmi, J. Partanen, K.-S. Paloheimo, J. Tuomi, T. Närhi, and J. Seppälä, "Novel additive manufactured scaffolds for tissue engineered trachea research.," *Acta Otolaryngol.*, vol. 133, no. 4, pp. 412–7, Apr. 2013.

[153] S. S. Crump, "Apparatus and method for creating three-dimensional objects," 5.121.3291992.

[154] M. Van Baal, "weg met octrooien," *Mens & Molecule*, pp. 6–7, 2013.

[155] P. Y. Noritomi, A. L. L. Filho, H. Lipson, P. Y. C. Cheung, H. Kang, J. V. L. da Silva, J. T. Butcher, N. Colangelo, P. I. Neto, and E. Malone, "Construction and adaptation of an open source rapid prototyping machine for biomedical research purposes?a multinational collaborative development," in *Innovative Developments in Design and Manufacturing*, CRC Press, 2009.

[156] S. Van Vlierberghe, V. Cnudde, P. Dubruel, B. Masschaele, A. Cosijns, I. De Paepe, P. J. S. Jacobs, L. Van Hoorebeke, J. P. Remon, and E. Schacht, "Porous Gelatin Hydrogels: 1. Cryogenic Formation and Structure Analysis," *Biomacromolecules*, vol. 8, pp. 331–337, 2007.

[157] S. Yang, K.-F. Leong, D. Zhaohui, and C. Chua, "The Design of Scaffolds for Use in Tissue Engineering. Part I. Traditional Factors," *Tissue Eng.*, vol. 7, no. 6, pp. 679–689, 2001.

[158] E. Saito, H. Kang, J. M. Taboas, A. Diggs, C. L. Flanagan, and S. J. Hollister, "Experimental and computational characterization of designed and fabricated 50:50 PLGA porous scaffolds for human trabecular bone applications.," *J. Mater. Sci. Mater. Med.*, vol. 21, no. 8, pp. 2371–83, Aug. 2010.

[159] S. Yang, K.-F. Leong, D. Zhaohui, and C. Chua, "Review The Design of Scaffolds for Use in Tissue Engineering. Part II. Rapid Prototyping Techniques," *Tissue Eng.*, vol. 8, no. 1, pp. 1–11, 2002.

[160] H. Xu, J. Dong, G. Chai, Z. Yu, and W. Lang, "Rapid prototyped PGA / PLA scaffolds in the reconstruction of mandibular condyle bone defects," *Int. J. Med. Robot. Comput. Assist. Surg.*, vol. 6, no. December 2009, pp. 66–72, 2010.

[161] D. W. Hutmacher, "Scaffolds in tissue engineering bone and cartilage.," *Biomaterials*, vol. 21, no. 24, pp. 2529–43, Dec. 2000.

[162] a. Ovsianikov, B. Chichkov, O. Adunka, H. Pillsbury, a. Doraiswamy, and R. J. Narayan, "Rapid prototyping of ossicular replacement prostheses," *Appl. Surf. Sci.*, vol. 253, no. 15, pp. 6603–6607, May 2007.

[163] C. W. Hull, "Apparatus for production of three-dimensional objects by stereolithography," 4.575.3301986.

[164] V. I. Lozinsky, I. Y. Galaev, F. M. Plieva, I. N. Savina, H. Jungvid, and B. Mattiasson, "Polymeric cryogels as promising materials of biotechnological interest.," *Trends Biotechnol.*, vol. 21, no. 10, pp. 445–51, Oct. 2003.

[165] V. B. Djagny, Z. Wang, and S. Xu, "Gelatin: a valuable protein for food and pharmaceutical industries: review.," *Crit. Rev. Food Sci. Nutr.*, vol. 41, no. 6, pp. 481–92, Sep. 2001.

[166] M. Schuster, C. Turecek, G. Weigel, R. Saf, J. Stampfl, F. Varga, and R. Liska, "Gelatin-Based Photopolymers for Bone Replacement Materials," *J. Polym. Sci. Part A Polym. Chem.*, vol. 47, pp. 7078–7089, 2009.

[167] "Group T amino acid composition." .

[168] S. Van Vlierberghe, "Cell-Interactive Biopolymer-based Hydrogels designed for Tissue Engineering(PhD)," 2007.

[169] I. Van Nieuwenhove, "Development of Hydrogel Precursors for Stem Cell-based Tissue Engineering," Ghent university, 2013.

[170] G.-J. Graulus, "Development of biopolymers for bioreactor applications," Ghent University, 2012.

[171] M. S. Lee and J. Kim, "Photodependent Release from Poly (vinyl alcohol)/ Epoxypropoxy Coumarin Hydrogels," *J. Appl. Polym. Sci.*, vol. 124, pp. 4339–4345, 2011.

[172] Y.-L. Chen, T.-C. Wang, K.-H. Lee, C.-C. Tzeng, Y.-L. Chang, and C.-M. Teng, "Synthesis of Coumarin Derivatives as Inhibitors of Platelet Aggregation," *Helv. Chim. Acta*, vol. 79, no. 3, pp. 651–657, 1996.

[173] J. R. Prado and S. Vyazovkin, "Melting of Gelatin Gels Containing Laponite, Montmorillonite, and Chhitosan Particles," *Macromol. Chem. Phys.*, vol. 215, no. 9, pp. 867–872, 2014.

[174] BASF, "Safety Data Sheet Irgacure ® 2959," New Jersey, 2014.

[175] T. R. Ramadhar, F. Amador, M. J. T. Ditty, and W. P. Power, "Inverse H-C ex situ HRMAS NMR experiments for solid-phase peptide synthesis.," *Magn. Reson. Chem.*, vol. 46, no. 1, pp. 30–5, Jan. 2008.

[176] M. J. Shapiro, J. Chin, R. E. Marti, and M. A. Jarosinski, "Enhanced Resolution in MAS NMR for Combinatorial Chemistry," *Tetrahedron Lett.*, vol. 38, no. 8, pp. 1333–1336, 1997.

[177] J. Rueda, R. Suica, H. Komber, and B. Voit, "Synthesis of New Polymethyloxazoline Hydrogels by the 'Macroinitiator' Method," *Macromol. Chem. Phys.*, vol. 204, no. 7, pp. 954–960, May 2003.

[178] S. W. Paddock, *Confocal Microscopy: Methods and Protocols*. Humana Press Inc., 1999, p. 464.

[179] O. Germaniuk, "Morimoto Laboratery: MTT Assay," 26-Aug-2010. [Online]. Available: http://groups.molbiosci.northwestern.edu/morimoto/research/Protocols/II. Eukaryotes/E. Cell Growth/Death/2. MTT.pdf. [Accessed: 20-May-2014].

[180] "ultimaker." [Online]. Available: www.ultimaker/com. [Accessed: 30-Jan-2014].

[181] S. Buchatip, A. Petchsuk, and K. Kongsuwan, "Synthesis and Mechanical Properties of Poly (LLA-co-DLLA) Copolymers," *J. Met. Mater. Miner.*, vol. 18, no. 175, pp. 175–180, 2008.

[182] D. Garlotta, "A Literature Review of Poly (Lactic Acid)," *J. Polym. Environ.*, vol. 9, no. 2, pp. 63–84, 2002.

[183] E. Seeram, *Computed Tomography: Physical Principles; Clinical Applications, and Quality Control*, Third edit. Missouri: Saunders, Elsevier, 2013, p. 560.

[184] M. L. Bouxsein, S. K. Boyd, B. a Christiansen, R. E. Guldberg, K. J. Jepsen, and R. Müller, "Guidelines for assessment of bone microstructure in rodents using micro-computed tomography.," *J. Bone Miner. Res.*, vol. 25, no. 7, pp. 1468–86, Jul. 2010.

[185] D. Roylance, "STRESS-STRAIN CURVES." Massachusetts Institute of Technology: Department of Materials Science and Engineering, Cambridge, pp. 1–14, 2001.

[186] J. Cailloux, O. O. Santana, E. Franco-Urquiza, J. J. Bou, F. Carrasco, and M. L. Maspoch, "Sheets of branched poly(lactic acid) obtained by one-step reactive extrusion–calendering process: physical aging and fracture behavior," *J. Mater. Sci.*, vol. 49, no. 11, pp. 4093–4107, Feb. 2014.

[187] P. Pan, B. Zhu, and Y. Inoue, "Enthalpy Relaxation and Embrittlement of Poly (L -lactide) during Physical Aging," pp. 9664–9671, 2007.

[188] P. Pan, B. Zhu, T. Dong, K. Yazawa, T. Shimizu, M. Tansho, and Y. Inoue, "Conformational and microstructural characteristics of poly(L-lactide) during glass transition and physical aging," *J. Chem. Phys.*, vol. 129, no. 18, 2008.

[189] J. Gamez-Perez, "Fracture behavior of quenched poly(lactic acid)," *eXPRESS Polym. Lett.*, vol. 5, no. 1, pp. 82–91, Dec. 2010.

[190] J. Van Rie, "Fine-tuning the 3D Architecture of PCL Hydrogel Combination Scaffolds," Ghent University, 2013.

[191] J. Goldstein, D. Newbury, P. Echlin, C. Lyman, D. Joy, E. Lifshin, L. Sawyer, and J. R. Michael, *Scanning Electron Microscopy andd X-Ray Microanalysis*, 3rd editio. Kluwer Academic/Plenum Publishers, 2003.

[192] B. R. S. Siffert, "The Role of Alkaline Phosphatase in Osteogenesis," *J. Exp. Med.*, vol. 93, no. 5, pp. 415–426, 1951.

[193] J. D. Watson, T. A. Baker, S. P. Bell, A. Gann, M. Levine, and R. Losick, *Molecular Biology of the Gene*, Fifth edit. 2004, p. 733.

[194] T. Komori, "Regulation of Osteoblast Differentiation by RUNX2," in *Osteoimmunology, Advances in Experimental Medicine and Biology*, vol. 658, Y. Choi, Ed. Boston, MA: Springer US, 2010, pp. 43–49.

[195] J. a Saal and J. S. Saal, "Intradiscal electrothermal treatment for chronic discogenic low back pain: prospective outcome study with a minimum 2-year follow-up.," *Spine (Phila. Pa. 1976).*, vol. 27, no. 9, pp. 966–73; discussion 973–4, May 2002.

[196] D. S. Choy, "Percutaneous laser disc decompression (PLDD): twelve years' experience with 752 procedures in 518 patients.," *J. Clin. Laser Med. Surg.*, vol. 16, no. 6, pp. 325–31, Dec. 1998.

[197] C.-C. Wu, S.-H. Yang, T.-L. Huang, C.-C. Liu, D.-H. Lu, K.-C. Yang, and F.-H. Lin, "The interaction between co-cultured human nucleus pulposus cells and mesenchymal stem cells in a bioactive scaffold," *Process Biochem.*, vol. 47, no. 6, pp. 922–928, Jun. 2012.

[198] Y. Lu, G. Mapili, G. Suhali, S. Chen, and K. Roy, "A digital micro-mirror device-based system for the microfabrication of complex, spatially patterned tissue engineering scaffolds.," *J. Biomed. Mater. Res. A*, vol. 77, no. 2, pp. 396–405, May 2006.

[199] M. Emons, K. Obata, T. Binhammer, A. Ovsianikov, B. N. Chichkov, and U. Morgner, "Two-photon polymerization technique with sub-50 nm resolution by sub-10 fs laser pulses," *Opt. Mater. Express*, vol. 2, no. 7, p. 942, Jun. 2012.

[200] W. Denk, J. H. Strickler, and W. W. Webb, "Two-photon laser scanning fluorescence microscopy," *Science (80-.).*, vol. 248, no. 4951, pp. 73–76, Oct. 1990.

[201] O. Bastidas, "Cell Counting with Neubauer Chamber: Basic Hemocytometer Usage." www.celeromics.com, pp. 1–6.

Addendum G: Nederlandstalige samenvatting

Het voornaamste doel van deze studie is om de mogelijkheid van een combinatie van verschillende SFF technieken voor de productie van poreuze draagstructuren voor weefselregeneratie te evalueren. Meer bepaald wil deze studie de haalbaarheid nagaan om twee photon polymerisatie toe te passen om een gedefinieerde, op maat gemaakte cel-bevattende gelatine-microstructuur te verkrijgen binnenin een PLA draagstructuur geproduceerd via FDM. Het gebruik van twee photon polymerisatie kan niet alleen een toename op het gebied van cel-uitzaai efficiëntie binnenin de 3D structuren betekenen, maar biedt tevens perspectieven met betrekking tot de productie van draagstructuren die de ideale omgeving zijn voor de (re)generatie van een welbepaald doelweefsel. Een hydrogel materiaal kan pas geschikt zijn voor de voorgaande toepassingen indien het stabiel is bij lichaamstemperatuur (e.g. fotovernetbaar in geval van gelatine), over relatief gunstige mechanische eigenschappen beschikt en voldoende cel-interactieve eigenschappen bezit. Om materialen te verkrijgen die aan de voorgaande eigenschappen voldoen, werden drie belangrijke pistes geëvalueerd.

In een eerste luik werden geschikte gelatine-derivaten ontwikkeld om een fotovernetbaar materiaal te bekomen. Een eerste derivatisatie mogelijkheid was het inbouwen van dubbele bindingen, meer bepaald methacrylamiden via de reactie van de primaire amines met methacrylzuuranhydride en methacrylaten via de functionalisatie van de carbonzuren in gelatine met aminoethylmethacrylaat. Deze groepen werden dan in aanwezigheid van een foto-initiator en na aanwenden van UV-licht succesvol gepolymeriseerd. Een alternatief voor deze strategie bestond erin om de primaire amines te laten reageren met een coumarine derivaat. Op deze manier kan een reversibel netwerk gevormd worden via bestraling met UV licht met een geschikte golflengte in afwezigheid van een foto-initiator. Ondanks het optreden van een geslaagde modificatie, is de vorming van een netwerk tot op heden nog niet succesvol geweest. In de toekomst zal de mogelijkheid onderzocht worden om dit materiaal te vernetten met behulp van laserlicht met een geschikte golflengte. Naast de voorgaande methoden zijn er tevens preliminaire experimenten uitgevoerd om de mogelijkheid na te gaan tot introductie van een foto-initiator (i.e. Irgacure 2959) in gelatine. Op deze manier zou een in situ vernetbare hydrogel zonder additieven gevormd kunnen worden. De details van deze testen zijn niet opgenomen in huidig werk.

In een tweede luik werden de methacrylaat- en de methacrylamide-derivaten verwerkt tot twee-dimensionaal vernette films via film casting gevolgd door UV vernetting. Irgacure 2959 werd hierbij aangewend als foto-initiator. De gegenereerde films werden vervolgens gekarakteriseerd

via een legio aan technieken zoals HR-MAS ^{1}H-NMR spectroscopie, gel-fractie bepaling, zweltesten en rheologie. Uit deze testen is gebleken dat het inbouwen van additionele methacrylaat-groepen in gel-MOD via de modificatie van carbonzuren met AEMA niet alleen resulteerde in een toename aan mechanische sterkte, maar bovendien ook in een toename van de crosslink efficiëntie. Naast de materiaaleigenschappen hebben preliminaire celtesten aangetoond dat de biocompatabiliteit van gel-MOD-AEMA in dezelfde grootteorde lag als deze van gel-MOD. Deze observaties werden zowel gemaakt voor vernette als voor onvernette systemen en dit ondanks een verdubbeling van het aantal dubbele bindingen in gel-MOD-AEMA ten opzichte van gel-MOD. Gezien het bewezen succes van gel-MOD voor weefselregeneratie, bieden deze resultaten perspectieven naar de toepassing van gel-MOD-AEMA voor tissue engineering. [1][2][3]

In een derde luik van deze studie, werden gel-MOD hydrogelen met uitstekende biocompatibiliteit gecombineerd met 3D geplotte (via FDM) PLLA scaffolds vanwege hun mechanische eigenschappen. Om reproduceerbare poreuze scaffolds te bekomen, werd een programma geschreven in VBA dat precieze controle over poriegroottes en externe dimensies mogelijk maakte. De combinatie van de gelatine hydrogelen met de poreuze scaffolds verliep op twee manieren. Enerzijds werd de geïntroduceerde gel-MOD hydrogel onderworpen aan een cryogene behandeling na UV-vernetting om een poreuze gelatine-microstructuur met cel-interactieve eigenschappen in de PLA scaffolds te introduceren. Anderzijds werd een MC3T3 cel-bevattende gel-MOD oplossing vernet met behulp van UV-licht na introductie in de PLA draagstructuren om een meer uniform bezaaide 3D structuur te verkrijgen. De scaffolds geproduceerd via de cryogene behandeling werden onderworpen aan verschillende karakterisatiemethoden zoals zweltesten, rasterelektronenmicroscopie, digitale microscopie en µ-CT. Via deze technieken kon de aanwezigheid van een poreuze gelatinemicrostructuur binnenin de PLA scaffolds aangetoond worden. Op dit moment worden deze scaffolds bovendien onderworpen aan celtesten om de invloed van verschillen in porositeit en poriëngrootte (als gevolg van variërende polymeerconcentraties en de toepassing van verschillende cryo-parameters) op de celviabiliteit na te gaan. De draagstructuren verkregen via de tweede methode ondergingen reeds succesvolle celtesten. Hieruit bleek dat de cellen niet alleen een UV-behandeling overleefden, maar tevens dat de geëncapsuleerde cellen hun mogelijkheid tot differentiatie naar volwassen osteoblasten behielden.

In eerste instantie heeft deze studie aangetoond dat celencapsulatie in hydrogelprecursoren gevolgd door UV vernetting mogelijk is. Dit opent interessante perspectieven naar een meer uniforme celuitzaaiing voor 3D hydrogel-gebaseerde scaffolds. Voorts blijkt een combinatie van

de ontwikkelde hydrogelmaterialen met de poreuze PLA scaffolds een veelbelovende aanpak met het oog op de combinatie van twee materiaalklassen en twee SFF technieken om te resulteren in de ideale op maat gemaakte draagstructuur voor weefselregeneratie.

Referenties

[1]   S. Van Vlierberghe, E. Vanderleyden, V. Boterberg, and P. Dubruel, "Gelatin Functionalization of Biomaterial Surfaces: Strategies for Immobilization and Visualization," *Polymers (Basel).*, vol. 3, no. 4, pp. 114–130, Jan. 2011.

[2]   T. Billiet, E. Gevaert, T. De Schryver, M. Cornelissen, and P. Dubruel, "The 3D printing of gelatin methacrylamide cell-laden tissue-engineered constructs with high cell viability.," *Biomaterials*, vol. 35, no. 1, pp. 49–62, Jan. 2014.

[3]   P. Dubruel, R. Unger, S. Van Vlierberghe, V. Cnudde, P. J. S. Jacobs, E. Schacht, and C. J. Kirkpatrick, "Porous gelatin hydrogels: 2. In vitro cell interaction study.," *Biomacromolecules*, vol. 8, no. 2, pp. 338–44, Feb. 2007.

Addendum H: English Article

Tunable Hydrogel-Polyester Combination Scaffolds for Tissue Engineering Purposes

J. Van Hoorick*[a], H. Declercq[b], M. Cornelissen[b], M. Markovic[c], A. Ovsianikov[c], T. Fowler[d], O. Hoffman[d], S. Van Vlierberghe[a] and P. Dubruel[a]

[a] Department of Organic Chemistry, Polymer Chemistry & Biomaterials Research Group, University of Ghent, 9000 Belgium
[b] Department of Basic Medical Sciences, University of Ghent, 9000 Belgium
[c] Institute of Materials Science and Technology, Vienna University of Technology (TU Wien), Austria
[c] Department of Pharmacology and Toxicology, University of Vienna, Austria
*jasper.vanhoorick@Ugent.be

In the present work, photo-crosslinkable gelatin-based hydrogel materials have been developed to be applied for intervertebral disc regeneration. Crosslinked films have been prepared using methacrylamide and additional methacrylate functionalized gelatins. In parallel, photo-reversible coumarin functionalities have been incorporated in an attempt to generate a photoreversible hydrogel network. The material characterization results indicated that networks generated by the introduction of additional methacrylate functionalities exhibited superior mechanical properties over crosslinked methacrylamide-functionalized materials while maintaining their bio-interactive properties. In a final part of the present study, methacrylamide-functionalized gelatin hydrogels have been combined with PLA scaffolds produced using fused deposition modelling (FDM) either via the application of a cryogenic treatment or through in situ crosslinking of a cell-containing gel-MOD solution as preliminary approach aiming at the application of two-photon polymerization (2PP). Preliminary cell work not only revealed a reasonable cell survival, but the ability to enable differentiation was unhampered by the UV treatment.
Keywords: hydrogel, gelatin, PLA, tissue engineering, FDM, UV-curing

Introduction

Low back pain is one of the most common complaints throughout the modern western society.[1][2][3][4][5] It can lead to a chronic disability for 10% of the patients resulting in a huge economic burden for society. Lower back pain often goes concomitant with intervertebral disc (IVD) degeneration.[3][4][6] The origin of the degeneration is not completely clear to date, however, a IVD is a rather avascular system with poor regenerative capabilities.[7] As a result, surgical intervention is essential in order to reduce the associated complaints. However, state of the art surgical techniques currently focus on a treatment of the symptoms instead of aiming at a fundamental cure. In addition, these treatments are often associated with additional complications.[2][3] As a result, tissue engineering solutions for IVD gained increasing attention during the last decade.[8][2][9][10][11] An IVD is characterized by three main areas including a gelatinous core (i.e. nucleus pulposus, NP) which is encapsulated by a fibrous-like annulus fibrosus (AF). Moreover, both areas are contained in between two cartilaginous endplates.[2] In the present work, attention has been paid to the development of a gelatin-based hydrogel material because of its proven bio-interactivity due to the presence of arginine-glycine-aspartic acid

(RGD) sequences. In addition, hydrogels are hydrophilic polymer networks, often obtained via crosslinking of several macromonomers which exhibit the ability to take up large amounts of water without dissolving.[12][13][14] This large water uptake renders the material very suitable towards NP regeneration as 85% of the mass of an NP can be attributed to water.[2][5][15] To generate a hydrogel with sufficient mechanical properties, the primary amines will be functionalized with photo-crosslinkable methacrylamide functionalities followed by the introduction of additional crosslinkable methacrylate functionalities via the reaction of the carboxylic acids present in the aspartic and glutamic acid residues present in the gelatin backbone. The obtained hydrogel materials will be characterized in depth via HR-MAS ^{1}H-NMR spectroscopy, rheology, swelling tests, determination of the gel fraction as well as *in vitro* cell interaction studies. In a second part of the study, a combination of gelatin hydrogels with PLA scaffolds will be evaluated in order to obtain a scaffold with suitable mechanical properties towards AF repair. To produce the scaffolds, a rapid prototyping method (i.e. fused deposition modelling, FDM) will be applied as it enables precise control and generation of perfectly tailored scaffolds which is essential to mimic the complex fibrotic AF structure.[3][16][15][17][18][19] To this end, the methacrylamide-derivatized gelatin will be introduced in the PLA scaffold followed by a cryogenic treatment to generate a porous microstructure.[20][21][22] In parallel, a cell-containing gel-MOD solution will be crosslinked inside the PLA scaffolds to assess the cell viability following the UV irradiation, as a pilot experiment towards the potential of 2PP of cell-encapsulating gelatin materials.[23][24][25]

Experimental

<u>Materials</u>

Gelatin type B isolated from bovine hides using an alkaline treatment was obtained from Rousselot (Ghent, Belgium). The PLA filament was obtained from bitsfrombytes.com (UK). The dialysis membranes (Spectra/Por 4, MWCO 12000-14000 Da) were obtained from Polylab (Antwerp, Belgium), Irgacure 2959 was purchased from BASF (Kaisten, Germany). 2-Aminoethyl methacrylate hydrochloride was obtained from Polysciences. 1-Ethyl-3-(3-dimethylaminopropyl)carbodiimide (EDC), methacrylic anhydride, NaOH and D_2O were obtained from Aldrich (Bornem, Belgium). 7-Hydroxycoumarin (umbelliferrone), acetone, chloroform, epichlorohydrin and NaCl were obtained from Sigma-Aldrich (Diegem, Belgium). DMSO, NHS, KH_2PO_4 and Na_2HPO_4 were obtained from Acros (Geel, Belgium).

<u>Methods</u>

All compression tests were performed using a Hounsfield THE Universal tester 10-KM. The applied load cell was 1000 N. Program and data acquisition was performed using QMAT software. Data analysis was performed using Microsoft Excel 2010. For the cryogenic treatment, the cooling rate and the final freezing temperature of the cryogels was controlled using a Julabo, type FP40-ME cryostat in combination with a thermo-electric cooler (DuraTec DT12, Marlow industries) for the application of a temperature gradient. The gelatin thermograms were obtained through differential scanning calorimetry (DSC) on a TA instruments Q 2000 (40 mg gelatin solution, T_{zero} pan, hermetic lid, reference milliQ) using a temperature program as described by Prado et al.[26]

To obtain the hydrogel films, gel-MOD and gel-MOD-AEMA were dissolved at 40°C in the presence of Irgacure 2959 followed by injection in between two glass plates separated by a silicone spacer (0.5 mm thick) (1 hour physical gelation at 6°C followed by 30 min UV-A crosslinking at 365 nm and 8mW/cm² using a Ultra Violet Products transilluminator). The PLA scaffolds were produced using an Ultimaker 1 (nozzle diameter 400 μm) in combination with a self-developed Gcode writing program (V1.8) and Cura 13.06.4 software to control the printer. All ^{1}H-NMR spectra were recorded at 40°C using a Brüker 500MHz NMR-spectrometer. The

HR-MAS NMR spectroscopy measurements were performed using a Brüker Avance II 700 Spectrometer (700.13 MHz) in combination with an HR-MAS probe. The digital microscopy images were obtained using either a Keyence VHX 2000 series system or a Keyence VHX-5000 series system. Micro-computed tomography (μCT) was performed using a scanner consisting of an open type Feinfocus Tra tube combined with a Varian 2520V Paxscan detector. The 3D reconstructions of the obtained radiographs were performed using Octopus software. All rheological measurements were performed using an Anton Paar Physica MCR-301 rheometer with a normal force of 0.2 N starting from solutions at 40°C (15 min physical gelation at 5°C followed by 30 min UV crosslinking and 10 minutes post curing at a strain of 0.05 % and a frequency of 1 Hz. SEM analysis was performed on a Fei Quanta 200F (field emission gun) scanning electron microscope. Sample preparation consisted of samples being cut in half followed by gold sputtering using a K550X automatic gold sputter coater.

Cell experiments: The applied cells for the characterization of the 2D films were human foreskin fibroblasts (HFF) while the 3D cell experiments were performed using mouse MC3T3 preosteoblasts.

Synthesis and characterization of gel-MOD: The methacrylation of gelatin B occurred in PBS buffer (pH 7,3) via a protocol described by Van Vlierberghe et al[20] using 2,5 equivalents of methacrylic anhydride. The degree of substitution (DS) was determined using ^{1}H-NMR spectroscopy in D_2O at 40°C with the signal of the Val, Leu and Ile at 1.01 ppm as a reference.

Synthesis and characterization of gel-MOD-AEMA: 10 g gel-MOD (DS 87% or 97%) (cfr. 10.980 mmol carboxylic acids) was dissolved in 200 ml DMSO at 50°C under reflux conditions in argon atmosphere (three times degassed) under continuous magnetic stirring. After complete dissolution, 1 equivalent EDC (2100 mg; 10.980 mmol) and 1.5 equivalents NHS (1895 mg; 16.48 mmol) were added to the mixture. After 30 min stirring, 2 equivalents AEMA.HCl were added (3.6353g; 21.96 mmol) together with 0.01 equivalents of 4-tert-butyl catechol (i.e. inhibitor). The solution was shielded from light and stirred at 50°C overnight. Afterwards, the reaction was precipitated in a tenfold excess of cold acetone and filtered on a glass filter n°4. The precipitate was redissolved in MilliQ and dialyzed using Milli-Ro (MWCO: 12000-14000 Da) at 40°C for 24 hours (water changed 5 times). After dialysis, the solution was transferred to petridishes and frozen at   -20°C enabling the subsequent removal of ice via lyophilization. The DS was determined using ^{1}H-NMR spectroscopy in D_2O at 40°C using the signal of the Val, Leu and Ile at 1.01 ppm as reference.

Synthesis and characterization of gel-coumarin: In a first step, 7-(2,3-epoxypropoxy)coumarin was synthesized using a protocol described by Chen et al.[27]
Next, 0.2358 g 7-(2,3-epoxypropoxy)coumarin (1.155 mmol) was dissolved in 10 ml DMSO in a two-neck flask under reflux conditions under argon atmosphere (2 times degassed) while stirring continuously. Next, gelatin B (1 g, 0.385 mmol amines) was added and the set-up was degassed twice while the temperature was increased to 50°C. The mixture was reacted for two days followed by precipitation in a tenfold excess of cold acetone. The precipitate was filtered off on a glass filter (P4) and redissolved in MilliQ water prior to dialysis using MilliRo (MWCO: 12000-14000 Da) for 24 hours at 40°C (water changed 5 times) followed by freezing at -20°C prior to lyophilization. The DS was determined via ^{1}H-NMR spectroscopy at 50°C in DMSO-d using the Val/Leu/Ile signal as reference.

Results & Discussion

Material synthesis and characterization

Characterization of gel-MOD: The obtained DS varied from 82% to 87%. In order to obtain a higher DS, the gel-MOD developed was subjected to an additional methacrylation cycle applying 1 additional equivalent of methacrylic anhydride which resulted in a DS of 97%.

Characterization of gel-coumarin: For the coumarin derivative, a DS of 45% was obtained as indicated via ^{1}H-NMR spectroscopy. However, to date crosslinking has not been successful due to absence of a suitable photo-reactor.

Characterization of gel-MOD-AEMA

Gel-MOD materials with sufficiently high degrees of substitution were applied to prevent zero-length crosslinking. The obtained DS for the carboxylic acids ranged from 27 to 41%. Interestingly, the developed gel-MOD-AEMA hydrogel precursors were soluble at room temperature in contrast to the gel-MOD derivatives. This phenomenon can probably be related to the fact that, during the modification, both the primary amines as well as the carboxylic acids present in gelatin have been consumed. It can be anticipated that this modification could potentially inhibit the formation of triple helices to a certain extent. To further investigate this phenomenon, DSC was performed on the gelatin derivatives similar to Prado et al.[26]
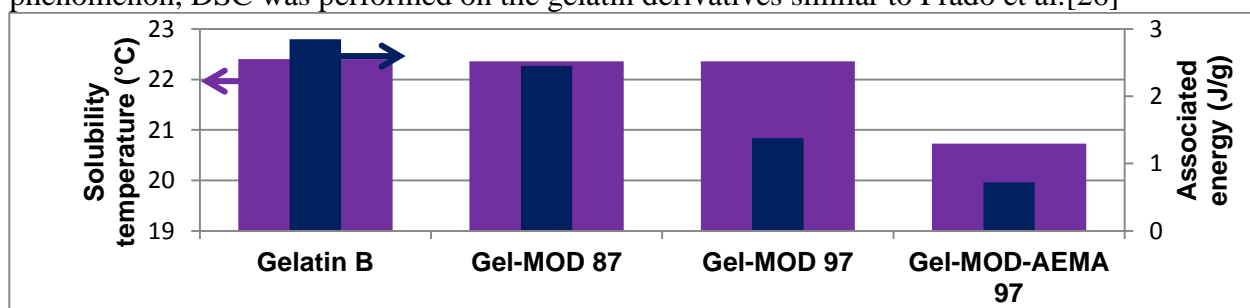

Figure 1. Plot depicting the UCST and the associated heat exchange for gelatin B, gel-MOD 87 (DS$_{amines}$ 87%), gel-MOD 97 (DS$_{amines}$ 97%) and gel-MOD-AEMA (DS$_{amines}$ 97%; DS$_{carboxylic acids}$ 41%)

Interestingly, the modification of the amines of gelatin does not influence the UCST, yet, it will inhibit the formation of triple helices to some extent as reflected by the smaller difference in heat capacity upon gelation. Furthermore, this effect is more pronounced upon increasing the degree of modification of the primary amines. For gel-MOD-AEMA, a small transition could still be observed despite its solubilization at room temperature. However, this transition takes place at a lower temperature while the energy associated with this transition is drastically decreased. These results further support the postulated idea that the modification of both the amines as well as the carboxylic acids will partially inhibit the formation of triple helices.

Characterization of hydrogel films developed

Four different hydrogel films have been prepared starting from gel-MOD (DS: 82%), gel-MOD (DS: 97%) gel-MOD-AEMA (DS$_{amines}$: 87%, DS$_{carboxylic acids}$: 30%) and gel-MOD-AEMA (DS$_{amines}$: 97%, DS$_{carboxylic acids}$: 27%). In the course of this article, these films will be referred to as gel-MOD 82, gel-MOD 97, gel-MOD-AEMA 87, gel-MOD-AEMA 97.

Swelling tests and gel fraction determination: To determine the swelling capacity of the crosslinked hydrogel films, swelling experiments have been performed in PBS buffer at 37°C. In addition, the gel fraction was determined to obtain a semi-quantitative indication of the degree of crosslinking (DC) as the gel fraction represents the amount of covalently incorporated precursor.
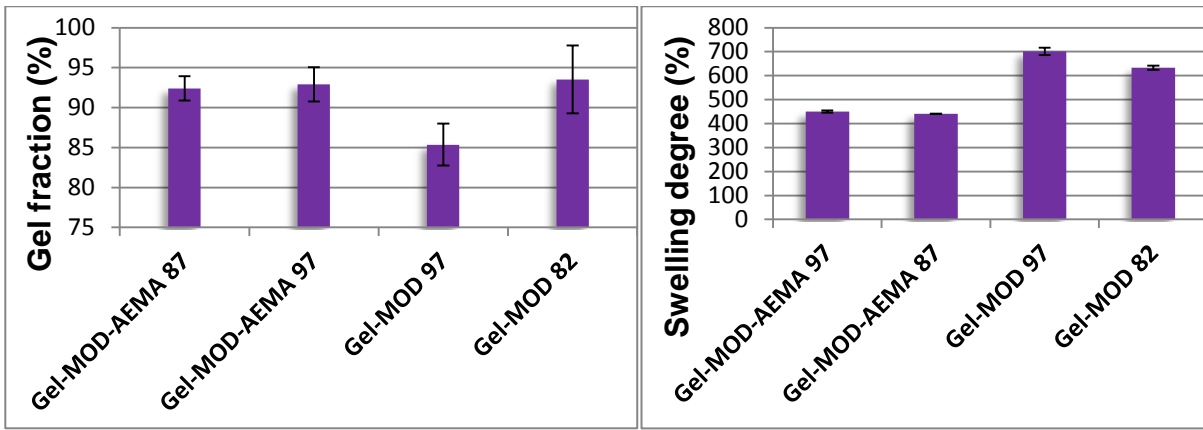
Figure 2. Plots depicting the obtained gel fractions (left) and the swelling degrees for the produced hydrogel films (right).

Figure 2 (left) depicts an overview of the different gel fractions obtained for the hydrogel films developed. Generally, a relatively high gel fraction was obtained which is beneficial for tissue engineering applications as the probability for leaching out of potentially harmful hydrogel precursors will be limited. The gel-MOD 97 film exhibited a significantly (T-test, p<0.05) lower crosslinking degree which is anticipated to originate from a lower initial molecular weight as a result of additional hydrolysis during the second methacrylation cycle. A lower molecular weight results in a shorter chain length and thus in a reduced number of crosslinkable functionalities present per chain.

Figure 2 (right) depicts the equilibrium swelling degrees obtained during the swelling experiment. As anticipated, the plot reveals that gel-MOD-AEMA hydrogels exhibit a much lower swelling degree compared to the gel-MOD hydrogels. The introduction of the AEMA functionalities doubled the amount of crosslinkable groups present in gelatin, thus a denser network possessing more junction knots per volume unit was formed. These crosslinking points will limit the swelling capacity as this is an osmotically driven process and the mobility of the polymer chains inside the network is hampered.

HR-MAS ^{1}H-NMR spectroscopy: To obtain a quantitative insight in the DC of the produced hydrogel films, the integration of the signals corresponding to the methacrylamide and methacrylate functionalities present in gel-MOD and gel-MOD-AEMA was compared prior to and after crosslinking. To realize a quantitative comparison, the samples were first normalized using the Val/Leu/Ile reference signal at 1.1 ppm. Application of equation (1) resulted in the calculation of the DC

$$DC(\%) = \left[\frac{\left(\frac{I^i_{5.75ppm}+I^i_{6.20ppm}}{I^i_{1.1ppm}}\right)-\left(\frac{I^c_{5.75ppm}+I^c_{6.20ppm}}{I^c_{1.1ppm}}\right)}{\left(\frac{I^i_{5.75ppm}+I^i_{6.20ppm}}{I^i_{1.1ppm}}\right)}\right] * 100 \% \qquad (1)$$

$i = initial\ uncrosslinked\ material \quad c = crosslinked\ material$
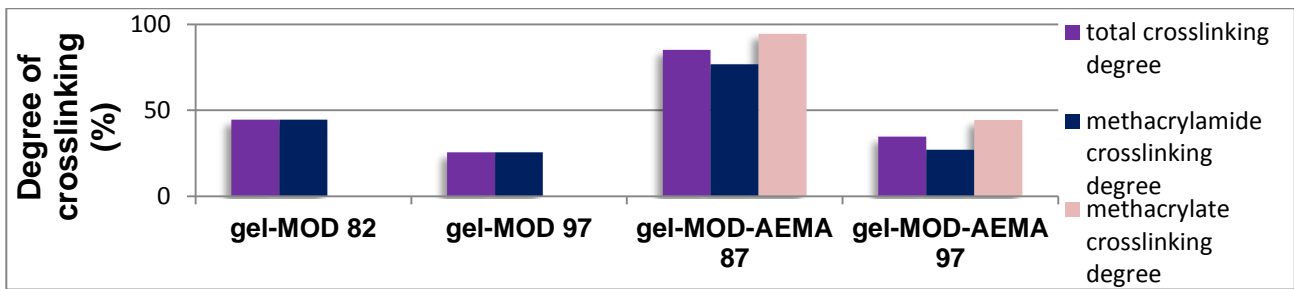
Figure 3. **Crosslink efficiency of the methacrylamide and the methacrylate functionalities as well as the combined efficiency of both functionalities determined using HR-MAS ^{1}H-NMR spectroscopy.**

Figure 3 depicts the obtained DC both for the methacrylate as well as for the methacrylamide functionalities and combinations thereof for the hydrogel films developed. The results illustrate that crosslinking was less proficient for the films with a higher amount of methacrylamide functionalities (i.e. gel-MOD 97 versus gel-MOD 82), which is in agreement with the gel fraction determination and the swelling behavior and probably results from a reduction in initial molecular weight of gel-MOD 97. As anticipated, the gel-MOD-AEMA derivatives exhibit a higher crosslinking degree, as an increase in the amount of crosslinkable functionalities will increase the probability for two functionalities to reside in close proximity to one another during UV irradiation. In addition, the crosslinking of the methacrylate functionalities seems to be more efficient compared to the crosslinking of the methacrylamide functionalities.

Rheology: To compare the evolution of the storage modulus (G') of a gel-MOD hydrogel in the presence and absence of additional methacrylates during crosslinking, a rheological experiment was performed.
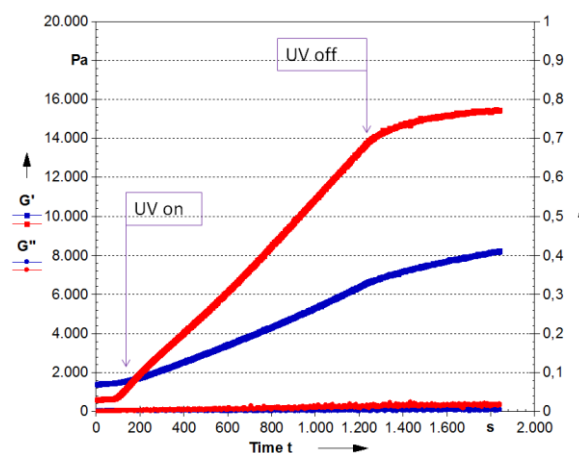

Figure 4: Mechanical behavior under the influence of photo-crosslinking of gel-MOD (blue) and gel-MOD-AEMA (red).

Figure 4 depicts the influence of the UV crosslinking on the storage modulus and the loss modulus for two gelatin derivatives (i.e. gel-MOD-AEMA 97 versus gel-MOD 97). The plots indicated that the initial storage modulus decreases with increasing degree of modification due to a poorer physical gelation. Secondly, the increase in storage modulus upon UV crosslinking of gel-MOD-AEMA is about two times higher compared to the gel-MOD derivative originating from additional crosslink points in the network.

Cell viability tests: To assess the potential of the gelatin hydrogel materials developed towards tissue engineering purposes, a live/dead staining was performed on the developed materials in the crosslinked state. In parallel, an MTT assay was performed on the hydrogel precursors to generate more quantitative results regarding cell viability.
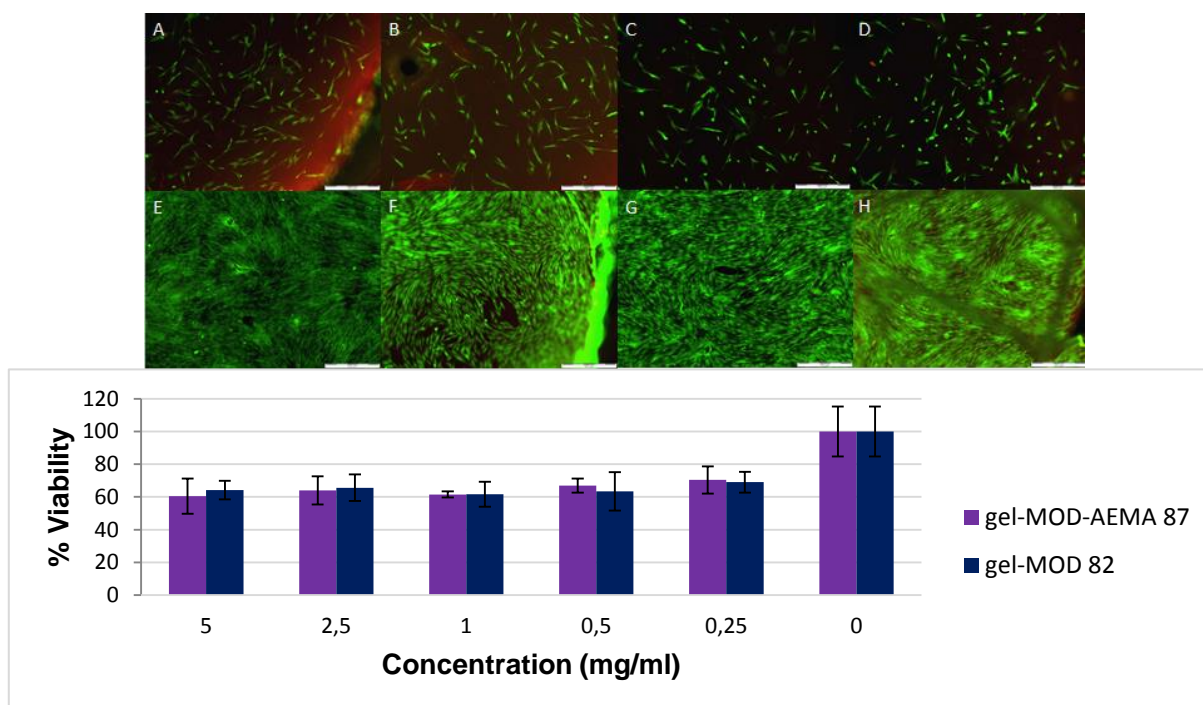
Figure 5: Live/dead staining images obtained via confocal microscopy one and seven days after seeding for gel-MOD 82 (A, E), gel-MOD 97 (B, F), gel-MOD-AEMA 87 (C, G) and gel-MOD-AEMA 97 (D, H) (scale bars represent 500µm) (upper panel); Plot depicting the cytotoxicity of several concentrations of hydrogel precursors relative to a control obtained via an MTT assay (lower panel).

The results of the cytotoxicity tests indicate that, despite the incorporation of additional double bonds, no increase in cytotoxicity could be observed both for the crosslinked as well as for the uncrosslinked gel-MOD-AEMA when compared to the gel-MOD hydrogels which have already proven their biocompatibility.[28] Interestingly, the developed gel-MOD-AEMA hydrogels not only exhibit better mechanical properties compared to gel-MOD, but they are also very suitable towards tissue engineering purposes considering their biocompatibility.

Development and characterization of poly(lactic acid)-hydrogel combination scaffolds
The combination of both materials occurred via two approaches. On the one hand, a gel-MOD hydrogel was introduced in the PLA scaffold followed by UV crosslinking and exposure to a cryogenic treatment followed by lyophilization prior to cell seeding. In parallel, a gel-MOD solution was blended with MC3T3 preosteoblast cells prior to its introduction in the PLA scaffolds followed by UV crosslinking.

Development and characterization of PLA-cryogel combination scaffolds
Gel-MOD was first introduced into the PLA scaffolds in the presence of a suitable photo-initiator (Irgacure 2959), followed by applying a vacuum treatment, enabling one hour gelation at 6°C and 2 hours UV-A irradiation to crosslink the material prior to the application of a cryogenic treatment during which the samples were cooled down to -30°C over the course of 5h30 either with or without the application of a temperature gradient of 30°C between top and bottom of the scaffold.[22]
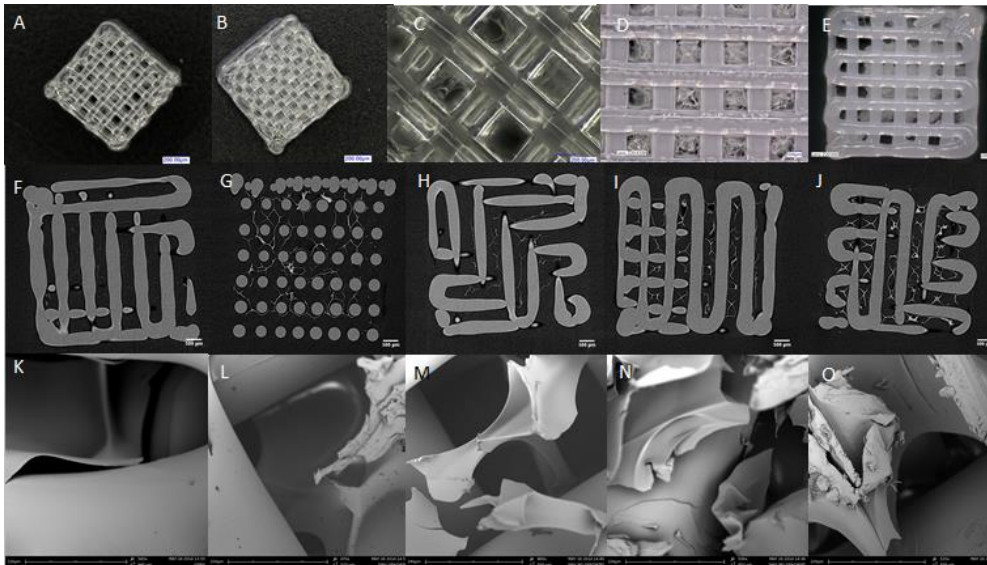
Figure 6: Digital microscopy images of a scaffold containing a 2 w/v% solution in the absence of a temperature gradient prior to incubation at 40°C (A, C); a scaffold containing a 5 w/v% hydrogel solution in the absence of a temperature gradient prior to incubation (B) and following incubation (D, E). µ-CT images of PLA scaffolds containing respectively a 2 and 5 w/v% gelatin solution with the application of a temperature gradient (F, G); a 2, 5 and 10 w/v% gelatin solution in the absence of a temperature gradient (H, I, J). SEM images of the 5 w/v% gelatin microstructure inside the PLA scaffold with temperature gradient (L); a 2, 5 and 10 w/v% solution in the absence of a temperature gradient (M, N, O) and a PLA strut physically coated with a 10 w/v% solution of non-modified gelatin (K).

Characterization via digital microscopy, SEM and µ-CT: The images (Figure 6) obtained via different techniques show the presence of a gelatin microstructure inside the PLA scaffolds. In addition, the less concentrated the solution, the lower the final amount of gelatin present inside the scaffolds as a result of leaching out during the physical gelation prior to UV curing. Furthermore, a denser network was obtained for solutions with higher gelatin concentrations. In addition, the images obtained after leaching (D and E) still reveal the presence of gelatin, indicating that the PLA scaffolds are sufficiently transparent for UV-A light to induce successful crosslinking. Moreover, the SEM images show that the PLA struts are physically coated with crosslinked gelatin which will render them more suitable towards cellular attachment (see Figure 6, K).

Water uptake capacity: To assess whether or not the gelatin cryogels inside the PLA scaffolds still exhibit sufficient water uptake capacity, water uptake capacity tests were performed by incubation in PBS buffer at 37°C.
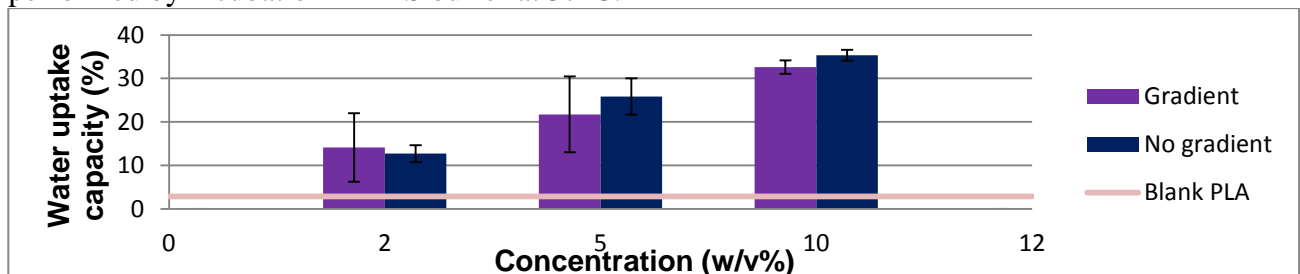

Figure 7: Maximum water uptake capacity of the PLA-gel-MOD combination scaffolds with varying gelatin concentrations.

Surprisingly, an increase in water uptake capacity was observed with increasing gelatin concentrations. The latter is contradictory to the results obtained by Van Vlierberghe *et al.* which illustrated an increase in water uptake capacity of gelatin-based cryogels upon decreasing the

140

gelatin concentration,[29] as higher gelatin concentrations lower the porosity of the cryogel thereby resulting in a larger obstruction towards water uptake. In addition, higher polymer concentrations generally result in a higher crosslinking degree and, consequently, a lower water uptake.[20] However, the obtained results can be explained by a poorer physical gelation and thus a reduced viscosity of the lower gelatin concentrations (i.e. 2 and 5 w/v% versus 10 w/v%). Consequently, part of the gel-MOD solution was leached out from the scaffolds containing the lowest gelatin concentration prior to crosslinking. As the dry gelatin fraction in the PLA scaffolds increases with increasing gelatin concentration, the water uptake capacity of the scaffolds will increase concomitant.

Development of PLA scaffolds with cell-encapsulating gel-MOD solution

PLA scaffolds were immersed in gel-MOD dissolved in culture medium containing MC3T3 cells in the presence of 0.05 wt% Irgacure 2959 followed by UV irradiation for 10 minutes. After 7 days, the scaffolds were stimulated with differentiation medium (DM) to check whether the crosslinking hampered the ability of the cells encapsulated to differentiate.

Characterization of cell viability and proliferation:
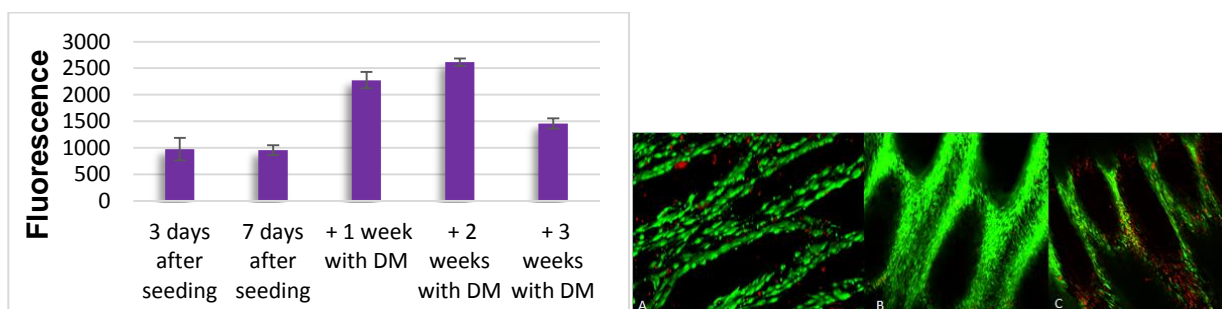Determination of the metabolic activity: Presto Blue staining

Figure 8: Presto blue fluorescence recorded at different time points as an indication of metabolic activity (left). Live/dead staining of the cells present on the scaffolds 1, 2 and 3 weeks after stimulation with DM (A, B, C) (right).

Evaluation of the generated fluorescence in the scaffolds after Presto Blue staining confirmed an increase in cell proliferation with a maximum after 3 weeks in culture. This increase in metabolic activity probably originates from two effects. On the one hand, the cell proliferation increases, which results in a higher overall metabolic activity. In addition, introducing the differentiation medium is likely to increase the metabolic activity of the viable cells.

Live/dead staining
Figure 8 (right), A reveals the presence of a few dead cells, probably as a consequence of the UV irradiation. Interestingly, B depicts an almost complete absence of dead cells indicating that cell proliferation occurred. Three weeks after the addition of DM, however, an increase in dead cells was again observed, which is in agreement with the results obtained via presto blue staining. The origin of this phenomenon, however, remains unclear to date.
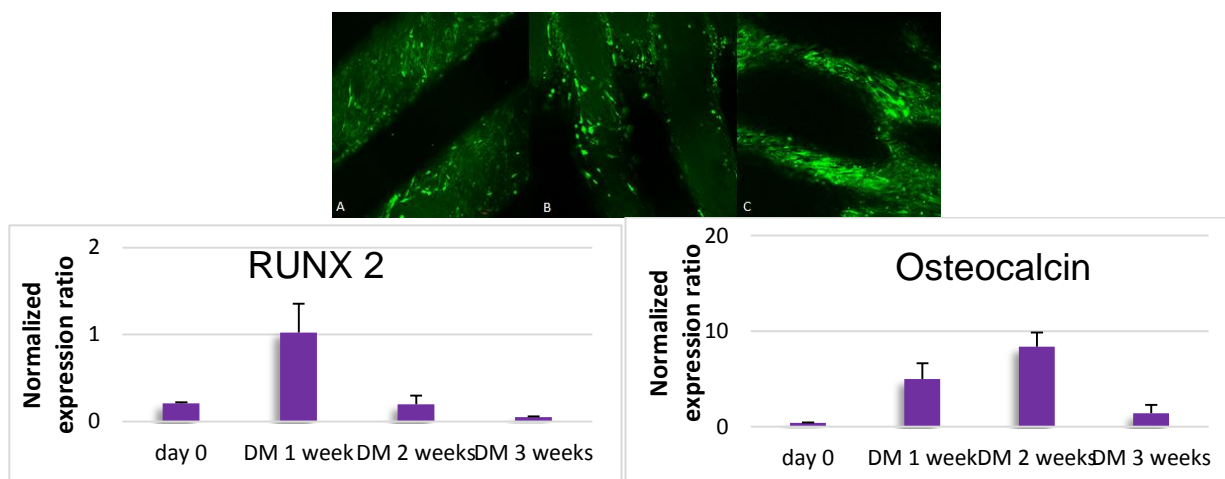
Figure 9: ALP staining performed 1, 2 and 3 weeks after addition of differentiation medium (A, B and C respectively) (above). RUNX2 expression (left) and osteocalcin expression (right) determined via qRT-PCR as a function of time.

ALP staining: The ALP staining images (Figure 9, upper panel) revealed an increase in the amount of cells exhibiting green fluorescence as a function of time as a consequence of the presence of alkaline phosphatase which is a marker for osteogenesis. Even after three weeks, an increase in osteogenesis was still observed despite the drop in cell number, proving that the osteoblasts are mature, mineral-forming and healthy.

Gene expression: RUNX2 and osteocalcin are important markers in the process of osteogenesis. The plot in Figure 9 (left) indicates an initial increase of the RUNX2 gene followed by a decrease after 3 weeks. Alongside this effect, Figure 9 (right) indicates an increase in the osteocalcin formation. These results indicate the presence of mature osteoblasts starting from 3 weeks after differentiation. The presence of both effects was anticipated as upon maturation of osteoblasts, the production of RUNX2 is inhibited while the osteocalcin production is upregulated.[30] Both the ALP staining as well as the gene expression experiments indicated that the cells maintained their ability to differentiate even after a UV-A treatment.

Conclusions

Successful modification of the primary amines in gelatin B was performed to yield both coumarin- functionalized gelatin as well as methacrylamide-functionalized gelatin. In addition, by subsequent reaction of the carboxylic acids with aminoethyl methacrylate, additional methacrylate functionalities could be introduced. These gave rise to a higher crosslink efficiency and, consequently, an increase in the mechanical properties while maintaining comparable cell-interactive properties. These results indicate that the gel-MOD-AEMA material can be a very promising candidate towards applications for the regeneration of the nucleus pulposus.

In addition, the combination of a gel-MOD hydrogel with a PLA scaffold via a cryogenic treatment resulted in the formation of a porous gelatin network inside the scaffold. Swelling tests proved that the incorporated gelatin maintained its water uptake capabilities. However, the introduction of a lower concentrated gel-MOD needs further optimization to prevent hydrogel leaching from the scaffolds prior to crosslinking. In addition, the gelatin microstructure could still be observed after incubation in water at 40°C which indicates that the PLA scaffolds could sufficiently be penetrated by UV-A irradiation to result in a successful crosslinking of the gelatin derivative. Furthermore, the crosslinking of a cell containing gel-MOD solution inside a PLA scaffold has proven that preosteoblasts cannot only survive these harsh conditions, but in addition, maintain their ability to differentiate into mature osteoblasts. The positive results of this

study clear the road towards the application of 2PP of a cell-encapsulating gel-MOD inside a PLA scaffold to generate the optimally tailored AF regenerative system with the potential to closely mimick its complex fibrous morphology.

Acknowledgments

References

[1]   E. George, "Low back pain," *Bull. World Health Organ.*, vol. 81, no. 9, pp. 671–676, 2003.

[2]   P. P. Raj, "Intervertebral Disc : AnatomyPhysiology-Pathophysiology-Treatment," *World Inst. Pain, Pain Pract.*, vol. 8, no. 1, pp. 18–44, 2008.

[3]   S. M. Richardson, R. V Walker, S. Parker, N. P. Rhodes, J. a Hunt, A. J. Freemont, and J. a Hoyland, "Intervertebral disc cell-mediated mesenchymal stem cell differentiation.," *Stem Cells*, vol. 24, no. 3, pp. 707–16, Mar. 2006.

[4]   B. R. Whatley, J. Kuo, C. Shuai, B. J. Damon, and X. Wen, "Fabrication of a biomimetic elastic intervertebral disk scaffold using additive manufacturing.," *Biofabrication*, vol. 3, no. 1, p. 015004, Mar. 2011.

[5]   K. D. Hudson, M. Alimi, P. Grunert, R. Härtl, and L. J. Bonassar, "Recent advances in biological therapies for disc degeneration: tissue engineering of the annulus fibrosus, nucleus pulposus and whole intervertebral discs.," *Curr. Opin. Biotechnol.*, vol. 24, no. 5, pp. 872–9, Oct. 2013.

[6]   Y. Yamamoto, J. Mochida, D. Sakai, T. Nakai, K. Nishimura, H. Kawada, and T. Hotta, "Upregulation of the viability of nucleus pulposus cells by bone marrow-derived stromal cells: significance of direct cell-to-cell contact in coculture system.," *Spine (Phila. Pa. 1976).*, vol. 29, no. 14, pp. 1508–14, Jul. 2004.

[7]   R. J. Moore, "The vertebral end-plate: what do we know?," *Eur. Spine J.*, vol. 9, no. 2, pp. 92–6, Apr. 2000.

[8]   J. L. Bron, L. a Vonk, T. H. Smit, and G. H. Koenderink, "Engineering alginate for intervertebral disc repair.," *J. Mech. Behav. Biomed. Mater.*, vol. 4, no. 7, pp. 1196–205, Oct. 2011.

[9]   E. Y.-S. See, S. L. Toh, and J. C.-H. Goh, "Effects of Radial Compression on a Novel Simulated Intervertebral Disc–Like Assembly Using Bone Marrow–Derived Mesenchymal Stem Cell Cell-Sheets for Annulus Fibrosus Regeneration," *Spine (Phila. Pa. 1976).*, vol. 36, no. 21, pp. 1744–1751, Oct. 2011.

[10] M. Bhattacharjee, S. Miot, A. Gorecka, K. Singha, M. Loparic, S. Dickinson, A. Das, N. S. Bhavesh, A. R. Ray, I. Martin, and S. Ghosh, "Oriented lamellar silk fibrous scaffolds to drive cartilage matrix orientation: towards annulus fibrosus tissue engineering.," *Acta Biomater.*, vol. 8, no. 9, pp. 3313–25, Sep. 2012.

[11] K.-I. Lee, S.-H. Moon, H. Kim, U.-H. Kwon, H.-J. Kim, S.-N. Park, H. Suh, H.-M. Lee, H.-S. Kim, H.-J. Chun, I.-K. Kwon, and J.-W. Jang, "Tissue engineering of the intervertebral disc with cultured nucleus pulposus cells using atelocollagen scaffold and growth factors.," *Spine (Phila. Pa. 1976).*, vol. 37, no. 6, pp. 452–8, Mar. 2012.

[12] S. Van Vlierberghe, P. Dubruel, and E. Schacht, "Biopolymer-based hydrogels as scaffolds for tissue engineering applications: a review.," *Biomacromolecules*, vol. 12, no. 5, pp. 1387–408, May 2011.

[13] P. Dubruel and F. Du Prez, "Polymer Materials." University of Ghent, Ghent, 2012.

[14] N. a Peppas, P. Bures, W. Leobandung, and H. Ichikawa, "Hydrogels in pharmaceutical formulations.," *Eur. J. Pharm. Biopharm.*, vol. 50, no. 1, pp. 27–46, Jul. 2000.

[15] P. a Revell, E. Damien, L. Di Silvio, N. Gurav, C. Longinotti, and L. Ambrosio, "Tissue engineered intervertebral disc repair in the pig using injectable polymers.," *J. Mater. Sci. Mater. Med.*, vol. 18, no. 2, pp. 303–8, Feb. 2007.

[16] L. Ambrosio, A. Gloria, and R. De Santis, *Biomedical composites*. Woodhead Publishing Limited and CRC Press LLC, 2010, pp. 178–200.

[17] L. Jin, A. L. Shimmer, and X. Li, "The challenge and advancement of annulus fibrosus tissue engineering.," *Eur. Spine J.*, vol. 22, no. 5, pp. 1090–100, May 2013.

[18] S. a Skoog, P. L. Goering, and R. J. Narayan, "Stereolithography in tissue engineering.," *J. Mater. Sci. Mater. Med.*, Dec. 2013.

[19] A. a Mäkitie, J. Korpela, L. Elomaa, M. Reivonen, A. Kokkari, M. Malin, H. Korhonen, X. Wang, J. Salo, E. Sihvo, M. Salmi, J. Partanen, K.-S. Paloheimo, J. Tuomi, T. Närhi, and J. Seppälä, "Novel additive manufactured scaffolds for tissue engineered trachea research.," *Acta Otolaryngol.*, vol. 133, no. 4, pp. 412–7, Apr. 2013.

[20] S. Van Vlierberghe, "Cell-Interactive Biopolymer-based Hydrogels designed for Tissue Engineering(PhD)," 2007.

[21] S. Van Vlierberghe, P. Dubruel, E. Lippens, B. Masschaele, L. Van Hoorebeke, M. Cornelissen, R. Unger, C. J. Kirkpatrick, and E. Schacht, "Toward modulating the architecture of hydrogel scaffolds: curtains versus channels.," *J. Mater. Sci. Mater. Med.*, vol. 19, no. 4, pp. 1459–66, Apr. 2008.

[22] S. Van Vlierberghe, V. Cnudde, P. Dubruel, B. Masschaele, A. Cosijns, I. De Paepe, P. J. S. Jacobs, L. Van Hoorebeke, J. P. Remon, and E. Schacht, "Porous Gelatin Hydrogels: 1. Cryogenic Formation and Structure Analysis," *Biomacromolecules*, vol. 8, pp. 331–337, 2007.

[23] F. P. W. Melchels, J. Feijen, and D. W. Grijpma, "A review on stereolithography and its applications in biomedical engineering.," *Biomaterials*, vol. 31, no. 24, pp. 6121–30, Aug. 2010.

[24] K. Arcaute, B. K. Mann, and R. B. Wicker, "Stereolithography of three-dimensional bioactive poly(ethylene glycol) constructs with encapsulated cells.," *Ann. Biomed. Eng.*, vol. 34, no. 9, pp. 1429–41, Sep. 2006.

[25] Y. Lu, G. Mapili, G. Suhali, S. Chen, and K. Roy, "A digital micro-mirror device-based system for the microfabrication of complex, spatially patterned tissue engineering scaffolds.," *J. Biomed. Mater. Res. A*, vol. 77, no. 2, pp. 396–405, May 2006.

[26] J. R. Prado and S. Vyazovkin, "Melting of Gelatin Gels Containing Laponite, Montmorillonite, and Chhitosan Particles," *Macromol. Chem. Phys.*, vol. 215, no. 9, pp. 867–872, 2014.

[27] Y.-L. Chen, T.-C. Wang, K.-H. Lee, C.-C. Tzeng, Y.-L. Chang, and C.-M. Teng, "Synthesis of Coumarin Derivatives as Inhibitors of Platelet Aggregation," *Helv. Chim. Acta*, vol. 79, no. 3, pp. 651–657, 1996.

[28] P. Dubruel, R. Unger, S. Van Vlierberghe, V. Cnudde, P. J. S. Jacobs, E. Schacht, and C. J. Kirkpatrick, "Porous gelatin hydrogels: 2. In vitro cell interaction study.," *Biomacromolecules*, vol. 8, no. 2, pp. 338–44, Feb. 2007.

[29] S. Van Vlierberghe, P. Dubruel, E. Lippens, M. Cornelissen, and E. Schacht, "Correlation between cryogenic parameters and physico-chemical properties of porous gelatin cryogels," *J. Biomater. Sci. Polym. Ed.*, vol. 20, no. 10, pp. 1417–1438, 2009.

[30] T. Komori, "Regulation of Osteoblast Differentiation by RUNX2," in *Osteoimmunology, Advances in Experimental Medicine and Biology*, vol. 658, Y. Choi, Ed. Boston, MA: Springer US, 2010, pp. 43–49.